Development of carbon reinforced polymer-ceramic composites for bone tissue engineering

Tejinder Kaur

Department of Biotechnology and Medical Engineering
National Institute of Technology Rourkela

Development of carbon reinforced polymer-ceramic composites for bone tissue engineering

Dissertation submitted to the

National Institute of Technology Rourkela

in partial fulfillment of the requirements for the degree of

Doctor of Philosophy

in

Biotechnology and Medical Engineering

by

Tejinder Kaur

(Roll Number: 512BM1006)

under the supervision of

Prof. Arunachalam Thirugnanam
and

Prof. Krishna Pramanik

September, 2017

Department of Biotechnology and Medical Engineering
National Institute of Technology Rourkela

Department of Biotechnology and Medical Engineering
National Institute of Technology Rourkela

September, 2017

Certificate of Examination

Roll Number: 512BM1006
Name: Tejinder Kaur
Title of Dissertation: Development of carbon reinforced polymer-ceramic composites for bone tissue engineering

We the below signed, after checking the dissertation mentioned above and the official record book (s) of the student, hereby state our approval of the dissertation submitted in partial fulfillment of the requirements of the degree of Doctor of Philosophy in Biotechnology and Medical Engineering at National Institute of Technology Rourkela. We are satisfied with the volume, quality, correctness, and originality of the work.

Prof. K. Pramanik
Co-Supervisor

Prof. A. Thirugnanam
Principal Supervisor

Prof. Indranil Banerjee
Member (DSC)

Prof. Amit Biswas
Member (DSC)

Prof. J. Srinivas
Member (DSC)

Prof. Sourabh Ghosh
Examiner

Prof. A. Satapathy
Chairman (DSC)

Department of Biotechnology and Medical Engineering
National Institute of Technology Rourkela

Prof. Arunachalam Thirugnanam
Assistant Professor

Prof. Krishna Pramanik
Professor

September, 2017

Supervisor's Certificate

This is to certify that the work presented in this dissertation entitled "*Development of carbon reinforced polymer-ceramic composites for bone tissue engineering"* by "*Tejinder Kaur*", Roll Number 512BM1006, is a record of original research carried out by her under my supervision and guidance in partial fulfilment of the requirements of the degree of *Doctor of Philosophy* in *Biotechnology and Medical Engineering*. Neither this dissertation nor any part of it has been submitted for any degree or diploma to any institute or university in India or abroad.

---	---
Prof. Krishna Pramanik	*Prof. Arunachalam Thirugnanam*
Co-Supervisor	Principal Supervisor

Dedication

This thesis is dedicated to my parents, my brothers and my supervisor for making me who I am.

Declaration of Originality

I, *Tejinder Kaur*, Roll Number *512BM1006* hereby declare that this dissertation entitled *"Development of carbon reinforced polymer-ceramic composites for bone tissue engineering"* represents my original work carried out as a doctoral student of NIT Rourkela and, to the best of my knowledge, it contains no material previously published or written by another person, nor any material presented for the award of any other degree or diploma of NIT Rourkela or any other institution. Any contribution made to this research by others, with whom I have worked at NIT Rourkela or elsewhere, is explicitly acknowledged in the dissertation. Works of other authors cited in this dissertation have been duly acknowledged under the section "References". I have also submitted my original research records to the scrutiny committee for evaluation of my dissertation.

I am fully aware that in case of any non-compliance detected in future, the Senate of NIT Rourkela may withdraw the degree awarded to me on the basis of the present dissertation.

September 1st, 2017 Tejinder Kaur
NIT Rourkela 512BM1006

Acknowledgement

Successful completion of my Ph.D. is the outcome of incessant guidance and assistance from many people and I am extremely fortunate to have got these all along the completion of the project.

First and foremost, I owe my sincere gratitude and respect to my project supervisor, **Prof. A. Thirugnanam**, Department of Biotechnology and Medical Engineering, NIT Rourkela for his invaluable academic support, professional guidance, regular encouragement and motivation. His guidance helped me at various stages of this project from performing experiments to writing thesis. I am deeply grateful to my co-supervisor **Prof. K. Pramanik**, whose insights and ideas have contributed so much to this thesis. My sincere thanks also goes to **Prof. Indranil Banerjee** and **Prof. Sirsendu Ray** who provided me access to their laboratories and research facilities. I place on record my sincere gratitude to **Prof. Mukesh Kumar Gupta**, Head of Department, Department of Biotechnology and Medical Engineering, NIT Rourkela for his constant encouragement.

I would like to thank **Mr. K. Senthilguru, Mr. Joseph Christakiran** and **Ms. Abhinaya Bala** without whose precious support this project would have been a distant reality. I am especially grateful to my lab mates **Ms. Veena Vyas, Mr. Sumanta Kar, Mr. Omkar Majumder, Mr. Kartikeya Singh, Ms. Sulagna Sahu, Mr. Krishna Kumar Ramajayam, Ms. Protima, Mr. Kiran Vajanthari, Mr. Gaurav Mohan Sakhare, Mr. S.N. Naveen, Mr. Vivek Soni** and **Ms. Reshmi Dey** for their regular support, help and motivation. I would also thank my institution and faculty members. I wish to thank Department of Ceramic Engineering, Department of Physics and Department of Metallurgical and Materials Engineering for extending facilities. I also extend my thanks to my parents and family for supporting me throughout the difficulties.

September 1st, 2017 Tejinder Kaur

NIT Rourkela Roll No. 512BM1006

Abstract

Carbon based materials have attracted tremendous attention owing to their captivating electronic, mechanical and thermal properties. These materials are also being introduced in biological systems, considering the fact that life on earth is carbon based. However, limited information is available concerning the potential effects of different structures of these carbon materials on biological systems. In the present study, carbon reinforced (i.e. carbon nanotubes (CNTs-1D), graphene nanoplatelets (GNPs-2D) and activated carbon (AC-3D)) polymer-ceramic (nano-hydroxyapatite (nHA)) composite scaffolds have been developed. Poly(vinyl alcohol) (PVA) and poly(lactic-co-glycolic acid) (PLGA) have been used as polymer matrix. Initially, four different reinforcements i.e. nHA, CNTs, GNPs and AC were reinforced in PVA matrix by varying their concentrations and characterized for their physicochemical, mechanical and biological properties to find an optimum concentration. The proper dispersion of reinforcement materials up to threshold concentration enhanced the mechanical properties of the composites and provided the most favorable microenvironment for cell attachment and growth. The threshold (optimum) concentrations of different reinforcements were found to be 3% w/v for nHA, 1 wt% for CNTs, 1 wt% for GNPs and 2.5 wt% for AC, respectively, above which the agglomeration of reinforcements had reduced effect on the scaffold properties.

The optimum concentrations of each carbon were then reinforced into PVA along with 3% w/v of nHA to develop 3 component composite systems (PVA-nHA-carbon). Further, the optimum concentrations of each carbon reinforcement were also added to PLGA matrix without (PLGA-carbon) and with hydroxyapatite (PLGA-nHA-carbon). These composites containing threshold concentration of reinforcements were then characterized for their physicochemical, mechanical and biological properties. Along with the hemocompatible nature, the composites also exhibited good swelling ratio, degradation percentage and *in-vitro* bioactivity. The effective stress transfer between the homogenously dispersed

reinforcement materials and polymer matrix increased the tensile strength, Young's modulus and energy at break for the composites many folds. A significant enhancement in cell attachment, viability and differentiation was observed in all the composites. The suitable surface properties i.e. wettability, surface roughness and surface charge stimulated the protein adsorption on the carbonaceous composites making them suitable for MG-63 cell attachment, proliferation and differentiation. The augmented collagen secretion, ALP activity and matrix mineralization confirmed the improved bone forming ability of the cells. Owing to their nanostructure, both CNTs and GNPs exhibited better results in comparison to the AC.

Amongst all composites, GNPs along with nHA showed the strongest effect on the properties of PVA and PLGA based composites due to the sheet like 2D structure of GNPs. More functional groups and larger area exposed in case of GNPs lead to highest protein adsorption and hence, improved its cellular responses. The larger interface directed effective load transfer between polymer matrix and GNPs. These results demonstrate the potential of carbonaceous composites of polymer-nHA for accelerating bone tissue regeneration.

Keywords: poly(vinyl alcohol); poly(lactic-co-glycolic acid); carbon nanotubes; graphene; bone tissue engineering; tensile properties; osteoblast cells.

Contents

Certificate of Examination ..... **ii**
Supervisor's Certificate ..... **iii**
Dedication ..... **iv**
Declaration of Originality ..... **v**
Acknowledgement ..... **vi**
Abstract ..... **vii**
List of Figures ..... **xiii**
List of Tables ..... **xvii**
List of Abbreviations ..... **xviii**
1. Introduction **1**
1.1. Bone 1
1.2. Bone tissue engineering 3
1.3. Cells for bone tissue repair and regeneration 4
1.4. Scaffolds for bone tissue engineering 5
1.5. Scaffold fabrication techniques 6
1.6. Biomaterials used for bone scaffold preparation 8
1.6.1. Polymers 9
1.6.2. Ceramics 12
1.6.3. Metals 13
1.6.4. Carbon based materials 14
1.7. Summary 15
2. Literature review **17**
2.1. Tissue engineering 17
2.2. Bone tissue engineering (BTE) 18
2.3. Biomaterials for bone tissue engineering 21
2.3.1. Biodegradable polymers 21

2.3.2. Ceramics 27
2.3.3. Carbon based materials 28
2.4. Scope 32
2.5. Objectives 33
2.6. Outline of the chapters 33
2.7. Summary 34
3. Materials and methods 35
3.1. Materials 35
3.2. Preparation of composite scaffolds 36
3.2.1. PVA-nHA scaffolds 36
3.2.2. PVA-CNTs scaffolds 36
3.2.3. PVA-GNPs scaffolds 38
3.2.4. PVA-AC scaffolds 38
3.2.5. Carbonaceous PVA-nHA composite scaffolds 38
3.2.6. Carbonaceous PLGA composite scaffolds 39
3.2.7. Carbonaceous PLGA-nHA composite scaffolds 39
3.3. Characterization 39
3.3.1. Physicochemical characterization 39
3.3.2. *In-vitro* swelling studies 40
3.3.3. *In-vitro* degradation studies 40
3.3.4. *In-vitro* bioactivity studies 41
3.3.5. *In-vitro* hemocompatibility studies 41
3.3.6. Protein adsorption studies 42
3.3.7. Tensile properties 42
3.3.8. *In-vitro* biocompatibility studies 42
3.4. Summary 45
4. Results and discussion 46
4.1. Optimization of reinforcement concentration 46
4.1.1. Transmission electron microscopy 46
4.1.2. Scanning electron microscopy analysis 47
4.1.3. X-ray diffraction 52
4.1.4. Fourier transform infrared analysis 55
4.1.5. Contact angle measurements 60

4.1.6. *In-vitro* swelling studies 61
4.1.7. *In-vitro* degradation studies 64
4.1.8. *In-vitro* hemocompatibility studies 67
4.1.9. *In-vitro* bioactivity studies 69
4.1.10. Protein adsorption studies 73
4.1.11. Tensile properties 76
4.1.12. Cell viability 80
4.1.13. Cell morphology 84
4.1.14. Alkaline Phosphatase (ALP) activity 89
4.1.15. Mineralization assay 91
4.2. Effect of 1D/2D/3D carbon structures 93
4.2.1. Scanning electron microscopy analysis 93
4.2.2. X-ray diffraction 95
4.2.3. Fourier transform infrared spectroscopy 97
4.2.4. Contact angle measurements 98
4.2.5. *In-vitro* swelling studies 102
4.2.6. *In-vitro* degradation studies 104
4.2.7. *In-vitro* hemocompatibility studies 107
4.2.8. *In-vitro* bioactivity studies 107
4.2.9. Protein adsorption studies 110
4.2.10. Tensile properties 114
4.2.11. Cell viability 116
4.2.12. Cell morphology 119
4.2.13. Alkaline Phosphatase (ALP) activity 122
4.2.14. Confocal microscopy and quantification of cell morphology 124
4.2.15. Live cell staining 129
4.2.16. Collagen quantification 131
4.2.17. Mineralization assay 133
4.3. Summary 136
5. Conclusion 138
Scope for future research 140
References 141
Dissemination 158

Vitae **160**
Index **165**

List of Figures

Fig. 1.1 Schematic representation of bone tissue engineering process using cellular scaffold. 3

Fig. 1.2 Molecular structure of poly(vinyl alcohol). 11

Fig. 1.3 Molecular structure of poly(lactic-co-glycolic acid). 11

Fig. 3.1 Schematic representation of the sample preparation and characterization.……... 37

Fig. 4.1 (a) TEM micrographs and (b) SAED patterns of nHA, AC, CNTs and GNPs.....48

Fig. 4.2 FESEM micrographs of (a) PVA, (b) PHA 1, (c) PHA 2, (d) PHA 3, (e) PHA 4 and (f) PHA 5. 49

Fig. 4.3 FESEM micrographs of (a) PCN 0, (b) PCN 0.5, (c) PCN 1 and (d) PCN 1.5. Surfaces of (e) PCN 1 and (f) PCN 1.5 observed at higher magnification. (Arrows show the agglomeration in PCN 1.5.) 50

Fig. 4.4 FESEM micrographs of (a) PGN 0, (b) PGN 0.5, (c) PGN 1 and (d) PGN 1.5. Scaffolds (e) PGN 1 and (f) PGN 1.5 at higher magnification. (Arrows represent the well dispersed GNPs and asterisks represent the agglomeration of GNPs.) ...51

Fig. 4.5 FESEM micrographs of (a) PC 0, (b) PC 0.5, (c) PC 1, (d) PC 1.5, (e) PC 2, (f) PC 2.5, (g) interconnected pores in PC 2.5 and (h) higher magnification micrograph of PC 2.5 scaffolds. 52

Fig. 4.6 XRD patterns of (a) different reinforcements, (b) PVA-nHA, (c) PVA-CNTs, (d) PVA-GNPs and (e) PVA-AC composites. 54

Fig. 4.7 FTIR spectra of (a) different reinforcements, (b) PVA-nHA, (c) PVA-CNTs, (d) PVA-GNPs and (e) PVA-AC composites. 58

Fig. 4.8 Fourier self-deconvolution of FTIR spectra of various samples…… 59

Fig. 4.9 Swelling studies of (a) PVA-nHA, (b) PVA-CNTs, (c) PVA-GNPs and (d) PVA-AC composites……...62

Fig. 4.10 Degradation studies of (a) PVA-nHA, (b) PVA-CNTs, (c) PVA-GNPs and (d) PVA-AC composites……...65

Fig. 4.11 (a) FESEM micrographs and (b) XRD spectra of PVA-nHA composite scaffolds after immersion in SBF for 21 days. 70
Fig. 4.12 (a) FESEM micrographs and (b) XRD spectra of PVA-CNTs composite scaffolds after immersion in SBF for 21 days. 71
Fig. 4.13 (a) FESEM micrographs and (b) XRD spectra of PVA-GNPs composite scaffolds after immersion in SBF for 21 days. 72
Fig. 4.14 (a) FESEM micrographs and (b) XRD spectra of PVA-AC composite scaffolds after immersion in SBF for 21 days. 74
Fig. 4.15 MTT assay results of (a) PVA-nHA, (b) PVA-CNTs, (c) PVA-GNPs and (d) PVA-AC composites. 82
Fig. 4.16 Trypan blue exclusion assay results showing total cell count (a, c, e and g) and live to total cells ratio (b, d, f and h) for various scaffolds. 83
Fig. 4.17 FESEM micrographs of PVA-nHA composite samples cultured with MG-63 cells. 85
Fig. 4.18 FESEM micrographs of PVA-CNT composites cultured with MG-63 cells. 86
Fig. 4.19 FESEM micrographs of PVA-GNPs composites cultured with MG-63 cells.....87
Fig. 4.20 FESEM micrographs of PVA-AC composites cultured with MG-63 cells……..... 88
Fig. 4.21 ALP activity results of (a) PVA-nHA, (b) PVA-CNTs, (c) PVA-GNPs and (d) PVA-AC composites……. 90
Fig. 4.22 Alizarin red stain assay results for (a) PVA-nHA, (b) PVA-CNTs, (c) PVA-GNPs and (d) PVA-AC composites.....92
Fig. 4.23 FESEM micrographs of (a) PL, (b) PLCN, (c) PLGN and (d) PLAC composites. 94
Fig. 4.24 FESEM micrographs of (a) PH, (b) PHCN, (c) PHGN and (d) PHAC composite scaffolds.....95
Fig. 4.25 FESEM micrographs of (a) PLH, (b) PLHCN, (c) PLHGN and (d) PLHAC composite scaffolds. 96
Fig. 4.26 XRD patterns of (a) PLGA-carbon, (b) PVA-nHA-carbon and (c) PLGA-nHA-carbon composites. 97
Fig. 4.27 FTIR spectra of (a) PLGA-carbon, (b) PVA-nHA-carbon and (c) PLGA-nHA-carbon composites. 99
Fig. 4.28 FSD of the FTIR spectra of various composites. 100

Fig. 4.29 Swelling studies of (a) PLGA-carbon, (b) PVA-nHA-carbon and (c) PLGA-nHA-carbon composites. 103

Fig. 4.30 Degradation studies of (a) PLGA-carbon, (b) PVA-nHA-carbon and (c) PLGA-nHA-carbon composites……..... 105

Fig. 4.31 (a) FESEM micrographs and (b) XRD spectra of carbon reinforced PLGA composite scaffolds after immersion in SBF for 21 days…… 109

Fig. 4.32 (a) FESEM micrographs and (b) XRD spectra of carbon reinforced PVA-nHA composite scaffolds after immersion in SBF for 21 days…….. .111

Fig. 4.33 (a) FESEM micrographs and (b) XRD spectra of carbon reinforced PLGA-nHA composite scaffolds after immersion in SBF for 21 days. 112

Fig. 4.34 MTT assay results of (a) PLGA-carbon, (b) PVA-nHA-carbon and (c) PLGA-nHA-carbon composites. 117

Fig. 4.35 Trypan blue exclusion assay results showing the total cell count (a, c, e and g) and live to total cells ratio (b, d, f and h) for various scaffolds. 118

Fig. 4.36 FESEM micrographs of (a) PL, (b) PLCN, (c) PLGN and (d) PLAC composites cultured with MG-63 cells.....120

Fig. 4.37 FESEM micrographs of (a) PH, (b) PHCN, (c) PHGN and (d) PHAC composites cultured with MG-63 cells.....121

Fig. 4.38 FESEM micrographs of (a) PLH, (b) PLHCN, (c) PLHGN and (d) PLHAC composites cultured with MG-63 cells.....122

Fig. 4.39 ALP activity results of (a) PLGA-carbon, (b) PVA-nHA-carbon and (c) PLGA-nHA-carbon composites after 7 days of culturing.....123

Fig. 4.40 Confocal micrographs of MG-63 cells seeded on (a) PL, (b) PLCN, (c) PLGN, (d) PLAC and (e) quantification of cell area on different scaffolds……..... 126

Fig. 4.41 Confocal micrographs of MG-63 cells on (a) PH, (b) PHCN, (c) PHGN, (d) PHAC and (e) quantification of cell area. Inset (A) shows well spread cells on PHGN sample at lower magnification and (B) shows cells migrated inside the porous scaffold……... 127

Fig. 4.42 Confocal micrographs of MG-63 cells seeded on (a) PLH, (b) PLHCN, (c) PLHGN, (d) PLHAC and (e) quantification of cell area on different scaffolds. Inset shows the 3D micrograph of PLHGN sample confirming the presence of cells throughout the sample……... 128

Fig. 4.43 Live cell staining of MG-63 cells seeded on (a) PL, (b) PLCN, (c) PLGN and (d) PLAC composites…….. 130

Fig. 4.44 Live cell staining of MG-63 cells seeded on (a) PH, (b) PHCN, (c) PHGN and (d) PHAC composites. 131

Fig. 4.45 Live cell staining of MG-63 cells seeded on (a) PLH, (b) PLHCN, (c) PLHGN and (d) PLHAC composites. 132

Fig. 4.46 Quantification of collagen produced by MG-63 cells seeded on (a) PLGA-carbon, (b) PVA-nHA-carbon and (c) PLGA-nHA-carbon composites. 133

Fig. 4.47 Alizarin red stain assay results for (a) PLGA-carbon, (b) PVA-nHA-carbon and (c) PLGA-nHA-carbon composites. 134

List of Tables

Table 2.1 Commercially available tissue engineering products.....19
Table 2.2 Properties of different biomaterials used for bone repair and regeneration...22
Table 4.1 Average contact angles of different composites.....61
Table 4.2 Degradation rate coefficient for the developed composites……66
Table 4.3 Percentage (%) hemolysis of different composites…….68
Table 4.4 Protein adsorption on different composites…….75
Table 4.5 Mechanical properties of different composites……...78
Table 4.6 Average contact angles of different composites with threshold reinforcement concentrations……...101
Table 4.7 Degradation rate coefficient for the developed composites……. 106
Table 4.8 Percentage (%) hemolysis of different composites……...108
Table 4.9 Protein adsorption on different composites……...113
Table 4.10 Mechanical properties of different composites…….115

List of Abbreviations

AC	Activated carbon
ALP	Alkaline phosphatase
ARS	Alizarin red stain
ATR-FTIR	Attenuated total reflectance-Fourier transform infrared spectroscopy
BCP	Biphasic calcium phosphate
BMPs	Bone morphogenetic proteins
BSA	Bovine serum albumin
BTE	Bone tissue engineering
CNTs	Carbon nanotubes
DMEM	Dulbecco's Modified Eagle's medium
DWCNTs	Double-walled carbon nanotubes
ECM	Extracellular matrix
FESEM	Field emission scanning electron microscope
GNPs	Graphene nanoplatelets
GO	Graphene oxide
HA	Hydroxyapatite
MSCs	Mesenchymal stem cells
MTT	3-(4,5-dimethyl-2-yl)-2,5-diphenyltetrazolium bromide
MWCNTs	Multi-walled carbon nanotubes
nHA	Nano-hydroxyapatite
PBS	Phosphate buffer saline
PC	Poly(vinyl alcohol) – activated carbon
PCL	Polycaprolactone
PCN	Poly(vinyl alcohol) – carbon nanotubes

PDLLA	Poly(D, L-lactic acid)
PGA	Poly(glycolic acid)
PGN	Poly(vinyl alcohol) – graphene nanoplatelets
PHA	Poly(vinyl alcohol) - nano-hydroxyapatite
PHAC	Poly(vinyl alcohol) - nano-hydroxyapatite – activated carbon
PHCN	Poly(vinyl alcohol) - nano-hydroxyapatite – carbon nanotubes
PHGN	Poly(vinyl alcohol) - nano-hydroxyapatite – graphene nanoplatelets
PLA	Poly(lactic acid)
PLAC	Poly(lactic-co-glycolic acid) - activated carbon
PLCN	Poly(lactic-co-glycolic acid) - carbon nanotubes
PLGN	Poly(lactic-co-glycolic acid) - graphene nanoplatelets
PLH	Poly(lactic-co-glycolic acid) - nano-hydroxyapatite
PLHAC	Poly(lactic-co-glycolic acid) - nano-hydroxyapatite – activated carbon
PLHCN	Poly(lactic-co-glycolic acid) - nano-hydroxyapatite – carbon nanotubes
PLHGN	Poly(lactic-co-glycolic acid) - nano-hydroxyapatite – graphene nanoplatelets
PVA	Poly(vinyl alcohol)
ROS	Reactive oxygen species
SAED	Selected area electron diffraction
SWCNTs	Single-walled carbon nanotubes
TCP	Tri-calcium phosphate
TEM	Transmission electron microscopy
XRD	X-ray diffraction

Chapter 1

Introduction

This chapter gives an introduction to bone tissue engineering by providing an overview of basic requirements of the tissue engineering. The chapter begins with a summary of structure, functions and properties of bone. The current techniques of bone repair, their limitations and the need for bone tissue engineering will be discussed. Various types of biomaterials (polymers, ceramics, metals and carbon) and techniques for scaffold fabrication will also be discussed.

1.1. Bone

Bone is an organ of skeletal system with a highly complex and a well-organized structure [1]. Its main functions are to provide mechanical support to the body, to protect internal organs and to serve as a mineral reservoir. It also maintains calcium and phosphate homeostasis, helps in blood production and blood pH regulation [2]. It consists of a mineral phase, an organic phase and water [3]. In most of the bones, the mineral content ranges from 60-70% of its dry weight and is mainly composed of hydroxyapatite. The organic phase contains type 1 collagen (~90%), noncollagenous proteins (~5%) and lipids (~2%). The hydroxyapatite crystals are arranged parallel to the collagen fibrils of the organic phase [3]. The adult human skeleton is composed of 20% trabecular bone (cancellous and spongy) and 80% cortical bone (compact and dense). Bone development occurs by two processes: intramembranous or endochondral ossification. In intramembranous ossification, the mesenchymal stem cells directly differentiate into osteoblast cells and form bone. In contrast, endochondral ossification involves the formation of a cartilage template which converts to bone after calcification and invasion of blood vessels.

Bone has a unique ability to grow, model and remodel itself continuously throughout the lifetime [4]. In response to the physiological conditions or applied stress, bone keeps changing its shape and this process is known as bone modeling. To maintain bone strength and homeostasis bone remodeling occurs. In the bone remodeling process, old bone is resorbed and new bone is formed by osteoclast and osteoblast cells. This process starts before birth and continues till death. In most of the cases, after trauma or any disease, bone expresses excellent intrinsic capacity to repair and regenerate without the formation of any scar tissue. Studies have shown that the natural mechanism of bone repair closely resembles to the normal bone formation process [5]. However, the natural bone repair process has many disadvantages as it is limited to bone defects that have adequate vascular supply and it takes long time for proper healing of bone. Also it is inadequate to repair the large bone defects, as observed after nonunion fractures, bone tumor resections and endoprosthetic loosening. Therefore, bone grafts such as autografts and allografts are used to enhance bone repair and regeneration in such cases.

Currently, autografts, which involve harvesting bone from the patient's iliac crest and transplanting to the injured site, are the gold standard for bone grafts. Autografts are non-immunogenic and histocompatible, that possess the essential components of bone regeneration like osteoprogenitor cells, osteoinductive growth factors (i.e. bone morphogenetic protein (BMPs)) and bone supporting matrix. However, autografts have limitations including expensive procedures, donor site morbidity, scarring and many surgical risks. The second most common bone grafting technique is known as allografting that uses bone from human cadaver. Allografts have risk of immunoreactions and infections. Additionally, the supply of bone grafts is much less than the demand. Any untreated injury or defect in bone structure can intensely alter patient's body equilibrium and quality of life. Hence, there is a need for new bone defect repair strategies. Engineered bone tissues are considered to be a potential alternative to the conventional bone repair methods.

1.2. Bone tissue engineering

Tissue engineering is a promising strategy to develop new tissue structures by using a combination of cells and matrix scaffolds. It is defined as an interdisciplinary field applying the principles of life science and engineering for the development of biological substitutes that repair, maintain and improve tissue functions [6]. In terms of its application to engineer a bone, the aim is to guide and enhance the osteogenic differentiation of cells cultured on three-dimensional matrix. The field of bone tissue engineering was initiated almost 30 years ago, and it has developed rapidly since then. The key objective of bone tissue engineering is to repair or regenerate bone in such a way that the new bone formed is integrated structurally with the surrounding bones. Different bone tissue engineering strategies are available to develop bone constructs. In the most promising strategy, cells with osteogenic potential are isolated and seeded on a scaffold to produce extracellular matrix (ECM) which is implanted to the bone defect site (Fig. 1.1). Other methods include direct implantation of scaffold with or without cells immediately to the defected site [2, 7]. Along with the cells and ECM, intercellular communication, cell-matrix interaction and growth factors also play an important role in bone tissue engineering.

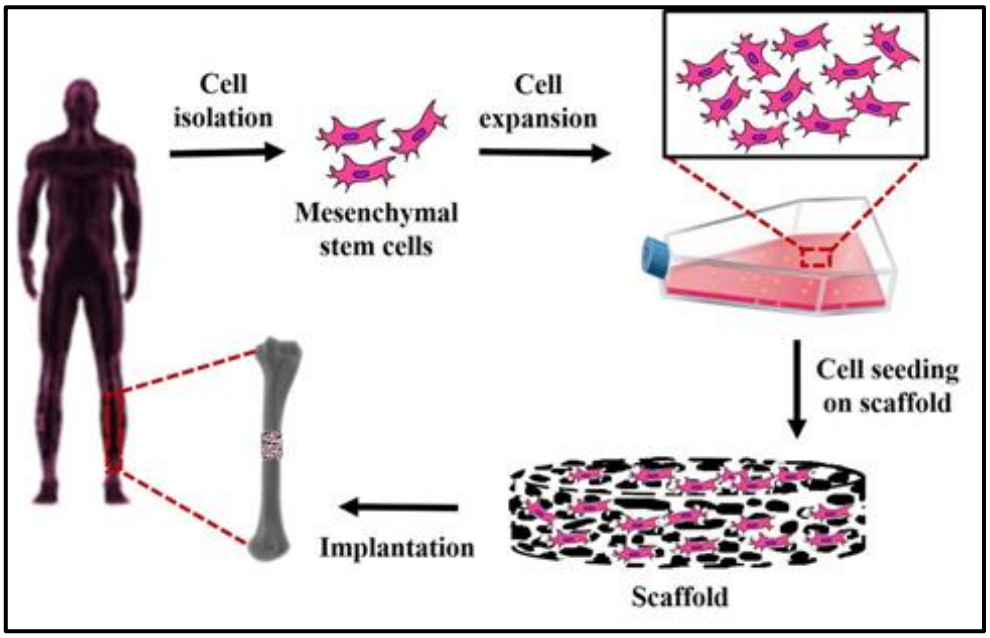

Fig. 1.1 Schematic representation of bone tissue engineering process using cellular scaffold.

1.3. Cells for bone tissue repair and regeneration

One of the major requirements for bone tissue engineering is the cells that are capable of producing bone. These cells are isolated from many sites and expanded into high numbers to produce a clinically sized engineered bone tissue. An ideal cell source should be non-immunogenic, expandable to a large number of cells and possesses osteogenic potential. Osteoblasts and mesenchymal stem cells are potential cell sources and also have been found to produce biomimetic bone tissue [8]. Primary osteoblast cells are advisable to use as they can be taken from patient itself (autologous) and would produce bone matrix immediately after implantation. These cells increase the extent of bone regeneration and produce bone specific proteins and enzymes (e.g. osteocalcin, alkaline phosphatase and collagen). Using enzymatic extraction, the osteoblast cells are extracted from bone and expanded by culturing them *in-vitro*. However, primary pre-differentiated osteoblast cells present some limitation such as low expansion rate and less number of cells. Therefore, stem cells are considered to be a promising alternative for primary osteoblast cells. Stem cells are undifferentiated cells which have the ability of self-renewal and can differentiate into many different cell lineages. Various types of stem cells have been utilized for bone regeneration such as mesenchymal stem cells, embryonic stem cells, adipose derived stem cells and induced pluripotent stem cells [9]. Amongst all, mesenchymal stem cells (MSCs) have attracted special interest in bone tissue engineering due to their role in the natural bone formation process. MSCs have advantages like easy expansion, high proliferation potential, and can be cryo-preserved and differentiated into muscle, bone and cartilage tissue lineages [10]. Other than bone marrow, MSCs have also been isolated from umbilical cord blood, peripheral blood, amniotic fluid, adipose tissue, kidneys, brain, liver, heart and skin [11-16]. These cells have shown their potential in the repair of the femur and cranial bone defects [17]. The tissue engineered bones using MSCs exhibited mechanical strength similar to that of natural bone. The embryonic and induced pluripotent stem cells also have tissue regeneration capability. With limited literature available on tissue engineered bones from MSCs, extensive research is needed to evaluate their potential for bone regeneration and repair.

1.4. Scaffolds for bone tissue engineering

A scaffold is a three-dimensional (3D) structure that provides temporary mechanical support during bone regeneration and starts degrading as the tissue grows [18]. It also provides a suitable tissue specific environment for cells to proliferate, differentiate and form new bone. It functions as a reservoir of nutrients and growth factors. A scaffold should possess the following properties to meet the requirements for bone tissue engineering.

- **Biocompatibility**: The scaffold should support cellular activity without eliciting any local or systematic toxic effects to the host. It should also facilitate molecular signaling and generate beneficial tissue specific responses. The biocompatibility of a scaffold depends on factors like its structure, chemistry, morphology and material processing [19]. Different physical and chemical treatments are available to augment the biocompatibility of the scaffold material. Further, several biocompatible synthetic polymers have also been developed for bone tissue engineering such as poly(vinyl alcohol) (PVA), poly(lactic acid) (PLA), poly(glycolic acid) (PGA), polycaprolactone (PCL), and poly(lactic-co-glycolic acid) (PLGA), etc. [20].
- **Porosity**: The scaffold should possess a 3D interconnected porous structure with high surface area to volume ratio such that it allows cells to distribute and grow throughout the scaffolds. Porosity is required for diffusion of nutrients and gases to the cells inside scaffolds and to remove metabolic waste. Along with porosity, the pore size also plays an important role for cells to penetrate inside the scaffold. Different tissue regenerations have different pore size requirements according to the size of respective cells. Previous studies have reported the optimum pore size of 5 µm for neovascularization and fibroblasts, 20 µm for hepatocytes and 20-125 µm for adult mammalian skin cells [19]. The minimum required pore size for osteoblast cells has been reported as 100 µm [21]. Other important factors are pore volume, pore size distribution, pore shape and pore wall roughness.
- **Mechanical properties**: An ideal scaffold should have sufficient mechanical properties to endure the hydrostatic pressure and maintain spaces required for cells to grow inside the scaffold [22]. It should have mechanical strength matching to

that of host bone. Designing an ideal scaffold for bone regeneration is a challenging task owing to the geometry and wide variations in mechanical properties of the natural bone. Mechanical properties of cortical bone (Young's modulus: 15-20 GPa) and cancellous bone (Young's modulus: 0.1-2 GPa) vary widely [18]. Hence, it becomes difficult to develop scaffolds mimicking the bone tissue.

- **Biodegradability**: After repair and regeneration of bone tissue there is no need of implant anymore. Therefore, additional surgery is required to remove the implant leading to increased complications and cost. To avoid these complications, biodegradable scaffolds are being developed. After implantation, these scaffolds degrade itself with time and create space for the new bone to grow. The scaffolds should degrade at a controlled rate so that the injured bone is repaired completely before the scaffold is totally degraded.
- **Surface properties**: Surface properties of a scaffold have a strong influence on its cellular response. An ideal scaffold should have suitable surface properties to encourage cells attachment, proliferation and differentiation. Surface chemistry and topological features of a scaffold mediate the cell responses and direct the immunological responses. After implantation, the migration of osteogenic cells to the scaffold depends on its topographical properties. Further, the surface chemistry of scaffold material control the cell adhesion on scaffold surface via cell-protein-material interactions. Hence, surface properties are an imperative aspect in directing cell-material interactions.

1.5. Scaffold fabrication techniques

Several techniques have been used for fabrication of scaffolds for bone tissue engineering. The developed three dimensional (3D) scaffolds should encourage the cell distribution and proliferation. For fabrication of such scaffolds, general processing techniques include solvent casting, salt leaching, gas foaming, electrospinning, freeze drying and phase separation [23]. Other advanced techniques also exist based on the application of fabricated scaffold like self-assembly, rapid prototyping, fiber mesh, fiber bonding, melt molding, membrane lamination, etc. [24]. Each technique has its advantages and disadvantages. Most widely used techniques have been discussed below.

Solvent casting: It is the most widely used, easy and inexpensive technique for the preparation of scaffolds [24]. It is based on the evaporation of solvent from polymer (or polymer composite) solution when poured into a mold. However, the retention of toxic solvent in scaffolds may cause problems after implantation. Hence, to avoid this, the prepared scaffolds are dried under vacuum to remove solvent properly.

Particulate leaching: This method consists of a high density of particulates (porogens) dispersed in the polymer solution. The porogen is taken in a mold, and a polymer solution is poured into it. The polymer moves into the voids and settles there. After evaporation of solvent, the polymer gets hardened, and the porogen is leached out using water or alcohol. The leaching of porogen leads to the formation of a porous scaffold. Various porogens including salt, sugars, wax, and polymers have been successfully used to fabricate porous scaffolds. In this method, the pore size and pore volume can be controlled by using appropriate size and density of porogen [24]. However, the pore shape and pore interconnectivity cannot be controlled.

Gas foaming: High temperature and organic solvents used for the preparation of scaffolds may cause problems during *in-vitro* and *in-vivo* cell culture studies. To avoid such circumstances gas has been used as a porogen in gas foaming technique for development of porous scaffolds. Polymer discs prepared by compression molding are exposed to carbon dioxide at high pressure (800 psi) [25]. The porosity of the scaffold depends on the amount of gas porogen. At saturation level, the gas becomes unstable and form clusters which act as a porogen. The benefit of gas foaming techniques is that it provides interconnected pores; however, the pore size cannot be controlled.

Phase separation: This method involves the separation of the polymer solution into two phases: polymer lean phase (low polymer concentration) and polymer rich phase (high polymer concentration). In this technique, the polymer is dissolved, frozen to separate the liquid-liquid phase and then quenched forming a two-phase solid. Later, the solvent is removed from the system by evaporation, extraction, and sublimation resulting in a porous scaffold. The pores obtained by this method are relatively smaller in size and are not well distributed [26]. Hence, this technique has been combined with other scaffold fabrication methods to control the pore size, structure, and volume.

Freeze drying: Freeze drying, also known as lyophilization is based on the principle of sublimation. It involves freezing of polymer solution at (~ -70°C) and then removal of frozen solvent under high vacuum by sublimation. This method results in scaffolds with highly interconnected porous structure. The pore size of the scaffold depends on the freezing temperature, freezing rate and pH of the solution. The freeze drying method has already been explored to fabricate porous scaffolds using different polymers like PVA, PLGA, PLA, PGA, chitosan and their composites [27, 28]. The main advantages of this method are the elimination of organic solvent, high temperature, and leaching of the porogen.

Electrospinning: Electrospinning is widely used for fabrication of polymeric fibers with the diameter ranging from nanoscale (<1000 nm) to microscale (>1 µm) [29]. It uses high voltage electric field created between two electrodes, one placed in a polymer solution and another in a collecting target. The polymer solution is ejected from a needle forming a droplet. The generated electric field around the droplet overcomes its surface tension, and the fibers are formed as the polymer jet travels towards collecting target. The diameter of the fibers depends on the properties of polymer solution (viscosity, surface tension, conductivity, etc.), flow rate, strength of electric field and distance between the needle and collecting target. A wide range of polymers has been used to form nano fibrous scaffolds favorable for better cellular growth. However, the main disadvantage of his method is the use of organic solvents which can be toxic to cells.

1.6. Biomaterials used for bone scaffold preparation

Various natural and synthetic biomaterials have been investigated for better repair and replacement of the injured bone tissues [30]. An ideal biomaterial should be biocompatible, biodegradable, bioactive, porous, and mechanically compatible with the natural bone [31]. Biomaterials used for bone tissue engineering are broadly divided into the following categories: polymers, ceramics, metals, and carbon based materials.

1.6.1. Polymers

Both, natural and synthetic polymers have been extensively used to develop scaffolds for bone tissue engineering. Natural polymers such as collagen, chitosan, starch, silk, and hyaluronic acid have shown their potential for tissue engineering applications. These natural polymers exhibit bioactivity, low immunogenic potential and receptor-binding ligands for cells to attach. The drawbacks of natural polymers are that they have pathogenic impurities, weak mechanical strength, less supply, and high cost [32]. On the other hand, synthetic polymers (i.e. PVA, PGA, PLA, PLGA, etc.) represent the largest group of biomaterials used in tissue engineering. Synthetic polymers have already proven their potential in drug delivery, resorbable sutures and orthopedic fixation devices [33]. These polymers are biodegradable and have shown reasonable biocompatibility [34]. Their degradation products are non-toxic and can be eliminated from the body by normal metabolic pathways. The main advantage of synthetic polymers is their tunable properties which can be tailored according to the requirements. Also, the risk of toxicity and immunogenicity is low due to their known structures and they can be easily molded into differently designed shapes for different applications.

Poly(vinyl alcohol): Among various synthetic polymers, poly(vinyl alcohol) (PVA) has received intensive attention in tissue engineering, wound dressing and drug delivery owing to its suitable physicochemical properties [35]. PVA (Fig. 1.2) is a biodegradable, hydrophilic and biocompatible polymer, produced by partial or full hydrolysis of polyvinyl acetate. It dissolves in water at a temperature of 100°C with a holding time of 30 min. and its physical and chemical properties depend on the extent of hydrolysis. Moreover, semi-permeable nature of PVA allows the transportation of oxygen and other nutrients into the scaffold for cell survival and removal of wastes from the scaffold [36]. Owing to its good flexibility and mechanical properties, it has been used in both implantable and non-implantable devices. However, its poor cell adhesion, bioinert nature, and insufficient mechanical properties hinder its applications as a bone implant.

Poly(glycolic acid): Among polyesters, PGA is the only hydrophilic biodegradable thermoplastic polymer having hydroxyl and carboxyl groups on its two ends [34, 37]. This structure leads to the high crystallinity, elevated melting point and low solubility of PGA

in organic solvents. The properties such as biodegradability, hydrophilicity, suitable mechanical properties, non-toxicity, and formability attracted the attention of researchers towards the use of PGA for scaffold preparation by common fabrication methods. Owing to its suitable properties, PGA has been widely used to develop degradable synthetic suture [38]. The degradation of PGA is a two-step process: the first step includes random hydrolytic chain scission of the ester linkage in the amorphous phase after diffusion of water, followed by hydrolysis of the crystalline region in the second step [39]. The crystallinity of the polymer increases in the first stage and then decreases during the second stage. This degradation of PGA results into a natural metabolite, glycolic acid which is resorbable when present at high concentration. The rapid degradation of PGA in aqueous solution or *in-vivo* reduces its mechanical stability. Another limitation of PGA is the lack of specific cell recognition signals which decreases the cell attachment on its surface [40]. Thus, the regulation of degradation rate and the improvement of biological properties are required for the extensive biological applications of PGA.

Poly(lactic acid): The PLA is a polyester widely studied as a scaffold material owing to its biocompatibility, biodegradability and fascinating physical properties [41]. It can be synthesized into three isomeric forms: D-, L- and DL- isomers. The stereochemical structure of PLA influences its physiochemical properties as by varying the ratio of D- or L-isomer, the amorphous or crystalline nature of the polymer can be regulated. The degradation of PLA by hydrolysis results in lactic acid which is removed from the body by tricarboxylic acid cycle in the form of water and carbon dioxide. The presence of methyl group in the PLA structure makes it more hydrophobic and amorphous in comparison to the PGA. This decreased affinity toward water reduces the degradation rate of the polymer and maintains its mechanical integrity for months, both, *in-vitro* and *in-vivo* [38]. The L-isomer of PLA i.e. poly(L-lactic acid) (PLLA) is well known for its excellent mechanical properties due to the slower degradation rate when compared to DL-isomer i.e. poly(D, L-lactic acid) (PDLLA). However, PLA has to suffer from few drawbacks such as poor cell adhesion and stimulation of inflammatory responses *in-vivo* [42].

Poly(lactic-co-glycolic acid): The PLGA, a copolymer of PLA and PGA, is one of the most commonly used biodegradable polymer (Fig. 1.3) [43]. Its degradation (hydrolysis of ester bond) leads to the formation of lactic acid and glycolic acid which can be easily

removed from the body by metabolic pathways [44]. The PGA is hydrophilic in nature whereas PLA is comparatively hydrophobic due to the presence of methyl group. Hence, the degradation rate of PLGA can be controlled by varying the ratio of its monomers. Other properties like swelling degree, rate of hydrolysis and mechanical strength depend upon the crystallinity of PLGA which is again subjected to the ratio of its monomers. Owing to its highly biocompatible and biodegradable nature, PLGA has been widely used in bone tissue engineering. It has shown good results in controlled drug delivery and can also be fabricated in different forms and shapes. However, hydrophobicity, suboptimal mechanical strength and poor bioactivity of PLGA are the main disadvantages that often limit its applications [45].

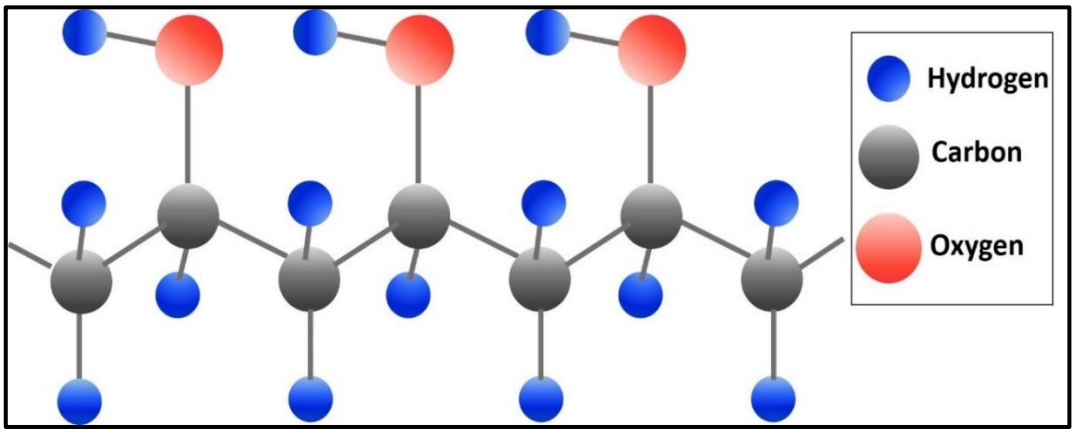

Fig. 1.2 Molecular structure of poly(vinyl alcohol).

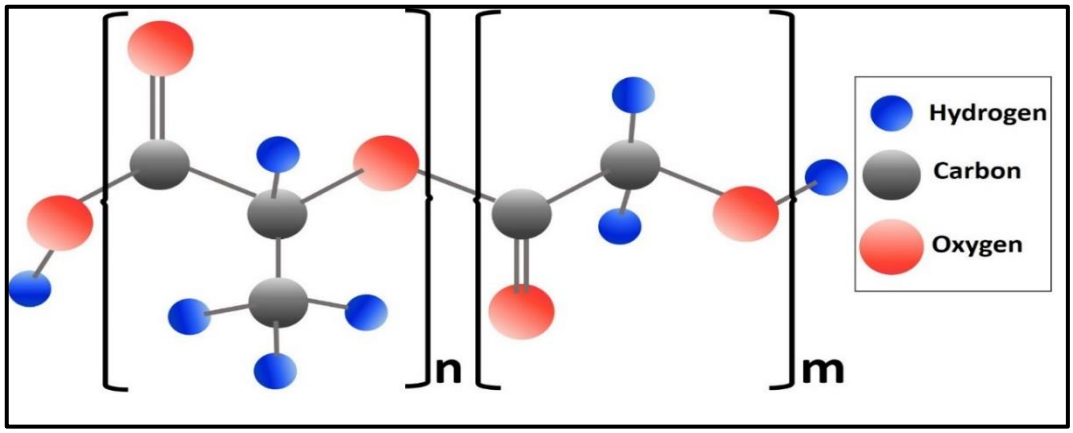

Fig. 1.3 Molecular structure of poly(lactic-co-glycolic acid).

1.6.2. Ceramics

Both, natural and synthetic ceramics have been used for the repair of bones. These are mainly used for filling bone defects, replacement of defected bone and fracture repair [46]. Ceramics are biocompatible, corrosion resistant and highly bioactive. Brittleness, low fracture toughness, and high stiffness are the main limitations of ceramics which restrain their applications. Natural ceramics such as corals are biocompatible and have interconnected porous structure with decent mechanical properties. They have shown their potential in the repair of bones such as distal phalanx of the thumb [7]. However, the high dissolution rate of these ceramics has restricted their clinical applications. Therefore, synthetic ceramics such hydroxyapatite (HA), tri-calcium phosphate (TCP), biphasic calcium phosphate (BCP), brushite, and monetite have been developed and evaluated for bone repair applications. Calcium phosphate based ceramics have similar mineral phase as that of bone. Due to their osteoconductivity (support osteoblast adhesion and proliferation) and osteoinductivity (stimulate bone formation), they have been considered for bone tissue engineering applications. These ceramics are highly bioactive and biodegradable also. Researchers have reported them as a carrier for osteogenic cells and osteoconductive growth factors [47]. TCP is a bioactive ceramic which has been used as bone filler in orthopedic applications [48]. Brushite and monetite have been evaluated for fracture treatment and bone augmentation respectively. Mostly ceramic materials are used as reinforcing materials in polymer matrices to develop biocomposite scaffolds for bone tissue engineering.

Hydroxyapatite: HA (chemical formula: $Ca_{10}(PO_4)_6(OH)_2$) is the most widely used ceramic for bone regeneration owing to its similar composition to that of bone mineral. It is highly biocompatible, osteoconductive, osteoinductive, and bonds chemically with the host tissue. These advantages make HA a suitable candidate for different applications such as bone repair and augmentation, bone fillers, hard tissue replacement implants, and coating of implants. Further, nano-hydroxyapatite (nHA) has been found to have improved mechanical properties and bioactivity [49]. However, its brittle nature, difficulty in shaping as a scaffold and low mechanical properties restrict its use as a scaffold material for load

bearing sites. Hence, to meet the requirements of tissue engineering, nHA reinforced polymer composites are developed with improved biological and mechanical properties.

Other ceramic materials: The biocompatibility, osteoconductivity and chemical similarity to the inorganic phase of natural bone make TCP an attractive biomaterial for bone tissue engineering applications. It exists in two phases, α and β, both of which possess similar chemistry but different crystal structures [50]. The Ca/P ratio of the stoichiometric TCP ($Ca_3(PO_4)_2$) is 1.5, and it is more soluble in aqueous environment owing to the instability of its phases in comparison to the HA. On the other hand, BCP, consisting of different concentrations of a stable phase (HA) and a soluble phase (β-TCP), has advantages of controlled bioactivity and biodegradation properties. By varying the concentration of HA and β-TCP, BCP with desired degradation time is developed for bone implant applications. Along with its ability to induce stem cell differentiation, BCP is attracting researchers as it can be easily tailored to different sizes and shapes. Nevertheless, the use of these ceramic materials is associated with few drawbacks including brittleness and poor mechanical properties. This shows that the additional efforts are required to further advance the applications of ceramics in bone tissue engineering.

1.6.3. Metals

A variety of biocompatible metallic materials have been used as a bone implant or a fixation device. Frequently used metallic bone implant materials include titanium alloys, stainless steel, cobalt-chromium alloys, tantalum, and magnesium. Metallic implants have extensive mechanical properties like high strength, fracture toughness and corrosion resistance making them suitable as implants for load bearing sites [51]. The major drawback of metallic implants is that it lacks biological recognition on its surface. To improve their surface biocompatibility several treatments and coating have been successfully used. Titanium is an inert and biocompatible materials which has osseointegration capability. Titanium alloys have shown superior biocompatibility and mechanical properties as compared to stainless steel and cobalt alloys [51]. They also have capability to carry growth factors which induce bone repair and regeneration. Titanium foams were developed and used as porous implant for total hip replacement and knee arthroplasty [52]. With the similar modulus of elasticity to that of bone, highly porous tantalum has shown its potential

for total knee arthroplasty. Recently, magnesium is gaining attention of researchers for its applications as scaffolds, screws and plates. Unlike other metallic scaffolds, it is a biodegradable material hence there is no need to remove it after repair and regeneration of bone. Magnesium and its alloys have good mechanical properties and their corrosion products can be easily removed from body by normal metabolic pathways [53]. However, more *in-vivo* studies are required to check the potential of magnesium and its alloys as a biomaterial for bone tissue engineering.

1.6.4. Carbon based materials

Carbon based materials like diamond, graphite, carbon fibers, activated carbon, nanotubes, nanowires and nanoribbons are being used from years for various electronics, optics, and sensor applications [54]. In recent years, carbon and its allotropes have attracted increased interests as reinforcing materials. Further, the developments in the field of nanotechnology have paved the way for the use of carbon nanomaterials as reinforcements in the polymer matrix. These nanomaterials have unique nanoscale dimensions, large surface area, biocompatibility with living tissues, and exceptionally good mechanical properties which make them promising material for orthopedic applications. Three types of carbon biomaterials widely being used in the field of bone tissue engineering are carbon nanotubes (CNTs), graphene nanoplatelets (GNPs) and activated carbon (AC).

Carbon nanotubes: Amongst various carbon based biomaterials, CNTs (1D) have drawn a great attention of researchers. Owing to their exceptional mechanical and biological properties, CNTs have been reinforced in different polymer matrices to develop composite scaffolds with improved properties. In addition, multi-walled CNTs (MWCNTs) have been found to accelerate the bone formation [55]. Nevertheless, owing to their intrinsic van der Waal interactions, pristine CNTs have the tendency to aggregate, resulting in the reduced dispersion and hence, cytotoxicity to human cells [56]. To overcome this problem, researchers have functionalized CNTs using different functional groups like hydroxyl, carboxylic acid, poly amino benzoic sulfonic acid, and poly(vinyl alcohol) etc. [57]. The functionalization increases CNTs dispersion and eliminate them easily from the body via renal excretion route. These functional groups also improve the bioactivity of the scaffolds by attracting calcium cations [58].

Graphene nanoplatelets: Graphene, a 2D sp^2 hybridized carbon sheet, is emerging as a potential biomaterial for bone tissue engineering. Its aromatic structure, strong bonding between carbon atoms, and active sites on the surface make graphene a unique material with exceptional physicochemical, thermal, electrical and mechanical properties. Graphene nanoplatelets (GNPs) are also gaining attention of researchers owing to their structural similarity to idealized graphene. GNPs provides an ameliorative substitute to CNTs as it contains no metallic impurities and its production is cost effective. Due to its high aspect ratio and sheet like structure, GNPs form percolated networks when reinforced in the polymer matrix. The large interfacial interaction between GNPs and polymer matrix helps in effective load transfer and improved mechanical properties of the composite. The defects present on the edges of GNPs promote the oxidative reaction with surrounding environment yielding hydrophilic structure due to oxygen containing functional groups [59]. Therefore, GNPs are less prone to agglomeration as compared to single layer graphene [60]. Functionalization of GNPs with different functional groups increases their water dispersibility. Moreover, GNPs have shown non-toxic behavior towards human osteoblast and mesenchymal stromal cells. In recent *in-vitro* cell culture studies, GNPs were found to stimulate the osteoblast cell attachment, growth, and differentiation.

Activated carbon: Activated carbon (AC), a quasi-graphitic form of carbon, is a highly porous biomaterial with large surface area to volume ratio. Due to its irreversible adsorption of toxic metabolites it is widely used to enhance cell growth and development in plant tissue culture [61]. The large surface area and powerful adsorption properties of AC fulfill the space requirement and help living cells to attach onto its surface. The adsorption of inflammatory cytokines by porous carbon decreases the inflammation. Owing to these properties AC is expected to encourage osteoblast cells growth and differentiation.

1.7. Summary

This chapter has provided essential basic information about the bone tissue engineering. The limitations of the existing bone repair and regeneration techniques along with the need of bone tissue engineering have been discussed. The requirements and fabrication

techniques for an ideal scaffold were described. Finally, various biomaterials and their advantages for better repair and replacement of the injured bone tissues were briefed.

Chapter 2

Literature review

This chapter provides a comprehensive literature review of the research field. A brief but informative review on tissue engineering and its application for bone tissue repair and regeneration will be presented. Following that, various biomaterials used for bone tissue engineering are described. The current research using hydroxyapatite and carbon materials as reinforcements in polymer matrices are also discussed in this chapter. Lastly, the scope, objectives of the present work and the outline of various chapters are also mentioned.

2.1. Tissue engineering

Many other instances of the vision of regenerative medicine and tissue engineering have been reported in ancient times. The Sanskrit texts like Sushruta Samhita have described the skin transplantation done by Koomas caste members in ancient India, during 2500-3000 BC [62]. Later, a famous painting named as “Healing of Justinian” from 278 AD depicted the homograft limb transplantation to a soldier [63]. In the 18th century, transplantation of teeth and skin proved to be a milestone in the modern tissue engineering. In the mid-1980s, tissue engineering term came into existence to represent the surgical manipulations of tissues. Y. C. Fung, a researcher working in the field of biomechanics submitted a proposal entitling “Center for the Engineering of Living Tissues” to NSF (in 1985) from which the term “tissue engineering” originated [64]. Dr. Eugene Bell further explained the tissue engineering by focusing on its applications [65]:

- providing cellular prostheses or replacement parts for the human body;
- providing formed acellular replacement parts capable of inducing regeneration;

- providing tissue or organ-like model systems populated with cells for basic research and for many applied uses such as the study of disease states using aberrant cells;
- providing vehicles for delivering engineered cells to the organism; and
- surfacing non-biological devices

The most frequently referred definition of tissue engineering was reported in a review paper by Robert Langer and Joseph P. Vacanti as [6]:

> "Tissue engineering is an interdisciplinary field that applies the principles of engineering and the life sciences toward the development of biological substitutes that restore, maintain, or improve tissue function".

Over the past 30 years, the field of tissue engineering has evolved significantly. It has been applied to regenerate a wide variety of organs and tissues. Tissue engineered skin, the first successful cell-based product, was marketed under the name of Epicel. As this product did not have a dermis, another product was developed consisting of collagen and chondroitin sulfate along with a silicone sheet as a temporary epidermis [66]. Even the advanced tissue engineered skin products have several limitations such as lack of cells, glands etc. High occurrence of joint diseases has increased the cartilage regeneration and repair demand. Currently, three different techniques are used for cartilage repair: osteochondral transplantation, marrow simulation, and cell based techniques. In 1994, the first commercially available cell based technique for cartilage repair, named as Carticel was developed [67]. Later, various engineered tissues have been or being developed throughout the world including skin, bone, cartilage, liver, blood vessels, kidney, heart valves, pancreas, breast, and lung [68]. Some of the commercial tissue engineering products and their uses have been summarized in Table 2.1. With increasing demand for tissue engineered products, several approaches are adopted to tailor its needs.

2.2. Bone tissue engineering (BTE)

Worldwide, millions of people suffer from bone disorders and injuries due to various reasons. Yearly, almost 8.9 million fractures occur only due to osteoporosis, and more than 26 million people suffer from bone disorders in India [69, 70]. It is estimated that by the

year 2050, 50% of global hip fractures will occur in Asia [71]. About, 2.2 million bone grafting surgeries are performed every year worldwide making the bone as most frequently transplanted tissue [72].

Table 2.1 Commercially available tissue engineering products [73, 74].

Tissue	Products	Company	Application
Skin	Integra Dermal Template	Integra Lifesciences	Burns
	TransCyte	Advanced Biohealing	Burns
	Apligraf	Organogenesis	Diabetic foot ulcers and venous leg ulcers
	Dermagraft	Organogenesis	Foot ulcer of diabetic patients
	Integra Flowable Wound Matrix	Integra Lifesciences	Ulcers
	Oasis Wound Matrix	Healthpoint	Ulcer and other types of wounds
	Xelma	Molnlycke	Leg ulcers
Bone	OP-1	Stryker	Bone injury
	INFUSE Bone Graft	Medtronic	Spinal fusion
	Vitoss Scaffold FOAM	Orthovita	Bone injury
	FortrOss	Pioneer surgical	Bone injury
	Bioset IC	Pioneer surgical	Bone injury
	GEM 21S	BioMimetic Therapeutics	Dental defects (bone and gum)
	BCT001	Bioceramic Therapeutics	Bone defects
Cartilage	Synvisc	Genzyme	Synovial fluid replacement

	CaReS	Arthro Kinetics	Articular cartilage injury
	Menaflex	Regenbiologics	Meniscus cartilage injury
	Bioseed-C	Biotissue Technologies	Articular cartilage injury
	MACI	Genzyme	Articular cartilage injury
Tendon and ligaments	GraftJacket	Wright Medical Technology	Tendon and ligament repair
	X-Repair	Synthasome	Tendon and ligament repair
Heart valve	CryoValve SG pulmonary human heart valve	CryoLife	Heart valve replacement
	Clearlink valve	Baxter Healthcare Corporation	Heart valve replacement
	Carbomedics standard aortic valve	CarboMedics	Heart valve replacement
	On-X heart valve	CryoLife	Aortic and mitral prosthetic valve replacement
	Medtronic Open Pivot mechanical heart valves	Medtronic	Valve replacement with mechanical valve
	CryoValve Aortic valve	CryoLife	Aortic valve replacement
Liver	Bioartificial liver system	ExcorpMedical	Liver replacement
	ELAD Artificial liver	Vital therapies	Liver replacement
Pancreas	Islet sheet	Cerci Medical	Diabetes mellitus
	Amcyte	ReNeuron	Diabetes mellitus

Current treatments for bone defects include autologous and allogenic bone grafts. Autografts are the gold standard for bone grafts owing to their osteoconductive, osteoinductive and non-immunogenic properties. These grafts are the second most commonly transplanted tissues. However, bone grafts have limitations such as high cost, donor site injury, scarring, inflammation, and infection. Additionally, high demand and less supply of bone grafts stimulated researchers to go for substitutes such as metal implants. After the failure of stainless steel and cobalt alloys implants, titanium was used as implant material back in 1930s. Although metallic implants provide mechanical support, they have certain disadvantages such as stiffness, stress shielding, poor integration with biological tissues, and risk of infection [1]. It has been reported that 13% of people are sensitive to different metals such as nickel, cobalt and chromium [75]. Given the limitations associated with the grafts and metallic implants, there is a need for a tissue engineered bone. Bone tissue engineering initiated almost three decades ago and it has progressed very fast over the years. It is an excellent option for full recovery of patients suffering from bone injuries by using engineered bone substitute that mimick the natural bone.

2.3. Biomaterials for bone tissue engineering

An ideal material for bone tissue engineering should be biocompatible and biodegradable with good mechanical strength. A number of natural and synthetic materials have been explored for bone applications. Based on the BTE requirements, biomaterials can be divided into various categories. Properties of these biomaterials used for bone repair and regeneration are mentioned in Table 2.2.

2.3.1. Biodegradable polymers

The use of biodegradable biomaterials for BTE has progressed in years to avoid the use of second surgery to remove implant material after bone recovery. The three types of biodegradable materials are polymers, ceramics, and metals. Natural biomaterials such as chitosan, alginate, hydroxyapatite, agarose, etc. have low mechanical properties making them unsuitable for bone tissue engineering [76-78]. To overcome these problems, synthetic biomaterials came into existence, but these materials lack adequate tissue interactions.

Table 2.2 Properties of different biomaterials used for bone repair and regeneration.

Materials	Origin	Properties	Applications	Ref.
Polymers				
Collagen	Natural	Biodegradable, biocompatible, porous, hydrophilic, weak mechanical strength	Scaffold, composite, drug delivery, guided bone regeneration	[79]
Chitosan	Natural	Osteoconductive, biodegradable	Scaffolds, microgranules, vertical bone augmentation	[1, 46]
Hyaluronic acid	Natural	Biodegradable, injectable, weak mechanical properties	Synthetic bone grafts, wound dressing	[19, 80]
PGA	Synthetic	Tunable degradation behaviour and mechanical properties	Bone grafts, scaffolds, bone internal fixation devices, synthetic suture	[81, 82]
PLA	Synthetic	Good mechanical strength	Fracture fixation, screws, scaffolds	[83, 84]

PLGA	Synthetic	Fast degradation, high mechanical strength, biocompatible, hydrophobic	Scaffolds, coating, microspheres, drug delivery system, monofilament suture, carrier for BMP	[19, 46, 85]
PCL	Synthetic	Biocompatible	Scaffolds, composites, coating	[86]
PVA	Synthetic	Biocompatible, hydrophilic,	Bone scaffolds, composites	[30]
Polydioxanone	Synthetic	Biodegradable properties	Fixation screws	[19]
Ceramics				
Corals	Natural	Biocompatible, porous, high dissolution rate	Repair of distal phalanx of the thumb	[7]
Hydroxyapatite (HA)	Synthetic	Biodegradable, tunable degradation rate, brittle, high mechanical strength	Bone regeneration scaffolds, composites, coatings, bone defect filler	[27, 87]
Brushite	Synthetic	Biodegradable, high strength	Controlled drug delivery system for bone healing	[88]
Alumina	Synthetic	Good strength	Joint replacement	[89]

Tri-calcium phosphate	Synthetic	Biodegradable	Bone filler, bone cement	[46]
Metals				
Titanium and its alloys	Synthetic	Non-biodegradable, resistant to corrosion and fatigue	Implant for load bearing site, screws, plates, fracture treatment, BMP carrier	[89, 90]
Stainless steel	Synthetic	Non-biodegradable, corrosive	Implant for load bearing site, screws	[91]
Magnesium	Synthetic	Degradable, corrosive	Implant for load bearing site, osteosynthesis device, screws, wires	[92, 93]
Carbon based biomaterials				
Carbon nanotubes	Synthetic	High mechanical strength, excellent electrical properties	Biomaterial reinforcement, cell and tissue labelling, drug delivery system	[54]
Graphene nanoplatelets	Synthetic	Large surface area, high mechanical strength	Biomaterial reinforcement, cell and tissue labelling	[54]
Activated charcoal	Synthetic	Highly porous, large surface area to volume ratio	Adsorption of toxic metabolites, plant tissue culture	[94]

Poly(glycolic acid): Owing to its biodegradability, biocompatibility and good mechanical properties, PGA has attracted the attention of researchers worldwide. Its applications include tissue engineered scaffolds, drug delivery systems, and orthopedic implants [95]. Conversely, a decrease in strength, an increase in localized pH and fibrous capsule formation after implantation of PGA, limit its suitability as scaffold material [96]. To improve the biocompatibility, various treatments have been performed on the PGA based scaffolds. Boland et al. have reported that the pretreatment of PGA scaffolds with concentrated hydrochloric acid (HCl) improves its cellular responses [37]. The acid pretreatment of PGA degrades the amorphous region present on its surface and releases the monomers prior to implantation. This results in a reduction of the localized pH decrease and improves the *in-vivo* responses. In another study, PGA grafted chitosan films were prepared to counteract the acidic degradation products of the PGA and to improve the degradation of chitosan [95]. After the degradation of chitosan, the released glucosamine neutralizes the acidic products and prevents the inflammatory tissue reactions. By taking advantage of the formability of PGA, β-TCP reinforced composite scaffolds, possessing improved biological properties, were also developed [97]. The presence of β-TCP in PGA matrix stabilized the physiological pH near the implant, increased the biocompatibility and encouraged the bone formation after implantation.

Poly(lactic acid): PLA has been widely used to provide the architectural cues for the repair and regeneration of large bone defects. The *in-vivo* implanted PLLA degrades itself by hydrolysis without the use of any enzyme and makes the surgical removal of implant unnecessary [98]. The low molecular weight PLLA was found to degrade at an adequate rate while maintaining its mechanical properties until the bone defect was healed properly [99]. The self-reinforced PLLA rods were also used as a scaffold for bone regeneration in muscle by free tibial periosteal grafts. After 6 weeks of implantation, new bone was generated in a predesigned cylindrical form [100]. In an attempt to design PLLA based scaffolds for load bearing applications, ceramic materials such as β-TCP and HA have been reinforced into the polymer matrix to improve its mechanical properties [101]. The reinforcement of β-TCP strengthens the PLLA composite along with the improvement in cell viability [102]. Similarly, silane modified HA has also increased the mechanical properties of the resulting composite scaffold [103]. The PLLA based microspheres and

microcapsules have shown their potential as drug delivery systems for prolonged administration of a wide range of drugs [104].

Poly(lactic-co-glycolic acid): PLGA, a copolymer of PLA and PGA, is preferred for BTE as it satisfies most of the requirements of scaffold fabrication. The PLGA microspheres with calcium phosphate cement have shown improved biological response after loading of bone morphogenetic protein (BMP-2) [105]. It has shown carbonated apatite growth when kept in simulated body fluid for 16 days [106]. It has also been explored as nanofibers, hydrogels, films and 3D scaffolds [107]. However, hydrophobicity, weak mechanical strength and poor bioactivity of PLGA are the critical issues of concern that often limit its applications [45]. Blending PLGA with other hydrophilic polymers (e.g. poly(vinyl alcohol)) or ceramics along with the surface treatments have shown improved biological properties [43, 108, 109]. The graphene oxide reinforced PLGA nanocomposites have enhanced surface chemical and mechanical properties. Coating PLGA with hydrophilic polymers have been found to slightly improve the cell adhesion on its surface [110]. However, the results obtained from these studies are non-satisfactory. Thus, reinforcing PLGA with a suitable biomaterial is required to potentially improve its biological and mechanical properties.

Poly(vinyl alcohol): Owing to its biodegradable and biocompatible nature PVA has been used as a scaffold material for BTE [30]. Most of the biodegradable polymers (PLA, PCL, PLGA) are hydrophobic nature, whereas PVA showed excellent hydrophilic nature. Furthermore, its semi-permeable nature allows transport of nutrients and oxygen to the cells inside the scaffolds [36]. Porous PVA scaffolds have been developed by using porogens like sodium chloride, sucrose and polyethylene glycol [111]. Selective laser sintering technique has also been used to develop PVA based porous scaffolds with improved osteoblast cell adhesion [112]. However, weak cellular affinity and mechanical properties limit its application as a scaffold material for bone tissue engineering. Research is being carried out to improve the cellular affinity and mechanical properties of PVA as a scaffold. The coating of bioactive glass was found to improve the tensile strength of PVA but reduced the elongation to failure value [113]. Thus, the composites of PVA with suitable reinforcements are required to potentially improve the biological and mechanical properties of scaffolds.

2.3.2. Ceramics

The compositional similarity of various calcium phosphate bioceramics to the bone mineral makes these materials an appropriate option for bone scaffold material. The commonly used calcium phosphate ceramics for bone tissue repair and regeneration are TCP, BCP and HA. Porous β-TCP scaffolds with 3D orthogonal periodic architecture were fabricated via selective laser sintering by using epoxy resin and nylon as adhesive [114]. The fabricated scaffolds with 55% porosity exhibited good mesenchymal stem cell attachment and growth on their surface. Tarafder et al. have reported the manufacturing of microwave sintered 3D printed TCP scaffolds with controlled interconnected macroporous architecture for bone tissue engineering [115]. The efficient densification obtained by microwave sintering increased the compression strength of the scaffolds many folds in comparison to the conventional sintering technique. The presence of both micro and macropores expedited the osteoid like bone formation in femoral defects of rats. In another study, the addition of strontium oxide and magnesium oxide in TCP improved the mechanical and biological properties of the scaffolds for BTE [116]. An increased bone formation and mineralization of the newly formed bone was observed in the strontium oxide and magnesium oxide doped 3D printed TCP scaffolds. In another study, the effect of an increasing amount of BCP granules (50-250 mg) on viability, morphology, adhesion, and differentiation of the total bone marrow cells was studied [117]. A decrease in cell viability, attachment and differentiation was observed with the increasing amount of BCP. These declined cellular responses could be explicated by calcium phosphate precipitation resulting to a reduction in calcium concentration with increasing BCP amount. A biomimetic BCP-collagen-apatite composite scaffold with improved biological properties was fabricated [118]. The BCP facilitated the formation of collagen matrix and strengthened the scaffold, whereas, collagen and apatite improved the cellular interactions.

Amongst the bioactive inorganic materials, nHA has gained a widespread application because of its biocompatibility, bioactivity, osteoconductivity, and osteoproductivity [87]. The nHA that mimics the stoichiometry of bone composition easily bonds with the living bone tissue by forming a new apatite layer. From decades nHA is being used in maxillofacial surgery as bone defect filler. The 3D scaffolds made up of nHA have shown migration of cells inside the porous scaffolds [119]. However, owing to its poor mechanical

properties like brittleness, low plasticity and fatigue strength, nHA is difficult to use as a monolithic in load-bearing applications. Therefore, HA has been used as a reinforcing material to the polymer matrices to develop composites with the improved mechanical and biological properties. The HA reinforced porous PVA bioactive composite scaffolds, when seeded with SaOS-2 cells, were found to encourage the cell penetration into pores and enhanced their proliferation [87]. In another study, PVA-nHA composites were developed by varying the concentration of nHA in PVA matrix [27]. It was observed that above a certain concentration (3% w/v), HA started agglomerating which deteriorated the properties (biological and mechanical) of the composites. The incorporation of nHA into polyamide (poly hexamethylene adipamide) was found to increase both, bioactivity and mechanical properties of the scaffold material [120]. The nHA coatings on polymeric, metallic and carbonaceous materials have always attracted the researchers. The coating of nHA on carbon matrix has shown positive effects on biological responses by up-regulating the corneal cell growth [121].

2.3.3. Carbon based materials

The unique properties of carbon based materials make them a suitable candidate for scaffold development and present new opportunities in the field of tissue engineering. The carbon nanomaterials provide a microenvironment similar to the biological ECM which improves the cellular responses. Different dimensional structures of various carbon materials play an important role in their application. Carbon based materials with 1D, 2D, and 3D structures are extensively being used in the field of bone tissue engineering.

Carbon nanotubes: In the year 1991, Sumio Iijima first reported the preparation of CNTs which fuelled research on CNTs [122]. Since then, CNTs are effectively being used in various fields of chemistry, electronics, physics, and material science. The unique electrical, biological and mechanical properties of CNTs have also attracted attention in the medical field. The CNTs have also been reinforced in different polymer matrices for potential use in various biomedical applications. However, in few studies, the agglomeration of pristine CNTs have shown toxic effects. To avoid this problem, CNTs are being functionalized with various functional groups to achieve better dispersion in polymer matrices. Polymer composites reinforced with CNTs have shown better growth of

various cell types such as osteoblast, fibroblast, skeletal myoblast, and stem cells. Researchers have shown that the reinforcement of functionalized CNTs in PCL matrix improves both, the stem cell osteogenesis and mechanical properties of the composite [123]. Lahiri et al. showed that the addition of CNTs in polylactide-caprolactone enhanced the osteoblast cell viability and mechanical properties of the composites [124]. Studies have also proven that the functionalized MWCNTs impart osteoinductive properties to the PCL composite with increased wettability. This increase in wettability of the matrix improves the protein and cell adhesion on the surface. Further, the incorporation of the carboxylated MWCNTs into PLGA films induced the mesenchymal stem cells to differentiate into osteoblast cells [44]. Polyethyleneimine functionalized single-walled CNTs (SWCNTs) promoted the neurite growth and branching due to the positive charge on their surface [125]. PVA matrix reinforced with 1 wt% carboxylic acid functionalized CNTs has shown an up-regulated osteoblast cell adhesion, proliferation, and differentiation [30]. Further, increase in concentration up to 1.5 wt% lead to agglomeration of CNTs which caused toxic effects. *In-vitro* studies have exposed the toxic effects of CNTs on the various types of cells. Different structures of CNTs are expected to play an important role in their toxicology towards osteoblast cells. Zhang et al. investigated the effect of SWCNTs, DWCNTs (double-walled CNTs) and MWCNTs on the various cellular responses of primary osteoblasts [126]. A time and dose-dependent reduction in cell proliferation and differentiation was observed in the order SWCNTs>DWCNTs>MWCNTs. They have also reported that the SWCNTs with the smaller diameter are intended to aggregate more due to their high surface energy in comparison to the MWCNTs [127]. Hence, more aggregation could be the reason for high toxicity of SWCNTs. At a concentration of 50 µg/ml, CNTs significantly inhibited the mineralization and expression of Runx-2 and Col-I proteins in osteoblasts. However, the ALP activity of the cells was found to be dependent on the time of interaction of the cell with CNTs instead of the CNTs dose. Another reason for cytotoxicity of CNTs is their ability to induce reactive oxygen species (ROS) and oxidative stress due to the presence of metallic impurities. In another study, authors have demonstrated the aggregation of MWCNTs in mouse embryonic stem cells leading to DNA damage through ROS generation [128]. This interaction with MWCNTs induced the apoptosis in cells and doubled the frequency of mutations. Few other studies have also shown cytotoxicity of CNTs depending on the concentration used. As both, positive and

negative effects of CNTs have been reported in the literature, in-depth study of cytotoxic effects of CNTs are required.

Graphene nanoplatelets: Graphene is considered as the basic building block of all other carbon allotropes. Graphene family nanomaterials like graphene, GNP, graphene oxide (GO), and reduced graphene oxide (rGO) have been used for various biomedical applications since their first application as a drug delivery system by Dai et al. [129]. Several studies have shown that graphene supports the adhesion and proliferation of osteoblast, mesenchymal stem cells, and fibroblast cells. Literature has reported an accelerated differentiation of human mesenchymal stem cells towards osteoblast lineages when cultured on graphene substrate [130]. Improved expression of osteocalcin and calcium deposition was observed due to the improved protein adsorption via π–π interactions. The surface morphology and chemistry also affected the osteogenic differentiation of cells on graphene. Kalbacova et al. demonstrated the osteoconductive behavior of graphene without any toxicity [131]. It was found biocompatible to both human osteoblast and mesenchymal stromal cells. The graphene oxide reinforced PLGA nanocomposites have enhanced surface chemical and mechanical properties [132]. Graphene hydrogels showed biocompatible nature by forming monolayers due to increased osteoblast cells adhesions and proliferation [133]. When GO was reinforced in chitosan matrix, increased swelling properties and hydrophilicity lead to better osteoblast cellular response [134]. However, the mechanical properties of the developed scaffolds are not suitable for bone tissue engineering applications. Mehrali et al. have reported that GNPs are less prone to agglomeration as compared to single layer graphene [60]. Further, GNPs have also shown positive effects on various biological and mechanical characteristics of composites when incorporated in poly(lactic acid) matrices. Pinto et al. showed that reinforcement of small amount of GO and GNPs (0.4 wt%) in PLA matrix significantly enhances Young's modulus and tensile strength of the composite [135]. In another study, Zhang et al. had reported improved mechanical and biological properties when hydroxyapatite was reinforced with GNPs [136]. A few studies have also testified the contradictory results showing toxicity of graphene depending on its concentration [137]. Studies are being performed to investigate the cytotoxic effects of graphene and its derivatives on mammalian cells. It has shown toxic effects to fibroblasts, epithelial cells,

osteoblasts, and blood cells. The graphene has been found to cause ROS generation and hindrance in nutrient uptake [134]. Similarly to CNTs, graphene has also shown size-dependent cytotoxicity. Smaller GO particles showed higher toxicity towards the cells by ROS generation [138]. They also led to increased hemolysis of erythrocytes with the decrease in GO size. The dose-dependent toxicity of GO decreased the fibroblasts cell adhesion and viability at a concentration above than 20 µg/ml [139]. The GO enters the cell cytoplasm and disturbs the cell energy metabolism, gene transcription and translation resulting into cell apoptosis. However, Zhang et al. have reported that at a concentration of 10 µg/ml, graphene induces mitochondrial injury and neuronal cell apoptosis due to the activation of caspase 3 [140]. Like CNTs, the aggregation of graphene also leads to enhanced toxic effects. On interaction with blood cells, GO exhibited higher hemolysis than the graphene sheets, whereas, on interaction with fibroblasts, graphene sheets caused more damages than the GO [141]. The GNPs induced the ROS generation and disruption of cell membranes at a dose of 5 $\mu g/cm^2$ [142]. The use of low concentration or functionalized carbon nanomaterials is expected to reduce their cytotoxic effects. Thus, more detailed research efforts are required to study the mechanical and biological effects of GNPs.

Activated carbon: Owing to its fine network of pores and large surface area, AC provides more surface for adsorption. It has been used in plant tissue culture to enhance the growth by adsorbing toxic compounds from culture medium [61]. As reported by Sandman et al., the adsorption of inflammatory cytokines by porous carbon matrix, suppressed the inflammation and increased the corneal cell growth on hydroxyapatite-coated porous carbon matrix [121]. They showed the adsorption of inflammatory cytokines by porous carbon matrix, hence, suppressing the inflammation and increasing cellular growth. Further in another recent study AC-ECM composite scaffolds facilitated the regeneration of damaged neural tissues by promoting neuronal differentiation [94]. The AC composite helped in concentrating the growth factors and cell adhesion proteins. The differentiation of stem cells in the presence of AC lead to more matured neuron- like cells. The AC has advantages like low cost and economical synthesis in comparison to other carbon based materials. However, in spite possessing better properties and low cost, AC has not been explored much in the field of tissue engineering.

2.4. Scope

It has been observed that most of the current biomaterials fail to fulfill all the requirements for an ideal bone scaffold. The mechanical properties of scaffolds are significantly low than those of natural bone. Therefore, there is need to combine two or more biomaterials to develop a composite scaffold material with improved properties. Different composites such as polymer-polymer, polymer-ceramics, polymer-metal, and ceramics-metal combinations have been developed and evaluated for bone tissue engineering. Inert biomaterials can be reinforced with osteoinductive and osteoconductive materials to encourage bone repair and regeneration. Similarly, osteoinductive brittle materials can be reinforced with a mechanically strong material. Owing to their biocompatibility and biodegradation properties, PVA and PLGA have been widely used in the field of tissue engineering. However, weak mechanical strength and inert nature of PVA, and hydrophobicity and poor bioactivity of PLGA are the critical issues of concern that often limit their applications. Amongst the bioactive inorganic materials, nHA has gained a widespread application because of its biocompatibility, bioactivity, osteoconductivity, and osteoproductivity. On the other hand, carbon based materials are fascinating due to their size, large surface area and well acceptance by the biological environment. Along with the favorable biological properties, the mechanical properties of these materials are also comparable to that of natural bone. All these verdicts establish the feasibility of using hydroxyapatite and carbon allotropes (CNTs, GNPs and AC) with different structures as ideal reinforcement materials in PVA and PLGA matrices for bone tissue engineering. The cytotoxic effects of carbon materials are also necessary to be studied further to evaluate their biocompatibility. Therefore, in the present study, optimized concentrations of nHA and carbon materials, with improved cellular responses and no toxicity, were obtained. These threshold concentrations were further used to develop carbonaceous polymer-ceramic composite materials with required biological and mechanical properties for better bone regeneration.

2.5. Objectives

From the literature review, the broad objectives of the thesis are:

- To develop polymer composite scaffolds by reinforcing hydroxyapatite and various carbon allotropes with different dimensional structures in PVA and PLGA matrices.
- To characterize the composite scaffolds for their physicochemical and mechanical properties.
- To perform *in-vitro* bioactivity and evaluate the biological properties of the composite scaffolds.

2.6. Outline of the chapters

- Chapter 1 provides an introduction to the field of bone tissue engineering, scaffold preparation techniques and various biomaterials used for scaffold preparation.
- Chapter 2 provides an overview of literature reported for bone tissue engineering applications using hydroxyapatite and various carbon based materials as reinforcements in polymer matrices.
- Chapter 3 reports the materials and methodology followed for development of carbon reinforced PVA/PLGA based composites with and without nHA. The techniques used to characterize and evaluate the mechanical and biological properties of the developed composites are provided.
- Chapter 4 delineates the results and discussion of the present research work. Results obtained from various characterizations of PVA based composites reinforced with varying concentrations of carbon materials and nHA are reported. The optimum concentrations obtained and their effects of these optimum concentrations on various properties of PVA and PLGA based composites are also reported.
- Chapter 5 discusses the final conclusions drawn from the present research work and recommendations for future research are also reported in this chapter.

2.7. Summary

This chapter provided an overview of the current research in the field of bone tissue engineering. Ongoing research on the development of various scaffolds for improved bone repair and regeneration has been discussed. Advantages and disadvantages of different biomaterials as reinforcements have been mentioned. From the literature survey it can be summarized that hydroxyapatite and carbon based materials have extensive potential for bone tissue engineering applications. Different shapes and aspect ratio of these biomaterials are expected to trigger diverse biological and mechanical effects. The effect of different dimensional structures of carbon reinforcements on PVA/PLGA matrices has not been explored much. Finally, the scope of the present work, objectives, and outlines of the chapters of the thesis have been reported.

Chapter 3

Materials and methods

This chapter describes various materials required and methods followed to perform the present research. The preparation and characterization of PVA based composite scaffolds using varying concentrations of different materials (nHA, CNTs, GNPs, AC) will be described to find the threshold (optimum) concentration of each reinforcement material, above which it deteriorates the composite properties. Further, the preparation of PVA/PLGA based composites using optimized reinforcement concentrations and their characterizations are explained to study the effects of different carbon structures.

3.1. Materials

PVA (hot water soluble), AC powder, antibiotic-antimycotic solution, phosphate buffer saline (PBS), Bradford reagent, bovine serum albumin (BSA) and 3-(4,5-dimethyl-2-yl)-2,5-diphenyltetrazolium bromide (MTT) assay kit from HiMedia Laboratories Pvt. Ltd., India; PLGA (lactide:glycolide = 75:25), carboxylic acid functionalized CNTs (multi-walled; diameter: 9.5 nm; length: 1.5 μm), Dulbecco's Modified Eagle's medium (DMEM), trypsin-EDTA solution, alkaline phosphatase (ALP) assay kit, alizarin red stain based (ARS) assay kit, TRITC-phalloidin stain, Hoechst stain and fetal bovine serum (FBS) were procured from Sigma-Aldrich, India; carboxylic acid functionalized GNPs (average thickness 6-8 nm, surface area 150 m^2g^{-1}) from Cheap tubes, USA, nano-hydroxyapatite (nHA) from Acros Organics, USA, calcein-AM from Thermo Fisher Scientific India Pvt. Ltd., India and the human osteoblast-like MG-63 cells (human osteosarcoma cell line) from

the National Centre for Cell Science (NCCS, Pune) India, were procured and used in this research work. All reagents used in this research work were of analytical grade.

3.2. Preparation of composite scaffolds

The present work is divided into two phases as shown in Fig.3.1. In the first phase, varying concentrations of four different materials (nHA, CNTs, GNPs and AC) were reinforced into PVA matrix to develop various composites. The developed composites were characterized for their physicochemical, biological and mechanical properties to find the optimum concentration of each reinforcement. In the second phase, the obtained optimum concentrations of different materials were further reinforced into polymer (PVA and PLGA) matrices to study the effect of different structures (1D, 2D, and 3D) of carbon.

3.2.1. PVA-nHA scaffolds

The PVA-nHA scaffolds were prepared by solvent evaporation method as a preliminary work to find optimum concentration of nHA. Five different PVA-nHA composite scaffolds were prepared by dissolving 10% w/v of PVA in distilled water, followed by addition of nHA by varying its concentration (1%, 2%, 3%, 4% and 5% w/v). The homogenous dispersion was achieved by sonication and continuous stirring (90°C), and the solution was poured into a glass mold and kept in a vacuum oven at 60°C for 24 h. The five resultant PVA-nHA composite scaffolds were designated as PHA 1, PHA 2, PHA 3, PHA 4 and PHA 5 respectively. Pure PVA scaffold was also prepared and coded as PVA. These composites were characterized, and their mechanical, and *in-vitro* biological properties were studied.

3.2.2. PVA-CNTs scaffolds

The PVA-CNTs nanocomposite scaffolds were prepared by freeze drying technique. To reduce the tendency of agglomeration, carboxylic acid functionalized CNTs were used. PVA (10% w/v) in distilled water was dissolved and stirred at 90°C for 3 h in a magnetic hot plate. Different concentrations of CNTs (0, 0.5, 1 and 1.5 wt% with respect to PVA) were added to the solution and stirred. The obtained solutions were frozen at -20°C for 24 h and then lyophilized in vacuum for 48 h to obtain porous PVA-CNTs nanocomposite

scaffolds. The obtained scaffolds by varying the CNTs (0, 0.5, 1 and 1.5 wt%) composition were coded as PCN 0, PCN 0.5, PCN 1 and PCN 1.5 respectively.

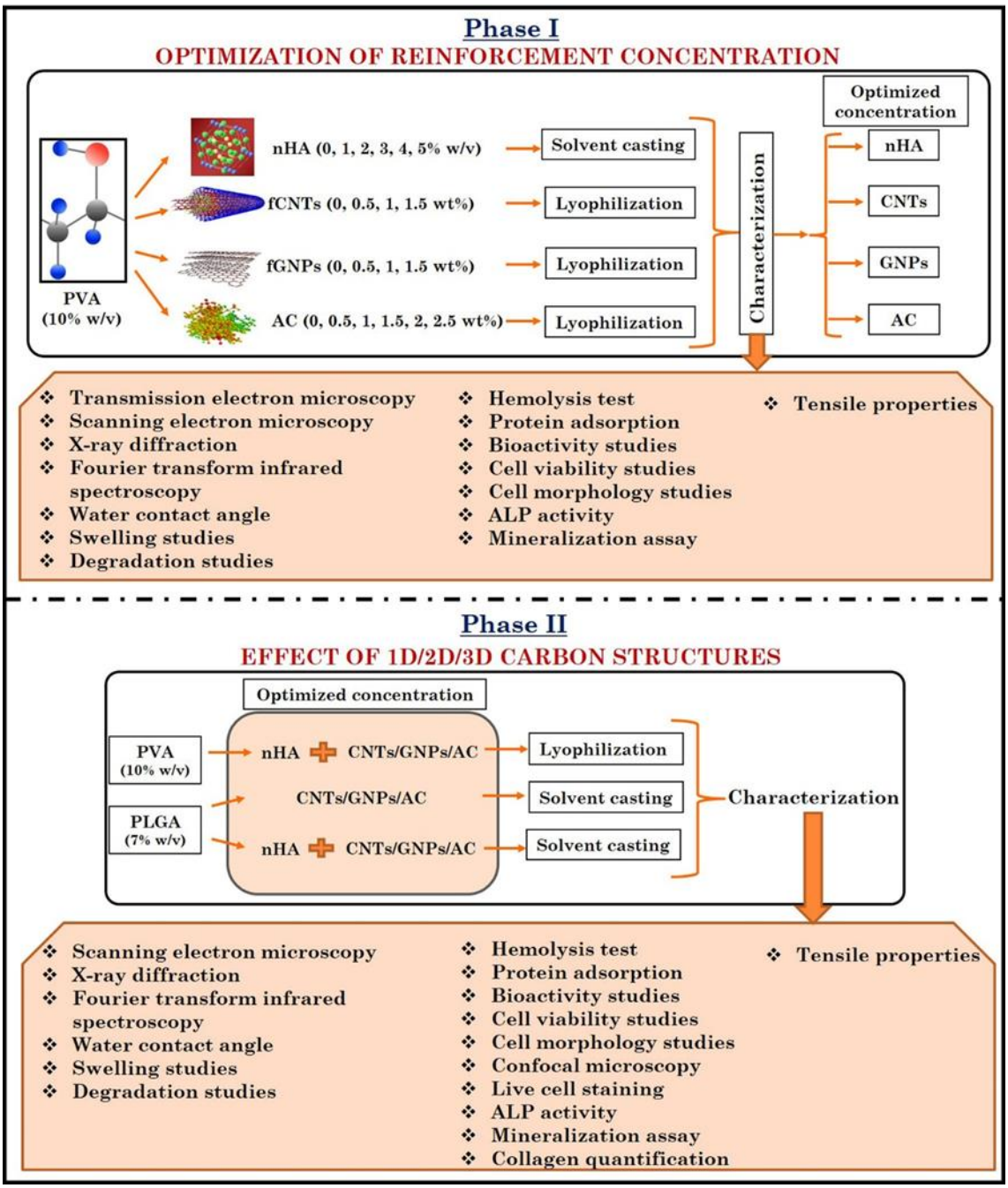

Fig. 3.1 Schematic representation of the sample preparation and characterization.

3.2.3. PVA-GNPs scaffolds

To prepare PVA-GNPs nanocomposite scaffolds by freeze drying technique, PVA (10% w/v) was dissolved in distilled water and stirred at 90°C for 3 h in a magnetic hot plate. Different concentrations of functionalized GNPs (0, 0.5, 1 and 1.5 wt% with respect to PVA) were dispersed in the prepared PVA solution. To obtain porous PVA-GNPs nanocomposite scaffolds the solutions were frozen at -20°C for 24 h and then lyophilized in vacuum for 48 h. The developed scaffolds by varying the GNPs (0, 0.5, 1 and 1.5 wt%) composition were coded as PGN 0, PGN 0.5, PGN 1 and PGN 1.5 respectively.

3.2.4. PVA-AC scaffolds

The porous PVA-AC scaffolds were prepared by freeze drying method. PVA (10% w/v) was dissolved in distilled water and stirred at 90°C for 3 h in a magnetic hot plate. Different concentrations of AC powder (0, 0.5, 1, 1.5, 2 and 2.5 wt% with respect to PVA) were added to the solution and stirred. The obtained PVA-AC composite solutions were frozen at -20°C for 24 h and lyophilized in vacuum for 48 h to obtain dry, porous PVA-AC composite scaffolds. The six scaffolds with different concentrations of AC powder were prepared and coded as PC 0, PC 0.5, PC 1, PC 1.5, PC 2 and PC 2.5 respectively.

3.2.5. Carbonaceous PVA-nHA composite scaffolds

The carbon reinforced PVA-nHA scaffolds were prepared by reinforcing PVA with optimized concentrations of nHA and carbon materials using freeze drying method. PVA (10% w/v) was dissolved in distilled water and stirred at 90°C (3 h) followed by addition of nHA (3% w/v). After proper dispersion of nHA, optimized concentration of respective carbon (1 wt% CNTs, 1 wt% GNPs, and 2.5 wt% AC) material was added and stirred. The obtained carbonaceous PVA-nHA composite solutions were frozen at -20°C for 24 h and lyophilized in vacuum for 48 h. Similarly, PVA-nHA composite scaffolds without addition of any carbon were also prepared. The four different scaffolds were coded as PH (PVA-nHA), PHCN (PVA-nHA-CNTs), PHGN (PVA-nHA-GNPs) and PHAC (PVA-nHA-AC).

3.2.6. Carbonaceous PLGA composite scaffolds

The PLGA-CNTs, PLGA-GNPs and PLGA-AC composite scaffolds were prepared by solvent casting technique. To obtain proper dispersion, 1 wt% of each of functionalized CNTs and GNPs, and 2.5 wt% of AC were sonicated in dichloromethane (DCM) at room temperature. The PLGA (7% w/v) polymer was dissolved in DCM separately and added to the above solutions. The solutions were then sonicated, poured in glass dish and vacuum dried overnight. The dried films were then kept in a vacuum oven at 37°C for 48 h. Similarly, pure PLGA film (PL) was also prepared. Thus obtained four different films were coded as PL, PLCN (PLGA-CNTs), PLGN (PLGA-GNPs) and PLAC (PLGA-AC) respectively.

3.2.7. Carbonaceous PLGA-nHA composite scaffolds

The carbon and nHA reinforced PLGA composite scaffolds were prepared by solvent casting method. The PLGA (7% w/v) polymer was dissolved in DCM followed by addition of respective carbon solutions (1 wt% of CNTs and GNPs, and 2.5 wt% of AC sonicated in DCM). While stirring, nHA (3 wt%) was added slowly to the PLGA-carbon composite solutions while stirring. The composite solutions were then sonicated, poured in glass dish, vacuum dried overnight and kept in oven at 37°C for 48 h. Similarly, PLGA-nHA composite (PLH) was also prepared. Thus obtained four different films were coded as PLH, PLHCN (PLGA-nHA-CNTs), PLHGN (PLGA-nHA-GNPs) and PLHAC (PLGA-nHA-AC) respectively.

3.3. Characterization

3.3.1. Physicochemical characterization

The initial structure and size of the nHA and carbon allotropes were studied using transmission electron microscopy (TEM). The samples were first sonicated using a probe sonicator in ethanol medium until homogenous dispersion. The dispersed solution is then placed on a carbon coated copper grids and then observed in transmission electron microscope (TEM-FEI Tecnai F30). The selected area electron diffraction (SAED) patterns

were also observed. The surface morphology of all the composite scaffolds was evaluated using a field emission scanning electron microscope (FESEM-FEI NovananoSEM 450). The samples were gold sputter coated prior to SEM imaging to avoid imaging artifacts from electrical charging. The phase and crystallinity of all the composites were studied using X-ray diffraction (XRD, RigakuUltima IV Diffractometer, Japan) technique. The XRD over a scan range of 15°-60° was performed with a scan speed of 5°/min and step size of 0.05° using CuKα radiation. Attenuated total reflectance-Fourier transform infrared spectroscopy (ATR-FTIR, AlphaE, Bruker, USA) was performed to characterize the functional groups present in composites. Transmittance spectra within the range of 600-4000 cm^{-1} were obtained. Further, the FTIR spectra were deconvoluted using Fourier self-deconvolution. The effect of different reinforcements on the hydrophilicity of composites was evaluated by measuring contact angles (DSA25, Kruss, Germany) at room temperature with distilled water using sessile drop method. Ten measurements of contact angle were measured for each sample.

3.3.2. *In-vitro* swelling studies

All the composite samples (triplicates) were subjected to swelling by immersing them in PBS (pH 7.4) at 37°C after measuring the initial weight (W_d). The samples were retrieved from PBS after 24 h, and wet weight (W_s) was measured. The swelling percentage was calculated from the following equation:

$$S\ (\%) = \frac{W_s - W_d}{W_d} \times 100 \qquad ...(1)$$

where W_s and W_d are the wet and dry weights of the samples respectively.

3.3.3. *In-vitro* degradation studies

The *in-vitr*o degradation studies were performed in triplicate to determine the weight loss of the composite scaffolds. The initial samples were weighted (W_i) and soaked in PBS for 4 weeks in a constant temperature environment of 37°C. The PBS was not refreshed during the experiment. At regular intervals, the samples were withdrawn, dried at 40°C for 4 days, and its final weights (W_f) were measured. The degradation percentage (D_w) of each sample was calculated in the form of weight loss as in equation (2):

$$D_w\,(\%) = \frac{W_i - W_f}{W_i} \times 100 \qquad ...(2)$$

where W_i and W_f are the initial and final weights of the samples respectively.

3.3.4. *In-vitro* mineralization activity studies

The *in-vitro* bioactivity study of the composites was carried out in simulated body fluid (SBF), an inorganic physiological solution having a similar composition to that of human blood plasma. The SBF was prepared following the standard procedure described by Kokubo and Takadama [143]. The composite samples were soaked in SBF and kept at 37°C in a constant temperature water bath for 21 days. The samples were then removed, gently rinsed with deionized water and dried. The apatite formation was evaluated by performing FESEM and XRD analysis.

3.3.5. *In-vitro* hemocompatibility studies

The hemocompatibility of the composite samples was studied by performing hemolysis and anticoagulant assays. To perform hemolysis assay, the samples in triplicates were equilibrated with a physiological saline solution for 24 h. The equilibrated samples were put into test tubes with fresh physiological saline (10 ml) and incubated for 30 min at 37°C. After addition of anticoagulant (potassium citrate), goat blood was diluted (v/v; 4/5) with physiological saline. The diluted goat blood (0.2 ml) was added to each tube containing samples with saline and incubated for 1 h at 37°C. To prepare positive and negative controls, diluted blood was added to distilled water and physiological saline respectively. After the incubation time, the samples were centrifuged (1000 rpm for 10 min) and its absorbance (OD) was taken from the supernatant liquid at 545 nm (double beam spectrometer 2203, Systronics, India). The percentage hemolysis was calculated using following equation:

$$\%\ \text{Hemolysis} = \frac{OD_{test} - OD_{neg}}{OD_{pos} - OD_{neg}} \times 100 \qquad \ldots(3)$$

where OD_{test}, OD_{neg}, and OD_{pos} are absorbance values for test samples, negative and positive controls, respectively.

3.3.6. Protein adsorption studies

To perform protein adsorption study, a calibration curve was drawn for standard BSA solution ranging from 200-1000 µg/ml. The Bradford assay was used for the quantification of adsorbed protein by composite samples. The samples (triplicates) were immersed in 1 ml BSA solution (1 mg/ml protein in PBS) for 24 h at 37°C. The samples were retrieved from the solution and then centrifuged at 4000 rpm for 10 min. After centrifugation, 100 µl of supernatant was mixed with 1 ml of Bradford reagent and 2 ml of distilled water followed by incubation in the dark for 10 min, and its absorbance was measured at 595 nm using a UV-spectrophotometer. The protein concentration was determined using the calibration curve.

3.3.7. Tensile properties

The tensile properties of the composites were obtained using a universal testing machine (ElectroPuls E1000, Instron, UK) with a load cell of 250 N at a strain rate of 2 mm/min. The test samples were cut following ASTM D3039 standard, and testing was done in triplicates [144].

3.3.8. *In-vitro* biocompatibility studies

MG 63 cell line, an established model for human osteoblasts was used to study the response of osteoblast cells on the developed composites. Human osteoblast like MG-63 cells were cultured in T-25 tissue culture flasks in a humidified atmosphere containing 5% CO_2 at 37°C in DMEM supplemented with 10% FBS, and 100 U/ml of penicillin-streptomycin. Prior to cell seeding, the samples were sterilized using UV and ethanol treatment for 20 min each. All the tests were performed in triplicates and compared with control i.e. tissue culture plate.

a. Cell viability

The cell viability of osteoblast cells cultured on the composites was evaluated using MTT assay and trypan blue exclusion assay. To perform MTT assay, the MG-63 cells (1 x 10^4 cells) were incubated on the samples in a tissue culture plate at 37°C in 5% CO_2. After 48

h, 20 µl of MTT solution at a concentration of 5 mg/ml was added to each well and incubated for 4 h. The removal of the MTT solution from tissue culture plate was followed by addition of dimethyl sulfoxide (DMSO) to solubilize the formazan crystals. After shaking plate gently for 15 min, its absorbance was measured at 595 nm. For trypan blue exclusion assay, cells (1.5 x 10^4) were seeded on the samples in a 24 well plate. After 48 h, the cells were trypsinized and stained with a 0.4% trypan blue solution. Live/dead cells were counted using a phase contrast microscope (Primo Vert, Carl Zeiss, Germany).

b. Cell morphology

The MG-63 cells (1 x 10^4 cells) were seeded on the sterilized samples into tissue culture plate and incubated (at 37°C in 5% CO_2). After incubation, the samples were washed gently with PBS to remove media. For fixing the samples, 2.5% glutaraldehyde solution (3 h) was used followed by dehydration in a graded series of ethanol solution (30, 50, 70, 90, 95 and 100%). Then the samples were vacuum dried, gold sputter coated and observed in FESEM to study the cell morphology and adhesion.

c. Alkaline Phosphatase (ALP) activity

The alkaline phosphatase activity of osteoblast cells cultured on composites was evaluated using ALP colorimetric assay. After 7 days of cell seeding, the samples were washed with PBS, followed by addition of lysis buffer and then p-nitrophenyl phosphate (pNPP) substrate for 1 h at 37°C. The reaction was stopped using 0.5 N NaOH, and the absorbance was measured at 405 nm.

d. Mineralization assay

The calcium deposition on the samples was measured using alizarin red stain (ARS) based colorimetric assay. The osteoblast cells seeded on the composites for 7 days were fixed with 70% ethanol for 1 h at 4°C, washed thrice with distilled water and stained with ARS for 30 min. After a series of distilled water washes, the stain was eluted with a destaining solution consisting of 10% cetylpyridinium chloride (CPC) and incubated for 30 min. The absorbance of the eluted dye was measured at 562 nm. A calibration curve was also plotted for known concentrations of ARS.

e. Confocal microscopy and quantification of cell morphology

To further evaluate the cytoskeletal organization of cells, double staining was performed only on the samples reinforced with optimized concentrations of reinforcements (carbonaceous composites of PLGA, PVA-nHA and PLGA-nHA). After 48 h of cell seeding, the cells were fixed with paraformaldehyde (4%) for 15 min and permeabilized with Triton-X 100 (0.25% in PBS) for 10 min. The actin cytoskeleton and nuclei of cells were stained with TRITC-phalloidin and Hoechst dyes, respectively. The stained samples were washed with PBS and observed under the confocal microscope (TCS-SP8, Leica). Further, to quantify the cell spreading on different scaffolds, the cell area was measured using ImageJ software. The cells present on five different confocal micrographs were evaluated for each sample.

f. Live cell staining

Live cell staining was performed by using calcein-AM (acetoxymethyl ester) to determine the number of viable cells on samples reinforced with optimized reinforcement concentrations. Calcein-AM is a marker of esterase activity of living cells. In live cells, esterase's remove the acetoxymethyl ester group of calcein-AM by hydrolysis converting it to calcein which produces green fluorescence. After 7 days of cell seeding, media was removed, and samples were washed with PBS. Calcein-AM (1 µl/ml) was added to each scaffold and incubated at 37°C for 30 min. The samples were washed with incomplete media and visualized under the fluorescence microscope (Olympus IX71, Japan).

g. Collagen quantification

The total collagen secreted by osteoblast cells on the scaffolds (with optimized reinforcement concentrations) was determined by using Sirius red colorimetric assay. After 7 days of cell culture, the cells were fixed on the scaffolds with Bouin's fluid. The fixation fluid was removed after 1 h, and the samples were washed with distilled water, air dried and then stained with Sirius red dye for 1 h. Thereafter, the samples were washed with 0.01 M HCl, and the bound dye was dissolved in 0.1 M NaOH. The absorbance of the solution was measured at 550 nm against 0.1 M NaOH as a blank.

3.3.9. Statistical Analysis

Data are expressed as mean ± standard deviation and one-way analysis of variance (ANOVA) was used for comparison. The level of significance was measured and data was represented at significant ($*p \leq 0.05$) level.

3.4. Summary

This chapter has described the materials used and methods followed to perform the present work. Preparation of various samples and their characterization techniques (physicochemical, biological and mechanical) to find optimum concentration of reinforcement have been explained in detail. The sample preparation using optimum reinforcement concentrations and their characterizations have also been mentioned to study the role of reinforcement structure.

Chapter 4

Results and discussion

This chapter provides the results obtained from the present research work. The results are divided into two phases. The first phase includes the results and discussion of optimization of reinforcement concentration. The optimum (threshold) concentration of each of the reinforcement material will be obtained after analyzing physicochemical, mechanical and biological properties of the developed composites with varying reinforcement concentrations. The second phase results include the effect of different carbon materials (1D, 2D, 3D) with and without nHA in the two polymer matrices, i.e. PVA and PLGA.

4.1. Optimization of reinforcement concentration

4.1.1. Transmission electron microscopy

TEM analysis was performed to investigate the initial structure and size of three carbon based materials and nHA used in this study to reinforce PVA and PLGA matrices. The TEM micrographs (Fig. 4.1) revealed the typical morphology of nHA, CNTs, GNPs and AC. The nHA showed nanorods, CNTs and GNPs showed their respective tubular and sheet like (platelets) structure whereas AC exhibited irregular structure. The SAED patterns indicated the amorphous nature of CNTs whereas nHA and GNPs displayed crystalline nature. The lack of distinct reflections in the SAED pattern indicated the poorly ordered structure of AC which is consistent with a turbostratic structure [145].

4.1.2. Scanning electron microscopy analysis

The surface topography and microstructure are important parameters in designing scaffolds for tissue engineering applications. The scaffold morphology significantly influences the *in-vitro* and *in-vivo* behavior of the composite scaffolds. Microstructural analysis was done on all composite scaffolds with varying concentrations of nHA, CNTs, GNPs and AC to analyze whether the homogeneous dispersion of different reinforcements in the polymer matrix has been achieved.

The FESEM micrographs of different PVA-nHA composite scaffolds are shown in Fig. 4.2. Agglomeration of nHA in the polymer matrix might affect composite properties whereas, homogeneous dispersion of nHA aids in the improvement of physical, mechanical and biological properties of the composite. The SEM micrographs have revealed the distribution of nHA in PVA matrix, which plays a major role in surface roughness of these composites as the concentration of nHA has been increased. The micrograph of PVA scaffold without nHA (Fig. 4.2 (a)) shows the smooth surface owing to the bio-inert nature of PVA. The micrographs show that on the addition of nHA in PVA matrix, the surface roughness was found to increase. The PHA 1 and PHA 2 samples have shown a homogeneous dispersion of uniformly sized clusters of nHA particles (Fig. 4.2 (b-c)). With further increase in the concentration of nHA particles, the roughness was found to increase as in PHA 3 (Fig. 4.2 (d)). The microstructural analysis also reveals that the agglomeration of nHA in PVA matrix increase with the increase in the concentration of nHA. The PHA 3 sample shows some regions of agglomerated nHA particles; with 3% w/v of nHA, whereas, PHA 4 and PHA 5 samples (Fig. 4.2 (e-f)) showed more agglomerated clusters. The formation of agglomerated nHA clusters might attribute to the charged inorganic ions that were not evenly distributed in PVA matrix and thereby getting agglomerated clusters under the effect of van der Waals force and Brownian motion. Brownian motion causes the collision of the nHA particles with each other and the van der Waals forces attract these particles leading to agglomeration [40]. So from the SEM micrographs, it was observed that with the increase in the concentration of nHA above a certain amount (3% w/v), more agglomeration was evident, which could affect the mechanical and biological properties of composites.

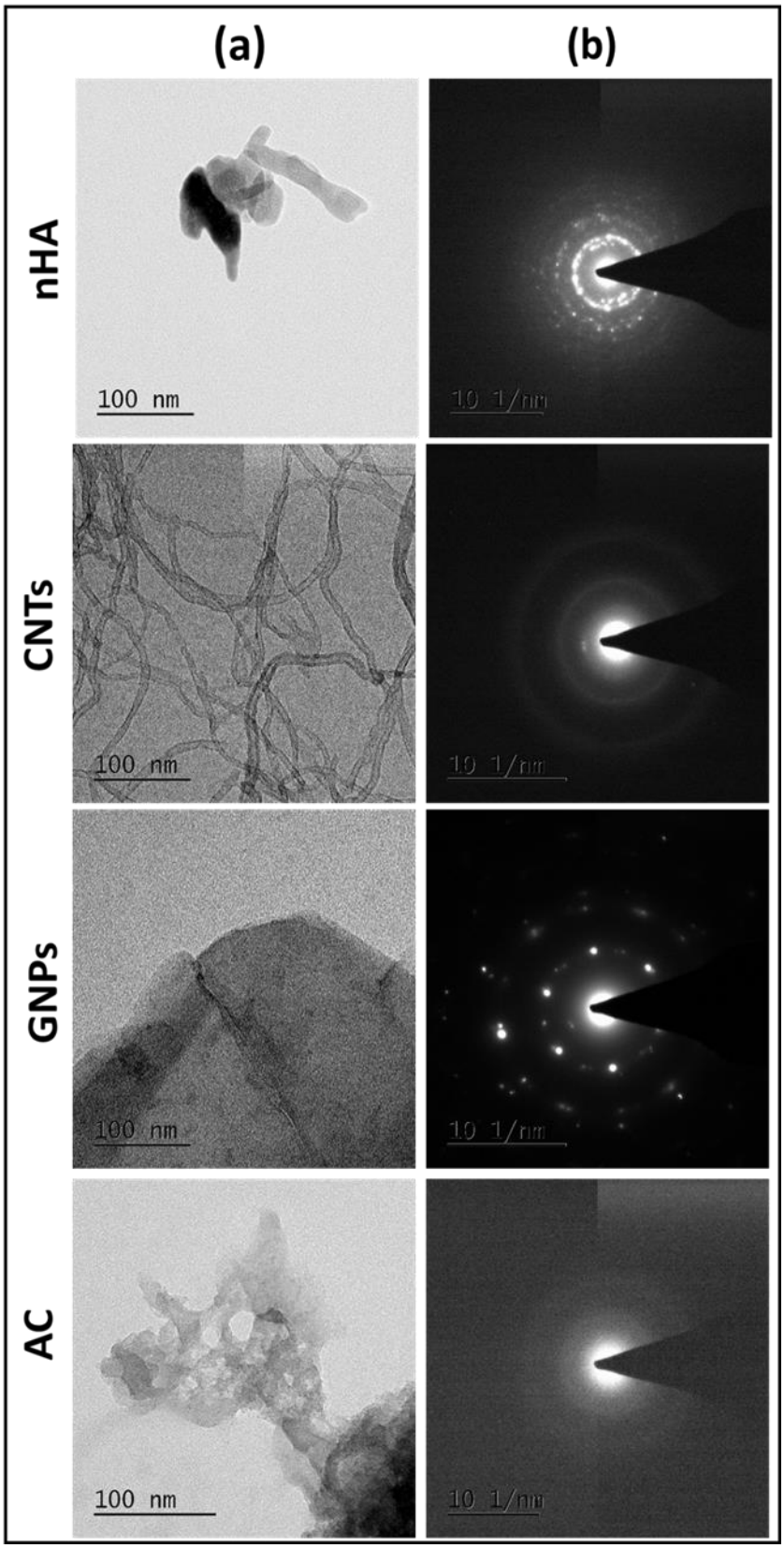

Fig. 4.1 (a) TEM micrographs and (b) SAED patterns of nHA, AC, CNTs and GNPs.

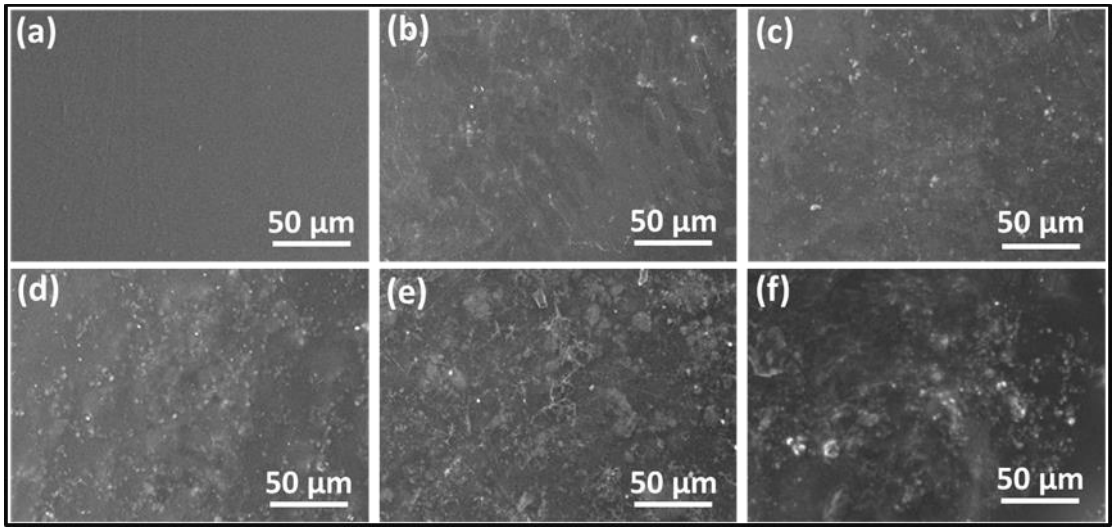

Fig. 4.2 FESEM micrographs of (a) PVA, (b) PHA 1, (c) PHA 2, (d) PHA 3, (e) PHA 4 and (f) PHA 5.

The cross-sectional surfaces of PVA-CNTs nanocomposite scaffolds with varying CNTs concentrations were analyzed using FESEM (Fig. 4.3). The micrographs have revealed the rough, interconnected and porous structure of the PVA-CNTs scaffolds that allow cells to attach, migrate and grow into the scaffold interior. Both micro (<50 µm) and macro (>50 µm) pores were observed in the nanocomposite scaffolds that increase the surface roughness. The pore size was found to decrease slightly with the addition of CNTs in PVA matrix. The pore size obtained in both, PCN 0.5 and PCN 1 (Fig. 4.3 (b-c)) were large enough to fulfill the requirements for osteoblast cell proliferation. However, sample PCN 1.5 (Fig. 4.3 (d)) was observed to have slightly smaller pores. Sample PCN 1 and PCN 1.5 (Fig. 4.3 (e-f)) were also observed at higher magnification to analyze the CNTs dispersion. Sample PCN 1 showed a uniform distribution of CNTs whereas, with further increase in concentration, CNTs started agglomerating. PCN 1.5 showed the presence of CNTs agglomerates in the PVA matrix. These agglomerates may diminish the mechanical and biological properties of the PCN 1.5.

A representative cross-sectional FESEM micrographs of PVA-GNPs composite scaffolds are shown in Fig. 4.4 (a-f). The FESEM micrographs revealed the porous network structure of all the scaffolds. Both, macro and micro sized pores were observed in all the samples which support the cell adhesion, growth and nutrients supply inside the scaffolds [146].

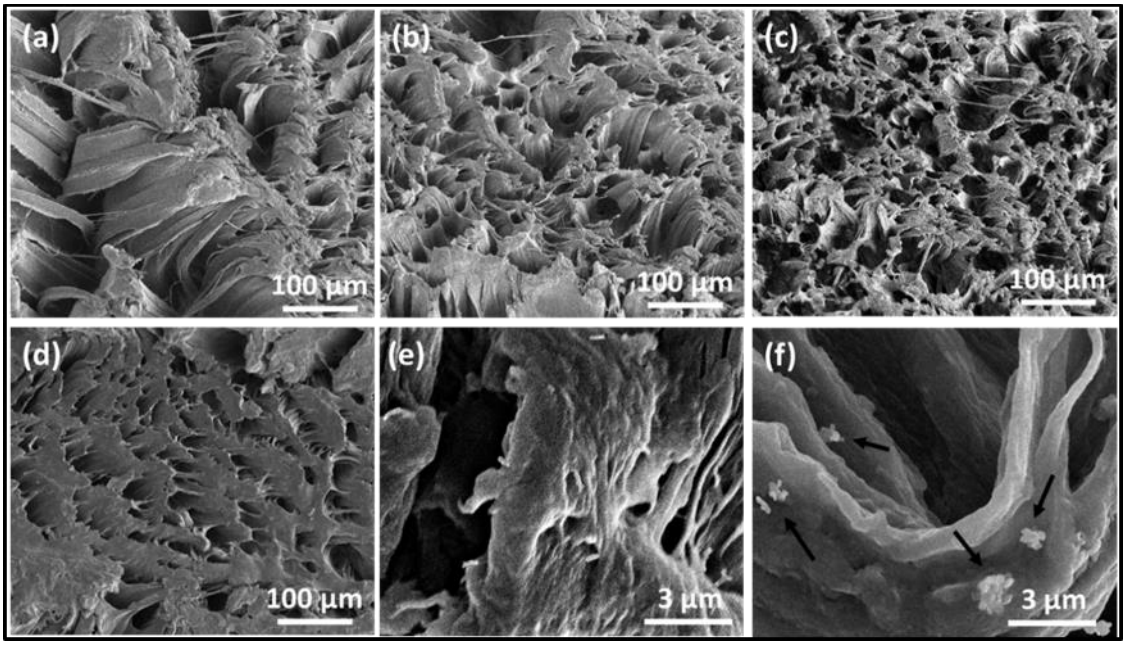

Fig. 4.3 FESEM micrographs of (a) PCN 0, (b) PCN 0.5, (c) PCN 1 and (d) PCN 1.5. Surfaces of (e) PCN 1 and (f) PCN 1.5 observed at higher magnification. (Arrows show the agglomeration in PCN 1.5.)

Lee et al. have reported that microporous scaffolds encouraged the MG-63 cell adhesion and proliferation, whereas increasing micropore size resulted in improved cell differentiation [147]. With the addition of GNPs in PVA matrix variation in pore architecture was obtained. Pore walls of PGN 0 (Fig. 4.4 (a)) scaffold were thin which led to crumbling of pores while addition of GNPs in PVA provided stability of pore structure by thick pore walls and prevented the pores from collapse, therefore, larger pores were observed in composite scaffolds. The large pore size and stable pore architecture play a significant role in providing mechanical interlocking with surrounding tissue [148]. The FESEM micrographs of PGN 1 and PGN 1.5 scaffolds at higher magnification have also been shown in Fig. 4.4 (e-f). The GNPs were homogeneously dispersed throughout in PGN 1 sample (Fig. 4.4 (e)). The homogeneous dispersion of GNPs is beneficial to enhance the mechanical properties of the scaffold. However, with the further increase of GNPs in PGN 1.5 (Fig. 4.4 (f)), the GNPs started to agglomerate due to van der Waals force [56]. These agglomerates in PGN 1.5 may result in the deterioration of the mechanical and biological properties.

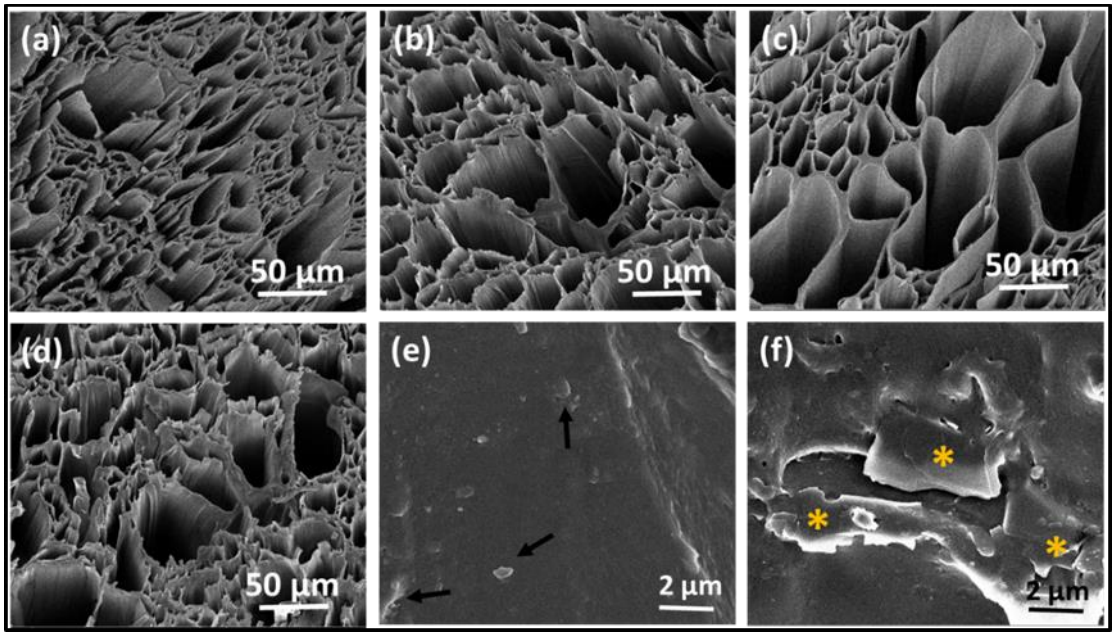

Fig. 4.4 FESEM micrographs of (a) PGN 0, (b) PGN 0.5, (c) PGN 1 and (d) PGN 1.5. Scaffolds (e) PGN 1 and (f) PGN 1.5 at higher magnification. (Arrows represent the well dispersed GNPs and asterisks represent the agglomeration of GNPs.)

The FESEM micrographs of the cross-sectional surface of PVA-AC composite scaffolds with varying AC concentrations are shown in Fig. 4.5. From these micrographs, it is evident that AC is homogenously dispersed, and there is no trace of agglomeration of AC in PVA matrix. The well dispersed AC was also observed in high magnification micrograph of PC 2.5 (Fig. 4.5 (h)). The cross-sectional morphology of all the composite scaffolds showed macro and micro pores which are an important requirement for influencing cell attachment and growth. Researchers have reported that the pore size plays an important role in encouraging cell attachment and differentiation on a surface roughened biomaterial that develops mechanical interlocking between the implant and surrounding tissues [149, 150]. The cross-section micrographs of PVA (Fig. 4.5 (a) revealed undefined pore shapes. Due to the flexible character of PVA polymer, shrinkage and collapse of the pore structure were observed in PC 0 scaffold. However, comparatively larger and homogenous pore architecture was obtained for PC composite (Fig. 4.5 (b-f)) scaffolds. The AC present in PVA matrix enhanced the stability of the structure and prevented the pores from collapse. The porosity obtained in the PC scaffolds fulfilled the pore size requirements for osteoblast cell to penetrate into the scaffolds. The micrographs of samples have shown the presence

of micropores that are essential for regulating cell migration and nutrient supply to the cells, thereby permitting cell growth inside the scaffold. The interconnected porosity observed in the PC 2.5 sample has been shown in Fig. 4.5 (g). Thus, the developed scaffolds have the required morphology and porosity which may help in osteoblast growth and proliferation.

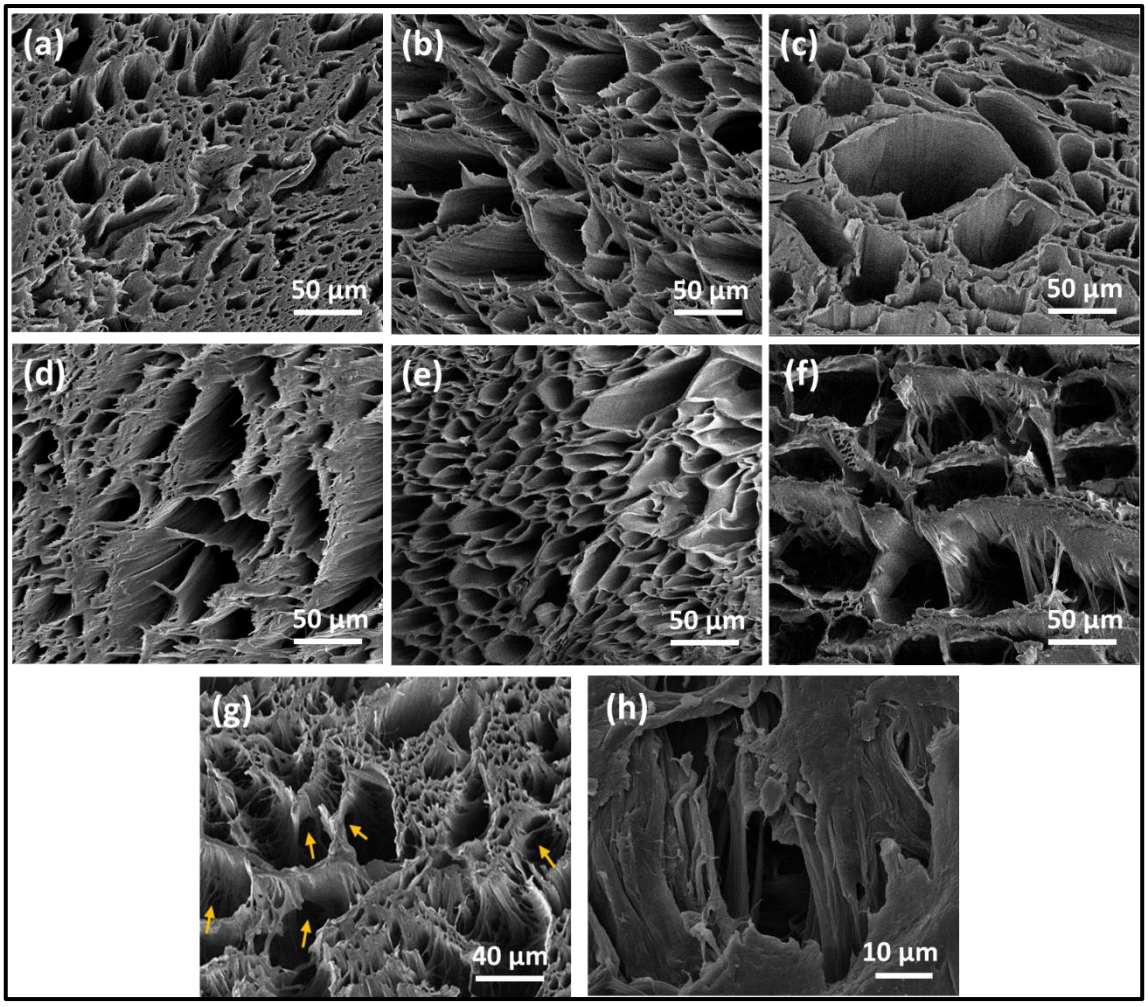

Fig. 4.5 FESEM micrographs of (a) PC 0, (b) PC 0.5, (c) PC 1, (d) PC 1.5, (e) PC 2, (f) PC 2.5, (g) interconnected pores in PC 2.5 and (h) higher magnification micrograph of PC 2.5 scaffolds.

4.1.3. X-ray diffraction

The XRD spectra of all four different reinforcements (nHA, CNTs, GNPs, AC) used in the present study are shown in Fig. 4.6 (a). The nHA showed characteristic peaks at 25.87°,

31.77° 32.1° and 32.90° similar to JCPDS standard for HA (PDF NO. 09-0432) [151]. Other peaks for nHA were found at 34.04°, 39.7°, 46.6° and 49.4°. Pure CNTs showed peaks at 25.6° and 42.7° corresponding to the (002) and (101) planes of CNTs respectively, as mentioned in JCPDS number 75-1621 [152]. For as received GNPs, the characteristic peak at 26.5° corresponding to the (002) plane reflection of GNPs was observed, as mentioned in JCPDS number 01-0646 [153]. Pure AC showed peaks at 26.5° and 43.5° indicating alignment of carbon planes [154].

The XRD spectra of PVA-nHA composite scaffolds with different nHA concentrations (Fig. 4.6 (b)) were obtained to investigate the formation of any new phase or contamination during processing. The broad diffused peak at 19.5° (101) corresponding to the characteristic peak of PVA demonstrates that PVA possesses a semi-crystalline structure that was observed in all composite scaffolds. No other peaks were found in PVA sample indicating that there is no phase contamination. The intensity of nHA peaks was found to increase from PHA 1 to PHA 5 samples as nHA concentration increases. No intermediate calcium phosphate phases like TCP or BCP were observed in all the processed PHA composite scaffolds.

In the XRD patterns of PVA-CNTs composites no strong CNTs characteristic peak was observed (Fig. 4.6 (c)). This might be due to the lower concentration of CNTs as compared to PVA in the composites. The broad peaks at 19.5° and 40.5° correspond well to the characteristic reflection of the (101) and (220) plane of the pure PVA (PCN 0) indicating its semi crystalline structure. These peaks were found in all the PVA-CNTs composite samples confirming the presence of PVA in all the samples.

The effect of GNPs addition to the PVA matrix can be very well seen in the XRD patterns of PVA-GNPs nanocomposites as shown in Fig. 4.6 (d). A sharp characteristic peak at 26.5° (002) corresponding to GNPs was observed, whereas PVA showed a peak at 19.5° (101) [155]. The characteristic peaks of PVA and GNPs were found in all the PVA-GNPs nanocomposite samples confirming the presence of PVA and GNPs. The intensity of the GNPs peak increased with the increase in the amount of the GNPs from PGN 0.5 to PGN 1.5.

A broad diffused characteristic peak at 19.5° (101) was observed in all PVA-AC samples corresponding to PVA (Fig. 4.6 (e)). This broad peak indicates that the PVA possesses semi-crystalline structure. There was no strong AC characteristic peak observed in PVA-AC composite scaffolds. This might be due to the lower concentration of AC as compared to PVA in the composites.

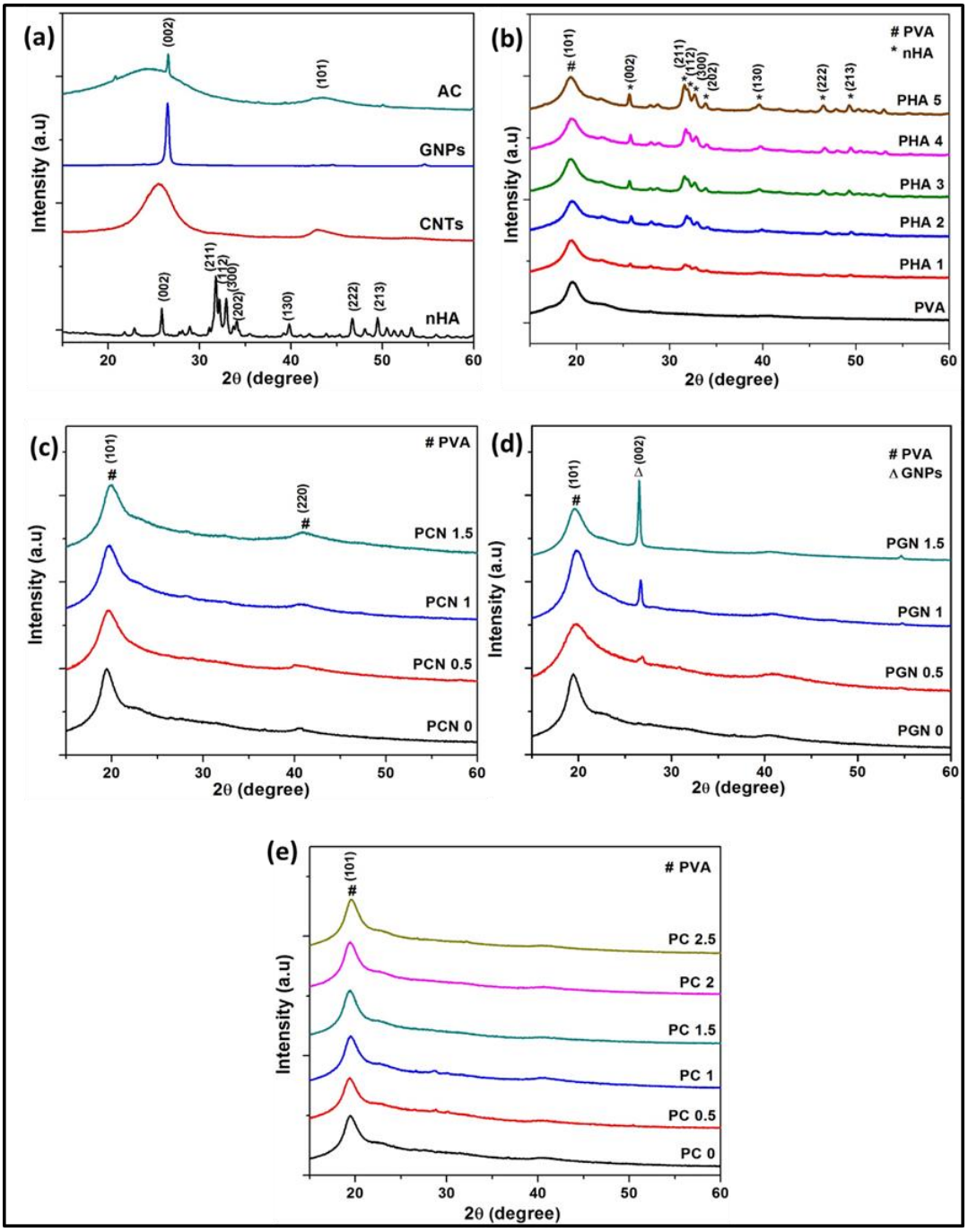

Fig. 4.6 XRD patterns of (a) different reinforcements, (b) PVA-nHA, (c) PVA-CNTs, (d) PVA-GNPs and (e) PVA-AC composites.

4.1.4. Fourier transform infrared analysis

After studying the morphology of the composite scaffolds, it is also important to understand the molecular interactions in the composites. In order to investigate the intermolecular interactions, ATR-FTIR analysis was carried out for all the composite samples, and their spectra are shown in Fig. 4.7. The deconvoluted spectra are also shown in Fig. 4.8.

The FTIR spectra of nHA, CNTs, GNPs and AC are shown in Fig. 4.7 (a) and the FSD spectra are given in Fig. 4.8. The spectra of nHA showed a high intensity peak at 1030 cm^{-1} along with the peaks at 1090 cm^{-1} and 960 cm^{-1} corresponding to the asymmetric stretching of PO_4^{3-} ions. Peak at 871 cm^{-1} corresponds to the out of plane bending mode of CO_3^{2-} ions. Stretching from adsorbed water was shown by a peak at 1642 cm^{-1}. Small intensity peaks around 3500 cm^{-1} and 600 cm^{-1} were observed due to stretching of O-H groups. The spectra of CNTs showed a peak at 3728 cm^{-1} attributing to the free O-H groups while the peak at 2361 cm^{-1} can be assigned to the O-H groups from strongly hydrogen bonded carboxyl groups [156]. Two peaks for C-H stretching were observed at 2922 cm^{-1} and 2850 cm^{-1}, whereas, the peaks for C=O stretching were obtained at 1738 cm^{-1} and 1682 cm^{-1}. Two peaks for C=C stretching around 1535 cm^{-1} and a weak peak at 1026 cm^{-1} correspond C=C stretching and C-O stretching. A unique peak for MWCNT was observed at 1450 cm^{-1} [157]. The GNPs IR spectra showed characteristic peaks at 3725 cm^{-1}, 1682 cm^{-1}, and 1513 cm^{-1} which can be assigned to free O-H groups, C=O and C=C stretching. The presence of C=O and O-H groups in FTIR spectra of both CNTs and GNPs confirmed their carboxylic acid functionalization. Further, AC showed weak intensity peaks for O-H and C=C bond stretching at around 3728 cm^{-1} and 1527 cm^{-1} respectively.

The ATR-FTIR spectra of PVA-nHA composite scaffolds showed the characteristic peaks corresponding to standard PVA and nHA (Fig. 4.7 (b)). PVA, a polar polymer having -CH, $-CH_2$ and -OH side groups with C-C backbone. On C-C backbone, PVA has O-H pendant groups that make PVA capable of physical crosslinking. All these characteristic functional groups were observed in the FTIR spectra of PVA. A broad absorption band obtained at about 3500 and 3000 cm^{-1} corresponds to the interaction of absorbed O-H group present in both nHA and PVA. The bonding between PVA and nHA became stronger because of the increase in number of O-H groups with the addition of nHA in PVA. This is due to the

attraction of Ca^+ ions onto the OH^- group of PVA. The peak at 2920 cm^{-1} indicates C-H stretching. Weak absorbance around 2474 cm^{-1} represents the interaction of hydrogen atoms of PVA with phosphorous atoms of nHA. Poursamar et al. also obtained a peak at 2430 cm^{-1} indicating PVA and nHA interactions [87]. The difference in concentration of nHA added might be the reason for the peak shift of ~40 cm^{-1}. The absorption band associated with the stretching of H_2O molecules was observed at 1640 cm^{-1}. Peaks with low intensity observed around 1470 cm^{-1} correspond to the stretching vibration of $-CO_3^{2-}$ ions due to atmospheric $-CO_2$ absorption. Absorption at around 1417 cm^{-1} originates from C-H bend and C-C stretching. The intensity of this peak was found to decrease with the increase in the concentration of nHA. The peak for C-O stretching was observed around 1083 cm^{-1}. The characteristic peaks for stretching vibration of phosphate ion (PO_4^{3-}) at 1030 cm^{-1} were observed at the higher concentration of nHA. This peak was absent in pure PVA scaffold. Other characteristic peaks for nHA were present at 960 cm^{-1} (symmetric P-O), 560 cm^{-1}, 570 cm^{-1} and 601 cm^{-1} (O–P–O bend).The intensity of these bands was very low because of less concentration of nHA used in processing from 1% w/v to 5% w/v.

The investigation of the intermolecular interactions in PVA-CNTs composites was performed by ATR-FTIR analysis and the obtained spectra is shown in Fig. 4.7 (c). The spectra of PVA (PCN 0) and other developed PVA-CNTs nanocomposites showed all the characteristic peaks corresponding to standard PVA. A broad absorption band observed between 3550 cm^{-1} and 3044 cm^{-1} indicates the stretching of free and hydrogen bonded hydroxyl groups in both, alcohol and carboxylic acid. The vibrational peaks at 2920 cm^{-1} and 2850 cm^{-1} refer to the stretching of C-H bond. The stretching vibration of C=O and C-O bonds in acetate groups was observed at 1654 cm^{-1} and 1081 cm^{-1}. The presence of C=O bonds in both CNTs and PVA confirms that the PVA can interact strongly with CNTs. Hence, the intensity of C=O peak (1654 cm^{-1}) was found to increase with the addition of CNTs in PVA. The absorptions at 1428 cm^{-1}, 1320 cm^{-1} and 837 cm^{-1} originate from the bending of C-H bond. The broadening of C-O peak (1081 cm^{-1}) occurred due to the formation of a new absorption peak at 1022 cm^{-1} in PCN 1 and PCN 1.5 samples attributed to the interfacial covalent reaction between PVA and CNTs [158]. Both, PCN 1 and PCN 1.5 samples showed O-H peak at 3728 cm^{-1} confirming the presence of functionalized CNTs in PVA matrix.

The spectra of pure PVA (PGN 0) and PVA-GNPs nanocomposites showed all the characteristic peaks corresponding to standard PVA (Fig. 4.7 (d)). A broad absorption band around 3272 cm^{-1} indicates the O-H stretching vibrations and the vibrational peak at 2920 cm^{-1} refers to the aliphatic stretching of C-H bond. The peaks at 1718 cm^{-1} and 1652 cm^{-1} are assigned to the stretching vibration of C=O whereas peak at 1082 cm^{-1} is assigned to the stretching vibration of C-O bond. With the increase in concentration of GNPs, the intensity of peaks at 1718 cm^{-1} and 1652 cm^{-1} was found to increase confirming the presence of carboxylated GNPs in nanocomposites. Further the absorptions at 1427 cm^{-1}, 1321 cm^{-1} and 837 cm^{-1} indicate the bending of C-H bond.

The ATR-FTIR analysis of the developed PVA-AC composite scaffolds was carried out to investigate the intermolecular interactions between the AC and PVA (Fig. 4.7 (e)). The spectra showed the characteristic peaks corresponding to standard PVA, a polar polymer having -CH, $-CH_2$ and O-H groups with C-C backbone. All these functional groups were observed in the FTIR spectra of PC 0 and all the PVA-AC composite scaffolds. A broad absorption band obtained at 3596-3024 cm^{-1} indicates the existence of free and intermolecular bonded hydroxyl groups of PVA and AC. The intensity of this band was found to decrease in PVA-AC composites as a result of carbonization of AC. The peaks at 2925 cm^{-1} and 2855 cm^{-1} correspond to the aliphatic stretching of C-H, which is a polar bond present in most of the polymers [159, 160]. The absorption bands associated with C=O and C-O stretching were observed around at 1726 cm^{-1} and 1651 cm^{-1}. The low intensity peak observed around 1527 cm^{-1} corresponds to C=C bond vibrations [161]. The absorption peak at 1416 cm^{-1} and 1320 cm^{-1} originate from C-H aliphatic bending [159]. However, in PVA-AC composites, the peak at 1320 cm^{-1} was not observed which might be due to the alteration of molecular arrangements as a result of AC addition. A strong peak for C-O stretching in alcohols was observed around 1084 cm^{-1}. The broadening of this C-O peak (1084 cm^{-1}) occurred with the formation of a new absorption peak at 1026 cm^{-1} in composite samples attributing to the interfacial covalent reaction between PVA and AC. The peak at 837 cm^{-1} for C-H bending in all the PVA-AC samples shifted to 816 cm^{-1} with AC addition. The absence and shifting of C-H bending peaks indicate that the addition of AC has obvious effects on the structure of PVA molecules.

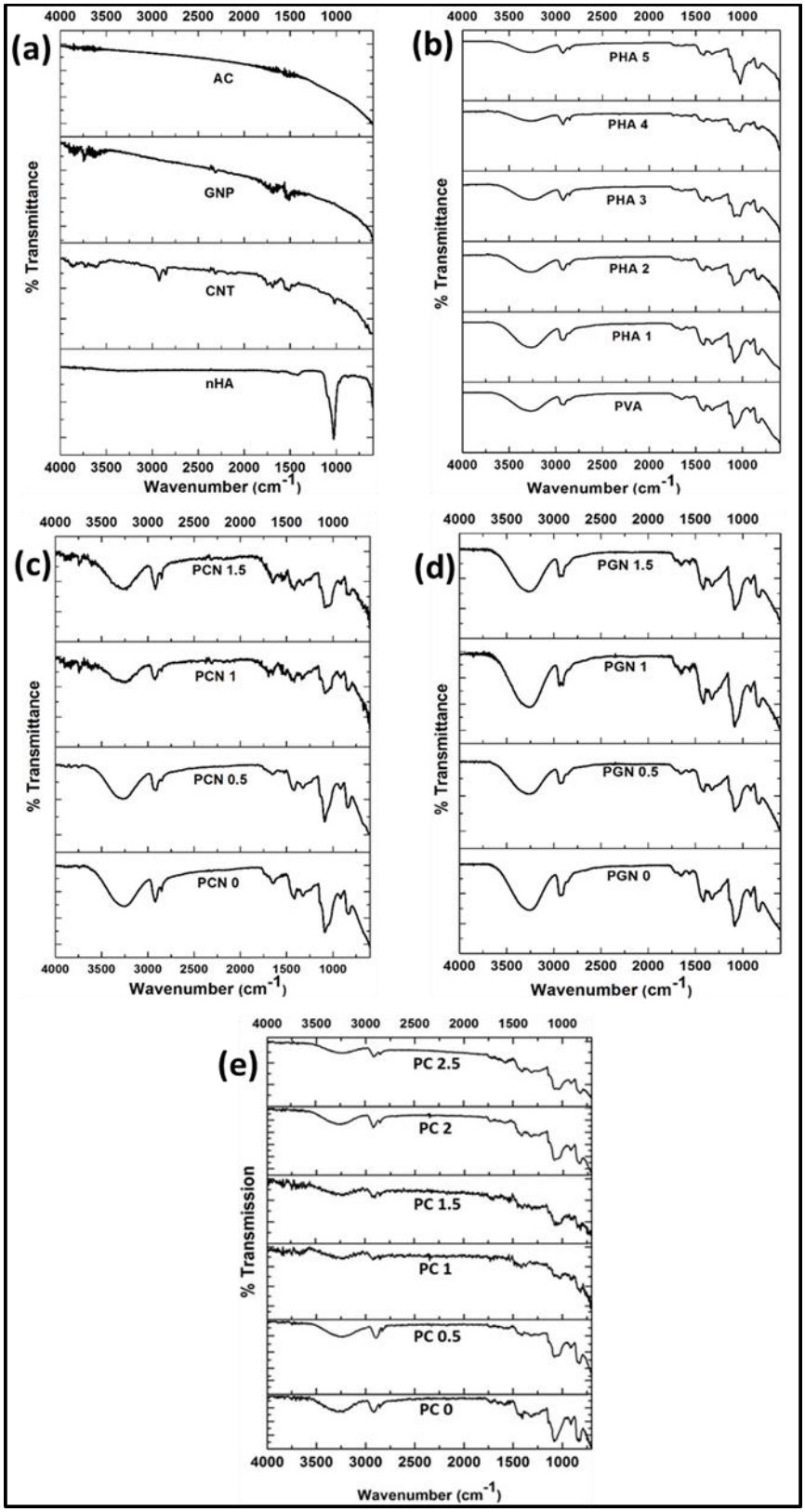

Fig. 4.7 FTIR spectra of (a) different reinforcements, (b) PVA-nHA, (c) PVA-CNTs, (d) PVA-GNPs and (e) PVA-AC composites.

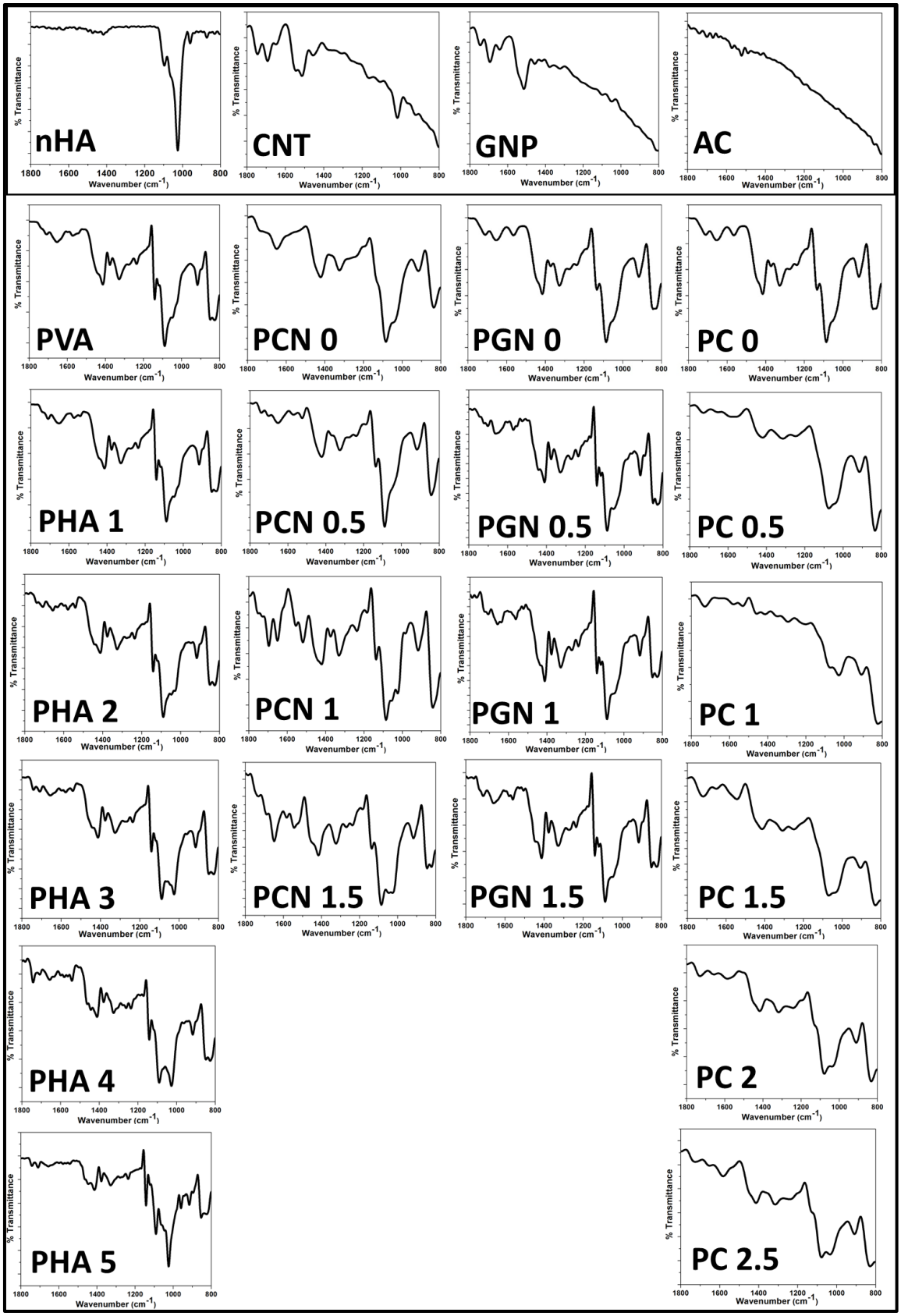

Fig. 4.8 Fourier self-deconvolution of FTIR spectra of various samples.

4.1.5. Contact angle measurements

Wettability is one of the key factors affecting the cell attachment and growth on the scaffold materials. To evaluate the effect of different reinforcements on the surface hydrophilicity, the water contact angles of composites were measured. The water contact angles of all the prepared composites are shown in Table 4.1.

The contact angles of all PVA-nHA composites were found to be less than 80°, indicating the hydrophilic behavior of the scaffolds. Pure PVA without nHA showed the lowest contact angle of 43.2°. The contact angles of PVA-nHA composites gradually increased with the increasing concentration of nHA. The increase in contact angles and the decrease in the hydrophilicity of the composite scaffolds correspond to the addition of hydrophobic nHA which made the developed composite comparatively hydrophobic.

With the reinforcement of CNTs into PVA, the contact angle of PVA-CNTs nanocomposite was found to increase. However, the increase in contact angles was not much significant due to the presence of hydrophilic carboxyl groups on the surface of CNTs and increase in surface roughness with the addition of CNTs. All the nanocomposites showed hydrophilic nature (contact angle less than 90°) that makes them suitable for osteoblast cell adhesion and growth.

Similarly, the contact angles of the PVA-GNPs samples were also found to increase comparing to the pure PVA, showing a small hydrophobic effect. As observed in above case, the increase in contact angles was not much significant due to the increase in surface roughness with the addition of nanofillers and the presence of hydrophilic functional groups on the surface of GNP.

In the case of PVA-AC composites, pure PVA (PC 0) sample showed the highest contact angle of 49.02°. The contact angle of the PVA-AC composite samples was found to decrease with an increase in AC compositions. This is due to the water absorbing properties of AC, which is homogenously embedded in PVA matrix.

The contact angle measurement results showed that all the composite samples have hydrophilic nature making them suitable for protein and cell attachment.

Table 4.1 Average contact angles of different composites.

Samples	Average contact angle (degree)	Samples	Average contact angle (degree)
PVA-nHA composites		**PVA-AC composites**	
PVA	43.2±3.42	PC 0	49.02±1.92
PHA 1	50.4±2.96	PC 0.5	47.28±1.34
PHA 2	51.8±4.78	PC 1	45.34±5.27
PHA 3	60.7±3.34	PC 1.5	45.06±0.56
PHA 4	67.3±6.10	PC 2	44.8±1.64
PHA 5	71.5±3.56	PC 2.5	43.56±1.63
PVA-CNTs composites		**PVA-GNPs composites**	
PCN 0	47.04±2.5	PGN 0	44.56±2.45
PCN 0.5	48.28±1.3	PGN 0.5	50.46±3.52
PCN 1	52.34±4.6	PGN 1	52.35±1.6
PCN 1.5	55.86±2.4	PGN 1.5	56.5±5.4

4.1.6. *In-vitro* swelling studies

Scaffolds are destined to swell when coming in contact with body fluids, but it should preserve its shape and mechanical stability for the extended time. The increase in pore size of the scaffold after swelling enhances the cell attachment and growth. However, undesirable swelling of the scaffold reduces its mechanical strength making it unsuitable for bone tissue engineering applications. The degree of swelling of the composite scaffolds

is dependent on their composition and hydrophilic nature. The influence of the different reinforcements on swelling behavior of composites in PBS is shown in Fig. 4.9 (a-d).

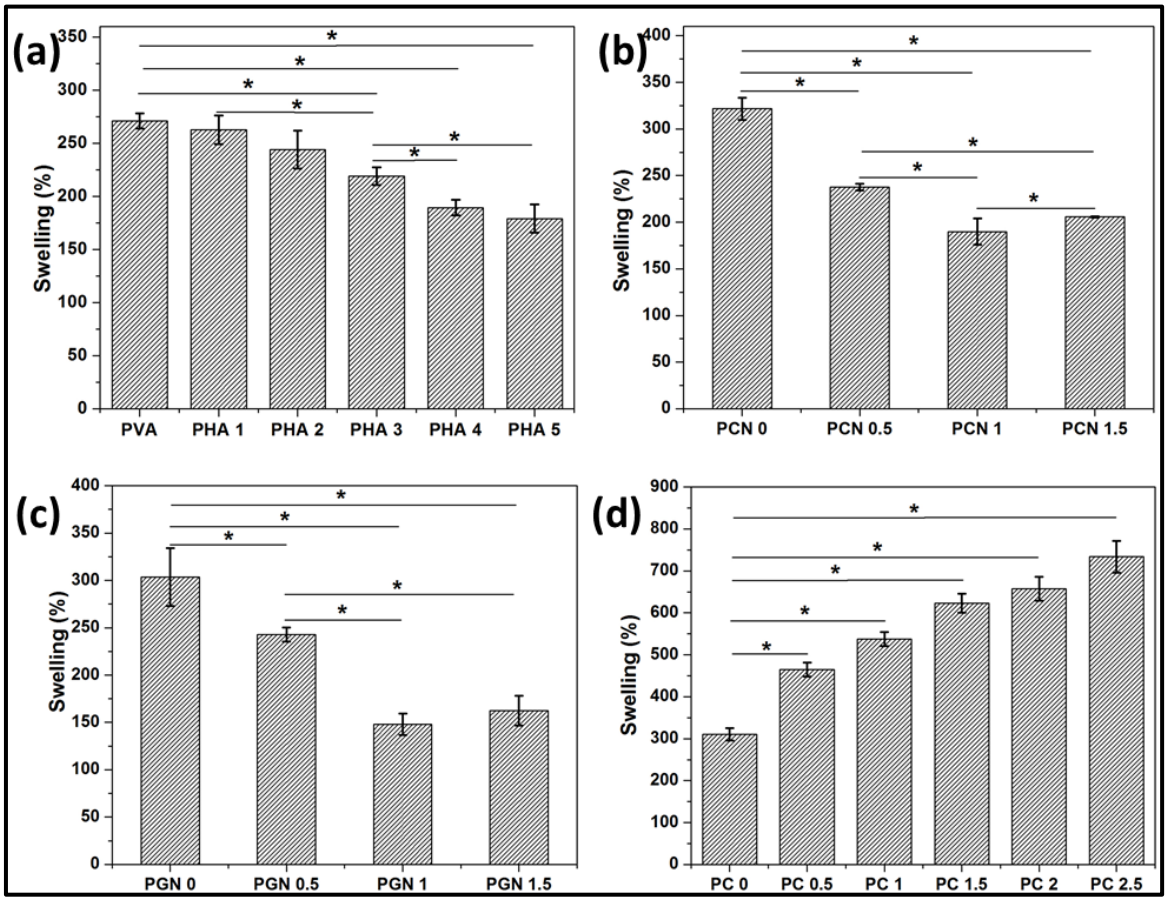

Fig. 4.9 Swelling studies of (a) PVA-nHA, (b) PVA-CNTs, (c) PVA-GNPs and (d) PVA-AC composites.

Reinforcement of nHA into the PVA matrix brings about a significant change in swelling behavior of PVA-nHA composite scaffolds (Fig. 4.9 (a)). PVA without nHA showed the highest degree of swelling equal to 271% after 24 h of soaking in PBS. With the increase in the concentration of nHA, the degree of swelling was found to decrease which is due to the lower hydrophilicity of nHA in comparison to the PVA, which is a hydrophilic polymer. The increase in crystallinity with an increase in nHA has led to the decrease in swelling. Reinforcement of nHA in PVA matrix made the composite stiffer which decreases the swelling of the composites in PBS. Researchers have reported that the addition of ceramic

material like HA into PVA matrix leads to the reduction in swelling behavior of composites [8].

The swelling percentages of various PVA-CNTs scaffolds are illustrated in Fig. 4.9 (b). As observed, PVA scaffolds showed the highest swelling percentage. With increase in CNTs content in the PVA matrix, the swelling percentage was found to decrease up to PCN 1 scaffold. This can be attributed to the increase in hydrophobicity and rigidity of the nanocomposites with the addition of CNTs [162]. In PCN 1.5, a slight increase in swelling was observed. Agglomeration of CNTs in PCN 1.5 might have increased the free volume by decreasing compactness of polymer matrix, and hence, resulted in more swelling of the scaffold as compared to PCN 1 scaffold. Similar results were also reported by Shirazi et al. for PVA nanocomposite membranes reinforced with CNTs [163]. The swelling was first found to decrease with the addition of CNTs in PVA matrix and then increased due to the aggregation of CNTs.

The swelling study results of the PVA-GNPs scaffolds are shown in Fig. 4.9 (c). Pure PVA (PGN 0) scaffolds showed highest swelling percentage as compared to PVA-GNPs composites. With addition of GNPs up to PGN 1, the swelling percentage was found to decrease. This decrease is due to the hydrophobic nature of the GNPs. Also, the reinforcement of GNPs in PVA matrix lowers the free volume of fluid uptake sites, hence reducing the swelling percentage. With further increase in GNPs (1.5 wt%), a slight increase in swelling was observed, which might be due to the agglomeration of nanoplatelets. The agglomeration increased the free volume of fluid uptake site which leads to increase in PBS uptake in PGN 1.5 scaffolds.

The incorporation of AC into PVA matrix brings about a significant change in swelling behavior of the composite scaffolds (Fig. 4.9 (d)). PVA without AC showed the lowest degree of swelling equal to 310% after 24 h of soaking in PBS. The swelling percentage increased with increase in AC content in the composites. This is due to the excellent absorption properties of AC. Also, the hydrophilic functional groups present in AC tends to absorb more fluid on its surface, thus increasing the swelling ratio.

4.1.7. *In-vitro* degradation studies

Biodegradability is an essential factor that has to be considered while developing a composite scaffold. Degradation rate influences the mechanical properties and inflammatory responses of the scaffold. It has been reported that biodegradable polymers provoke more intense inflammatory responses as compared to non-degradable polymers. Further degradation is influenced by many other factors like molecular weight, chemical structure, presence of reinforcement and its dispersion. The *in-vitro* degradation studies of PVA based composites scaffolds reinforced with nHA, AC, CNTs and GNPs are shown in Fig. 4.10 (a-d). In addition to the degradation percentage, the rate of degradation was also modeled and the degradation kinetics was evaluated using power law:

$$-\frac{dM}{dt} = k_d M^n$$

where M is the mass of the sample, t is the time, k_d is the coefficient of the degradation rate and n is the order of the reaction. The linear plots (inset of the Fig. 4.10 (a-d)) confirm the first order kinetics and the k_d values are given in Table 4.2 when the intercept was taken as zero.

Fig. 4.10 (a) shows the weight loss of the developed PVA-nHA composites in PBS over a period of 4 weeks. It was observed that the weight loss of PVA-nHA composites initially increased rapidly. The PVA scaffold without the addition of nHA showed higher degradation rate. With the addition of nHA, the degradation rate was found to decline due to the decrease in porosity in the PVA matrix. The degradation rate of PHA 1, PHA 2, PHA 3, PHA 4 and PHA 5 was 1.07, 1.15, 1.37, 1.47 and 1.27 times slower than the pure PVA. In the pure PVA scaffold, voids were reported through which fluid can diffuse and degrade the matrix [164]. With the reinforcement of nHA, the voids in PVA matrix were occupied by these nHA particles, thereby increasing the hydrophobic nature of the composites eventually decreasing the degradation rate of PHA samples as compared to pure PVA. On the contrary, the composite scaffold PHA 5 (k_d = 0.635) shows higher degradation rate than PHA 3 (k_d = 0.591) and PHA 4 (k_d = 0.548). This might be due to more agglomeration and improper dispersion of nHA in addition to the voids in PVA matrix. Due to this PBS must have penetrated to the matrix more easily and breaking the

bond between the agglomerated nHA and degrading the matrix in PHA 5 owing to higher degradation as compared to PHA 4 and PHA 3. Amongst all the composite scaffolds, PHA 3 showed nominal degradation rate due to uniform distribution of nHA in PVA matrix.

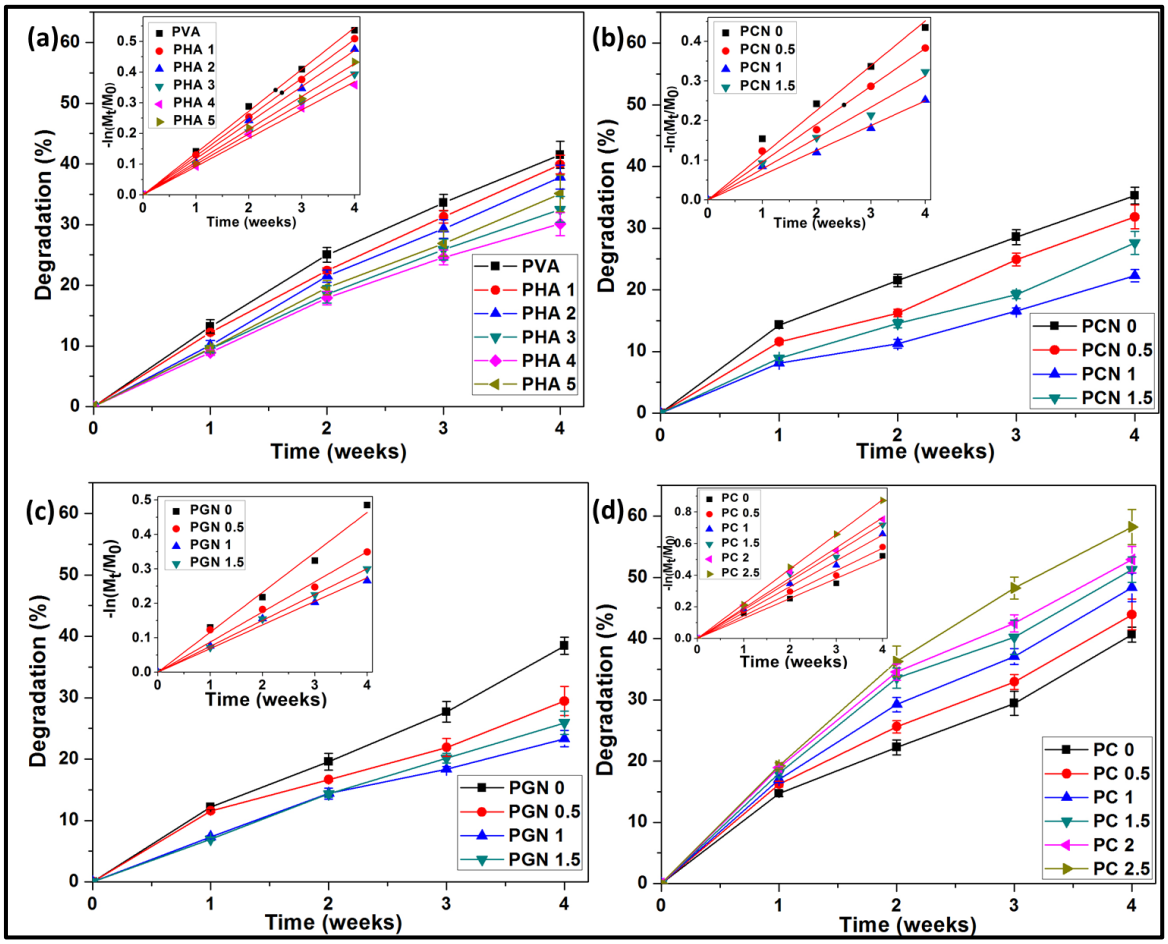

Fig. 4.10 Degradation studies of (a) PVA-nHA, (b) PVA-CNTs, (c) PVA-GNPs and (d) PVA-AC composites.

The weight loss curves observed in PVA-CNTs scaffolds are shown in Fig. 4.10 (b). The pure PVA (PCN 0) scaffold showed highest degradation percentage. The degradation of PVA was 1.17, 1.8 and 1.44 times faster than the PCN 0.5, PCN 1 and PCN 1.5, respectively. The reinforcement of CNTs in PVA matrix reduced the degradation rate of PVA-CNTs nanocomposite scaffolds. This can be attributed to the strong binding between CNTs and PVA matrix. The degradation results are also supported by results of contact angle measurements and swelling studies. The decrease in hydrophilicity and swelling rate

with the reinforcement of CNTs reduced the PBS uptake and hence retarded the degradation of the polymer backbone in nanocomposites. However, PCN 1.5 showed slightly higher degradation rate when compared to PCN 1 which might be due to the agglomeration of CNTs in PCN 1.5.

Table 4.2 Degradation rate coefficient for the developed composites.

Sample	**k_d (h^{-1}) ($x10^{-3}$)**	**Adj. R-Square**		**Sample**	**k_d (h^{-1}) ($x10^{-3}$)**	**Adj. R-Square**
PVA-nHA composites				**PVA-AC composites**		
PVA	0.811	0.999		PC 0	0.752	0.994
PHA 1	0.753	0.999		PC 0.5	0.848	0.995
PHA 2	0.700	0.999		PC 1	0.973	0.997
PHA 3	0.591	0.999		PC 1.5	1.077	0.995
PHA 4	0.548	0.998		PC 2	1.136	0.997
PHA 5	0.635	0.999		PC 2.5	1.305	0.999
PVA-CNTs composites				**PVA-GNPs composites**		
PCN 0	0.671	0.992		PGN 0	0.690	0.995
PCN 0.5	0.569	0.995		PGN 0.5	0.520	0.991
PCN 1	0.372	0.994		PGN 1	0.407	0.995
PCN 1.5	0.464	0.994		PGN 1.5	0.447	0.999

Similarly, in case of PVA-GNPs scaffolds also, the degradation rate was found to decrease with the addition of GNPs in PVA matrix (Fig. 4.10 (c). The PGN 0 sample with highest degradation rate coefficient degraded 1.32, 1.69 and 1.54 times faster than the PGN 0.5,

PGN 1 and PGN 1.5, respectively. The hydrophobic nature of GNPs in comparison to PVA matrix lead to low adsorption of PBS, resulting in reduced degradation rate. Both, PGN 1 and PGN 1.5 showed almost same degradation percentage till first 2 weeks. However, after 3 weeks higher degradation was observed in PGN 1.5 indicating the formation of voids due to agglomeration of GNPs.

The percentage degradation curves of PVA-AC composite scaffolds are shown in Fig. 4.10 (d). The PC 0 sample showed the slowest rate of degradation with k_d equals to 0.752×10^{-3} h^{-1}, whereas the samples containing AC showed increased degradation. The degradation of PC 0.5, PC 1, PC 1.5, PC 2 and PC 2.5 was 1.12, 1.29, 1.43, 1.51 and 1.73 times faster than the PC 0 sample. As observed in swelling studies, addition of AC lead to more adsorption of PBS due to its excellent absorption properties. Also, the hydrophilic functional groups present in AC tends to absorb more fluid on its surface. This increased absorption of PBS makes the scaffolds degrading faster. Hence, PC 2.5, with the highest degradation rate coefficient, is the fastest degrading PC composite.

4.1.8. *In-vitro* hemocompatibility studies

Blood compatibility is one of the most important properties that has to be tested on the scaffold material, as this scaffold on implantation in microenvironment has to be in contact with body fluids for a long period of time. During this time period, their interaction may lead to cell damage and blood clotting (thrombus). The damage in blood cells' membrane will release hemoglobin which in turn induces acute renal failure. So it is essential to study the interaction of blood components with scaffold material. Hemolysis test was performed to estimate the blood compatibility of the composite scaffolds. The hemocompatibility of scaffold material was estimated by quantifying the amounts of hemoglobin released from erythrocytes in whole blood when comes in contact with scaffolds. The percent hemolysis values of scaffolds were summarized in Table 4.3. Positive and negative control has shown 100% and 0% hemolysis respectively.

It can be observed from data that with increase in amount of nHA above 3% w/v, hemolysis has increased to 2% and 1.05% in PVA 4 and PVA 5 composite scaffolds, respectively. These data revealed that with the addition of nHA, blood compatibility decreases. This is

due to the interaction of ionic groups of nHA with blood leading to high hemolysis. As observed in XRD pattern, PHA 4 and PHA 5 samples were more crystalline and hence less distorted structure had a higher hemolysis rate when compared to less crystalline (PHA 1, PHA 2 and PHA 3) and semi-crystalline PVA.

Table 4.3 Percentage (%) hemolysis of different composites.

Samples	**Hemolysis (%)**	**Samples**	**Hemolysis (%)**
+ve control		100	
-ve control		0	
PVA-nHA composites		**PVA-AC composites**	
PVA	0.20±0.03	PC 0	0.26±0.15
PHA 1	0.96±0.05	PC 0.5	0.14±0.10
PHA 2	0.29±0.01	PC 1	0.29±0.10
PHA 3	0.92±0.04	PC 1.5	0.18±0.05
PHA 4	2.00±0.16	PC 2	0.11±0.05
PHA 5	1.05±0.08	PC 2.5	0.22±0.10
PVA-CNTs composites		**PVA-GNPs composites**	
PCN 0	0.12±0.05	PGN 0	0.15±0.06
PCN 0.5	0.78±0.12	PGN 0.5	0.58±0.15
PCN 1	1.01±0.40	PGN 1	1.12±0.45
PCN 1.5	1.04±0.43	PGN 1.5	1.14±0.35

The PVA-CNTs scaffolds have shown hemolysis in the range of 0.12-1.04% with an increase in CNTs concentration. The increase in hemolysis percentage is due to the roughness induced by the addition of CNTs in PVA matrix. However, the increase in hemolysis percent did not significantly differ in PCN 1 and PCN 1.5 samples.

The percentage hemolysis values for PVA-GNP nanocomposites varied from 0.15% to 1.14%. This minimal increase in hemolysis (%) is due to roughness induced by addition of GNP in PVA matrix. Also, the hydrophobic GNP adhere to the hydrophobic cell membrane and cause cell lysis.

From the hemolysis study it was observed that all the PVA-AC composite scaffold samples have negligible percent hemolysis indicating highly hemocompatible nature. The percent hemolysis values for PVA-AC scaffolds were found to vary from 0.11% to 0.29%.

The results have also confirmed the anti-hemolytic activity of the AC in the composite scaffold. All the hemolysis results were within the permissible limit. Therefore, from the hemolysis study, it can be concluded that the developed scaffolds are highly hemocompatible.

4.1.9. *In-vitro* mineralization activity studies

The *in-vivo* bioactivity is the ability of a scaffold material to bond to a living bone by the formation of bonelike apatite on its surface when implanted in the living body. It can be predicted by evaluating the apatite formation on the scaffold in *in-vitro* when immersed in SBF. The formation of apatite on composite scaffolds was confirmed by FESEM. Both, PVA and PLGA being bioinert materials do not support proper bone integration on its own. The addition of different biomaterials can make them bioactive and aid the bone to integrate with them.

The FESEM micrographs were taken to confirm the apatite formation on the PVA-nHA scaffolds (Fig. 4.11 (a)). The SEM result has shown enhanced bioactivity of PHA composite scaffolds than PVA. Reinforcement of nHA in PVA matrix has enhanced the apatite formation as PVA alone does not support it. It has been reported that an increase in crystallinity also increases the apatite formation. The XRD data has shown an increase in

crystallinity with the increase in the concentration of nHA. Micrograph of PHA 3 composite scaffold showed dense and homogeneous apatite formation when immersed in SBF. This is due to proper dispersion of nHA in PVA matrix leading to this apatite growth in SBF. The XRD analysis (Fig. 4.11 (b)) of the composite scaffolds after immersion in SBF showed the characteristic peaks of hydroxyapatite at 2θ = 26°, 32° and 46° confirming the presence of apatite. Thus, results show that the good dispersion of nHA in a polymer matrix influence the homogeneous distribution of apatite when soaked in SBF.

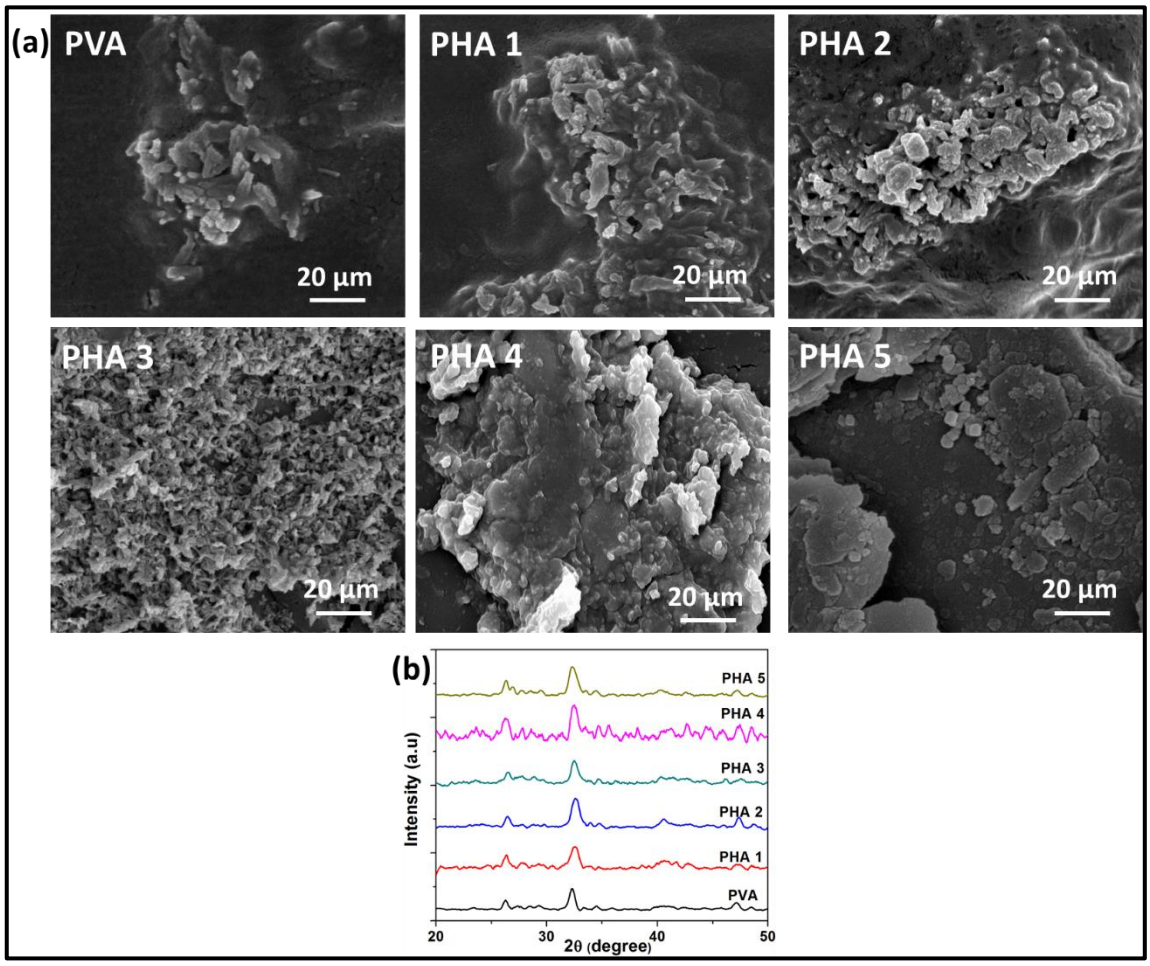

Fig. 4.11 (a) FESEM micrographs and (b) XRD spectra of PVA-nHA composite scaffolds after immersion in SBF for 21 days.

The PVA-CNTs composites showed dense apatite formation when compared to pure PVA after immersion in SBF for 21 days (Fig. 4.12 (a)). This increase is due to the presence of oxygen functionalities on the surface of carboxyl functionalized CNTs.

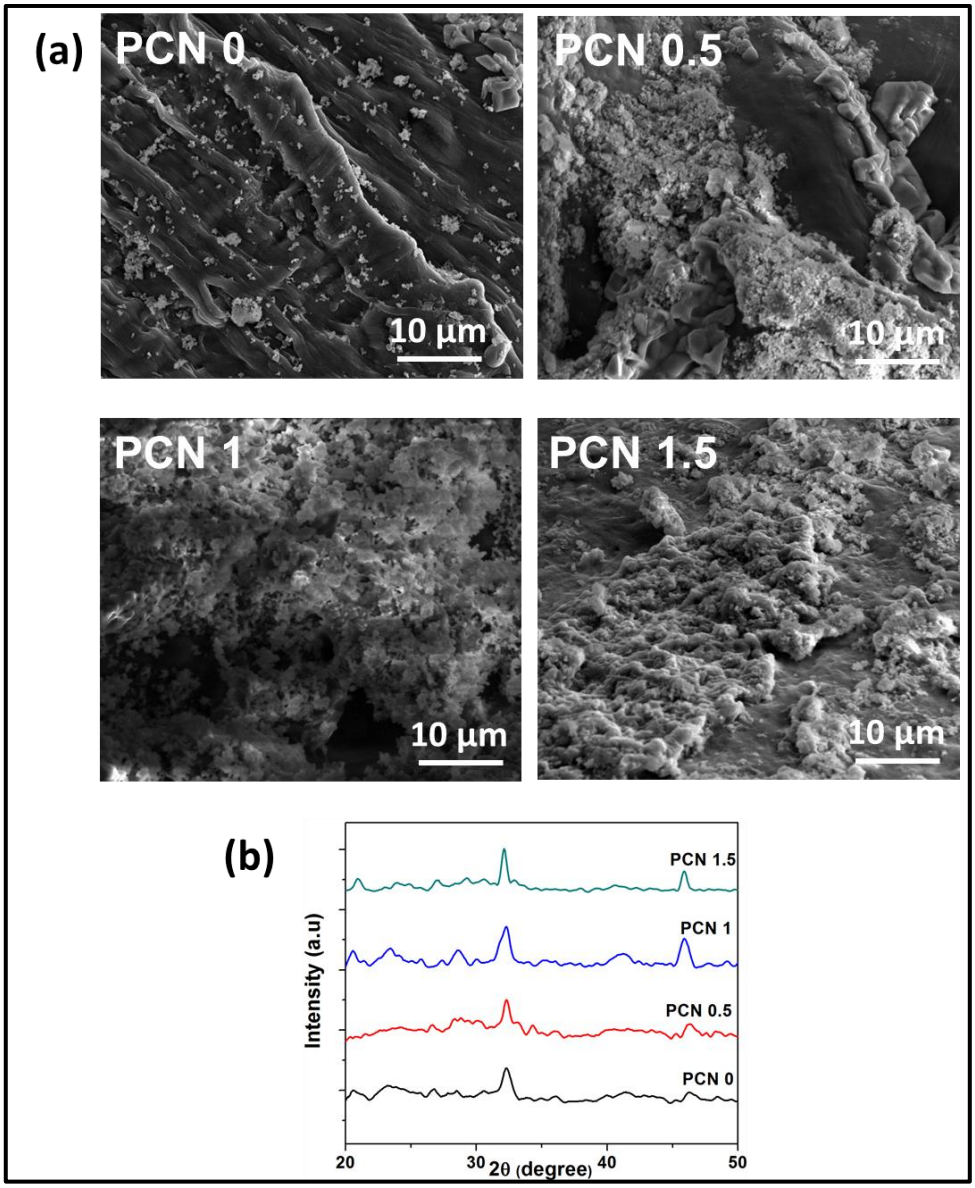

Fig. 4.12 (a) FESEM micrographs and (b) XRD spectra of PVA-CNTs composite scaffolds after immersion in SBF for 21 days.

The carboxyl groups having negative charge act as nucleation points for ionic clusters. The positively charged calcium ions (Ca^{2+}) get deposited on the negatively charged carboxyl groups, followed by phosphate ions (PO^{4-}), thus forming apatite layer. The PCN 1 sample showed homogeneous and dense apatite formation due to the proper dispersion of CNTs whereas PCN 1.5 showed less apatite as compared to PCN 1 sample. The agglomeration of CNTs in PCN 1.5 sample resulted in uneven apatite formation when soaked in SBF. The

XRD spectra (Fig. 4.12 (b)) of all the samples showed a peak at 2θ = 32° confirming the presence of apatite. Other characteristic peak for apatite was observed at 46°.

The apatite formation on PVA-GNPs scaffolds was confirmed by FESEM and results are shown in Fig. 4.13 (a). The PGN 0 sample showed the least formation of apatite, whereas a thick layer of apatite was observed in all PVA-GNPs composites. This apatite formation is due to the presence of carboxyl functional groups on the GNPs surface acting as a nucleation point for ionic clusters [60].

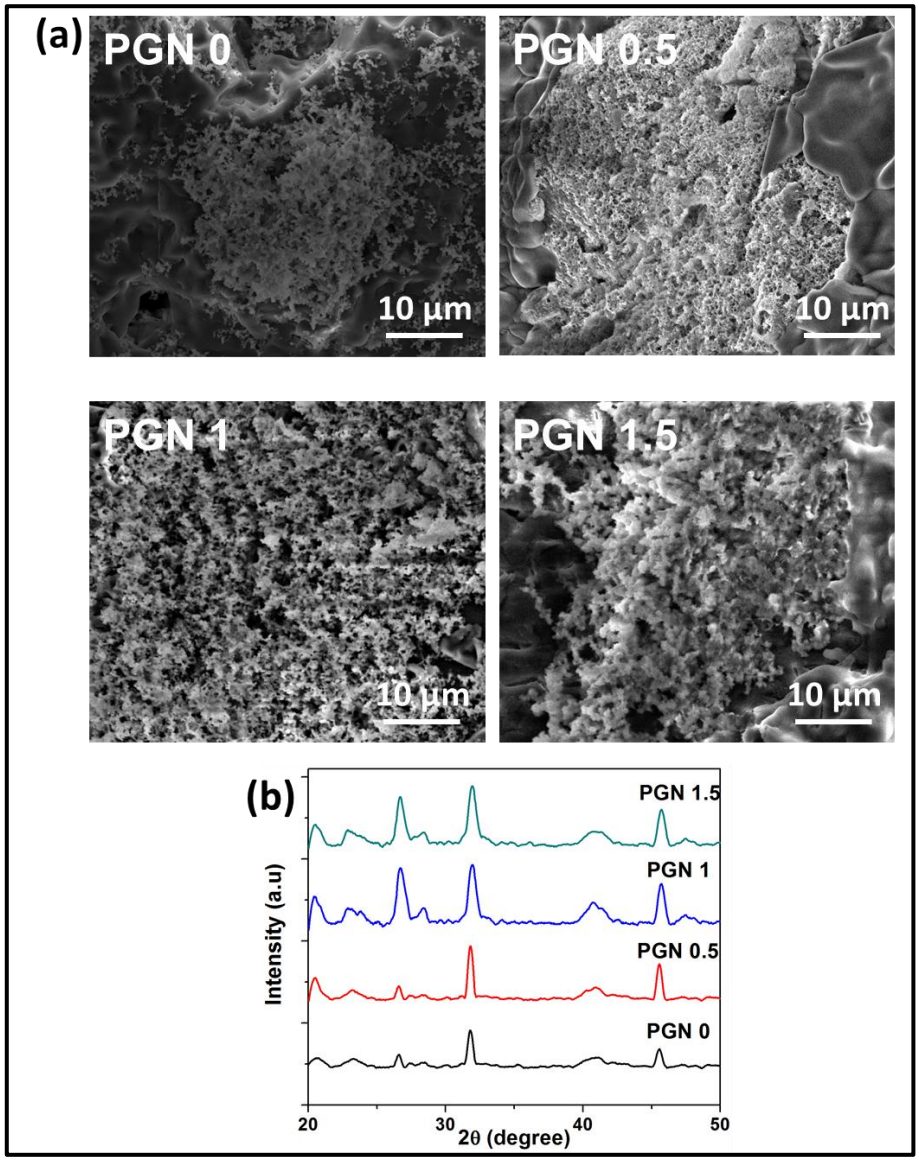

Fig. 4.13 (a) FESEM micrographs and (b) XRD spectra of PVA-GNPs composite scaffolds after immersion in SBF for 21 days.

The apatite layer grows by deposition of Ca^{2+} and PO^{4-} ions from the SBF on negatively charged functional groups of GNPs. The PGN 1 sample showed dense and well-formed apatite layer suggesting proper dispersion of GNPs in PVA matrix as compared to PGN 0.5 and PGN 1.5 samples. The apatite granules were homogeneously distributed all over the surface of PGN 1 which implies a strong bone-bonding ability between the scaffold and surrounding tissue. In contrast, uneven apatite deposition on PGN 1.5 scaffold was observed which is due to agglomeration of GNPs. The XRD peaks (Fig. 4.13 (b)) at 2θ = 26°, 32° and 46° confirmed the apatite formation on all the samples.

The PVA-AC composite scaffolds showed dense and homogenous apatite formation on the surface when immersed in SBF (Fig. 4.14 (a)). This is due to the presence of oxygen groups available on the surface of AC, which provides a favorable site for apatite nucleation. The negatively charged groups (carboxyl and carbonyl) electrostatically interact with positively charged calcium ions in SBF, which further attracts phosphate ions, thus forming calcium phosphate. The morphology of the apatite was found to be globular, but its size varied with AC concentration. With the addition of AC, the size of apatite particles was found to increase. The PC 0 sample also showed apatite formation, but the size of the apatite particles was smaller as compared to PVA-AC samples for the same time period. Further, the apatite formation was also confirmed by performing XRD analysis (Fig. 4.14 (b)) which showed sharp peaks at 32° and 46°.

4.1.10. Protein adsorption studies

The adsorption of proteins on the surface of an implant is among the leading events that occur immediately after implantation. When a scaffold is implanted in the human body a variety of cytoplasmic, transmembranal and extracellular proteins get adsorbed onto its surface when comes in contact with physiological fluids. These proteins facilitate the cell attachment and encourage tissue repair (cell responses). Protein adsorption is intensely influenced by the surface chemistry, surface charge, and hydrophobicity of the scaffold material. Bovine serum albumin (BSA) is a glycoprotein representing 50% of all the plasma proteins. Its molecular structure and functions are similar to those of human serum albumin [165]. Therefore, in the present study, the adsorption of BSA protein on composite scaffolds was evaluated by Bradford assay (Table 4.4).

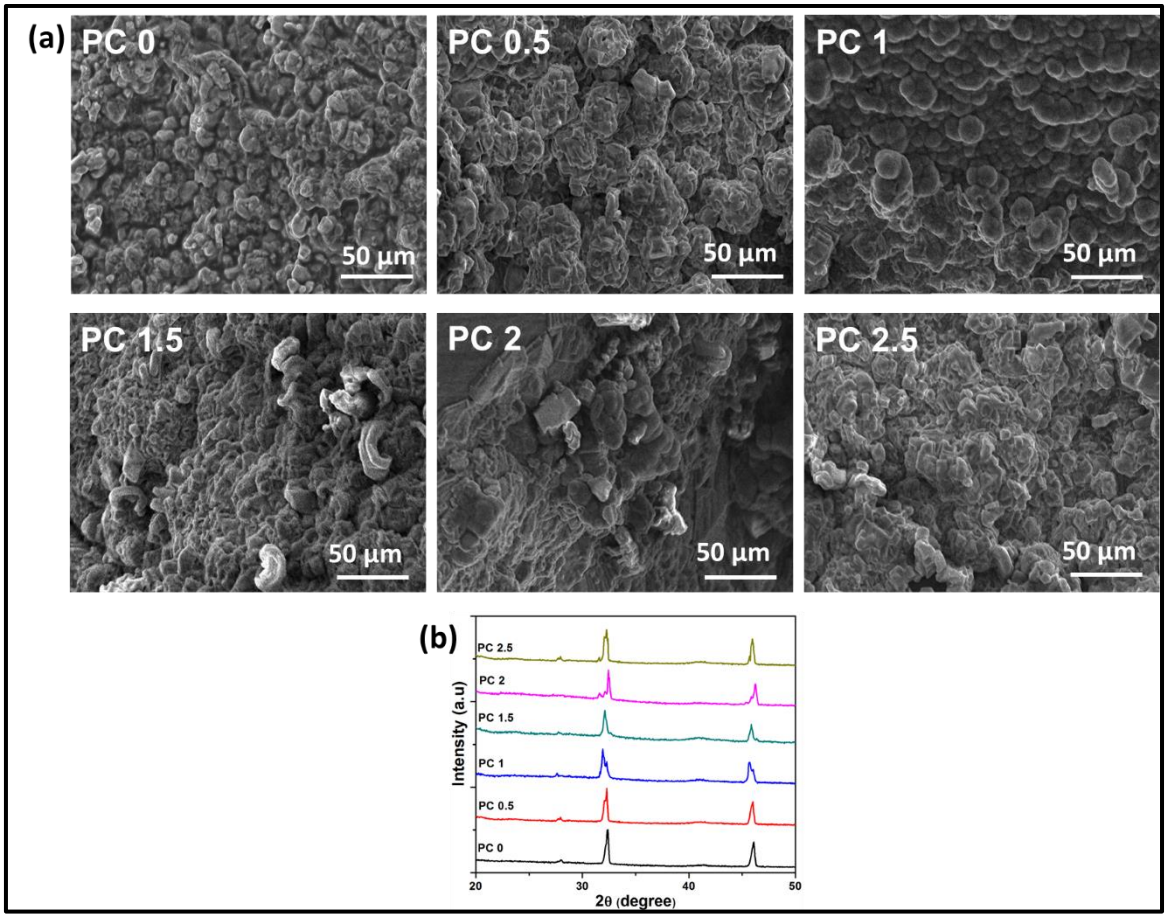

Fig. 4.14 (a) FESEM micrographs and (b) XRD spectra of PVA-AC composite scaffolds after immersion in SBF for 21 days.

In the PVA-nHA scaffolds, pure PVA showed least protein adsorption which was found to increase with the addition of nHA in PVA matrix. It is evident that hydrophobic surfaces tend to adsorb more proteins than hydrophilic surfaces [166]. The addition of nHA made the composite surface less hydrophilic as observed in contact angle measurement results. Therefore, more protein was absorbed on the surface of composite samples. However, sample PHA 4 and PHA 5 showed slightly less protein adsorption when compared to PHA 3 sample. The agglomerated nHA in these two samples led to decrease in BSA adsorption.

Amongst the PVA-CNTs composites, PCN 0 scaffold showed least protein adsorption, and it was increased with the addition of CNT. The hydrophilic functional groups (carboxylic and hydroxyl) present on the surface of functionalized CNTs adsorb proteins by interacting with the functional groups of protein molecules via electrostatic and van der Waals forces.

Hence, PVA-CNTs nanocomposites have shown enhanced protein adsorption making them biologically recognizable materials suitable for cell attachment.

Table 4.4 Protein adsorption on different composites.

Samples	Protein adsorbed (µg/ml)	Samples	Protein adsorbed (µg/ml)
PVA-nHA composites		**PVA-AC composites**	
PVA	250±13.51	PC 0	340.25±3.04
PHA 1	269.56±13.23	PC 0.5	376.90±1.55
PHA 2	286.43±15.30	PC 1	380.70±3.81
PHA 3	302.72±6.43	PC 1.5	399.10±5.37
PHA 4	295.09±10.16	PC 2	401.85±12.23
PHA 5	291.05±12.45	PC 2.5	405.68±2.26
PVA-CNTs composites		**PVA-GNPs composites**	
PCN 0	316.31±10.5	PGN 0	233.91±9.13
PCN 0.5	345.32±13.74	PGN 0.5	248.24±13.76
PCN 1	396.13±12.67	PGN 1	297.46±13.00
PCN 1.5	455.02±15.32	PGN 1.5	250.95±25.24

With the addition of GNPs, the hydrophilicity of the samples was decreased as shown by contact angle results of the as-cast nanocomposite, which has played an important role in enhancing protein adsorption on PVA-GNPs composites. The π electron cloud in graphene interacts with the inner hydrophobic cores of protein leading to increase in protein

adsorption. However, there was a slight decrease in amount of protein adsorbed for PGN 1.5 scaffolds which might be due to agglomeration which decreased the exposed surface of GNPs for protein adsorption. Hence, PGN samples have shown augmented protein adsorption making them suitable for cell attachment, proliferation, and mineralization.

The PC 0 scaffold showed least protein adsorption and was found to increase with the addition of AC. The hydrophilic functional groups present in AC interact with the functional groups of BSA molecules via electrostatic and van der Waals forces which induce the adsorption of protein molecules on the composite scaffolds. Further, an increase in the amount of AC provides more porosity, which means more surface area available for higher AC concentrations, thus paving more protein adsorption.

4.1.11. Tensile properties

To evaluate the effects of reinforcements on the mechanical properties of composite scaffolds, tensile testing was carried out. The tensile strength, Young's modulus and energy at break are tabulated in Table 4.5.

The tensile strength of the PVA-nHA composite scaffolds was found to increase initially with the increase in nHA concentration from PVA to PHA 3; 33.5% from PVA to PHA 3 composites. Later, it has been observed that the strength decreased for composite scaffolds PHA 4 and PHA 5 (higher concentration of nHA) with respect to PHA 3. The decrease in the tensile strength is due to agglomeration of nHA in PHA 4 and PHA 5 samples that hinder the effective stress transfer and deteriorates the tensile strength of the composite scaffolds [167]. The Young's modulus of the composites was found to increase with the increase in nHA concentration. This increase in Young's modulus is due to the improved rigidity of PVA-nHA composites on the addition of nHA; hence increasing the capability of the scaffolds to resist external forces. The lack of interfacial adhesion in PHA 4 and PHA 5 resulted in an early failure at the interface, leading to weak mechanical properties. The mechanical test results have revealed that the composite scaffold with 3% w/v nHA (PHA 3) has shown the best mechanical properties in comparison with the composite scaffolds PHA 4 and PHA 5.

In case of PVA-CNTs composites, PCN 0 sample showed lowest values for tensile strength, Young's modulus and energy at break. Increasing CNTs concentration in PVA matrix significantly improved the tensile properties of the nanocomposite scaffolds. The results showed that the tensile strength initially increased with increasing CNTs concentration up to 1 wt% (i.e., from 0.73±0.07 MPa for PCN 0 to 19.38±1.03 MPa for PCN 1 scaffold). This might be due the homogeneous dispersion of CNTs and strong interaction between CNTs and PVA matrix, which led to the effective stress transfer in the composite scaffolds leading to high tensile strength. With further increase in CNTs concentration (1.5 wt%), the tensile strength was found to decrease slightly (17.08±0.74 MPa) as compared to PCN 1 sample, which may be due to agglomeration of CNTs. The Young's modulus of the nanocomposites also showed a significant increase of 815% from PCN 0 to PCN 1 scaffolds. A substantial improvement in energy at break was also observed in nanocomposites as compared to PCN 0. Similarly, to tensile strength results, the energy at break also increased up to PCN 1 indicating more toughness of nanocomposites. This is due to the homogenous dispersion of CNTs up to 1 wt% concentration, resulting large interfacial area and hence increases the energy required to break the sample. A slight reduction in toughness was observed in PCN 1.5 which suggests that the further increase in CNTs concentration deteriorates the mechanical properties of the scaffold. Therefore, it can be concluded that PCN 1 scaffold showed overall good mechanical properties and further increasing the CNTs concentration has detrimental effect on PVA-CNTs nanocomposites.

As expected, the addition of GNPs into PVA matrix has a significant effect on the mechanical properties of the developed nanocomposites. The results have shown that the PGN 0 has least mechanical strength. The tensile strength of the nanocomposites increased with the addition of GNPs from 0 to 1 wt% and then diminished as the GNPs concentration reached 1.5 wt%. At 0.5 wt% of GNPs, the reinforcement effect is limited due to its less density in the matrix. However, a further increase in GNPs concentration (1 wt%, i.e. PGN 1) improved the tensile strength by 2068% when compared with pure PVA (PGN 0) scaffold. Similarly, the Young's modulus (stiffness) initially increased with the increase in GNPs concentration from 0 to 1 wt%, followed by a decrease in PGN 1.5 with 1.5 wt% of GNPs.

Table 4.5 Mechanical properties of different composites.

Samples	Tensile strength (MPa)	Young's modulus (MPa)	Energy at break (mJ)
PVA-nHA composites			
PVA	23.31±8.96	500.02±99.57	25.98±1.39
PHA 1	24.12±5.94	520.23±30.34	46.66±3.46
PHA 2	24.34±5.69	1000.34±80.45	156.94±6.38
PHA 3	31.15±8.33	1100.45±80.65	571.30±13.68
PHA 4	22.12±3.42	1700.00±40.36	29.26±1.52
PHA 5	26.13±3.62	1900.00±47.97	24.23±1.02
PVA-CNTs composites			
PCN 0	0.73±0.07	23.5±1.07	17.11±1.14
PCN 0.5	7.12±0.57	95.60±5.53	49.25±4.36
PCN 1	19.38±1.03	215.00±9.20	730.86±60.28
PCN 1.5	17.08±0.74	211.91±10.74	640.22±42.12
PVA-GNPs composites			
PGN 0	0.76±0.08	23.85±1.11	15.03±2.56
PGN 0.5	1.92±0.28	78.47±14.42	19.96±7.83
PGN 1	16.48±0.50	248.49±16.85	1106.85±67.56
PGN 1.5	10.53±1.62	10.61±1.35	202.78±64.93

PVA-AC composites			
PC 0	0.72±0.09	24.85±1.13	17.31±1.07
PC 0.5	1.00±0.15	29.32±6.105	24.80±2.00
PC 1	1.39±0.26	42.71±2.12	50.21±4.76
PC 1.5	1.45±0.11	43.04±6.00	51.90±5.29
PC 2	1.68±0.19	52.57±10.52	40.84±2.65
PC 2.5	2.21±0.25	111.57±15.91	44.64±2.45

The increase in mechanical strength can be ascribed to the homogeneous dispersion of GNPs in the polymer matrix which led to the effective stress transfer in the nanocomposites. At higher concentrations (>1 wt%), GNPs stack together forming layers due to strong van der Waals forces. This decreases the interaction between GNPs and matrix, generating a weak interface which prevents the effective stress transfer, deteriorating the mechanical properties of nanocomposites (PGN 1.5). Similar results have already been reported in the literature where the agglomeration of GNPs in polymer matrix decreases the mechanical strength of composites [168]. The critical concentration of GNPs, above which it starts agglomerating varies with the different matrices used. In the present work, a significant improvement in energy at break was also observed in all the nanocomposites as compared to PGN 0 making the nanocomposites tougher. Therefore, it can be concluded that the reinforcement of 1 wt% GNPs improves the overall mechanical properties of PGN 1 nanocomposite scaffolds.

The tensile strength of the scaffolds was found to increase (up to 207%) with an increase in AC concentration (i.e., from 0.72±0.09 MPa for PC 0 to 2.21±0.25 MPa for PC 2.5 sample). The same trend was also observed in the Young's modulus of the scaffolds that showed an increase of 349% from PC 0 to PC 2.5 sample. The increase in strength with AC concentration is attributed to the homogenous dispersion of AC in PVA matrix, which

helps the effective stress transfer in the composite scaffolds leading to high tensile strength. The PVA-AC composites showed a higher value of energy at break (toughness) as compared to PC 0 sample. This is due to the homogenous dispersion of AC, resulting large interfacial area and hence, increases the energy required to break the sample. A slight reduction in toughness was observed in PC 2 and PC 2.5 which suggests that the further increase in AC concentration may deteriorate the mechanical properties of the scaffold. From results it can be concluded that PC 2.5 scaffold showed overall good strength, toughness, and Young's modulus when compared to other composites.

4.1.12. Cell viability

Through preceding studies, it has been found that reinforcement of various carbon materials into polymer matrices (PVA) improves its biological and mechanical properties. Furthermore, it is also of interest to study in detail the effect of these reinforcements on the *in-vitro* cellular response like cell viability, proliferation, morphology, and differentiation. The ability of the scaffold material to encourage cell attachment and proliferation is a critical factor for osseointegration. The cell attachment and proliferation, controlled by the scaffold properties, further influence the cell differentiation [166]. The viability of MG-63 cells cultured on scaffolds was measured by MTT assay and trypan blue exclusion assay, and the results are shown in Fig. 4.15 and 4.16. The cell viability (%) of the cells cultured on the control was normalized to 100%.

At 48 h post cell seeding, the PVA-nHA scaffolds (Fig. 4.15 (a)) showed significantly higher cell proliferation as compared to the control (tissue culture plate). The MTT results showed that the addition of nHA encouraged the cell proliferation. This is due to the higher surface area to volume ratio of nHA which provides more space for the cells to proliferate. The cell viability and proliferation increased up to 3% nHA (PHA 3). With further increase in nHA concentration (PHA 4 and PHA 5), there was a slight decrease in the number of viable cells. Similar results were found by trypan blue exclusion assay (Fig. 4.16 (a-b). The PHA 3 sample exhibited highest total cell count, whereas, PHA 4 and PHA 5 showed a decrease in cell count and live/total cells ratio. This decrease is due to increase in crystallinity and contact angle of PHA 4, and PHA 5 might have inhibited the osteoblast cell proliferation.

It is evident from the results shown in Fig. 4.15 (b) and 4.16 (c-d) that the PVA-CNTs porous scaffold structures facilitate cell proliferation as compared to the control (tissue culture plate). The cell viability of the PVA-CNTs nanocomposite scaffolds was higher than that of pure PVA (PCN 0) scaffolds, suggesting that the CNTs encourage the MG-63 cell proliferation. The number of cells grown on the PCN 1 scaffold showed the highest cell proliferation when compared to other compositions and was found to be almost twice as compared to the control. The hydrophilic functional groups (carboxylic and hydroxyl) present on CNTs surface boosted the protein adsorption by nanocomposite scaffolds that further promoted the cell attachment. With further increase in CNTs concentration in sample PCN 1.5 (1.5 wt%), the cell viability was found to decrease. As shown in Fig. 4.16, PCN 1 sample showed highest cell count and all the scaffolds exhibited less number of dead cells than the control. In comparison to control, both PCN 0.5 and PCN 1 showed significantly higher live cell to total cell ratio. Hence, the results suggest that 1 wt% might be the threshold concentration of CNTs in PVA matrix, which potentially encourage the cell attachment and growth. Beyond that concentration (1 wt%), CNTs might have toxic effects on the osteoblast cells.

The results of osteoblast cell viability on the PGN scaffolds by MTT assay and trypan blue exclusion assay are shown in Fig. 4. 15 (c) and 4.16 (e-f). In MTT assay results, all the scaffolds showed significantly higher cell viability when compared to control, indicating that the porous scaffold structure facilitates cell proliferation. Among all the scaffolds, pure PVA showed the least cell viability. The addition of GNPs in polymer matrix promoted the cell attachment and proliferation which might be due to the high protein adsorption and surface roughness of the composite scaffolds. Also, the sheet like structure of GNPs contains more number of functional groups (when compared to functionalized CNTs) to interact with proteins and osteoblast cells. The nanocomposite scaffold with 1 wt% GNPs (PGN 1) exhibited the highest cell proliferation by facilitating its attachment. However, the cell proliferation on PGN 1.5 was significantly lesser than PGN 1 scaffold which might be due to the toxic effects of agglomerated GNPs. The concentration dependent toxicity of the graphene and its derivatives has already been reported in the literature [141, 166]. Mehrali et al. showed that the addition of 1 wt% GNPs into ceramics has positive effects on the proliferation of human osteoblast cells, whereas the further increase in GNPs concentration

lead to considerably lower cell viability [60]. Significantly higher total cell count and live cells to total cells ratio of PGN 1 than the control supported the MTT assay results. Hence, the results suggest that 1 wt% of GNPs potentially encourage the osteoblast cell attachment and growth.

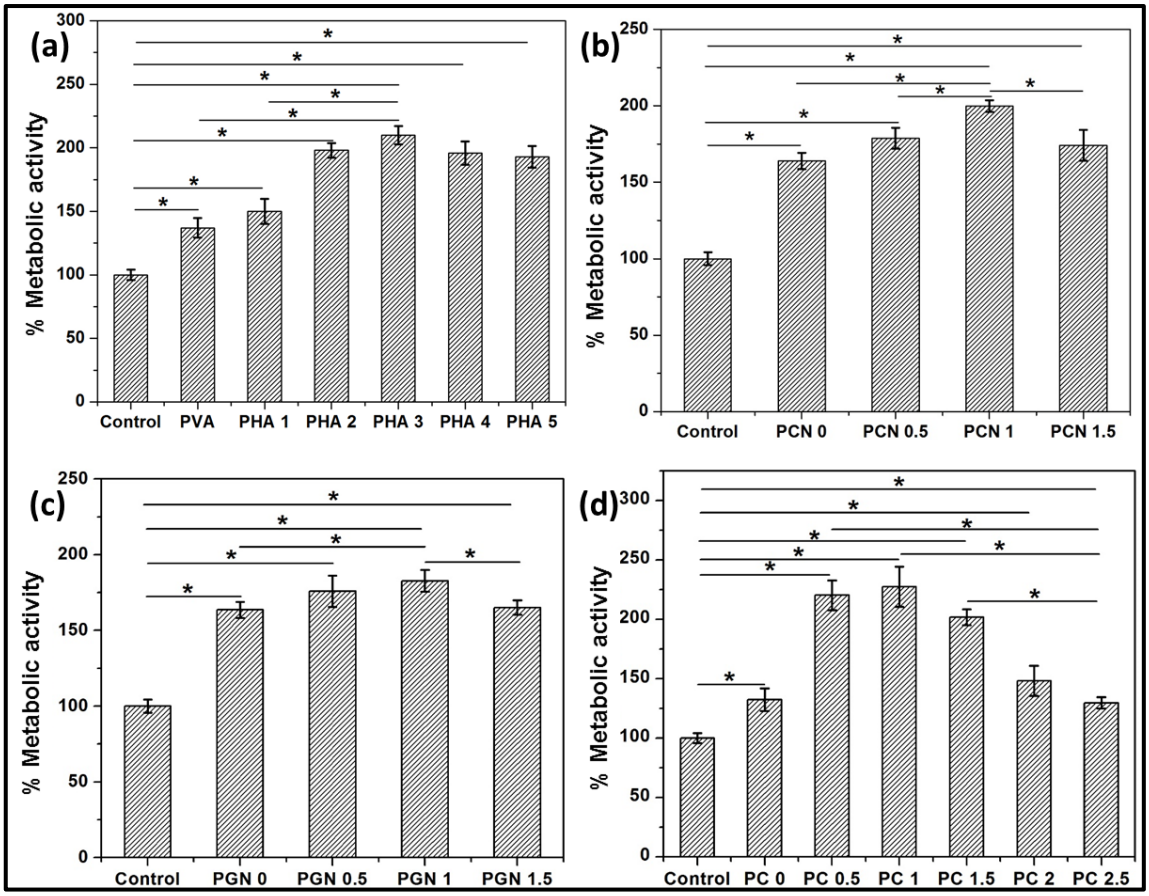

Fig. 4.15 MTT assay results of (a) PVA-nHA, (b) PVA-CNTs, (c) PVA-GNPs and (d) PVA-AC composites.

The MTT assay and trypan blue exclusion assay results of PVA-AC composite scaffolds are shown in Fig. 4.15 (d) and 4.16 (g-h), respectively. All the PVA-AC scaffolds showed higher cell proliferation than the control plate. It was observed from the MTT assay results that the addition of AC encouraged the cell proliferation. The hydrophilic functional groups present on AC enhanced the protein adsorption by composite scaffolds which further promoted the cell attachment. The PC 1 scaffold showed highest cell proliferation (230%) as compared to other compositions.

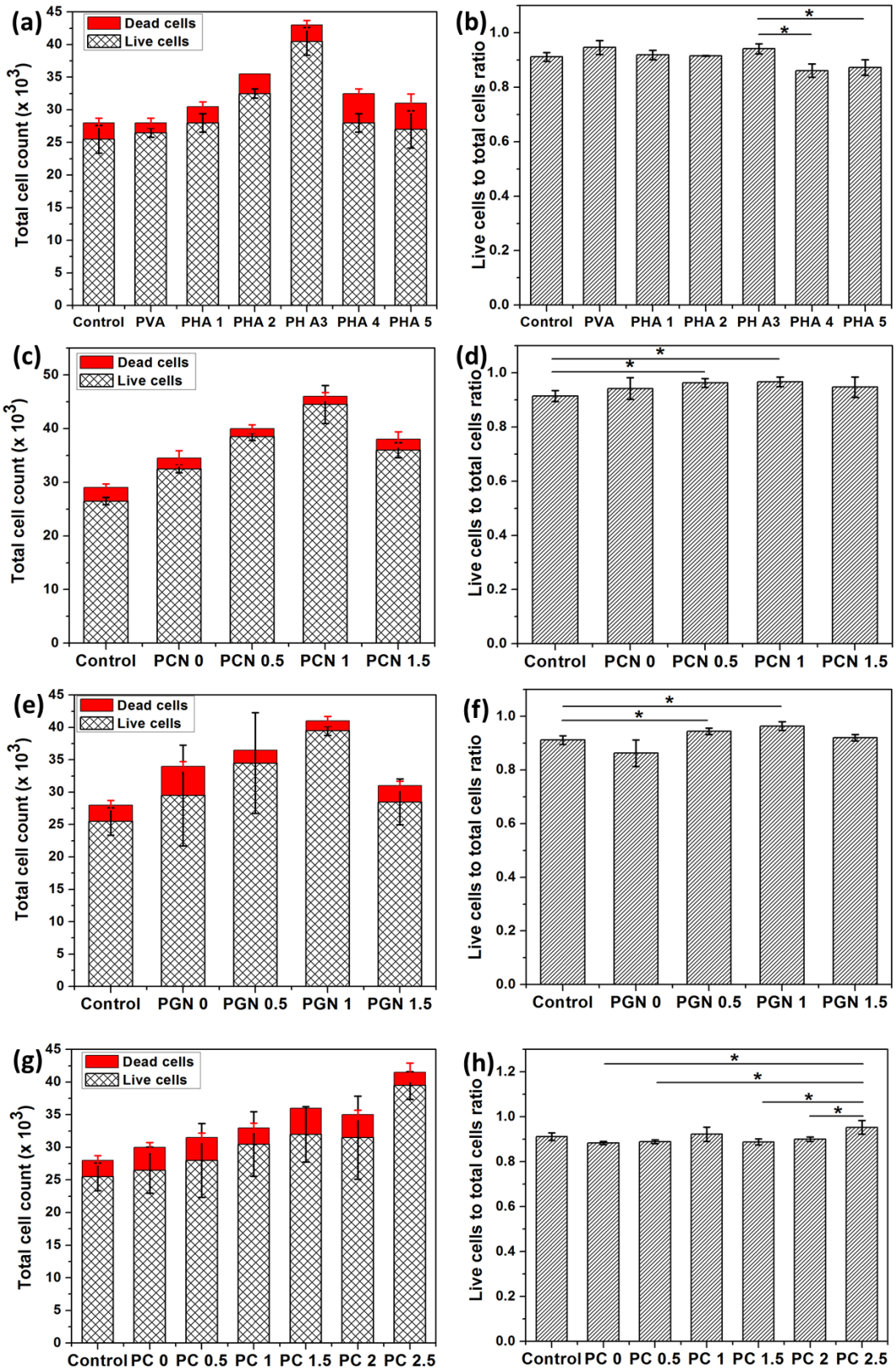

Fig. 4.16 Trypan blue exclusion assay results showing total cell count (a, c, e and g) and live to total cells ratio (b, d, f and h) for various scaffolds.

With further increase in the AC, the cell viability was found to decrease. This might be due to the differentiation of cells in scaffolds with higher concentrations of AC. However, in the trypan blue assay results PC 2.5 sample presented the highest cell count with the lowest number of dead cells. Briefly, the obtained results confirmed that PVA-AC composite scaffolds supported cell proliferation without inducing any cytotoxic effects.
Thus, the MTT and trypan blue assay results suggested that the carbon reinforcements in polymer matrix potentially increase the cell viability on composite samples.

4.1.13. Cell morphology

The ability of the scaffold material to encourage cell adhesion and proliferation is an important factor in determining the potential of scaffold for bone tissue engineering. The adhesion of osteoblast cells plays an important role in the expression of cell functions such as cell proliferation and differentiation [169]. It depends on different factors like surface charge, hydrophilicity and roughness of the material. The cells can sense surface topography and accordingly regulate their shape and cytoskeletal organizations. The FESEM analysis was performed to evaluate the effect of reinforcements on cell attachment, morphology and mineral production on different composite scaffolds.

Fig. 4.17 shows the FESEM micrographs of the human osteoblast-like MG-63 cells seeded on PVA-nHA scaffolds. The growth of the osteoblast cells on all the PHA composite scaffolds confirmed the biocompatibility of these scaffolds. The PVA scaffold showed globular shaped cells attached to its surface. The addition of nHA in PVA matrix enhanced the cell spreading and cell density on composite scaffolds. This might be due to a higher surface area to volume ratio of nHA that provides more space for cells to adhere and proliferate. The cells formed large groups on the scaffold surfaces. Nodule formation and mineralization were also observed in nHA containing scaffolds (PHA 2 and PHA 3). With further increase in nHA concentration (PHA 4 and PHA 5) the number of adhered cells and mineralization was decreased. This is due to the combined effect of an increase in crystallinity and contact angle of PHA 4 and PHA 5.

The growth of the osteoblast cells on all the PVA-CNTs nanocomposite scaffolds confirmed the biocompatibility of these scaffolds (Fig. 4.18). A less number of cells were

found in the PCN 0 samples, whereas more cells were attached to the nanocomposite scaffolds. The cells on PCN 0 scaffolds were localized and less spread indicating less favored interactions of osteoblast cells with pure PVA.

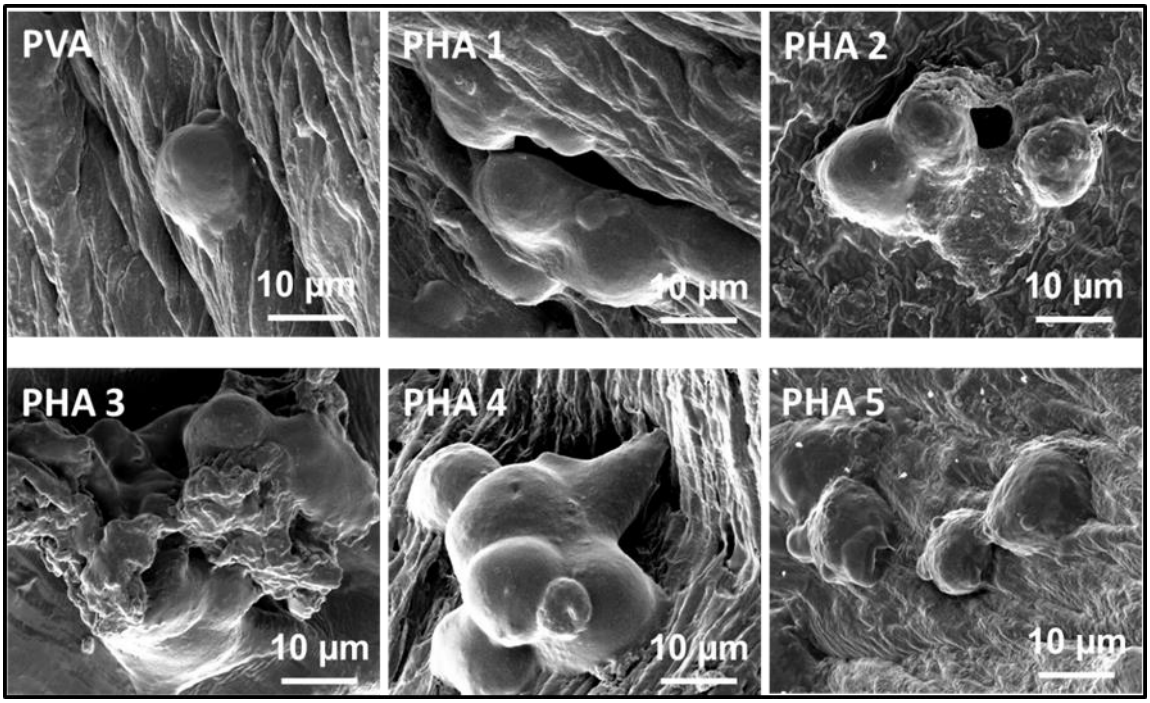

Fig. 4.17 FESEM micrographs of PVA-nHA composite samples cultured with MG-63 cells.

In contrast to PCN 0, MG 63 cells cultured on PVA-CNTs nanocomposite scaffolds were well spread and showed characteristic osteoblast cell morphology. The reinforcement of PVA with CNTs improved both, the cell density and growth on the nanocomposite scaffold samples. This might be due to the large surface area provided by CNTs to attach more cells and promote cell spreading and proliferation [170]. The increase in nanoroughness and protein adsorption with CNTs addition also mediated the osteoblast attachment on nanocomposite scaffolds [123]. Keselowsky et al. have also reported the improved osteoblast cell attachment on the surfaces having carboxyl functional groups [171]. In the case of PCN 1, cellular extensions were observed from the edges of cells. With further increase in CNTs concentration up to 1.5 wt% (PCN 1.5), reduced cell attachment and spreading was observed. The FESEM results of cell attachment support the MTT assay

results, suggesting 1 wt% concentration of CNTs as the threshold concentration of CNTs in PVA matrix for cell attachment and growth.

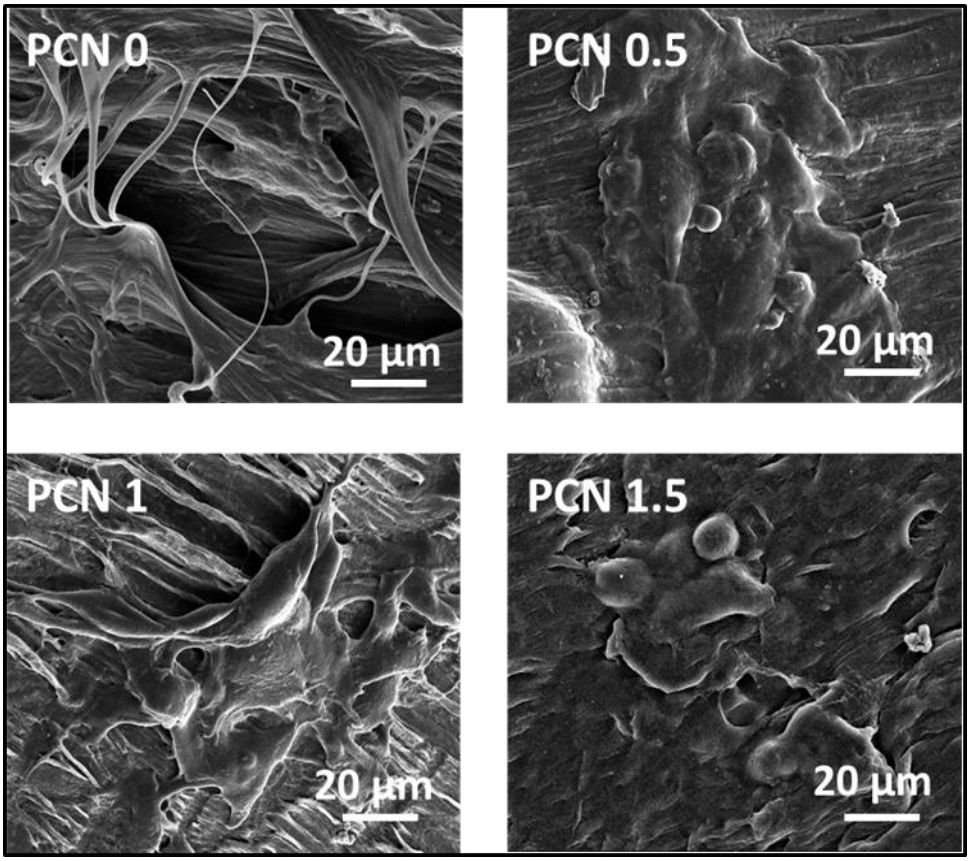

Fig. 4.18 FESEM micrographs of PVA-CNT composites cultured with MG-63 cells.

The FESEM micrographs of osteoblast cells (MG-63) attached to different PVA-GNPs scaffolds are shown in (Fig. 4.19). The results revealed that MG-63 cells were successfully attached to the scaffold surface. The growth of cells on all the PVA-GNPs scaffolds confirmed the biocompatibility of these scaffolds as supported by the MTT assay results. The cells on pure PVA (PGN 0) sample were localized and globular indicating less favored interactions of osteoblast cells. In contrast, more number of adhered and well-spread cells were observed on the surface of nanocomposites. The adjacent osteoblast cells were connected to each other through cytoplasmic extensions as shown in FESEM micrographs for PGN 1 scaffolds which are important for cell-cell communication required during cell differentiation. The mineralized nodules and elongated filopodia were also observed in the nanocomposite scaffolds. In the case of PGN 1, spherical cells were also found suggesting

that the few cells might be in dividing stage. The enhanced cell attachment on nanocomposites can be attributed to the large surface area and nanoscale surface roughness provided by GNPs for cells to attach on the nanocomposite scaffolds. Furthermore, high protein adsorption on nanocomposites makes more adhesion molecules available for cell adhesion [166]. Aryaei et al. have also shown the non-cytotoxic behavior of graphene towards the osteoblast cells [172]. A layer of graphene on bone implants was suggested for better osteoblast cell attachment and proliferation. However, in our study, a higher concentration of GNPs (1.5 wt%) was found to exert adverse effects on the cellular behavior. This might be due to the agglomeration of GNPs. Thus, the above results indicated that 1 wt% is the threshold concentration of GNPs in PVA matrix.

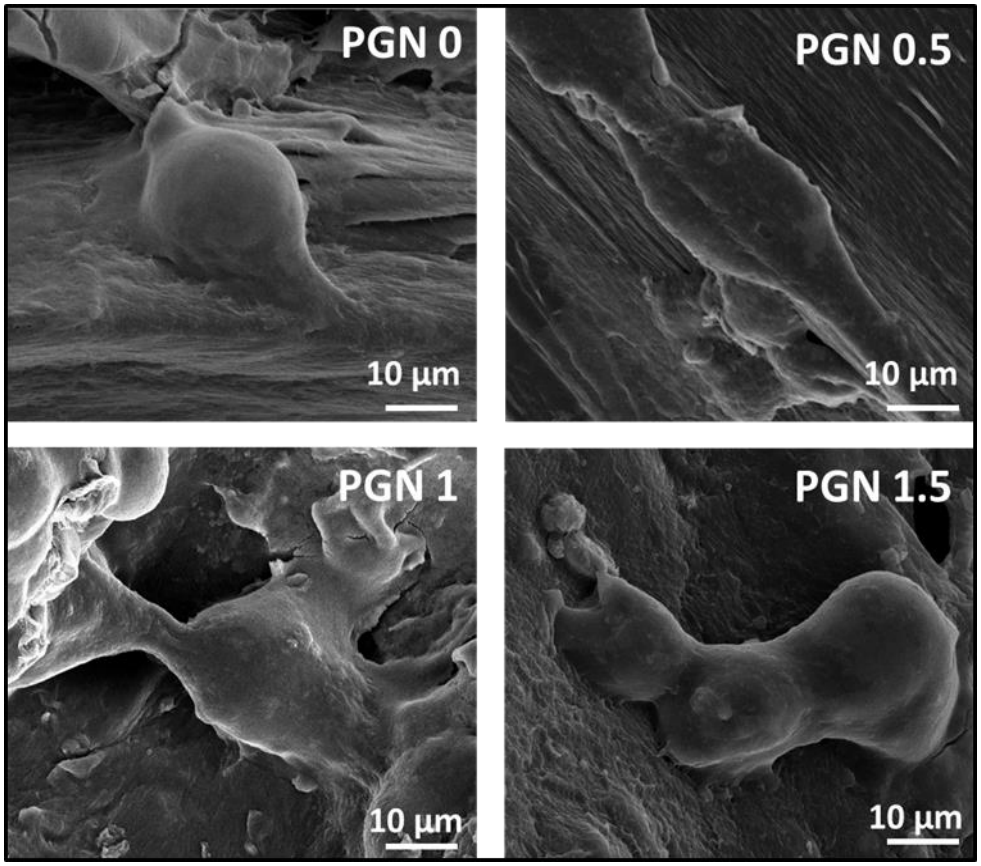

Fig. 4.19 FESEM micrographs of PVA-GNPs composites cultured with MG-63 cells.

In PVA-AC scaffolds (Fig. 4.20), the PC 0 scaffold showed round-shaped cells attached to its surface, whereas, MG-63 cells cultured on composite scaffolds started to spread and

showed characteristic morphology. The decrease in contact angle with AC addition increased the cell adhesion on the composite scaffolds surfaces. The cells formed groups on the surfaces and within pores of the scaffolds. Nodule formation was also observed in composite scaffolds as AC encouraged the formation of mineralized bone nodules and more number of mineralized bone nodules were observed in PC 2.5 sample. Clusters of matrix appeared inside the pores and on the surface of PC 2 and PC 2.5 scaffolds. Lee et al. have reported that the increasing pore size inhibits the cell proliferation but enhance the cell differentiation [173]. Similar results were also found in this study. With the addition of AC, the pore size was found to be larger as observed in FESEM (Fig. 4.5), which resulted in cell differentiation and matrix secretion in PC 2 and PC 2.5. This feature is very imperative for scaffold materials used in bone regeneration. Biomaterials often require growth factors and mineralization agents for improved cell responses [174]. The present study showed that the developed PVA-AC composites formed mineralized nodules without the addition of any extra agents.

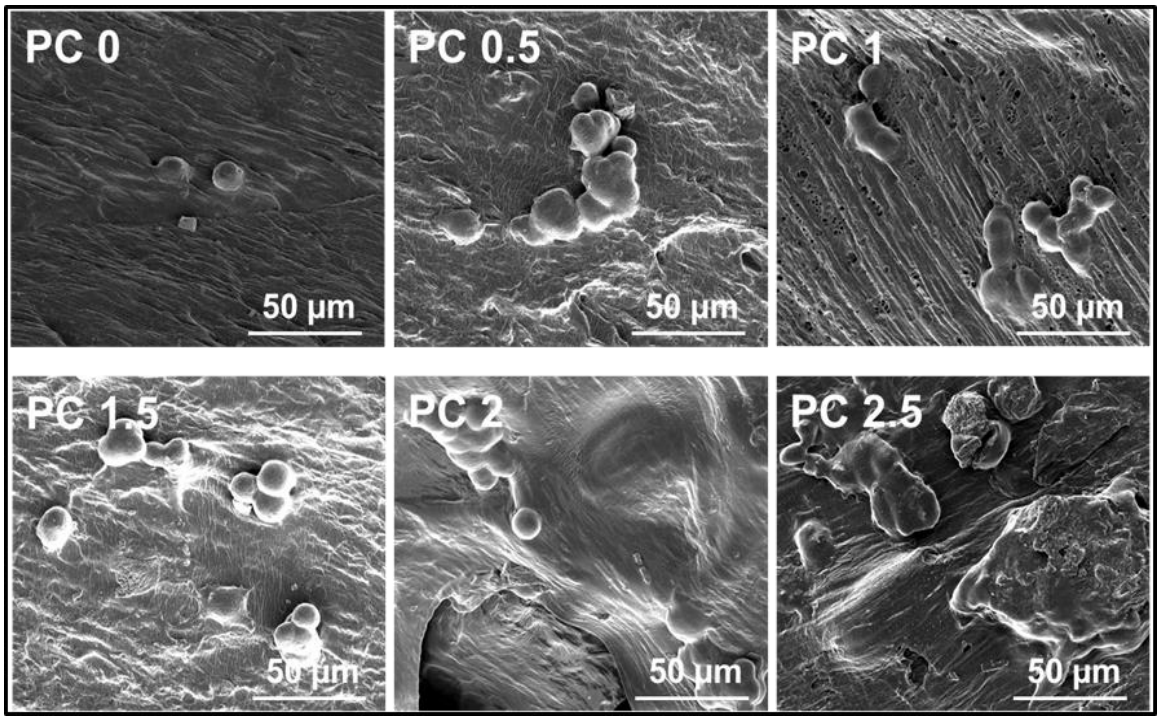

Fig. 4.20 FESEM micrographs of PVA-AC composites cultured with MG-63 cells.

4.1.14. Alkaline Phosphatase (ALP) activity

Alkaline phosphatase, an early and quantitative osteoblastic differentiation marker, is a key factor in the formation of hard tissue. The osteoblast cells mineralize bone matrix during their differentiation. The ALP helps in decreasing the concentration of extracellular pyrophosphate which is an inhibitor of mineralization, and it increases the inorganic phosphate concentration to promote mineral formation. Osteogenic differentiation of cells cultured on composites was estimated by quantifying ALP activity, and the results with respect to control (tissue culture plate) are shown in Fig. 4.21 (a-d).

As shown in Fig. 4.21 (a), the control showed the least ALP activity as compared to the PVA-nHA scaffolds. The ALP activity of cells grown on PVA-nHA composite scaffolds was higher than the PVA scaffold. With the addition of nHA, the ALP activity increases up to PHA 3 as the hydroxyapatite acts as a chelating agent for mineralization of osteoblast. There was a slight decrease in ALP activity with the further increase in nHA concentration which might be due to the less number of adhered cells on higher concentrations of nHA (PHA 4 and PHA 5) as demonstrated by cell viability study.

The addition of CNTs in polymer matrix resulted in significant up regulation of ALP activity in PVA-CNTs nanocomposites as compared to the PVA scaffold (Fig. 4.21 (b)). This increase might be attributed to the increase in surface roughness, hydrophobicity and hence, protein adsorption on the nanocomposite scaffolds. Watari et al. have also reported that the high protein adsorption with CNTs addition is responsible for improved osteoblast adhesion, growth and ALP activity [175]. With an addition of CNTs, the ALP activity increased up to PCN 1, whereas with further increase there was a slight decrease in ALP activity in PCN 1.5 due to the less number of adhered cells on higher concentrations of CNTs (PCN 1.5) as showed by MTT assay and FESEM results.

The ALP activity of the cells cultured on PGN scaffolds is shown in Fig. 4.21 (c). As expected, control (tissue culture plate) showed least ALP activity after 7 days of culturing. With the addition of GNPs, the ALP activity significantly improved in comparison to both control and pure PVA which suggested an osteogenic induction. Improved cell attachment and growth on the nanocomposite scaffolds as evidenced by MTT assay and cell

morphology results, exhibited an up-regulation of ALP activity. Better electric properties and surface topography of GNPs augment cell attachment and differentiation. A less number of not so well spread cells were observed on PGN 1.5 scaffold which led to less ALP activity on its surface.

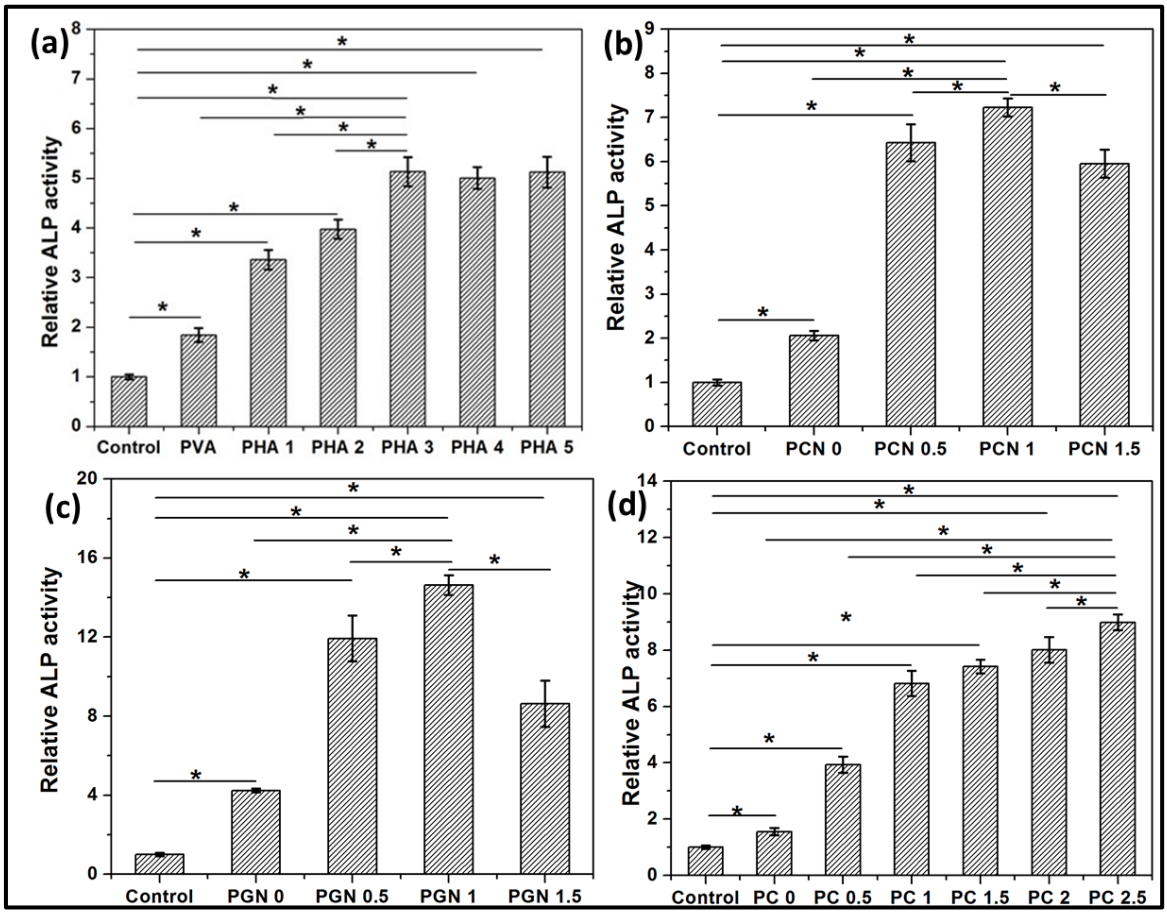

Fig. 4.21 ALP activity results of (a) PVA-nHA, (b) PVA-CNTs, (c) PVA-GNPs and (d) PVA-AC composites.

Fig. 4.21 (d) shows the ALP activity of PVA-AC samples with respect to the control (tissue culture plate). The control demonstrated the least ALP activity. The addition of AC in PVA matrix resulted in significant increase in ALP activity. The PC 2.5 sample showed highest ALP activity among all other composites. This increase might be due to the increase in surface roughness, protein adsorption and hence, cell adhesion with reinforcement of AC

in PVA matrix. Also, the hydrophilic nature of AC plays an important role in up-regulation of ALP activity of PC composites.

4.1.15. Mineralization assay

The calcium deposition on the samples cultured with cells indicates the matrix mineralization by osteogenic cell differentiation. The ARS based assay was performed to evaluate the matrix mineralization by quantifying calcium content on the developed composite samples, and the results are shown in Fig. 4.22 (a-d).

An increase in the concentration of ARS staining in PVA-nHA composites (Fig. 4.22 (a)) indicated a significant increase in calcium deposition and hence mineralization when compared to control. The results are consistent with SEM and ALP results. The control showed the least mineralization after staining. The mineralization was found to increase with an increase in nHA concentration up to PHA 3 composite scaffolds when compared to pure PVA scaffolds. The Ca^{2+} in HA might have contributed to this increase in osteoblast differentiation. The PHA 4 and PHA 5 samples showed a slight decrease in ARS staining indicating a reduction in mineralization. This might be due to direct contact of agglomerated HA particles with cells causing cell membrane damage *in-vitro*. Also, the crystalline nature and increase in hydrophobicity of PHA 4 and PHA 5 decreased the osteogenic differentiation, and hence less mineralization was observed.

As observed in PVA-CNTs scaffolds (Fig. 4.22 (b)), a significant increase in calcium deposition on nanocomposite scaffolds was observed after 7 days. The nanocomposite scaffold containing 1 wt% CNTs showed the highest amount of calcium deposition compared to other scaffolds. The researchers have reported the increased osteoblast attachment and differentiation on the surfaces containing hydroxyl and carboxyl groups [176]. These hydrophilic functional groups (-COOH, -OH) present on CNTs up regulated the ALP activity and matrix mineralization. However, the PCN 1.5 sample showed a slight decrease in ARS staining indicating the reduction in mineralization. The agglomeration of CNTs may expose a much less surface area for cells to interact, hence decreasing cell differentiation on PCN 1.5 scaffold.

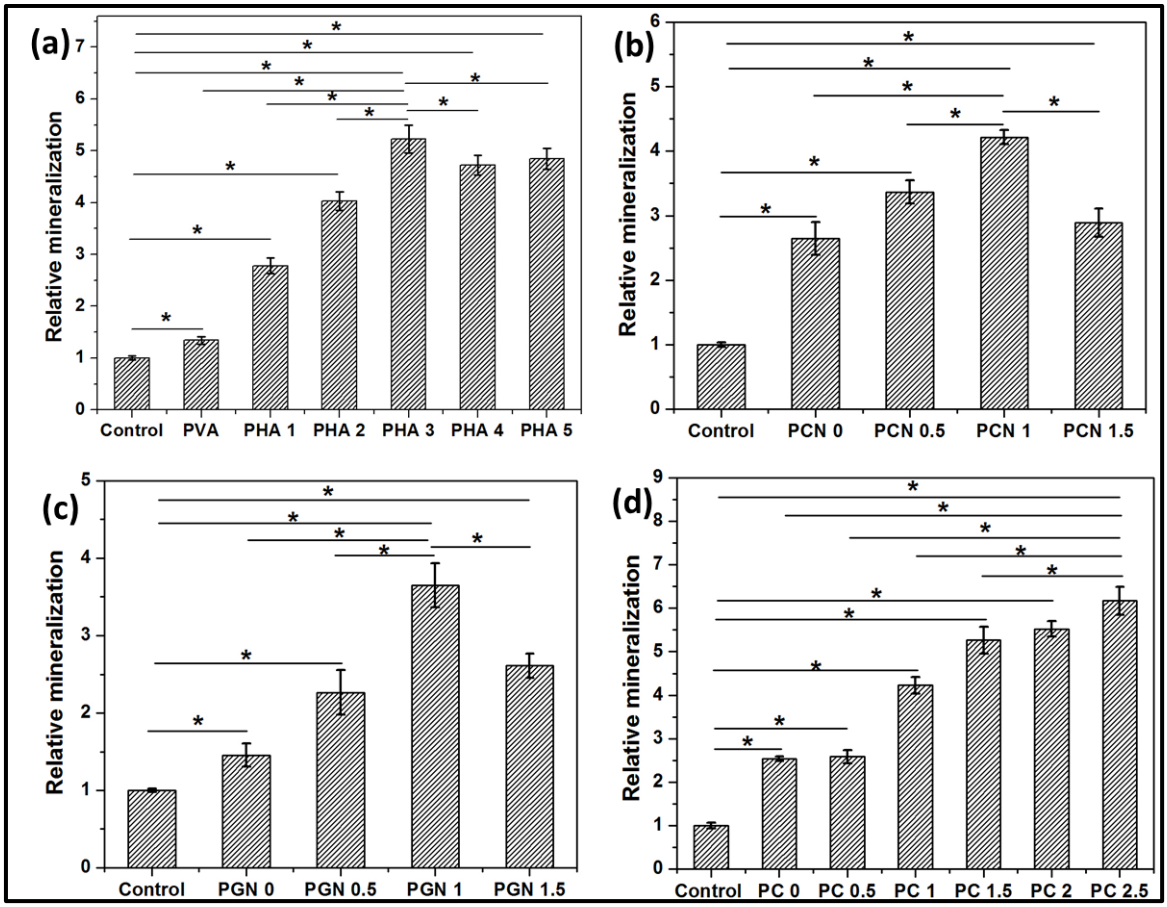

Fig. 4.22 Alizarin red stain assay results for (a) PVA-nHA, (b) PVA-CNTs, (c) PVA-GNPs and (d) PVA-AC composites.

A significant increase in calcium deposition was observed on PVA-GNPs scaffolds while control showed minimum deposition (Fig. 4.22 (c)). In particular, the scaffold containing 1 wt% GNPs exhibited the highest amount of calcium deposition. As serum proteins are known to directly mediate cellular proliferation and differentiation, this increase in matrix mineralization can be attributed to the ability of GNPs to adsorb more protein via π–π stacking. Graphene has an ability to pre-concentrate osteogenic inducers such as dexamethasone and β-glycerophosphate due to π–π stacking between the aromatic rings in the proteins and the basal plane of graphene [177]. The electrical conductivity of the GNPs could also be one of the reasons for improved mineralization. The agglomeration of abundant GNPs in PGN 1.5 scaffold adversely effected the cell proliferation and differentiation on scaffolds. Hence, the ALP activity and relative mineralization studies confirm that PGN 1 scaffold has osteogenesis promoting properties.

The Fig. 4.22 (d) shows the relative calcium deposition normalized to the control in PVA-AC scaffolds. These results were consistent with ALP results. As expected the control showed least calcium deposition after 7 days, and a significant increase in calcium deposition on PC composite scaffolds was observed. This increase in calcium deposition indicated the increase in encapsulated osteoblast mineralization. PC 0 and PC 0.5 showed almost same matrix mineralization, whereas a high mineral deposition was observed in all the other composites. Sample PC 2.5 showed highest cell differentiation as evidenced by ALP and mineralization assay results. Hence, the results showed that the addition of AC in polymer matrix makes the composites suitable as a scaffold material for bone tissue engineering.

4.2. Effect of 1D/2D/3D carbon structures

4.2.1. Scanning electron microscopy analysis

The cross-sectional surfaces of the PVA and PLGA based composites developed using threshold reinforcement concentration were also examined to investigate their cross-sectional morphology.

The FESEM micrographs of the cross-sectional surfaces of PLGA-carbon composite samples are shown in Fig. 4.23 (a-d). The PL (Fig. 4.23 (a)) surface was found to be smooth and flat, whereas, the addition of reinforcements in PLGA matrix made the composite surfaces relatively rough. This roughness is expected to improve the biological responses on composites. Nanomaterials like CNTs and GNPs tend to agglomerate in polymer matrices due to van der Waals forces. In the present study, carboxylic acid functionalized CNTs and GNPs were used; therefore, reinforcements were well dispersed in PLCN and PLGN samples and no agglomeration was observed (Fig. 4.23 (b-c)). Further, owing to the presence of oxygen containing groups, no agglomeration of AC in PLAC confirmed their well distribution throughout the matrix (Fig. 4.23 (d)). Hence, the FESEM results confirmed the successful reinforcement of carbon biomaterials in PLGA matrix.

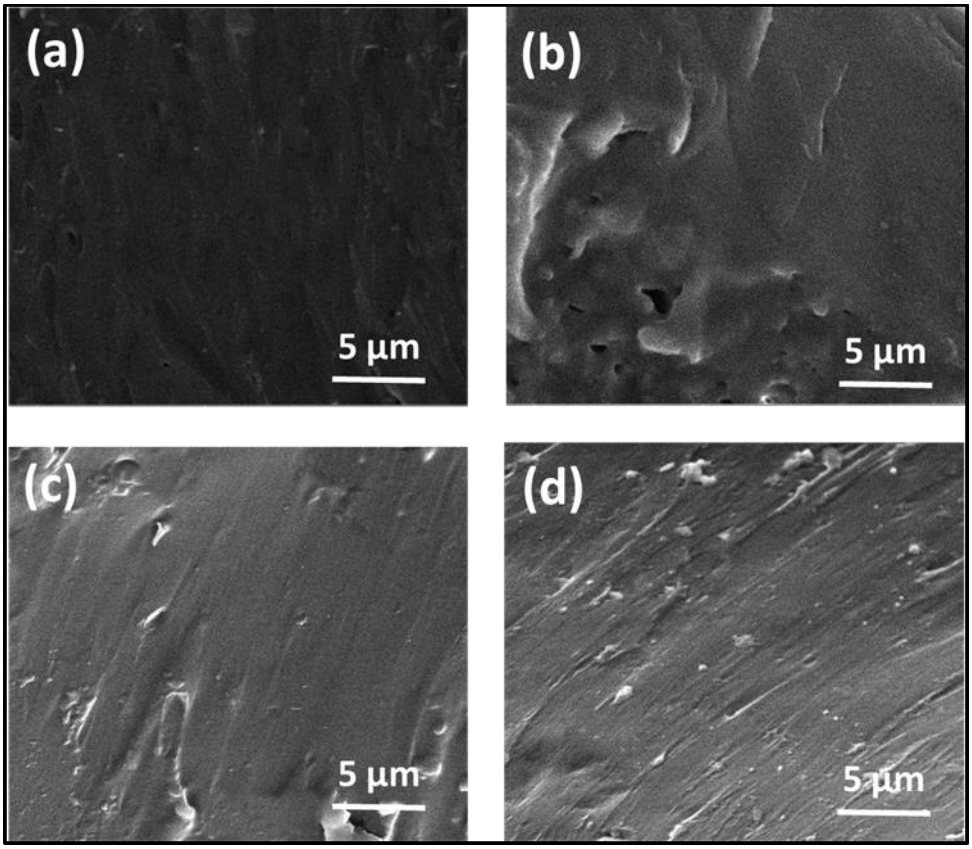

Fig. 4.23 FESEM micrographs of (a) PL, (b) PLCN, (c) PLGN and (d) PLAC composites.

The cross-sectional surfaces of various three component PVA-nHA-carbon composite scaffolds are shown in Fig. 4.24. The micrographs displayed the highly porous structure of all the composite scaffolds. However, all the scaffolds exhibited different pore size and shape. The PH scaffold showed larger but undefined pore structure, and the pore walls were crumbled in this sample. In contrast, the pore structure of carbon containing scaffolds was stable. The thick pore walls of PHCN and PHGN led to pore size of >100 µm which is highly suitable for osteoblast cells to migrate inside the scaffolds. Further, no agglomeration was observed in any of the scaffold. Hence, the obtained micrographs show that the developed scaffold structures are appropriate for osteoblast growth and proliferation.

The cross-sectional micrographs of PLGA-nHA based three component composites with and without carbon are shown in Fig. 4.25. The FESEM micrographs showed that the PLH sample has smooth surface. On the other hand, all the carbon containing samples were

comparatively rougher. This increased surface roughness is predicted to play an important role in enhancing the biological responses of these three component systems. In PLHCN and PLHGN composites, all the reinforced particles were wrapped in polymer matrix, whereas in PLHAC few particles were observed on the surface.

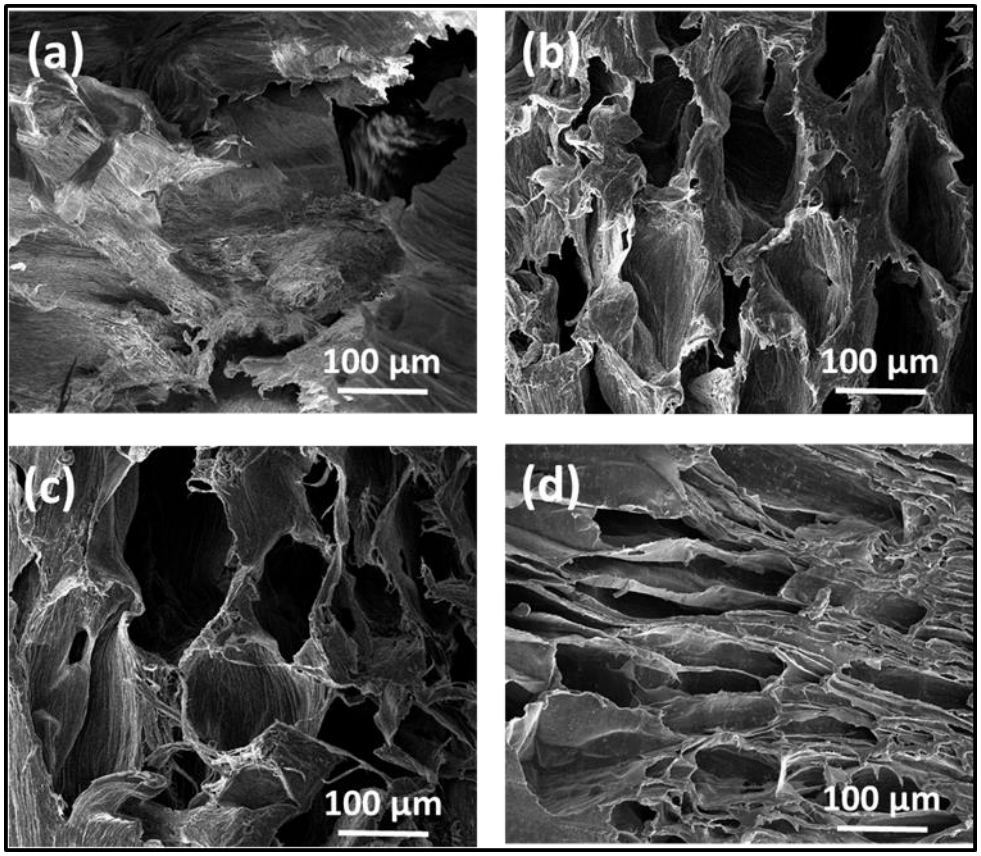

Fig. 4.24 FESEM micrographs of (a) PH, (b) PHCN, (c) PHGN and (d) PHAC composite scaffolds.

4.2.2. X-ray diffraction

The XRD patterns of all the composites developed after adding optimized concentrations of various reinforcements in both, PVA and PLGA composites are shown in Fig. 4.24 (a-c). As observed in the XRD patterns of PL and PLGA composites Fig 4.24 (a), PL showed a broad peak around 21° which confirmed the amorphous structure of PLGA. All the composite samples showed this characteristic peak of PLGA. However, the XRD pattern of PLCN composite did not reveal any characteristic peak for CNTs. This might be due to

its amorphous nature, less concentration and absence of CNTs at the surface of the composite. In contrast, both PLGN and PLAC composites displayed characteristic peaks for GNPs and AC, respectively.

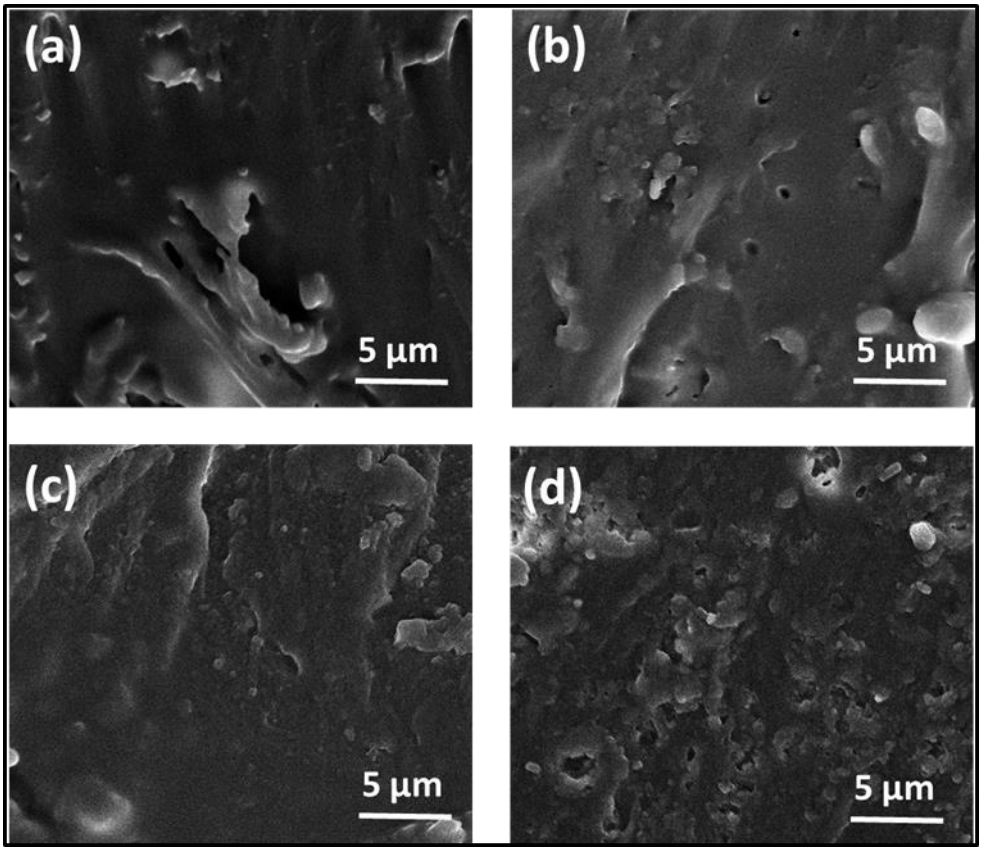

Fig. 4.25 FESEM micrographs of (a) PLH, (b) PLHCN, (c) PLHGN and (d) PLHAC composite scaffolds.

The XRD pattern of carbonaceous PVA-nHA composites are shown in Fig 4.26 (b). The PH composite showed all the characteristic peaks of both PVA (19.5°) and nHA (25.87°, 31.77° 32.1°, 32.90°, 34.04°, 39.7°, 46.6° and 49.4°). The reinforcement of CNTs and AC has not shown any change in the XRD pattern of PHCN and PHAC samples. This might be due to the amorphous nature (Fig. 4.6 (a)) and less amount of CNTs and AC as compared to the other two components (PVA and nHA) of the system. Further, in PHGN sample, a peak at 26.5° corresponding to the GNPs was observed along with the characteristic peaks for PVA and nHA.

The XRD pattern of PLGA-nHA composites with and without carbon reinforcements are shown in Fig. 4.26 (c). All the samples have shown a broad hump around 21° for PLGA and characteristic peaks for nHA. As described above, CNTs and AC have not shown any peak, whereas, GNPs have shown its characteristic peak at 26.5° corresponding to (002) plane.

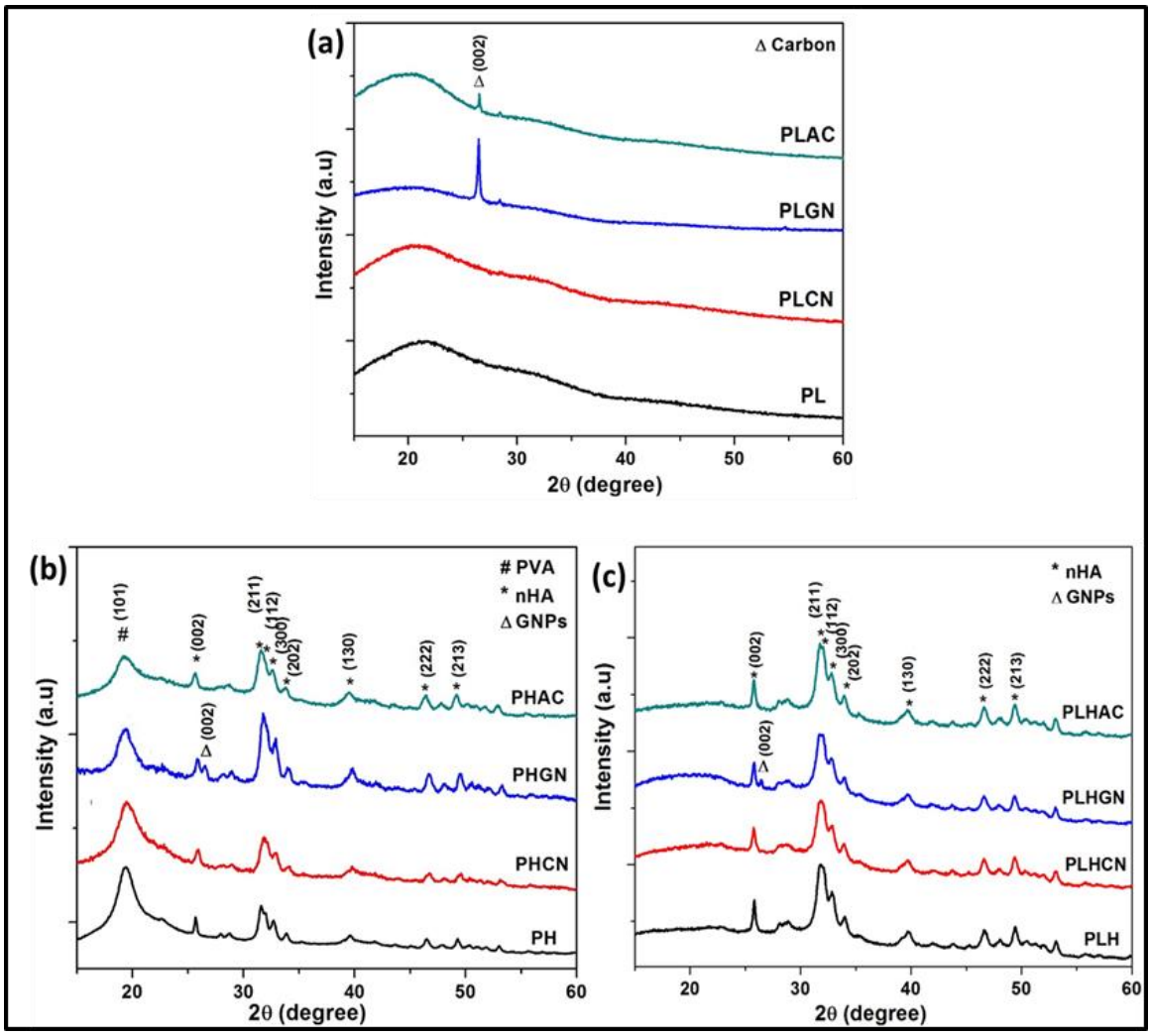

Fig. 4.26 XRD patterns of (a) PLGA-carbon, (b) PVA-nHA-carbon and (c) PLGA-nHA-carbon composites.

4.2.3. Fourier transform infrared spectroscopy

In order to investigate the intermolecular interactions in the composites FTIR analysis was carried out. The FTIR spectra and their respective FSD spectra are shown in Fig. 4.27 (a-

c) and Fig. 4.28. The chemical composition and intermolecular interactions in PLGA composites are shown in Fig. 4.27 (a). The pure PLGA (PL) sample showed sharp peaks at 1742 cm^{-1}, 1451 cm^{-1}, 1188 cm^{-1} and 1087 cm^{-1} attributing to C=O, C-H, C-O-C and C-O stretching, respectively. The above mentioned characteristic peaks for PLGA were also found in all PLGA composites. Additionally, PLCN and PLGN showed a sharp peak for C=O stretching at around 1682 cm^{-1} confirming the presence of carboxylic acid functionalized reinforcements in PLGA matrix. The O-H groups (3728 cm^{-1}) were also found in all the composites.

The FTIR spectra of PVA reinforced with optimized concentration of nHA and different carbon allotropes are shown in Fig. 4.27 (b). All the samples showed characteristic peaks for PVA and nHA, but the intensity of these peaks was slightly reduced with the addition of carbon in PHCN, PHGN and PHAC composites due to the strong interaction between PVA, nHA and carbon materials. In case of carbon reinforced composites, small peaks around 3728 cm^{-1} confirmed the presence of CNTs, GNPs and AC in PVA-nHA composites. The PH sample showed two peaks at 1083 cm^{-1} and 1030 cm^{-1} for C-O stretching and stretching vibration of PO_4^{3-} ions respectively. On the other hand, with the addition of carbon materials, one sharp peak at 1030 cm^{-1} was observed in carbonaceous composites along with a small peak at 1083 cm^{-1}.

The FTIR spectra of PLGA reinforced with optimized concentration of nHA and different carbon materials such as CNTs, GNPs and AC are shown in Fig. 4.27 (c). The PLH and carbon reinforced PLH samples showed characteristic peaks for pure PLGA and nHA as described earlier. Further, small peaks around 3728 cm^{-1} indicated the presence of O-H groups in the carbon reinforced composites, especially in PLHCN and PLHGN samples due to the carboxylic acid functionalized CNTs and GNPs.

4.2.4. Contact angle measurements

The wettability of the composite samples with the optimized reinforcement concentration was examined by performing contact angle measurements (Table 4.6). The PL sample showed a high water contact angle indicating its highly hydrophobic nature. This

hydrophobic nature of PLGA is a major concern as this could lead to its unfriendly behavior to cells and proteins [178].

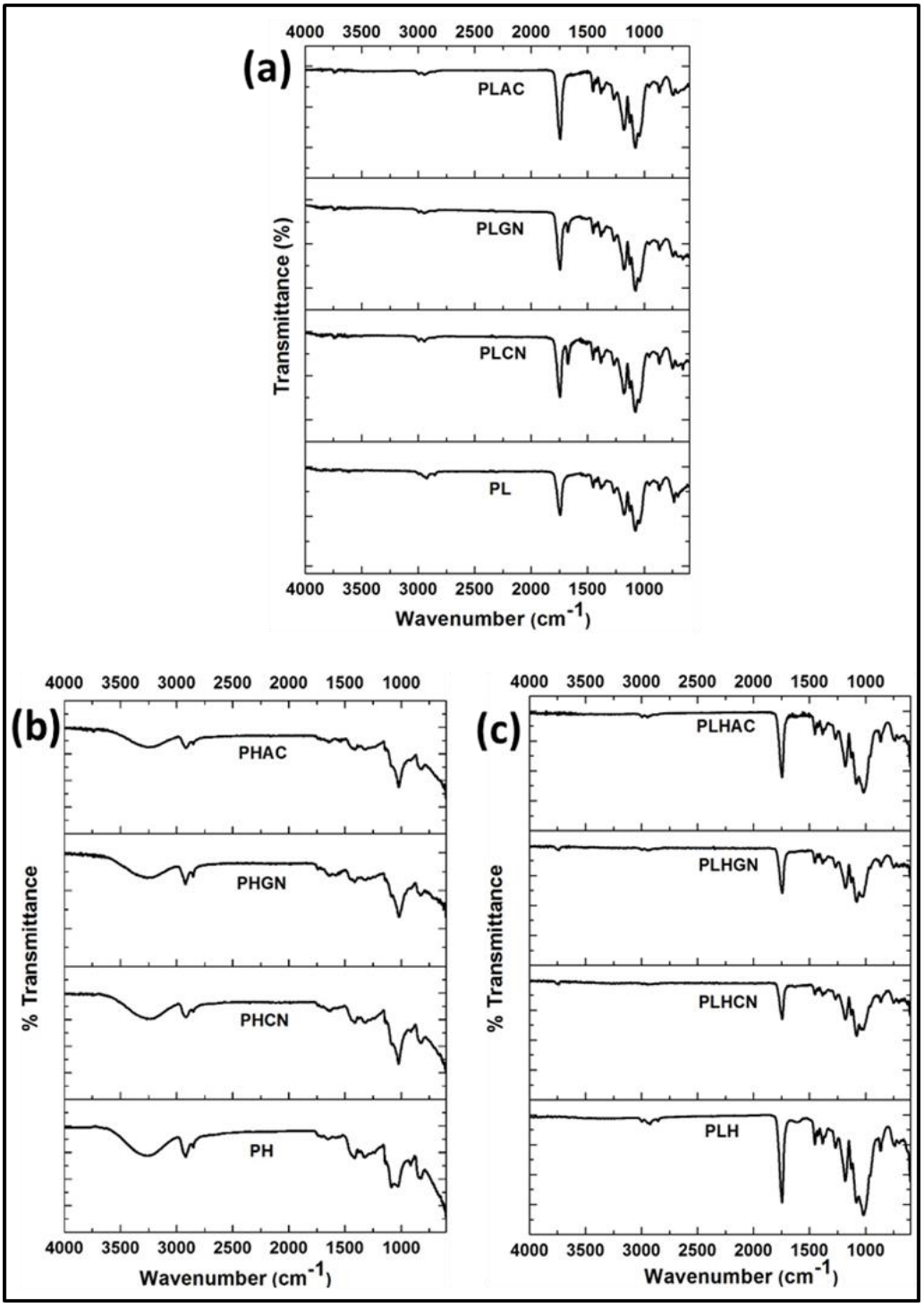

Fig. 4.27 FTIR spectra of (a) PLGA-carbon, (b) PVA-nHA-carbon and (c) PLGA-nHA-carbon composites.

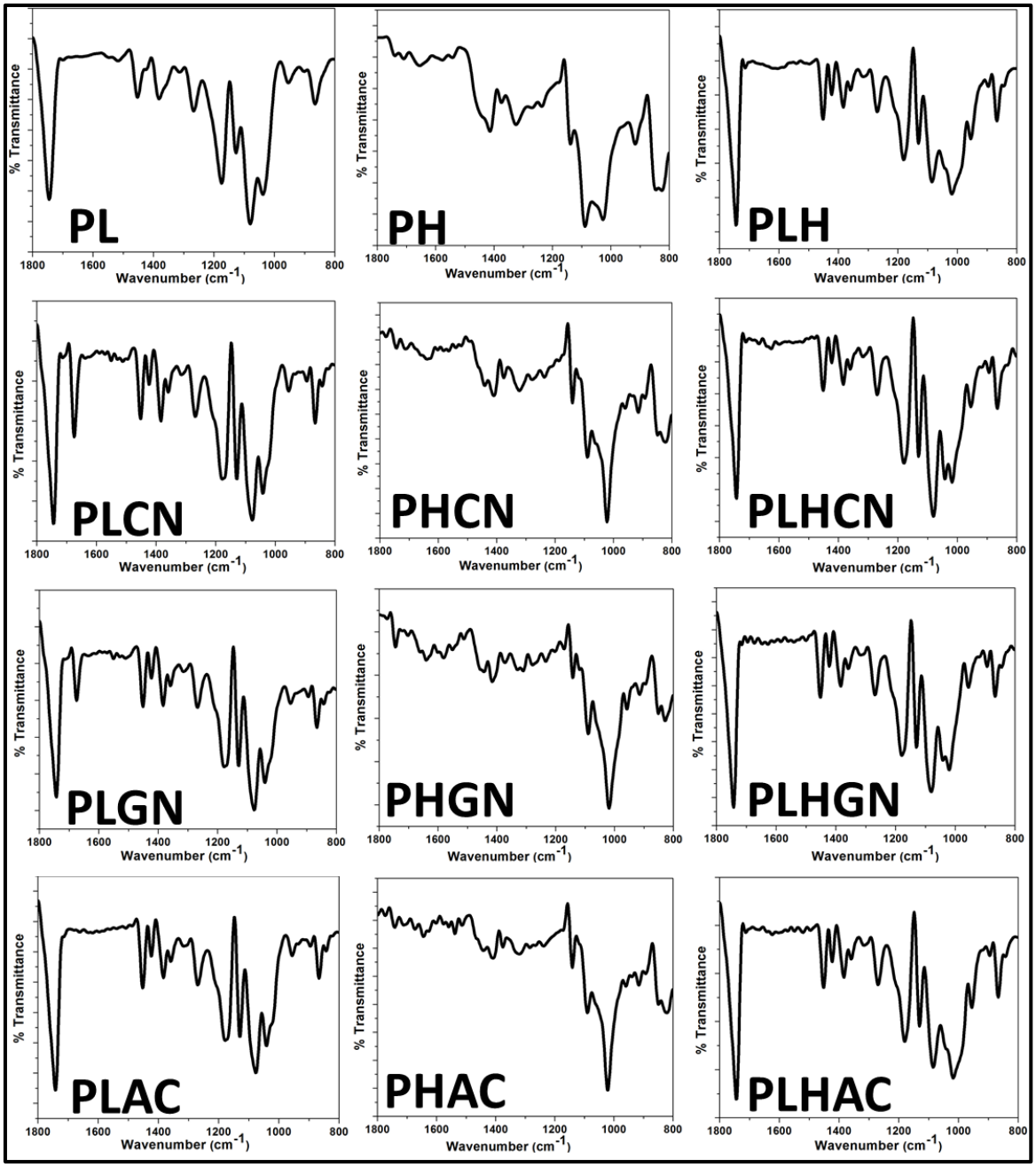

Fig. 4.28 FSD of the FTIR spectra of various composites.

A significant decrease in contact angle was obtained with the addition of carbon based reinforcements. The decrease may be owing to the comparative hydrophilic nature of carbon reinforcements exposed onto the composite surfaces. The oxygen containing functional groups in CNTs, GNPs and AC have hydrogen bond interactions with the water leading to decrease in contact angle and thus increase the hydrophilicity of the composites. Both, PLCN and PLGN showed almost similar contact angles i.e. 70° and 68° respectively,

whereas PLAC showed slightly higher contact angle (81°). This is due to the presence of more carboxyl acid groups on functionalized CNTs and GNPs than on AC used in this study.

Table 4.6 Average contact angles of different composites with threshold reinforcement concentrations.

Samples	Average contact angle (degree)
PLGA-carbon	
PL	94.97±6.50
PLCN	70.50±2.76
PLGN	68.87±3.12
PLAC	81.00±5.28
PVA-nHA-carbon	
PH	55.89±1.36
PHCN	61.24±2.87
PHGN	57.86±1.56
PHAC	63.01±2.78
PLGA-nHA-carbon	
PLH	85.53±3.23
PLHCN	67.14±2.45
PLHGN	62.34±2.98
PLHAC	70.47±2.89

In PVA-HA-carbon composites, carbon containing samples showed a slight increase in contact angle. This increase was not much significant due to the presence of less concentration of carbon materials. Furthermore, the concentration of nHA was same in all the composites, therefore, all the composites showed contact angle in the range of 55-63°.

In PLGA-nHA-carbon composites, the addition of carbon materials led to decrease in contact angle in all the composites making them hydrophilic in nature. The sample PLHGN showed the highest hydrophilicity with lowest contact angle values. As mentioned above, the oxygen containing functional groups in CNTs, GNPs and AC interact with the water leading to decrease in contact angle and thus increase the hydrophilicity of the composites. It can be seen that PLGA composites with nHA and carbon reinforcements showed higher hydrophilicity than the PLGA composites only with carbon. Therefore, the addition of nHA in PLGA matrix resulted in hydrophilicity.

Thus, the contact angle results suggest that all the developed composites have improved hydrophilicity which makes them suitable for proteins and cells attachment.

4.2.5. *In-vitro* swelling studies

The swelling behavior determines the infusion of nutrients and cellular products in the scaffold. It further affects the porosity, degradation and mechanical properties of scaffolds when implanted in the body. The swelling percentages of the developed composite samples are shown in Fig. 4.29 (a-c).

The *in-vitro* swelling degrees of the PLGA composite samples after 24 h of incubation in PBS are shown in Fig. 4.29 (a). As expected, pure PLGA showed least swelling percentage indicating its hydrophobic nature. The reinforcement of carbon biomaterials in PLGA matrix lead to increase in swelling percentage. This significantly improved swelling of all the composite samples is due to the oxygen containing functional groups on the surfaces of carbon reinforcements, which tends to absorbed more PBS increasing its swelling percentage. The PLGN composite showed highest swelling percentage (~40%) owing to the presence of more hydrophilic groups exposed on its larger surface area (due to sheet like structure of GNPs) when compared to PLCN and PLAC samples.

The effect of reinforcement of carbon biomaterials on swelling behavior of PVA-nHA composite scaffolds has been shown in Fig. 4.29 (b). The swelling results are in accordance with the contact angle results of PVA-nHA-carbon composites. The composite without carbon showed highest swelling degree. The addition of carbon biomaterials led to decrease in hydrophilicity of the composites resulting in decreased swelling percentage. Also, the less free volume for fluid uptake might have played a role in reducing the swelling percentage of the composites.

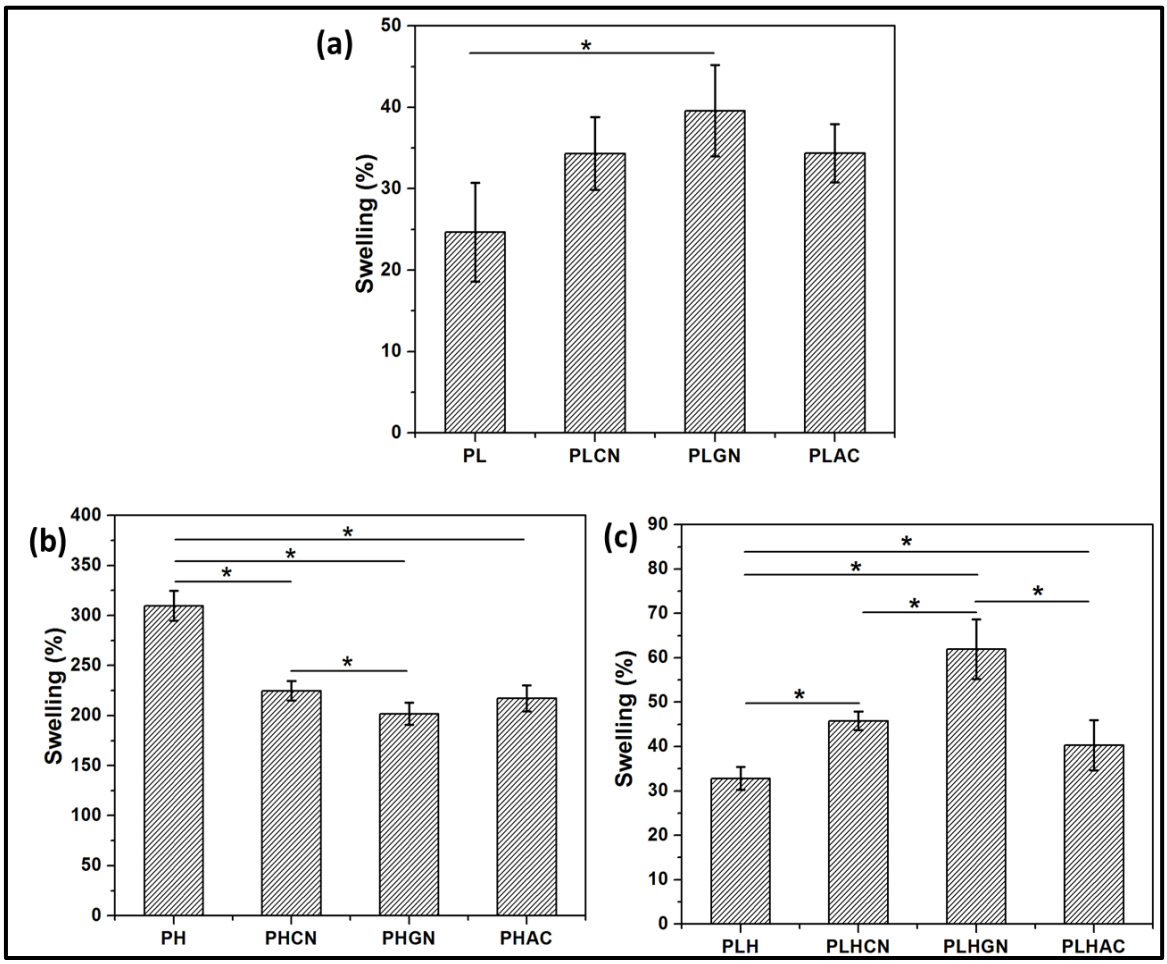

Fig. 4.29 Swelling studies of (a) PLGA-carbon, (b) PVA-nHA-carbon and (c) PLGA-nHA-carbon composites.

The swelling percentage of carbon reinforced PLGA-nHA composites after 24 h incubation in PBS is shown in Fig. 4.29 (c). The presence of hydrophilic functional groups on the carbon biomaterials resulted in increased swelling percentage of carbon reinforced

composites (PLHCN, PLHGN, PLHAC) when compared to PLH sample. These results are also supported by contact angle measurement values as the sample with lowest contact angle has shown highest swelling percentage value and vice versa. The PLHCN and PLHAC showed less swelling whereas, PLHGN composite showed highest swelling percentage (~60%) due to the presence of more hydrophilic groups on GNPs surface.

4.2.6. *In-vitro* degradation studies

The degradation rate of scaffold plays a significant role in engineering new tissue after implantation. Along with the percentage degradation (Fig. 4.30) of the developed composite samples, the rate of degradation was also modeled and their degradation kinetics was evaluated using power law:

$$-\frac{dM}{dt} = k_d M^n$$

where M is the mass of the sample, t is the time, k_d is the coefficient of the degradation rate and n denotes the order of the reaction. The plots are shown in the inset of the Fig. 4.30 and k_d values are given in Table 4.7 when the intercept was taken as zero.

The *in-vitro* degradation of the PLGA composites was evaluated and the results are shown in Fig. 4.30 (a). Initially, all samples showed slight reduction of weight for first few days. Similar to swelling studies, pure PLGA sample showed lowest degradation percentage. However, with the incorporation of carbon reinforcements in PLGA matrix, the degradation rate was accelerated. The k_d values showed that PLCN, PLGN and PLAC samples degraded almost 1.5, 1.7 and 1.3 times faster than the pure PLGA sample. All the samples showed first order kinetics as the plot of -ln (M_t/M_o) fitted linearly with respect to time. Until three weeks, all the composites showed almost same weight loss. After three weeks a dramatic increase in weight loss was observed in PLGN sample. The fast degradation process of the composite samples may be due to a higher interaction of carbon biomaterials with the PLGA matrix and the PBS. Also, the functionalized CNTs and GNPs create hydrophilic pockets in the composites which could fasten the hydrolytic degradation of PLGA. Further, the better interaction of sheet like structure of GNPs with PLGA matrix accelerated the degradation of PLGN composites. The degradation results are also

supported by results of swelling studies and contact angle. The increase in hydrophilicity of the composites speed up the degradation process leading to increased weight loss of composite samples.

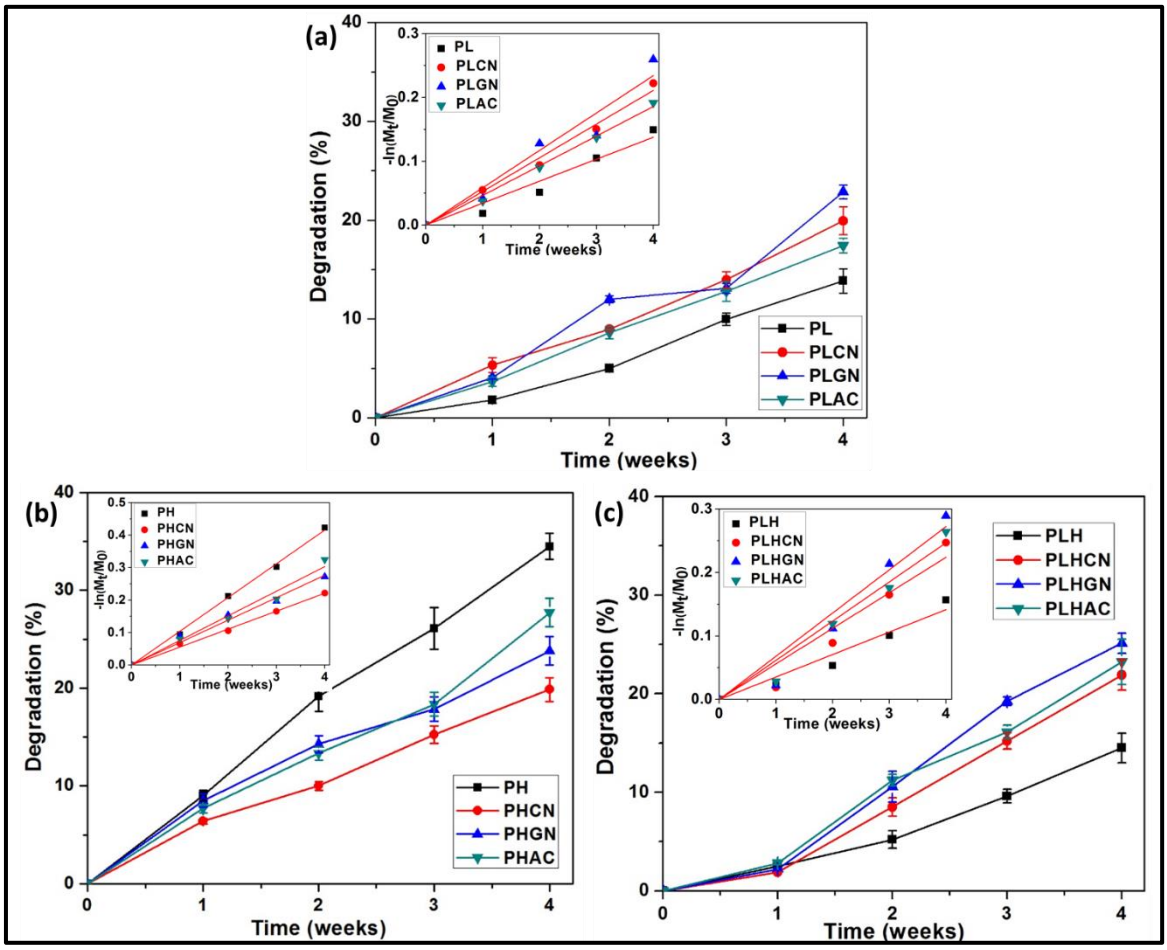

Fig. 4.30 Degradation studies of (a) PLGA-carbon, (b) PVA-nHA-carbon and (c) PLGA-nHA-carbon composites.

The results obtained from degradation studies of carbon reinforced PVA-nHA composites are shown in Fig. 4.30 (b) and the linear plot in inset shows that all the samples follow first order kinetics. The PVA-nHA (PH) composite without any carbon reinforcement showed highest degradation rate, whereas the carbon reinforced composites had comparatively lower degradation. As shown by the k_d values (Table 4.7), PHCN, PHGN and PHAC showed 1.88, 1.5 and 1.37 times lower degradation rate than the PH sample. The decrease in hydrophilic nature of the composites with the reinforcement of carbon materials reduced

the PBS uptake and hence delayed the degradation of the polymer backbone in composites. Among carbon reinforced PVA-nHA composites, PHCN showed lowest and PHAC showed the highest percentage of degradation. This is due to the high adsorption properties of the reinforced AC when compared to GNPs and CNTs.

Table 4.7 Degradation rate coefficient for the developed composites.

Sample	**k_d (h^{-1}) ($x10^{-3}$)**	**Adj. R-Square**		**Sample**	**k_d (h^{-1}) ($x10^{-3}$)**	**Adj. R-Square**
PLGA-carbon composites				**PVA-nHA-carbon composites**		
PL	0.204	0.975		PH	0.618	0.999
PLCN	0.313	0.995		PHCN	0.328	0.998
PLGN	0.348	0.972		PHGN	0.411	0.993
PLAC	0.276	0.997		PHAC	0.450	0.991
PLGA-nHA-carbon composites						
PLH	0.210	0.978				
PLHCN	0.333	0.968				
PLHGN	0.404	0.972				
PLHAC	0.366	0.983				

Further, the degradation studies of carbon reinforced PLGA-nHA composites were performed (Fig. 4.30 (c)). As expected the PLH sample showed lowest percentage degradation due to hydrophobic nature of both PLGA and nHA. The addition of carbon materials increased the degradation rate of the composites due to the improved hydrophilicity and water absorption. For all the samples, the degradation rate coefficients

were consistent with the degradation trend and the samples showed first order kinetics. The samples PLHCN, PLHGN and PLHAC exhibited 1.6, 1.9 and 1.7 times faster degradation than the PLH sample. The highest degradation rate of PLHGN shows that GNPs have hydrophilic groups which created hydrophilic pockets in the composites to absorb fluids and degrade the sample faster than other samples.

4.2.7. *In-vitro* hemocompatibility studies

Hemocompatibility is one of the most important properties to be evaluated for a scaffold material as they interact with blood and may cause cell damage. The hemolysis study was performed for all the samples and the results are shown in Table 4.8.

The percentage hemolysis values for PLGA-carbon, PVA-nHA-carbon and PLGA-nHA-carbon composites varied in the range of 0.90-1.32%, 0.82-1.09% and 1.06-1.44% (Table 4.8). The PL, PH and PLH samples showed least hemolysis, and found to increase for the carbon reinforced composites. This increase in hemolysis percentage is due to the roughness induced by carbon reinforcements. Further, it has been observed that CNTs reinforced PLGA, PLGA-nHA and PVA-nHA composites have shown higher hemolysis values when compared to AC and GNPs reinforced composites. This might be due to the toxic impurities retained during CNTs synthesis. However, the increase was not much significant, and the results for all the samples were in the permissible limit (<5%). According to the ISO 10993-4 standard, hemocompatible biomaterial having up to 5% hemolysis is permissible [179]. The percentage hemolysis values for all the samples were less than 5% showing the hemocompatible nature of the prepared composite scaffolds.

4.2.8. *In-vitro* mineralization activity studies

To mimic the *in-vivo* bond bonding ability of the developed scaffolds, *in-vitro* bioactivity studies were performed by soaking samples in SBF for 21 days. As confirmed by FESEM results (Fig. 4.31 (a)), the PL sample showed very less amount of apatite formed. On the contrary, a thick layer of apatite was observed on all the composite samples after 21 days. The presence of oxygen functionalities on the surface of different carbon reinforcements improved the bioactivity of the composites.

Table 4.8 Percentage (%) hemolysis of different composites.

Samples	Hemolysis (%)
+ve control	100
-ve control	0
PLGA-carbon	
PL	0.90±0.01
PLCN	1.32±0.09
PLGN	1.02±0.11
PLAC	1.12±0.04
PVA-nHA-carbon	
PH	0.82±0.06
PHCN	1.09±0.11
PHGN	1.02±0.08
PHAC	1.08±0.03
PLGA-nHA-carbon	
PLH	1.06±0.02
PLHCN	1.44±0.05
PLHGN	1.11±.06
PLHAC	1.41±0.06

The carboxyl groups present on the functionalized CNTs and GNPs trigger the apatite formation, leading to more bioactivity of PLCN and PLGN. Similarly, PLAC also showed good bioactivity. The characteristic XRD peaks (Fig. 4.31 (b)) for hydroxyapatite were obtained at 26° and 32°. The homogeneous layer of apatite on all the composites also confirmed the proper dispersion of reinforcements in the PLGA matrix demonstrating that the presence of carbon based biomaterials triggers the self-assembly of apatite.

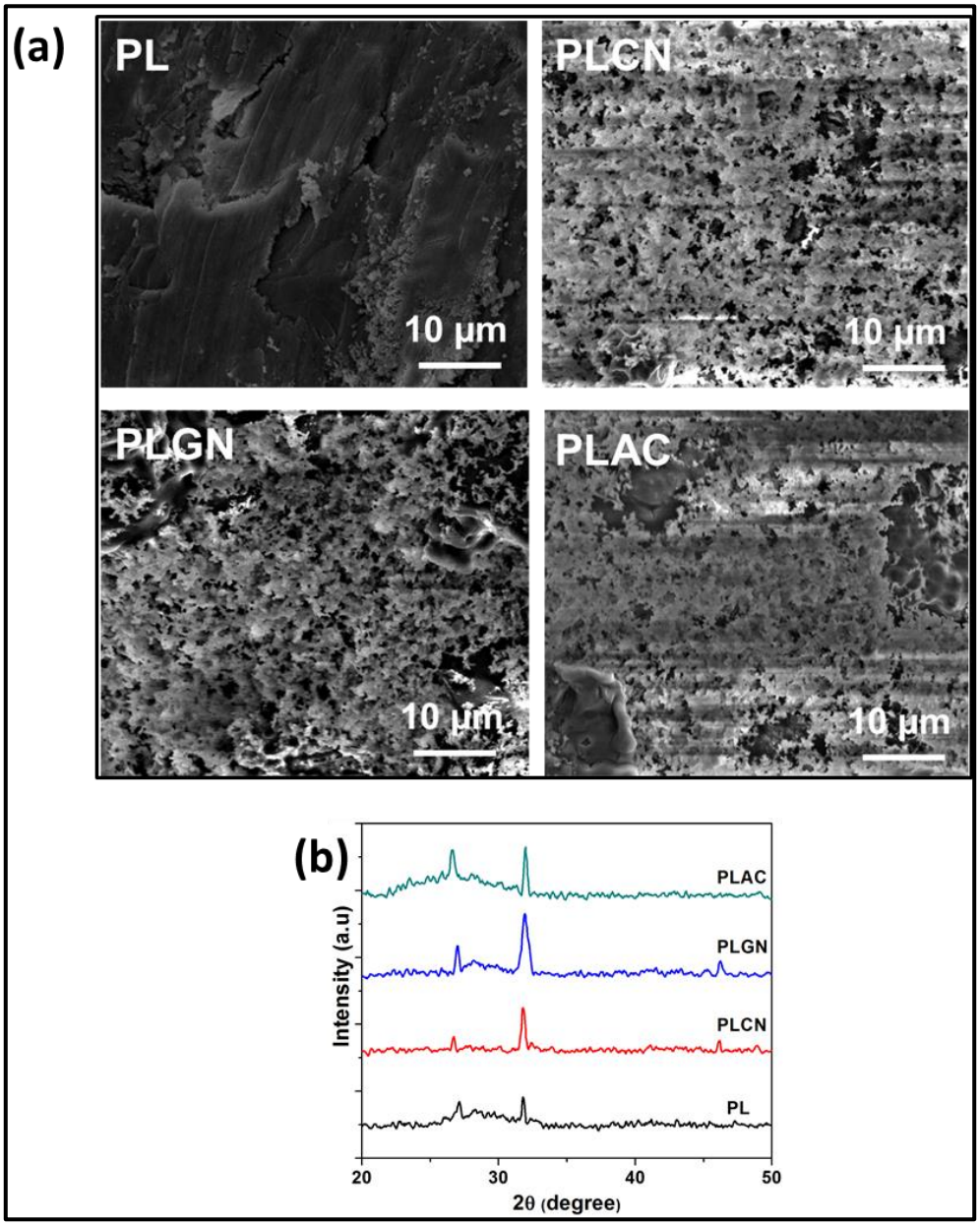

Fig. 4.31 (a) FESEM micrographs and (b) XRD spectra of carbon reinforced PLGA composite scaffolds after immersion in SBF for 21 days.

The FESEM micrographs of PVA-nHA-carbon composites after immersion in SBF for 21 days are shown in Fig. 4.32 (a) and it was observed that all the samples showed formation of apatite layer. Reinforcement of nHA in PVA supports the apatite formation as PVA alone does not support it much. The crystalline nHA increases the apatite formation. Further, the addition of carbon reinforcements makes the scaffold surface more suitable for apatite formation. The functional groups on the reinforcement's surface act as a nucleation point for ionic clusters and deposit Ca^{2+} and PO^{4-} ions from the SBF. Micrograph of PVA-nHA-GNPs (PHGN) scaffold showed dense and homogeneous apatite formation when immersed in SBF which is due to proper dispersion of nHA and GNPs in PVA matrix leading to more apatite growth in SBF. The sharp peaks at 26°, 32° and 46° in the XRD spectra (Fig. 4.32 (b)) of all the samples confirmed the apatite formation.

It has been shown already that pure PLGA has poor bioactivity. However, to enhance its bioactivity various bioactive materials can be reinforced in the PLGA matrix. The FESEM micrographs of nHA and carbon reinforced PLGA composites after immersion in SBF are shown in Fig. 4.33 (a). It has been observed that all the samples showed apatite formation, but PLH showed very less apatite deposition. On the other hand, the apatite formation on carbon containing samples was more and homogeneous which might be due to the synergistic effect of nHA and carbon reinforcements. A thick layer of apatite was observed on both PLHCN and PLHGN samples. The presence of negatively charged functional groups in nHA and carbon reinforcements trigger the apatite formation. Fig. 4.33 (b) shows the XRD spectra of the samples after incubation in SBF. The spectra displays the characteristic peaks of apatite at around 26°, 32° and 46°. Thus, the results exhibit that the presence of nHA and carbon based biomaterials with oxygen functionalities elicits the self-assembly of apatite.

4.2.9. Protein adsorption studies

When implanted, different proteins from physiological fluid get adsorbed on the surface of the scaffold and mediate biological responses. These adsorbed proteins further help in cell attachment, proliferation and growth on the scaffold surface. The protein adsorption is influenced by factors like surface chemistry, wettability, surface roughness and surface

charge. The BSA adsorption on composite scaffolds was evaluated by Bradford assay (Table 4.9).

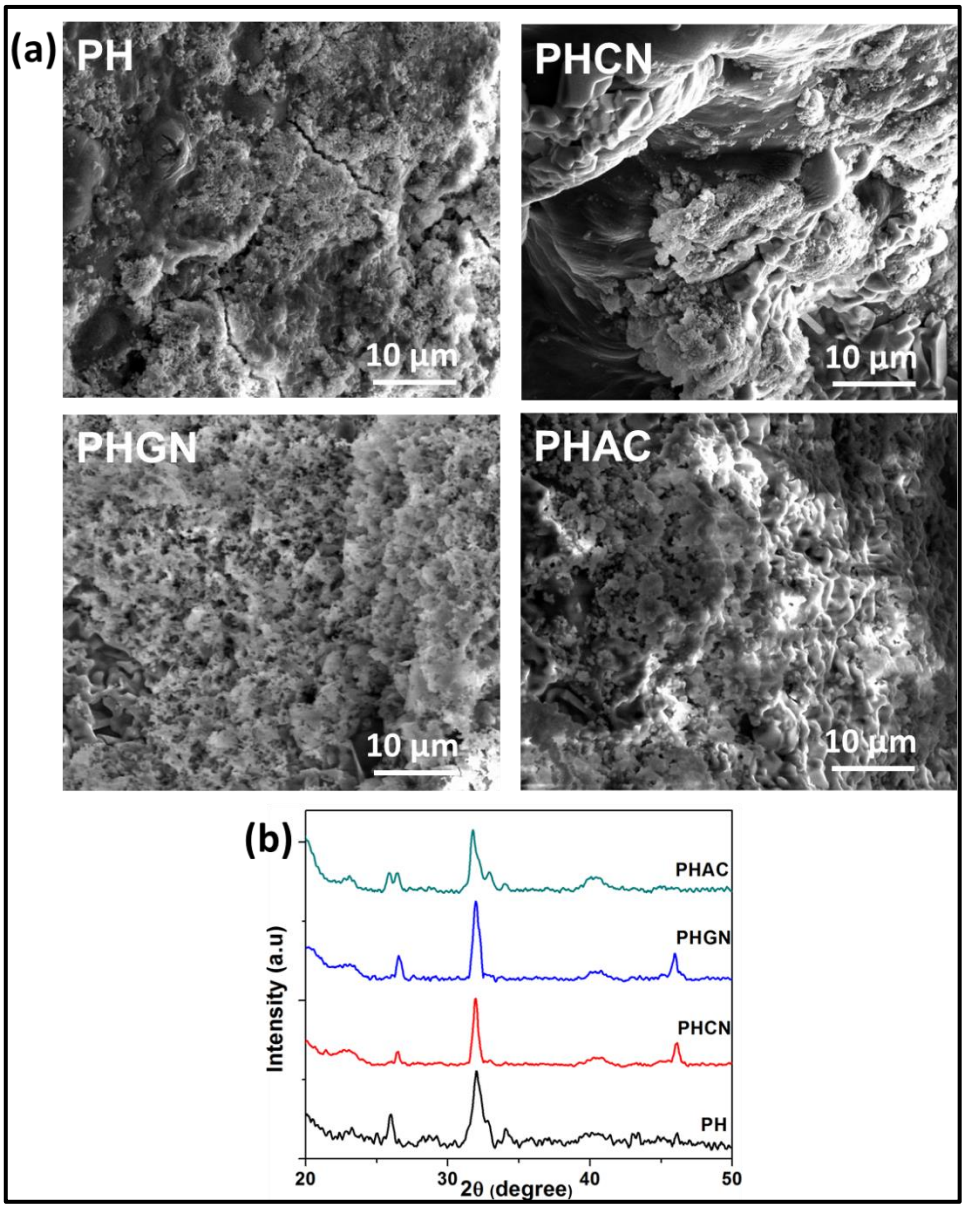

Fig. 4.32 (a) FESEM micrographs and (b) XRD spectra of carbon reinforced PVA-nHA composite scaffolds after immersion in SBF for 21 days.

The PL sample showed least protein adsorption, however an increase was observed on PLGA reinforced with carbon materials. The oxygen functionalities present on the surface promoted the protein adsorption of composites [170, 180]. This might be due to the

interaction of surface hydrophilic groups with the functional groups of BSA via van der Waals and electrostatic forces.

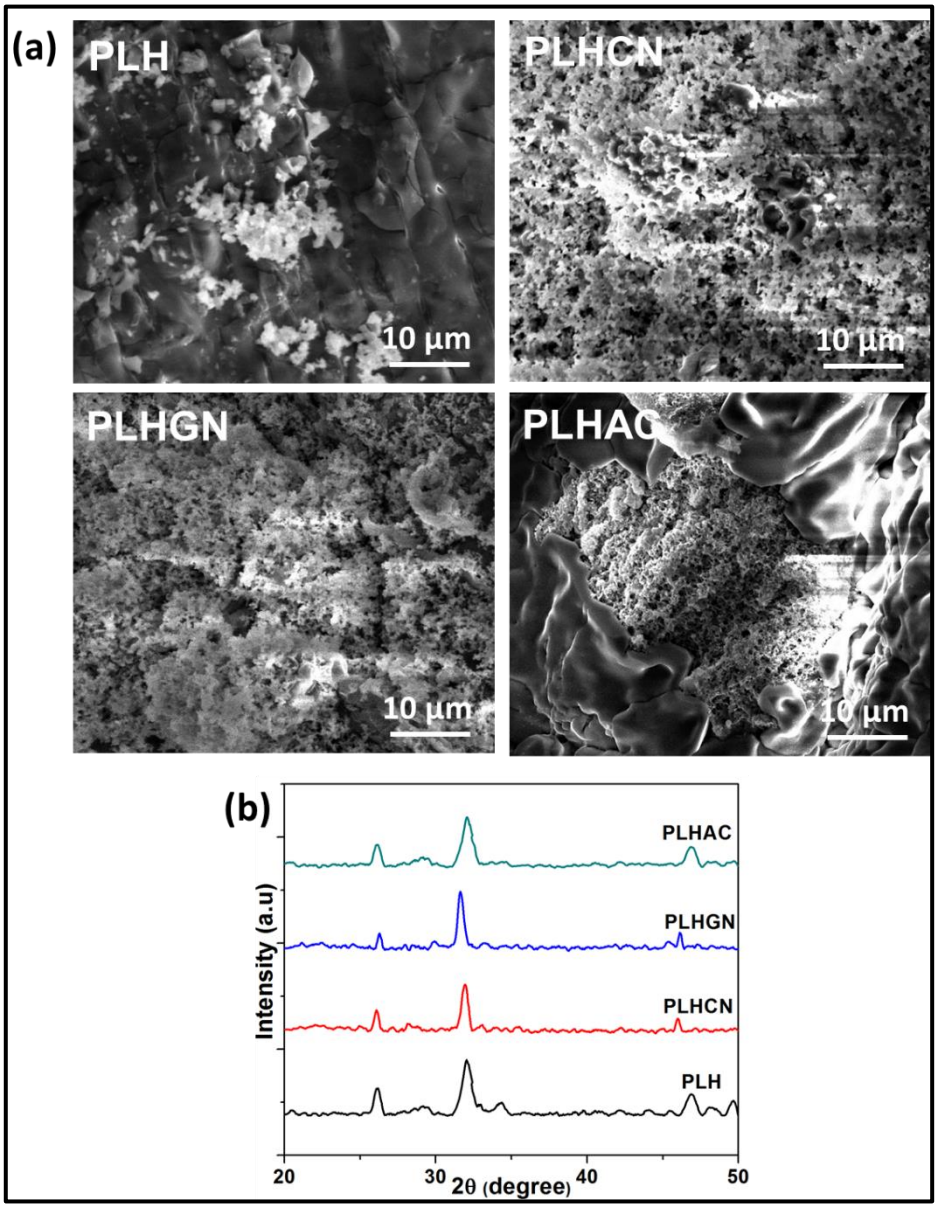

Fig. 4.33 (a) FESEM micrographs and (b) XRD spectra of carbon reinforced PLGA-nHA composite scaffolds after immersion in SBF for 21 days.

Carbon nanomaterials like CNTs and GNPs have induced more protein adsorption on PLCN and PLGN composites as the π electron cloud present on these graphite structures interact with the hydrophobic part of BSA proteins. Also, the presence of more functional groups on the sheet like (2D) structure of GNPs resulted in the highest protein adsorption

on PLGN samples. The protein adsorption on PLAC was almost similar to that on PLCN. The high adsorption properties of AC played an important role in such results.

Table 4.9 Protein adsorption on different composites.

Samples	Protein adsorbed (µg/ml)
PLGA-carbon	
PL	256.15±17.02
PLCN	326.23±10.56
PLGN	357.40±10.23
PLAC	325.12±20.25
PVA-nHA-carbon	
PH	482.52±16.06
PHCN	535.71±10.18
PHGN	527.1±20.08
PHAC	489.73±19.03
PLGA-nHA-carbon	
PLH	494.39±20.02
PLHCN	546.18±10.03
PLHGN	559.75±7.35
PLHAC	503.30±25.97

Further, the addition of nHA in PVA matrix along with different carbon materials significantly increased the protein adsorption. Both PH and PHAC showed almost similar protein adsorption. The high concentration of nHA might have suppressed the absorption properties of the AC in composite. Similarly, the protein adsorption on PHCN and PHGN was also not significantly different. The nHA reinforcement in carbonaceous PLGA composites significantly improved their protein adsorption. Among all the composites PLHGN showed the highest absorption of BSA. This is due to the synergistic effects of nHA and GNPs. It has been explained above that the addition of nHA and GNPs make the scaffold surface suitable for protein adsorption.

All the composite scaffolds have shown higher protein adsorption when compared to pure polymer matrices (PVA and PLGA). With the addition of fillers in polymer matrix, the surface roughness has been introduced to the scaffolds. The rough scaffolds provide a larger surface area to interact with the protein molecules. Also, PBS is a high ionic strength buffer that enhances these interactions between proteins and scaffold surface. Thus, the existence of nHA and carbon biomaterials in polymer matrix improved the protein adsorption on composites making them suitable for cell attachment.

4.2.10. Tensile properties

The mechanical properties of pure PLGA, PVA-nHA-carbon and PLGA-nHA-carbon composites were assessed by tensile strength, Young's modulus, and energy at break (Table 4.10). It was noticed that all the carbon reinforced PLGA composites demonstrated a significantly higher tensile strength when compared to pure PLGA sample. The addition of 1 wt% of CNTs, GNPs, and 2.5 wt% of AC in PLGA matrix resulted in 1.6, 2.0 and 1.3 folds increase in tensile strength of composites, respectively. Similarly, Young's modulus and energy at break were also found to increase making the composites stiffer and tougher in comparison to pure PLGA. The PLAC sample showed weaker tensile properties in comparison to other two composites. This might be due to the better dispersion of functionalized nano sized CNTs and GNPs in PLGA matrix. Also, the functional groups present on the surface of CNTs and GNPs form a hydrogen bond with the matrix and augment the interfacial adhesion. Further, PLGN composite showed 2.1 and 1.7 folds increase in Young's modulus and energy at break respectively, when compared to PL

sample. The 2D platelet structure of GNPs provides larger interface for effective load transfer between PLGA matrix and reinforcement in PLGN composites.

Table 4.10 Mechanical properties of different composites.

Samples	Tensile strength (MPa)	Young's modulus (MPa)	Energy at break (mJ)
PLGA composites			
PL	5.76±0.09	132.95±9.11	154.76±9.30
PLCN	9.62±0.8	275.67±19.13	228.43±10.70
PLGN	11.56±0.59	289.89±21.27	265.91±15.89
PLAC	7.85±1.58	216.28±23.07	202.83±12.86
PVA-nHA-carbon			
PH	6.78±0.63	197.16±6.83	48.54±3.14
PHCN	19.44±1.08	279.85±12.84	97.72±3.86
PHGN	21.49±1.57	285.74±13.95	102.24±5.63
PHAC	13.86±1.93	40.99±4.72	232.93±89.32
PLGA-nHA-carbon			
PLH	5.90±0.02	109.20±4.25	27.56±1.73
PLHCN	10.05±0.63	844.75±35.42	68.73±4.34
PLHGN	15.72±0.75	936.83±42.86	162.50±82.64
PLHAC	7.50±0.25	585.07±22.59	123.12±7.83

Further, the carbon reinforced PVA-nHA composites were assessed for their mechanical properties. The nHA reinforced PVA composite without carbon showed weakest tensile properties among all the PVA-nHA-carbon composites. As expected, the addition of carbon increased the mechanical properties of the composites many folds. Both tensile strength and Young's modulus were high for PHCN and PHGN as compared to PHAC samples. However, PHAC showed the highest energy at break. This shows that PHAC sample is soft but tough which makes it unsuitable for bone tissue engineering applications.

The mechanical properties of PLGA-nHA without and with carbons were assessed. The addition of different carbons i.e. CNTs, GNPs and AC in PLGA-nHA composite matrix resulted in 1.7, 2.66 and 1.27 folds increase in tensile strength of composites, respectively. The improvements in Young's modulus and energy at break made these composites stiffer and tougher in comparison to PLGA-nHA composite without carbons. The high energy at break and low tensile strength of PLHAC in comparison to PLHCN showed its comparatively soft but tough nature. The superior tensile properties of all the composites indicate the better dispersion of reinforcements in PLGA matrix. Though all the carbon reinforcements were found to improve the mechanical strength of composites, GNPs showed best results owing to its sheet like structure that provides larger interface for effective stress transfer between polymer matrix and reinforcement.

4.2.11. Cell viability

The MTT assay results of MG-63 cells cultured on PLGA composites are normalized and shown in Fig. 4.34 (a). It is evident from the results that all the samples including pure PL and PLGA composites, improved the cell metabolic activity when compared to control plate. Further, the cell viability of all the carbon reinforced PLGA composites was higher than that of pure PLGA samples. The trypan blue assay results are shown in Fig. 4.35 (a-b). The total cell count was found to be higher on all the carbon reinforced samples (PLCN, PLGN and PLAC) than the control plate and pure PL samples. This shows that the reinforcement of carbon biomaterials encourage the cell attachment and growth on the composite surfaces. The hydrophilic functional groups present on the carbon reinforcements improve the protein adsorption which further increases the cell adhesion and growth. The cells viability was highest on PLGN composites which might be due to

the fast proliferation of the cells on PLGN sample as compared with PLCN and PLAC samples.

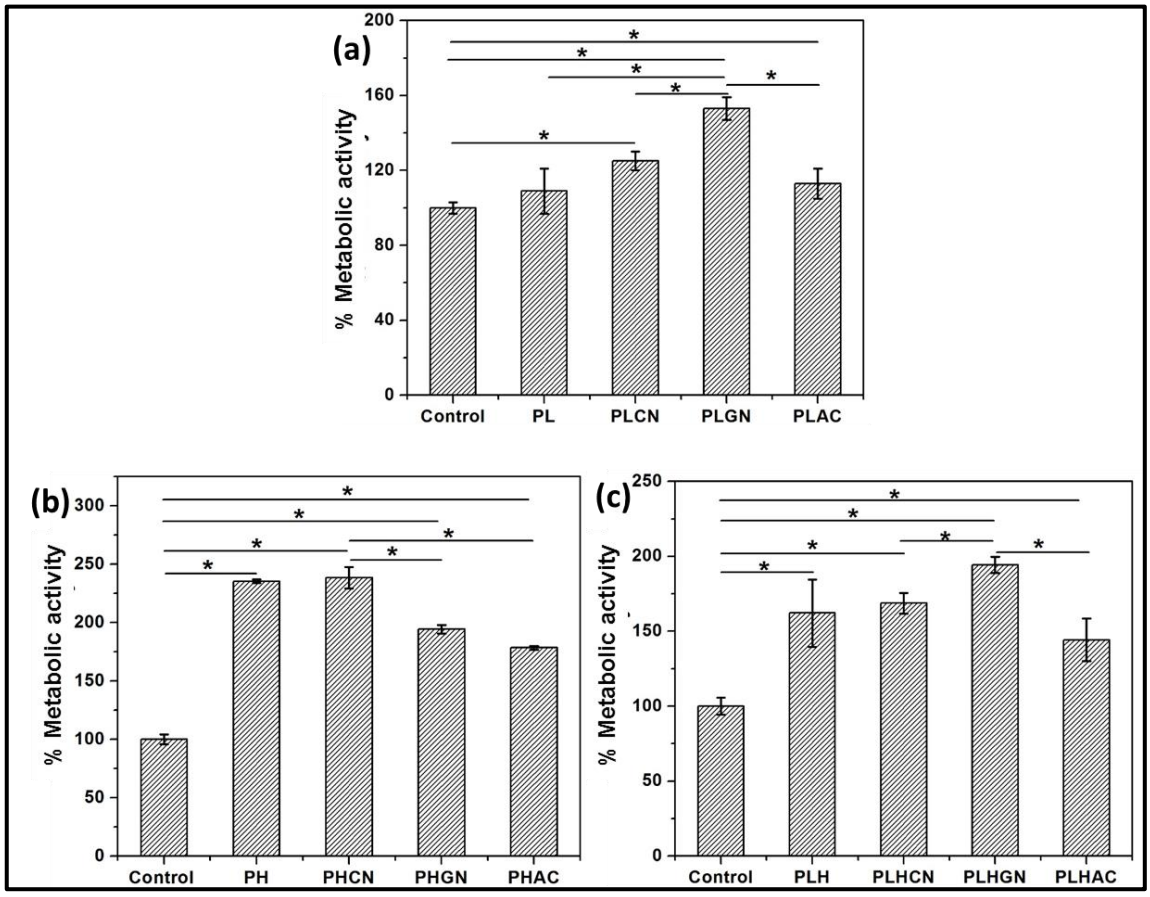

Fig. 4.34 MTT assay results of (a) PLGA-carbon, (b) PVA-nHA-carbon and (c) PLGA-nHA-carbon composites.

The cell viability results of MG-63 cells cultured on carbon reinforced PVA-nHA composites are shown in Fig. 4.34 (b) and 4.35 (c-d). Though all the scaffolds showed better percentage cell viability in MTT assay results, the PH and PHCN samples showed more than double cell viability (%) in comparison to control. The higher surface area to volume ratio of nHA and carbon reinforcements offers more space for the proteins and hence, cells to attach and proliferate. In the samples PHGN and PHAC, the cell viability was found to decrease. This might be due to the differentiation of cells in these scaffolds leading to reduced cell proliferation on PHGN and PHAC. Similarly, the total cell count was also found to increase in PH and PHCN samples, whereas a reduction was observed in

both, PHGN and PHAC samples. However, no significant difference was observed in live cells to total cells ratio.

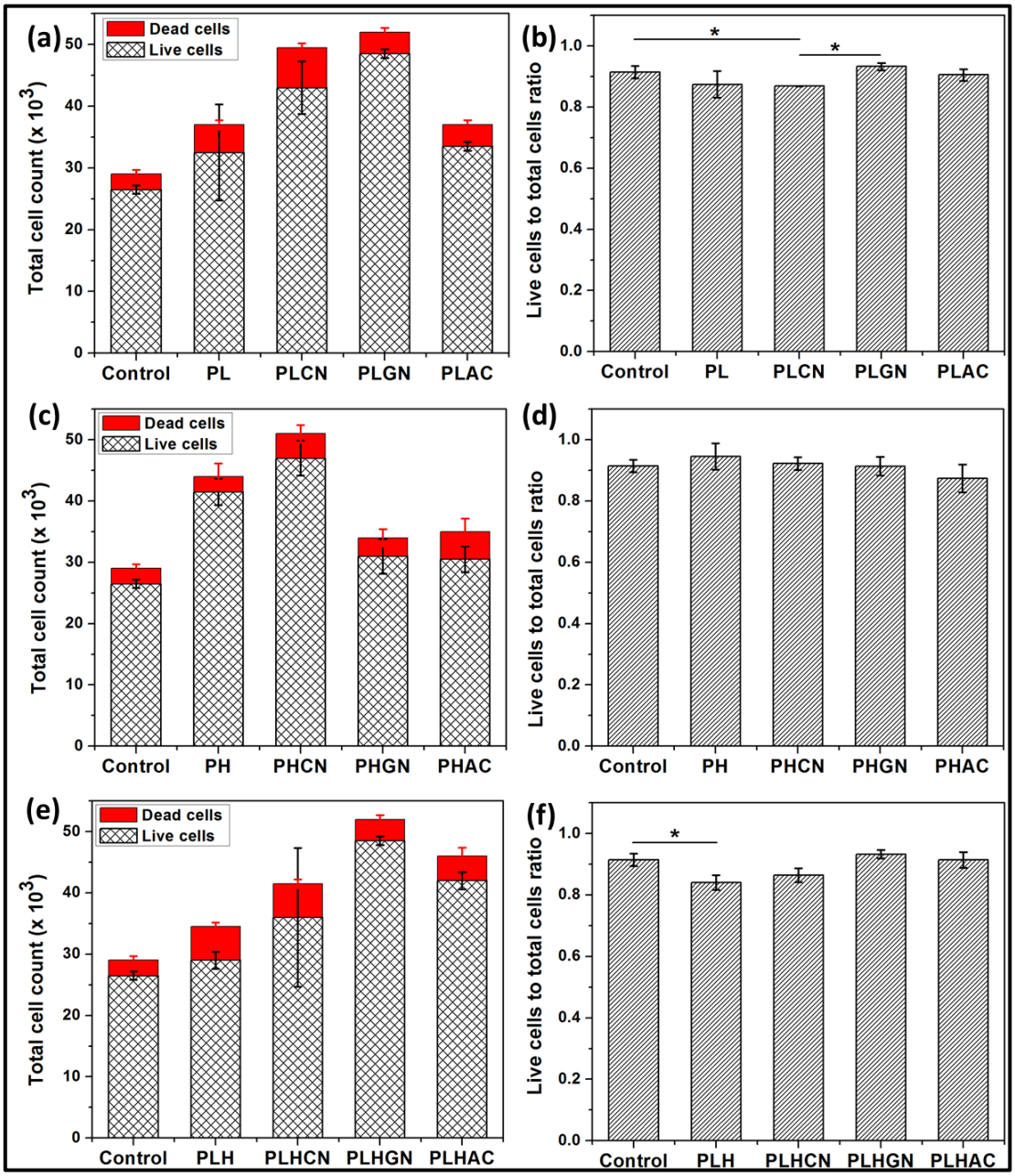

Fig. 4.35 Trypan blue exclusion assay results showing the total cell count (a, c, e and g) and live to total cells ratio (b, d, f and h) for various scaffolds.

The MTT assay and trypan blue exclusion assay results for PLGA-nHA-carbon composite scaffolds are shown in Fig. 4.34 (c) and Fig. 4.35 (e-f). It is evident from the MTT results

that all the composite samples facilitated cell proliferation when compared to control plate. The PLH, PLHCN, PLHGN and PLHAC samples showed 1.61, 1.68, 1.94 and 1.44 folds increase in proliferation than control. This is due to the high surface area to volume ratio and hydrophilic functional groups of the reinforcements (nHA, CNTs, GNPs, AC) which boosted the protein adsorption on the composite scaffolds. Further, the reinforcement of carbon biomaterials such CNTs, GNPs and AC in PLGA-nHA encourage the cell attachment and growth on the composite surfaces. As described earlier, the presence of more functional groups and high protein adsorption on GNPs encouraged the cell growth and cell viability on PLHGN composites as compared with PLHCN and PLHAC. Further, the trypna blue assay results showed the highest total cell count in case of PLHGN sample. All the composite samples showed improved cell count than the control plate. Amongst all the carbon reinforced samples, GNPs reinforced samples showed least number of dead cells.

Thus, the MTT assay and trypan blue exclusion assay results suggested that the nHA and carbon reinforcements in polymer matrix potentially increase the cell viability on composite samples.

4.2.12. Cell morphology

The osteoblast cell attachment and growth mainly depends on the scaffold surface properties like wettability, charge and surface roughness. The growth of the osteoblast cells on all the composite scaffolds confirmed their biocompatibility. The FESEM analysis was performed to evaluate the effect of reinforcements on cell attachment, morphology and mineral production on different composite scaffolds.

The morphology of the osteoblast cells cultured on carbon reinforced PLGA composites was evaluated by FESEM as shown in Fig. 4.36. It can be seen from the micrographs that the cells were round in shape and less spread on PL sample. However, on PLGA-carbon composite samples, cells were more spread and elongated. The propagation of filopodia was evident on composite samples. Cells were found to adhere to each other with cellular micro extensions. The osteoblast cells cultured on PLCN and PLAC samples showed spindle like morphology whereas on PLGN sample cells were fully spread and formed a group.

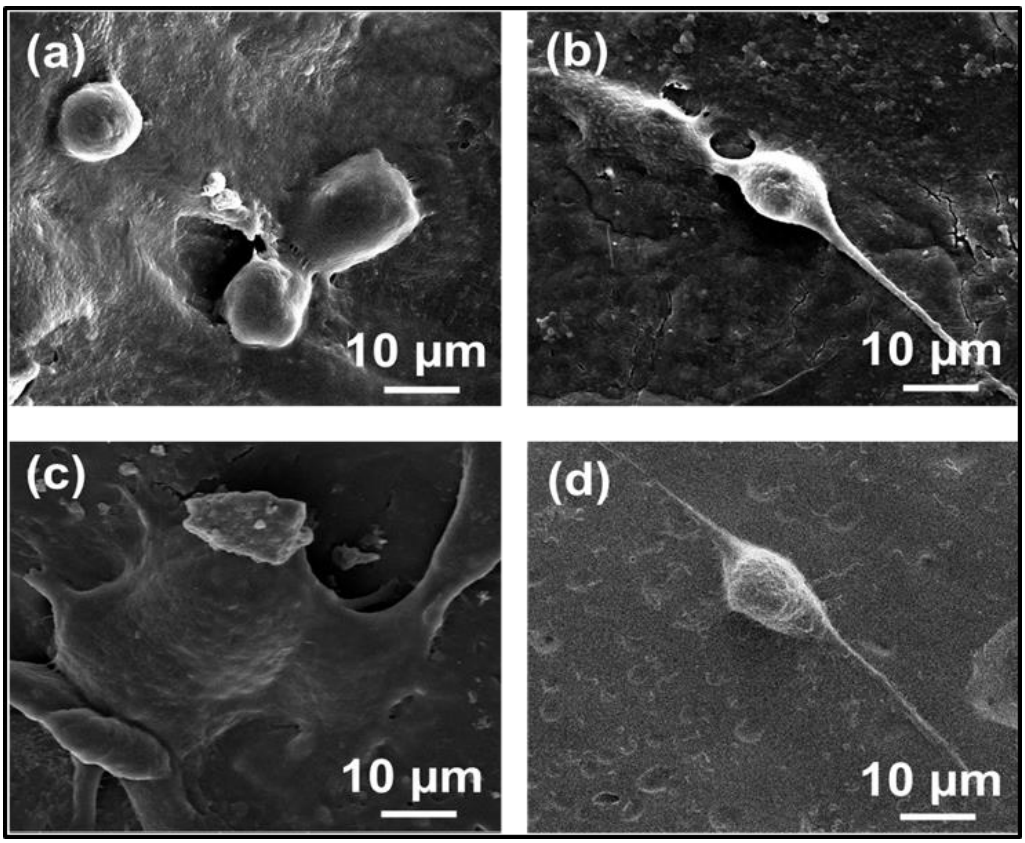

Fig. 4.36 FESEM micrographs of (a) PL, (b) PLCN, (c) PLGN and (d) PLAC composites cultured with MG-63 cells.

The SEM micrographs of osteoblast cell attachment and morphology on the PVA-nHA-carbon composites are shown in Fig. 4.37. Owing to the presence of nHA, all the samples have shown elongated morphology of the osteoblast cells. The addition of carbon materials along with nHA in PVA matrix enhanced the cell spreading and cell density on composite scaffolds. The surface of carbon containing samples was fully covered with well-spread cells. This might be due to higher surface area to volume ratio of nHA and carbon materials that provided more space for cells to adhere and proliferate.

The osteoblasts cell attachment and morphology on PLGA-nHA-carbon composite scaffolds was evaluated by SEM and the results are shown in Fig. 4.38. The growth of the MG-63 cells on all the scaffolds confirmed the biocompatibility of these scaffolds. Although cells were observed to be present on all the samples, carbon containing samples showed more number of cells attached to their surface.

The cells were found to be well spread on these samples compared to that on PLH sample. The formation of mineralized nodules was also observed on samples. The reinforcement of polymer matrices with carbon improved both, the cell density and growth on the composite scaffold samples owing to large surface area and nanoscale surface roughness provided by reinforcements. In GNPs containing PLGA-nHA scaffolds, cells were found to fully cover the scaffold surface and secreted matrix. Further, being a hydrophobic polymer, PLGA does not encourage cell adhesion. However, the addition of hydrophilic groups containing carbon materials improved the cell adhesion by lowering the contact angle of the PLGA based composite samples. The osteoinductive and osteoconductive properties of the nHA also played an important role. Hence, all the scaffolds showed biocompatible nature towards osteoblast cells.

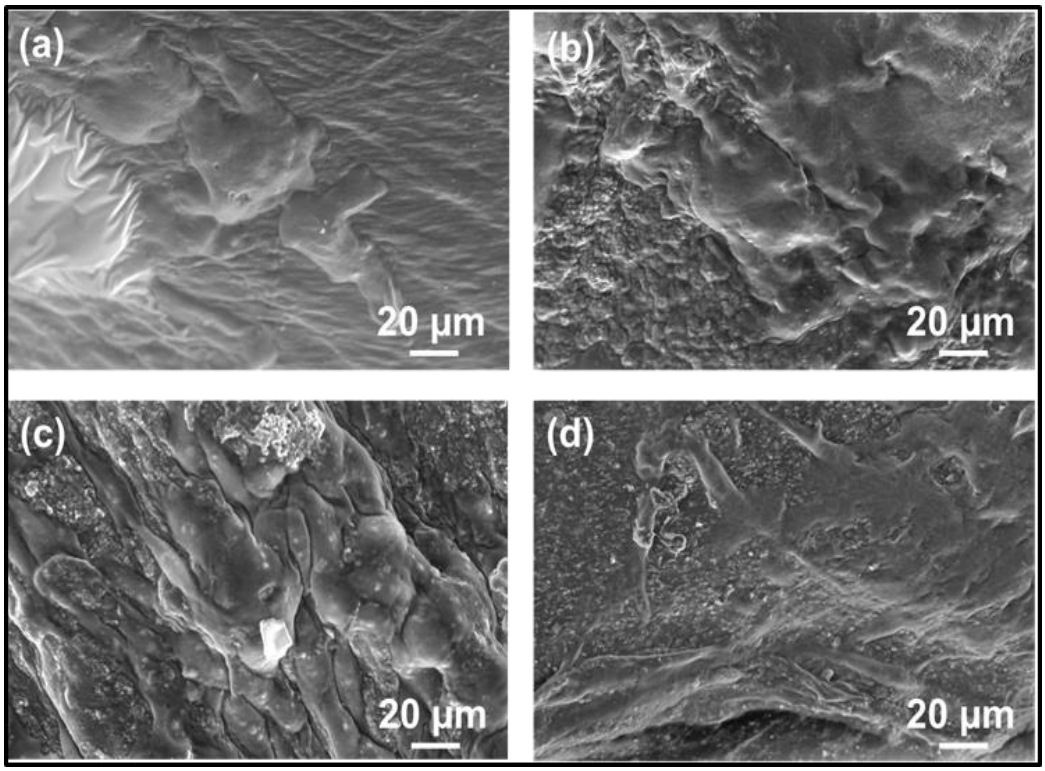

Fig. 4.37 FESEM micrographs of (a) PH, (b) PHCN, (c) PHGN and (d) PHAC composites cultured with MG-63 cells.

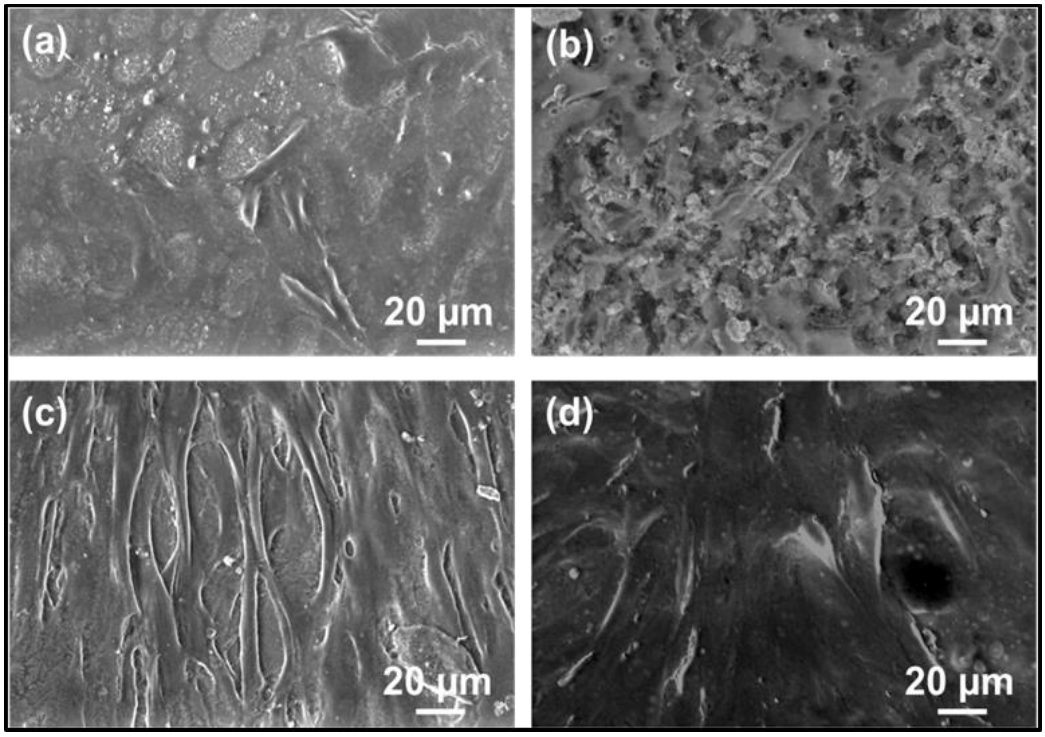

Fig. 4.38 FESEM micrographs of (a) PLH, (b) PLHCN, (c) PLHGN and (d) PLHAC composites cultured with MG-63 cells.

4.2.13. Alkaline Phosphatase (ALP) activity

Alkaline phosphatase (ALP) is an early osteogenic differentiation marker. To evaluate the bone forming ability of osteoblast cells cultured on various composite scaffolds, the ALP activity was examined quantitatively from the amount of p-nitrophenol produced after hydrolysis of pNPP and the results with respect to the control are shown in Fig. 4.39.

In carbonaceous PLGA composites, all the samples revealed up-regulation of ALP activity in comparison to control Fig. 4.39 (a). Further, the cells grown on composites displayed significantly higher ALP activity than those on pure PLGA sample. Thus, carbon reinforced PLGA composites supported higher osteoblast differentiation. Among these composites, the PLCN and PLGN samples showed better results than PLAC sample. The nanostructured CNTs and GNPs provide better surface topography and electric properties which play an imperative role in the promotion of cell differentiation. Consistent with the cell viability results, PLGN composite has shown the best ALP expression. This is due to

high protein adsorption on 2D structured GNPs with larger area and more functional groups to interact.

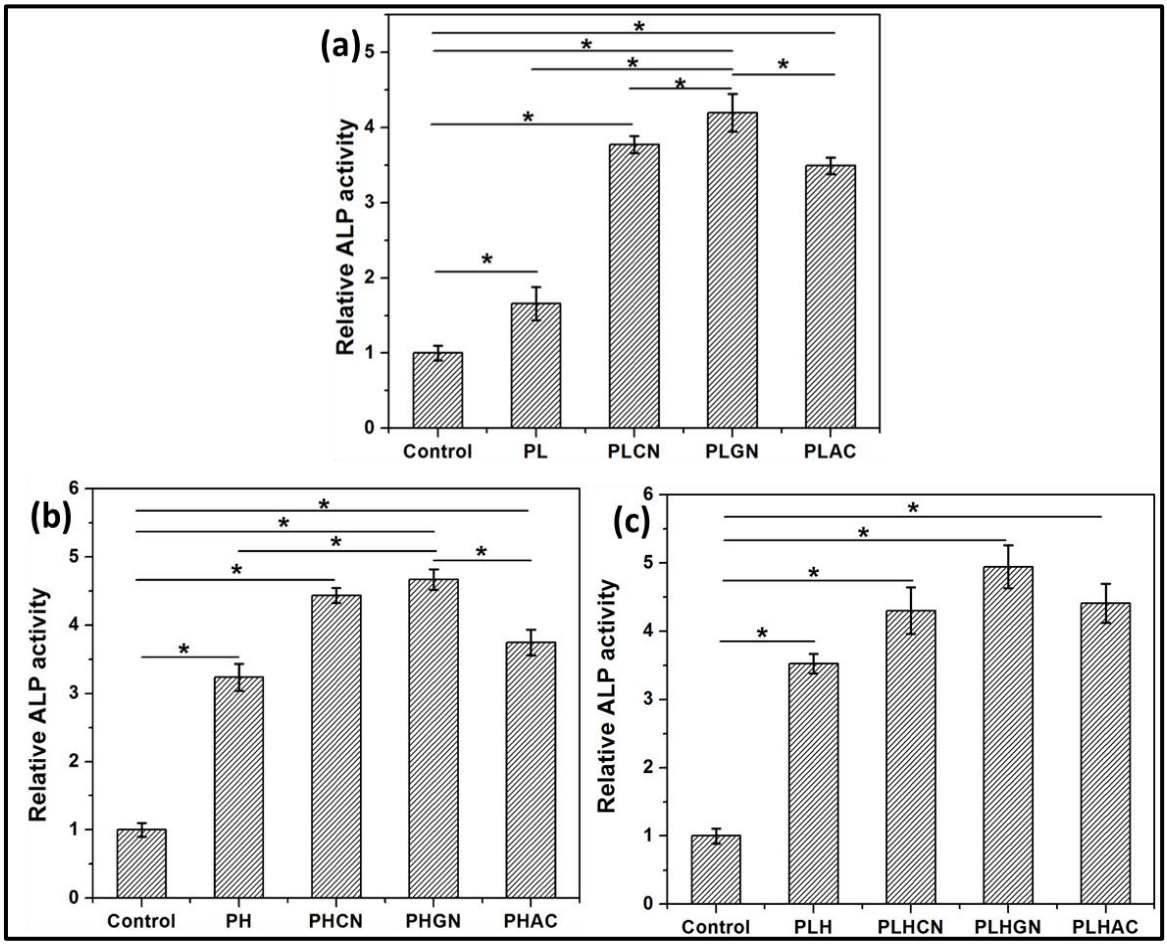

Fig. 4.39 ALP activity results of (a) PLGA-carbon, (b) PVA-nHA-carbon and (c) PLGA-nHA-carbon composites after 7 days of culturing.

The ALP activity of the carbon reinforced PVA-nHA composites is shown in Fig. 4.39 (b). The ALP activity was found to be in order of: control < PH < PHAC < PHCN < PHGN. All the carbon containing composite scaffolds showed better ALP activity than the control and PH sample. The increase in surface roughness due to the addition of nHA and carbon biomaterials led to improved protein adsorption and cell attachment which further resulted in the enhanced ALP activity of the composite scaffolds. The 2D structure of GNPs supported highest ALP activity of PHGN among all the other scaffolds. However, it was observed in MTT assay studies that PHGN showed less cell viability as compared to PH and PHCN. This might be due to the differentiation supporting ability of GNPs which

stopped the cell proliferation and started differentiation. Such behavior led to slow cell proliferation but high differentiation of the cells.

In the case of carbonaceous PLGA-nHA composite scaffolds, all the samples revealed up-regulation of ALP activity in comparison to the control plate (Fig. 4.39 (c)). The GNPs, CNTs and AC reinforcement supported higher osteoblast differentiation. As shown by protein adsorption and MTT assay results, nanostructured CNTs and GNPs might have provided better surface topography and electric properties to encourage protein adsorption and cellular responses [181-183]. Also, the excellent adsorption properties and hydrophilic groups present on AC made PLHAC sample suitable for cell differentiation. Moreover, high protein adsorption 2D structured GNPs (thus, larger area and more functional groups to interact) lead to adhere more cells on PLGN samples which expressed high ALP activity.

Thus, the ALP results showed that the carbon materials improve the cell differentiation on the scaffold surface in comparison to control plate. The synergistic effect of nHA and carbon materials up regulated the ALP activity of the three component composites many folds.

4.2.14. Confocal microscopy and quantification of cell morphology

The actin filaments are cytoskeletal proteins which mediate the cellular movement and provide structural support to cells. The cytoskeletal organization of cells cultured on different composite samples stained with TRITC-phalloidin (F-actin) and Hoechst (nuclei) was evaluated by confocal microscopy. The cell spreading is a crucial stage in cell adhesion prior to exponential growth phase. It can have an intense effect on cell adhesion, growth, proliferation, and differentiation. Therefore, in the present study, the cell morphology was quantified in terms of cell spreading area for each sample.

Fig. 4.40 (a-d) shows the cytoskeletal organization of cells cultured on PLGA-carbon composites after dual staining of nuclei and actin filaments. More number of cells were observed on composite samples as compared to PL sample. The reinforcement of carbon materials increases the surface roughness (especially with carbon nanomaterials such as

CNTs and GNPs) which is believed to improve cell adhesion and growth. This is due to the increase in protein adsorption on rough surfaces. It has also been reported that the presence of oxygen containing groups shows a positive response towards cell attachment and growth [109]. Amongst all the carbon containing composites, cells cultured on PLGN displayed better cytoskeleton organization and actin expression. In the PLGN sample, the cells were distributed on the entire surface and showed numerous filamentous extensions. Many layers of well-spread osteoblast cells with filopodia were observed and actin filaments were also clearly visible. Quantitative analysis (Fig. 4.40 (e)) also confirmed the better spreading of cells on composite scaffolds in comparison to pure PLGA. The average cell area for PL, PLCN, PLGN and PLAC was found to be 817μm^2, 886 μm^2, 1203 μm^2 and 857 μm^2, respectively. Therefore, the 2D structure of GNPs resulted in better adhesion and spreading of cells on composite samples.

The cytoskeleton of osteoblast cells cultured and stained on PVA-nHA and PVA-nHA-carbon composite scaffolds is shown in Fig. 4.41 (a-d). The cells cultured on PH and PHCN samples were observed to have globular morphology and formed clumps. On the other hand, the cells cultured on PHGN and PHAC samples were well-spread. Fig. 4.41 (c) shows the cytoskeletal organization of well spread cells on PHGN sample. Inset (A) shows many well spread cells on PHGN sample at lower magnification and inset (B) shows 3D micrograph of PHGN scaffold. It can be seen that the cells have migrated inside the porous scaffold. This might be a reason for the presence of less number of cells on the surface of all the scaffolds. The cell area quantification exhibited smaller size of cells on PH and PHCN samples. As observed from the box chart, most of the cells on these two samples (PH and PHCN) presented the same size, whereas, on PHGN and PHAC scaffolds, cells had comparatively larger size. The average cell area for PH, PHCN, PHGN and PHAC scaffolds was 102 μm^2, 205 μm^2, 1060 μm^2 and 550 μm^2, respectively. The GNPs reinforced scaffolds showed almost 10 times larger cells in comparison to the cells on PH scaffold. The large cell size indicated the suitability of the surfaces for better cell attachment and spreading.

Fig. 4.42 (a-d) shows the dual stained osteoblast cells on PLGA-nHA-carbon composite scaffolds. An increased number of cells were found attached to the carbon containing composites. The carbon reinforcements impart surface roughness and oxygen

functionalities on the scaffold surfaces making them suitable for cell attachment and growth. Moreover, the better protein adsorption on these scaffolds promotes interaction between cells and sample surface.

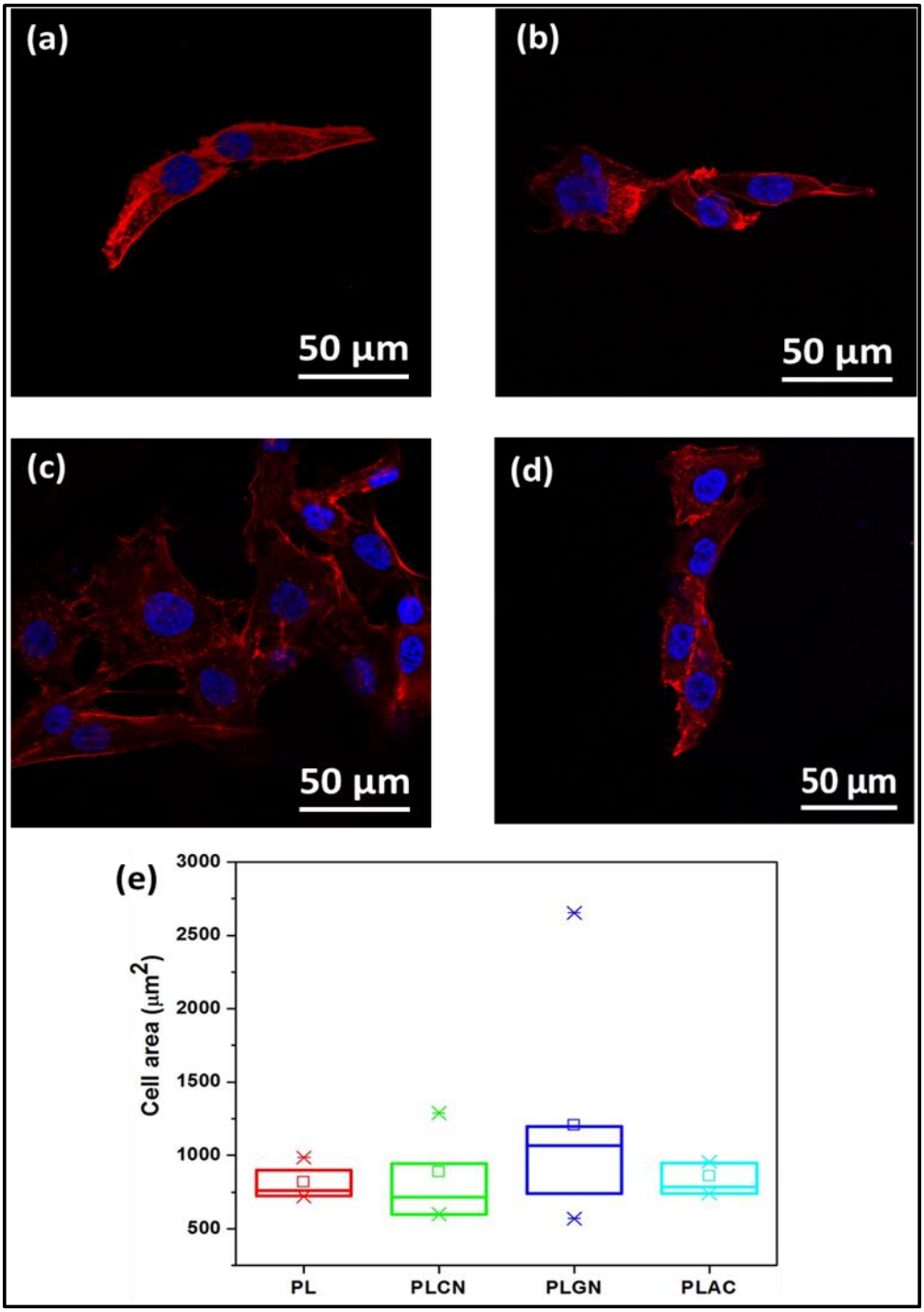

Fig. 4.40 Confocal micrographs of MG-63 cells seeded on (a) PL, (b) PLCN, (c) PLGN, (d) PLAC and (e) quantification of cell area on different scaffolds.

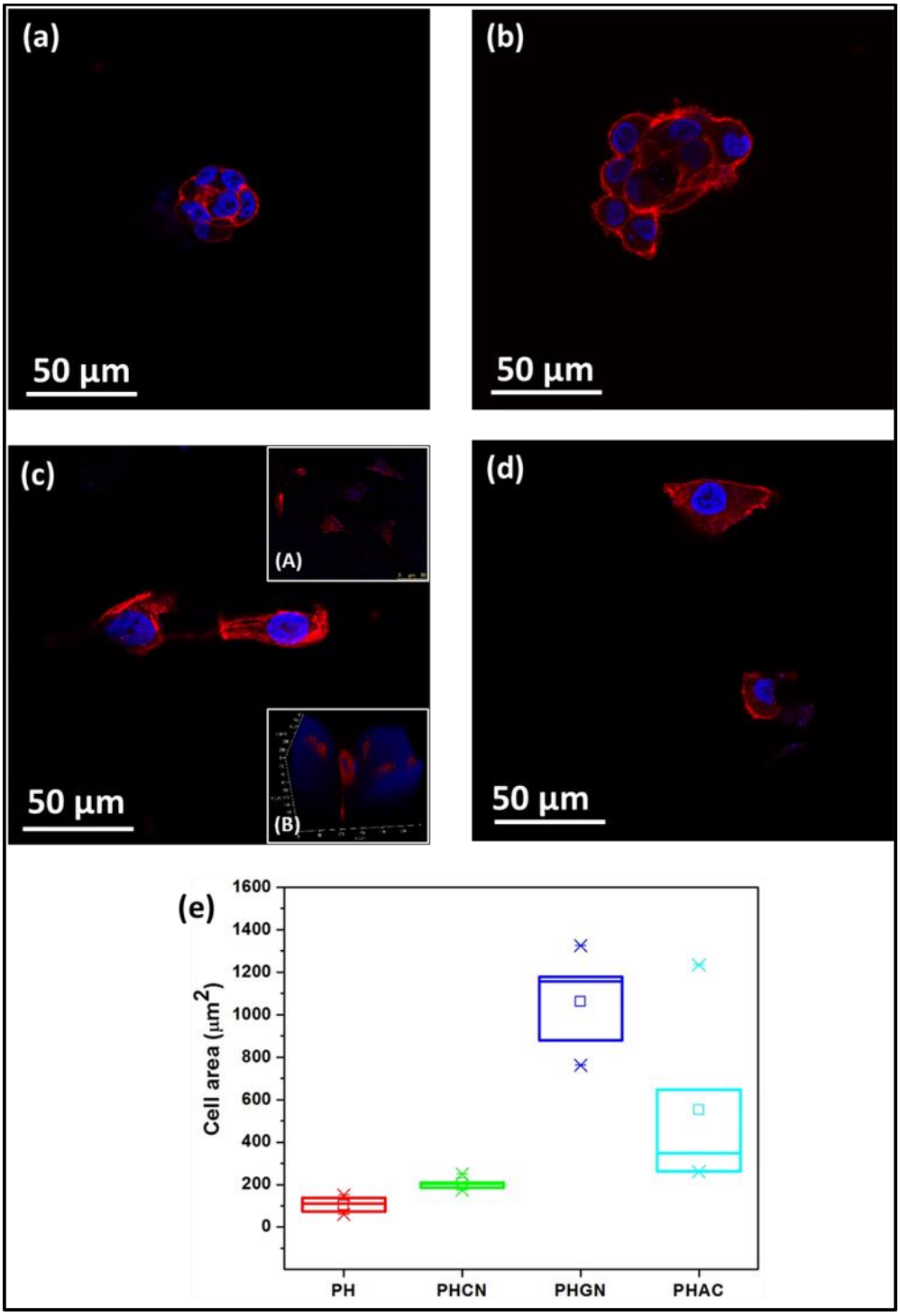

Fig. 4.41 Confocal micrographs of MG-63 cells on (a) PH, (b) PHCN, (c) PHGN, (d) PHAC and (e) quantification of cell area. Inset (A) shows well spread cells on PHGN sample at lower magnification and (B) shows cells migrated inside the porous scaffold.

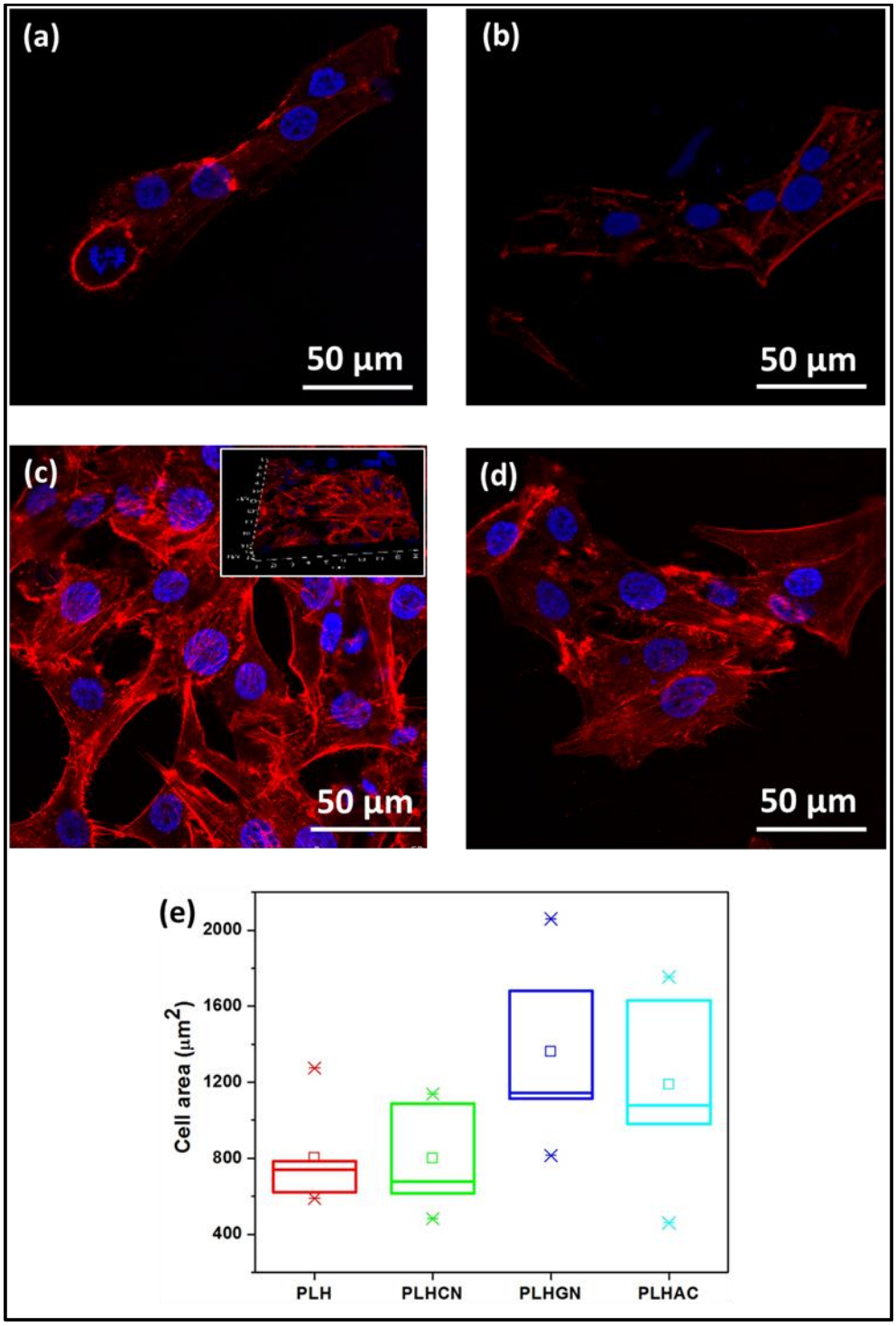

Fig. 4.42 Confocal micrographs of MG-63 cells seeded on (a) PLH, (b) PLHCN, (c) PLHGN, (d) PLHAC and (e) quantification of cell area on different scaffolds. Inset shows the 3D micrograph of PLHGN sample confirming the presence of cells throughout the sample.

The micrographs demonstrated that the cells adopted typical spindle like morphology of osteoblast. Further, PLHGN sample showed both improved cell growth and proliferation. The 3D micrograph of this sample (inset of Fig. 4.42 (c)) revealed that the cells were distributed evenly throughout the sample. Several filamentous extensions were observed along with the well-organized actin filaments. This is due to the presence of GNPs which provided more surface area for proteins and cells to adhere. Additionally, cell area quantification results are shown in Fig. 4.42 (e). The cells on PLHGN sample showed highest cell area followed by PLHAC, PLHCN and PLH. The average cell area for PLH, PLHCN, PLHGN and PLHAC samples was observed to be 799 μm^2, 800 μm^2, 1361 μm^2 and 1187 μm^2, respectively. This confirms that GNPs provided more surface area for proteins adhesion which encouraged the better cell attachment, proliferation and growth.

From the confocal micrographs, it can be concluded that the reinforcement of carbon biomaterials with and without nHA stimulated the cell adhesion and growth. The structure of carbon materials played an imperative role in cell attachment. The presence of 2D material (GNPs) with more number of functional groups provided better surface for cells to attach and grow.

4.2.15. Live cell staining

The *in-vitro* live cell attachment and viability on various scaffolds was studied by staining the cells with calcein-AM stain which stains the cytoplasm of living cells. The retention of the stain by live cells is detected as green fluorescence.

Fig. 4.43 shows the live cell micrographs of carbon reinforced PLGA composites. This is evident from the micrographs that the cells attached on pure PLGA sample were not so well spread and were present in globular shape. On the other hand, the carbon reinforced samples exhibited more number of well-spread cells attached to their surface. It was shown from the micrographs that the graphene reinforced sample (PLGN) supported the cell attachment and growth more in comparison to the other samples.

Further, the fluorescence staining results of cells cultured on PVA-nHA-carbon composite scaffolds are shown in Fig. 4.44. Similar to the FESEM results, the cells on PVA based composites were not spread well. The PH sample showed globular cells, whereas carbon

reinforced PVA-nHA composites showed the presence of both globular and spread cells. The presence of less number of cells on all PVA-nHA-carbon samples might be due the penetration of cells into the porous structure of the scaffolds.

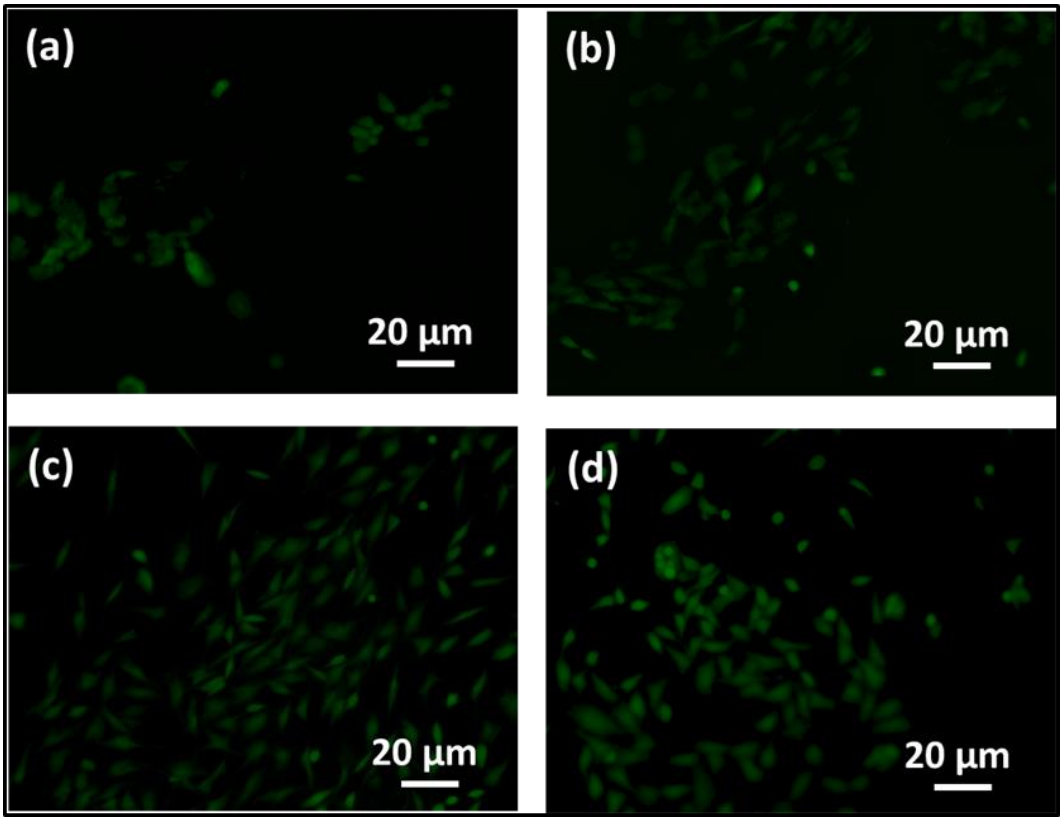

Fig. 4.43 Live cell staining of MG-63 cells seeded on (a) PL, (b) PLCN, (c) PLGN and (d) PLAC composites.

The live cell staining micrographs of PLGA-nHA-carbon composites are shown in Fig. 4.45. All the samples have been found to support the cell attachment and growth. The sample surfaces were covered with calcein stained cells indicating the presence of a large number of viable cells. Amongst all the carbon materials, GNPs reinforced sample (PLHGN) exhibited strongly adhered viable cells on the scaffold. Further, the cells were found to form cell-cell contact over large distances. Other carbonaceous PLGA-nHA composites (PLHCN and PLHAC) also showed firmly attached cells with elongated morphology. Multiple layers of cells were observed on the carbon and nHA reinforced samples. This is due to the synergistic effect of optimized concentrations of carbon materials and nHA that encourage cell adhesion without causing any toxic effects.

Hence, the calcein-AM staining results have confirmed the suitability of carbon reinforced composite scaffolds for better cell attachment and growth.

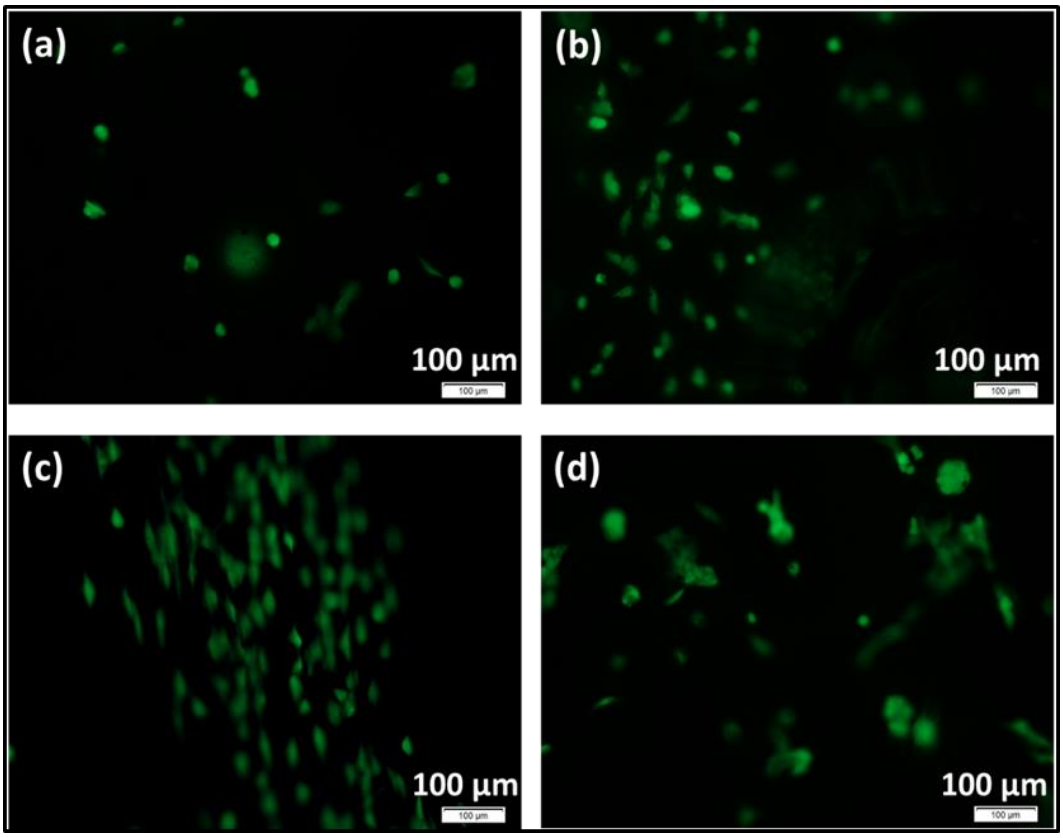

Fig. 4.44 Live cell staining of MG-63 cells seeded on (a) PH, (b) PHCN, (c) PHGN and (d) PHAC composites.

4.2.16. Collagen quantification

Collagen is an important component for cell proliferation and tissue formation. The collagen production in scaffolds by osteoblast cells indicates the formation of ECM within the scaffolds. The collagen content secreted by cells seeded on various scaffolds was quantified by staining with Sirius red dye (Fig. 4.46).

Less amount of collagen was observed in control plate (tissue culture plate), whereas, the total collagen content within all the scaffolds was notably higher. In PLGA-carbon composite scaffolds (Fig. 4.46 (a)), pure PLGA showed least collagen secretion, that was found to increase with the addition of carbon reinforcements. There was no significant

difference in the amount of collagen synthesized by cell seeded on both, PLCN and PLGN samples; however it was higher than pure PLGA and PLAC samples. This is due to the presence of nano sized CNTs and GNPs.

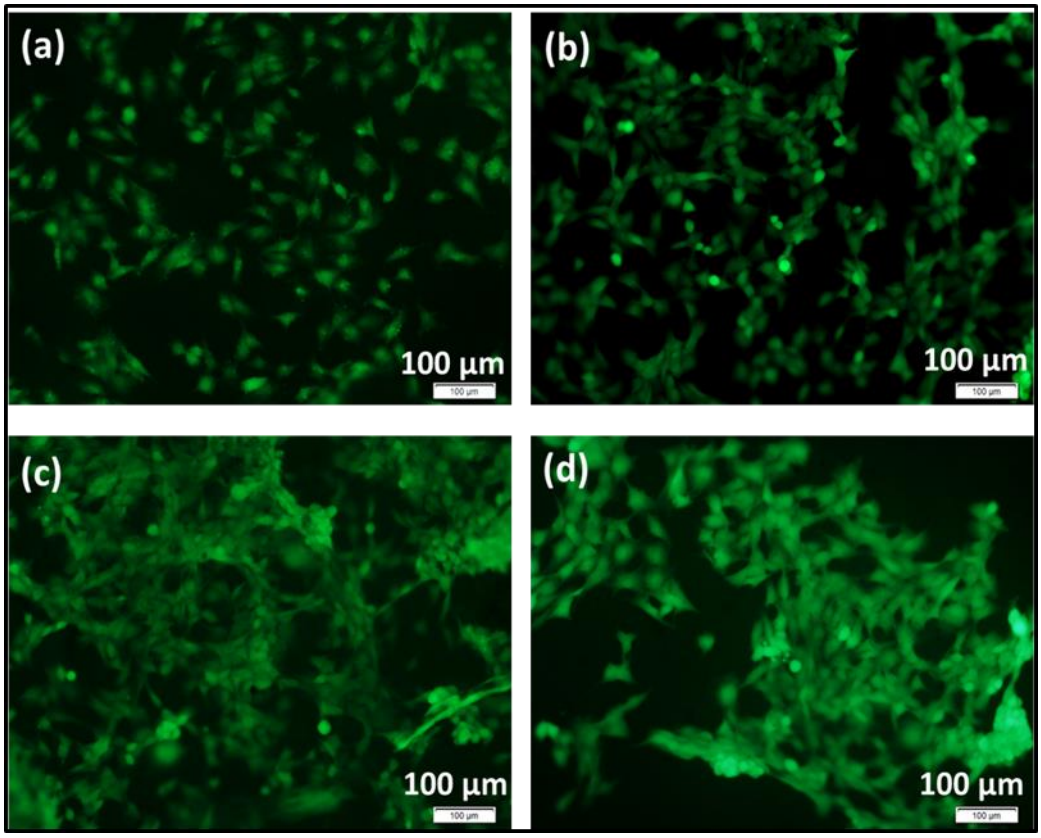

Fig. 4.45 Live cell staining of MG-63 cells seeded on (a) PLH, (b) PLHCN, (c) PLHGN and (d) PLHAC composites.

Further, in PVA-nHA-carbon scaffolds (Fig. 4.46 (b)), the addition of all the three carbon materials up-regulated their collagen secretion. Amongst PVA-nHA composites, PHGN exhibited the highest amount of collagen production. The cells cultured on carbonaceous composites of PLGA-nHA (Fig. 4.46 (c)) revealed many folds increase in the amount of collagen secreted in comparison to both, control plate and PLH scaffold. This might be due to the synergistic effect of carbon materials and hydroxyapatite added to the PLGA matrix. The GNPs reinforced PLGA-nHA composites (PLHGN) secreted significantly higher amount collagen in comparison to all other samples. The larger surface area, more

functional groups and hence, high protein adsorption values of the 2D structured GNPs lead to higher cell adhesion and differentiation.

The augmented collagen secretion on all the composite scaffolds suggested the positive effects of nHA and GNPs on cellular responses. Thus, the results confirmed the osteogenesis promoting properties of carbonaceous composites.

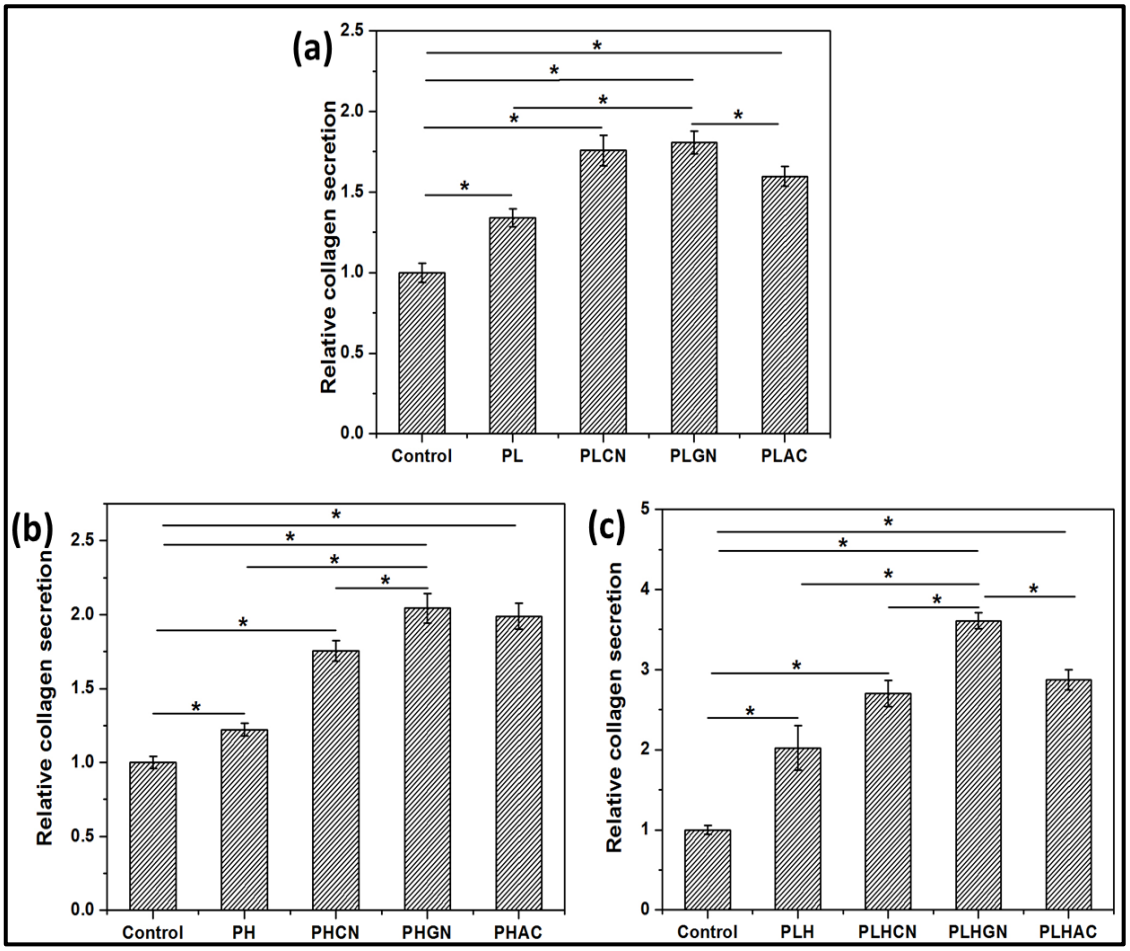

Fig. 4.46 Quantification of collagen produced by MG-63 cells seeded on (a) PLGA-carbon, (b) PVA-nHA-carbon and (c) PLGA-nHA-carbon composites.

4.2.17. Mineralization assay

The mineralized matrix on the scaffold samples cultured with osteoblast cells is the sign of the osteoblast differentiation. The calcium deposition due to matrix mineralization was

analyzed using Alizarin Red stain (ARS) based assay and the results were normalized to the control (Fig. 4.47 (a-c)).

Fig. 4.47 (a) shows the relative mineralization results of carbonaceous PLGA composites normalized to the control. As expected from other biological results, the calcium deposition was lowest on control in comparison to PL and PLGA composites. The carbon reinforced samples demonstrated significantly higher calcium depositions than the pure PLGA sample after 7 days of cell culturing. Amongst PLGA composites, PLGN showed highest amount of bone nodule formation. The functionalized reinforcements impart negative charge to the surface of composite. These negative surfaces encourage heterogeneous nucleation and growth of hydroxyapatite. It has been reported that the presence of carboxyl groups induce calcium deposition even after a short period of cell culturing [180].

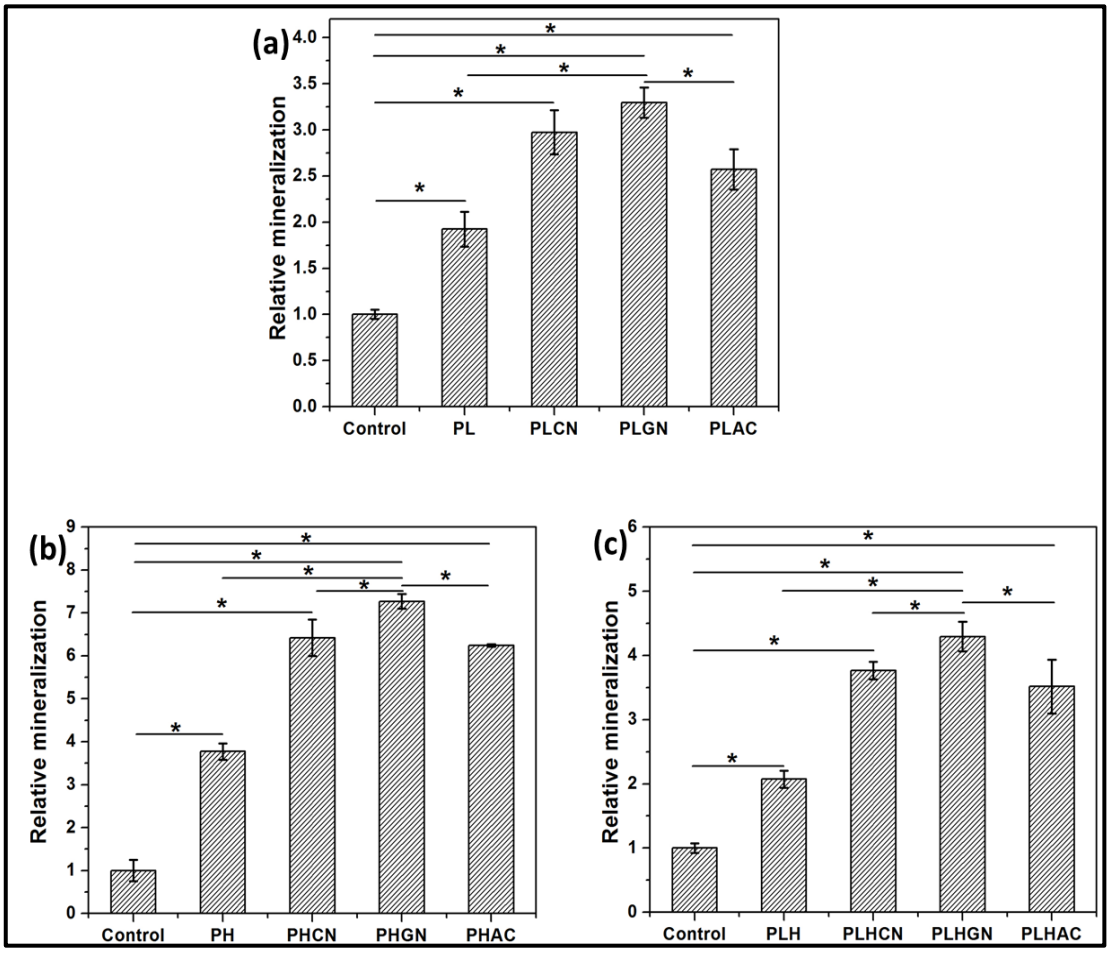

Fig. 4.47 Alizarin red stain assay results for (a) PLGA-carbon, (b) PVA-nHA-carbon and (c) PLGA-nHA-carbon composites.

The relative mineralization of the cell cultured on PVA-nHA-carbon composites are shown in Fig. 4.47 (b). Though all the scaffolds showed better results, the carbon containing scaffolds showed more mineralization as compared to control plate and PH sample. Both nHA and carbon biomaterials supported the cell differentiation on the scaffolds. More than 7 folds increase was observed in calcium deposition on PHGN sample in comparison to the control. The electrical conductivity and unique (sheet like, 2D) nanostructure of the GNPs encourage the cellular differentiation in PHGN scaffolds.

In the case of carbonaceous PLGA-nHA composites, PLH sample showed almost double mineralization than control plate (Fig. 4.47 (c)). As expected from above results, the carbon reinforcements further improved the mineralization deposition on scaffolds. Upon implantation, surface chemistry of the material plays an imperative role in regulating the cellular responses towards implant. The cellular responses such as cell attachment, proliferation, differentiation and matrix formation, depends on the protein adsorption on implant. The oxygen containing functional groups present on three carbon reinforcement used in this study act as bioactive molecules by providing sites for protein adsorption. Also, the interaction of π electrons of graphite structure and the hydrophobic part of protein encourage the protein adsorption on carbon nanomaterials (CNTs and GNPs) [177]. These interactions specifically adsorb proteins which enhance cell proliferation and differentiation, resulting in up regulation of ALP activity and matrix mineralization. Among CNTs and GNPs reinforced samples, PLHGN has shown the highest mineralization.

The differences in the morphology of three different carbon materials lead to different results. The exceptional electric properties of CNTs and GNPs played an important role in improving cellular responses as compared to AC. In spite of having same electric properties and graphitic structure, the GNPs showed better responses in comparison to the CNTs. This is mainly due to the sheet like structure of GNPs which is different from tubular CNTs. The unique 2D nanostructure of GNPs with more number of functional groups was available for proteins and cells to attach. Therefore, GNPs displayed stronger enhancement in cell proliferation and differentiation. From the results, it can be seen that carbon reinforced PLGA-nHA composites not only supported cell attachment and proliferation, but it also improved the cell differentiation.

4.3. Summary

In this chapter, the results obtained from the present study have been reported and discussed. The optimized concentrations of the various reinforcement materials (such as nHA, CNTs, GNPs and AC) have been obtained by characterizing the developed composite scaffolds for their physicochemical, biological and mechanical properties.

Micrograph of PHA 3 composite (3% w/v) showed even and homogenous distribution of nHA in PVA matrix. PHA 3 composite scaffold has shown nominal swelling studies and degradation studies; as well as dense and homogenous apatite formation on immersion in SBF for a duration of 4 weeks. On the other hand, the composite scaffolds PHA 4 and PHA 5 has shown non-homogenous apatite formation on immersion in SBF due to agglomeration of nHA in PVA matrix. The osteoblast adhesion, proliferation, ALP activity, and mineralization were significantly higher on composite scaffolds. PHA 3 also showed the highest tensile strength, whereas PHA 4 and PHA 5 exhibited less strength and undergone brittle failure. Hence, 3% w/v can be concluded to be the optimum composition of nHA amongst the other composite scaffolds and can be engineered further for bone tissue engineering application.

The presence of porous AC in the PVA matrix improved the porosity, hydrophilicity, bioactivity, hemocompatibility and protein adsorption of the composite scaffolds. The efficient load transfer between PVA and AC enhanced the mechanical properties of the composites many folds. Further, the hydrophilic nature and high protein adsorption of composite scaffolds encouraged the osteoblast cell adhesion and growth. It can be concluded that the reinforcing polymer matrix with porous AC (2.5 wt%) improves the mechanical as well as biological properties of the composite without compromising with the porosity of the scaffolds.

The physical interactions of carboxylic acid functionalized CNTs and GNPs with PVA enabled homogeneous dispersion of them in PVA matrix individually, leading to enhanced *in-vitro* biological and mechanical properties of the nanocomposites. The presence of CNTs and GNPs in the PVA matrix improved the surface morphology, bioactivity, protein adsorption, and mechanical properties of the nanocomposite scaffolds. The mechanical

properties were enhanced many folds with reinforcement of 1 wt% of each of CNTs and GNPs in PVA matrix without compromising much with the porosity of the scaffold. However, with further increase in reinforcement (1.5 wt%) concentration, mechanical properties were found to decrease due to the agglomeration of materials. Among all the nanocomposites, both PCN 1 and PGN 1 (1 wt%) provided the most favorable microenvironment for cell proliferation and differentiation. Hence, the presented results suggest that 1 wt% might be the threshold concentration of CNTs and GNPs in PVA matrix, below which they were well dispersed, and the scaffold surface was best suitable for cell attachment, proliferation, and differentiation.

Hence, obtained optimum concentrations of 4 different reinforcements were used to further study the effect of different structures of carbon reinforcements. The PLGA, PVA-nHA, and PLGA-nHA were reinforced with threshold concentrations of different carbon materials. The PVA based composites showed decrease in hydrophilicity, swelling and degradation, whereas the PLGA based composites exhibited improvement in these properties. The enhanced protein adsorption and bioactivity was obtained in comparison to control sample. The tensile strength of all the samples was drastically improved with reinforcement of each carbon material. The carbon reinforcement in polymer and polymer-ceramic matrices stimulated the enhancement in cell biological behavior. Improvement in osteoblast cell responses was observed from proliferation, ALP activity, mineralization assay and collagen quantification assay.

Chapter 5

Conclusion

In the present work, different reinforcing materials (nHA, CNTs, GNPs and AC) of different concentrations were reinforced in polymer (PVA) matrix. The optimum concentrations of the different reinforcements were obtained after conducting systematic mechanical and biological studies. The optimum concentrations of carbon materials were reinforced into PVA and PLGA along with nHA. The following conclusion was arrived from the study.

a. With the increase in the concentration of reinforcement materials, the mechanical and biological properties of the developed composites were improved up to threshold (optimum) concentration. At the threshold concentration, the reinforced material was homogenously dispersed in the polymer matrix providing a larger interface between the matrix and reinforcement for effective stress transfer. The well dispersed reinforcement materials also exhibited improvement in the protein adsorption, cell adhesion, proliferation, and differentiation in the composite samples with optimum reinforcement concentration. The homogenous dispersion of reinforcement materials provided suitable surface properties (wettability, roughness, surface charge and surface chemistry) to the scaffolds for protein and cell adhesion.

b. It was observed that above the threshold concentrations, the reinforced materials start to agglomerate in polymer matrix which results in deterioration of biological and mechanical properties of the composite scaffolds. The agglomerated materials

at higher concentration reduced the load transfer from polymer to reinforcement material weakening the mechanical properties of the composites. Moreover, the agglomerated reinforcement materials have also shown cytotoxicity to the osteoblast cells. Therefore, 3% w/v of nHA, 1 wt% of CNTs, 1 wt% of GNPs and 2.5 wt% of AC were considered as the threshold concentration at which reinforcements were well dispersed in the polymer matrix.

c. Further, the effect of different structures of carbon materials (1D, 2D, 3D) was studied by reinforcing polymer matrices (PVA and PLGA) with threshold concentrations of CNTs, GNPs and AC along with nHA. The synergistic effect of nHA and carbon materials improved the protein adsorption, bioactivity and tensile properties of the composites. The up regulated ALP activity and mineralization on the three component composite scaffolds confirmed the improvement in the bone forming ability of osteoblast cells. In spite of having different structures, all three carbon materials showed good osteogenic capacity when reinforced along with nHA. The different dimensional structures of reinforcements played an important role in tailoring the mechanical and biological properties of the composites. Both CNTs and GNPs reinforced composites revealed better tensile strength and Young's modulus as compared to AC owing to the good mechanical properties of the reinforcements. The improved surface properties i.e. roughness, charge, wettability and chemistry showed a positive effect on the biological properties of the nanocomposites. The high aspect ratio and exceptional electrical properties of the nanomaterials up regulated the proliferation and differentiation of the composites.

d. Although both CNTs and GNPs have similar graphitic structure and electric properties, GNPs exhibit greater advantages for reinforcing both polymer and polymer-ceramic composites over CNTs. The sheet like 2D structure of GNPs provided more number of functional groups for protein adsorption and cell attachment in comparison to tubular CNTs (1D). The high ALP activity, collagen secretion, and matrix mineralization confirmed that the GNPs reinforced composites provide the most favorable microenvironment for osteoblast cell

proliferation and differentiation. Also, their larger interface resulted in the effective load transfer between polymer matrix and GNPs. The results from the mechanical and biological studies suggested that the structure of reinforcement plays an imperative role in developing a suitable composite scaffold. Overall, from the above study, it can be concluded that the polymer-ceramic based carbonaceous composites possess osteogenesis promoting properties along with the improved mechanical properties for bone tissue engineering.

Scope for future research

In the present research, carbon reinforced polymer-ceramic composite scaffolds have been developed for improved bone tissue regeneration. However, there is a scope for future research to further improve the characterization process of the composite scaffolds.

- Detailed mechanical studies (compression, flexural behavior) can be studied in *in-vitro* environmental condition.
- The interaction of primary osteoblast cells with the developed scaffolds can also be studied.
- *In-vivo* studies using animal models can be performed to validate the *in-vitro* results.

References

[1] Salgado AJ, Coutinho OP, Reis RL. Bone tissue engineering: state of the art and future trends. Macromolecular bioscience 2004;4:743-65.

[2] Porter JR, Ruckh TT, Popat KC. Bone tissue engineering: a review in bone biomimetics and drug delivery strategies. Biotechnology Progress 2009;25:1539-60.

[3] Boskey AL. Bone composition: relationship to bone fragility and antiosteoporotic drug effects. BoneKEy reports 2013;2.

[4] Clarke B. Normal bone anatomy and physiology. Clinical journal of the American Society of Nephrology 2008;3:S131-S9.

[5] Deschaseaux F, Sensébé L, Heymann D. Mechanisms of bone repair and regeneration. Trends in molecular medicine 2009;15:417-29.

[6] Langer R, Vacanti JP. Tissue Engineering. Science 1993;260:920-6.

[7] Frohlich M, Grayson WL, Wan LQ, Marolt D, Drobnic M, Vunjak-Novakovic G. Tissue engineered bone grafts: biological requirements, tissue culture and clinical relevance. Current stem cell research & therapy 2008;3:254-64.

[8] Gentleman E, Swain RJ, Evans ND, Boonrungsiman S, Jell G, Ball MD, et al. Comparative materials differences revealed in engineered bone as a function of cell-specific differentiation. Nature materials 2009;8:763-70.

[9] Amini AR, Laurencin CT, Nukavarapu SP. Bone tissue engineering: recent advances and challenges. Critical Reviews™ in Biomedical Engineering 2012;40.

[10] Bruder SP, Kurth AA, Shea M, Hayes WC, Jaiswal N, Kadiyala S. Bone regeneration by implantation of purified, culture-expanded human mesenchymal stem cells. Journal of Orthopaedic Research 1998;16:155-62.

[11] Bianco P, Riminucci M, Gronthos S, Robey PG. Bone marrow stromal stem cells: nature, biology, and potential applications. Stem cells 2001;19:180-92.

[12] Rosada C, Justesen J, Melsvik D, Ebbesen P, Kassem M. The human umbilical cord blood: a potential source for osteoblast progenitor cells. Calcified Tissue International 2003;72:135-42.

[13] Kuznetsov SA, Mankani MH, Gronthos S, Satomura K, Bianco P, Robey PG. Circulating skeletal stem cells. The Journal of cell biology 2001;153:1133-40.

[14] Scherjon SA, Kleijburg-van der Keur C, de Groot-Swings GM, Claas FH, Fibbe WE, Kanhai HH. Isolation of mesenchymal stem cells of fetal or maternal origin from human placenta. Stem cells 2004;22:1338-45.

[15] Zuk PA, Zhu M, Ashjian P, De Ugarte DA, Huang JI, Mizuno H, et al. Human adipose tissue is a source of multipotent stem cells. Molecular biology of the cell 2002;13:4279-95.

[16] Crisan M, Yap S, Casteilla L, Chen C-W, Corselli M, Park TS, et al. A perivascular origin for mesenchymal stem cells in multiple human organs. Cell stem cell 2008;3:301-13.

[17] Hollinger JO, Einhorn TA, Doll B, Sfeir C. Bone tissue engineering: CRC press; 2004.

[18] Bose S, Roy M, Bandyopadhyay A. Recent advances in bone tissue engineering scaffolds. Trends in biotechnology 2012;30:546-54.

[19] Dhandayuthapani B, Yoshida Y, Maekawa T, Kumar DS. Polymeric scaffolds in tissue engineering application: a review. International Journal of Polymer Science 2011;2011.

[20] Cholkar K, Acharya G, Trinh HM, Singh G. Chapter 1 - Therapeutic Applications of Polymeric Materials. Emerging Nanotechnologies for Diagnostics, Drug Delivery and Medical Devices. Boston: Elsevier; 2017. p. 1-19.

[21] O'Brien FJ, Harley B, Yannas IV, Gibson LJ. The effect of pore size on cell adhesion in collagen-GAG scaffolds. Biomaterials 2005;26:433-41.

[22] Leong K, Cheah C, Chua C. Solid freeform fabrication of three-dimensional scaffolds for engineering replacement tissues and organs. Biomaterials 2003;24:2363-78.

[23] Zhu N, Chen X. Biofabrication of tissue scaffolds: INTECH Open Access Publisher; 2013.

[24] Subia B, Kundu J, Kundu S. Biomaterial scaffold fabrication techniques for potential tissue engineering applications: INTECH Open Access Publisher; 2010.

[25] Sachlos E, Czernuszka J. Making tissue engineering scaffolds work. Review: the application of solid freeform fabrication technology to the production of tissue engineering scaffolds. Eur Cell Mater 2003;5:39-40.

[26] Ma PX. Scaffolds for tissue fabrication. Materials today 2004;7:30-40.

[27] Kaur T, Thirugnanam A, Pramanik K. Tailoring the in vitro characteristics of poly (vinyl alcohol)-nanohydroxyapatite composite scaffolds for bone tissue engineering. Journal of Polymer Engineering.

[28] Loh QL, Choong C. Three-dimensional scaffolds for tissue engineering applications: role of porosity and pore size. Tissue Engineering Part B: Reviews 2013;19:485-502.

[29] Reneker DH, Chun I. Nanometre diameter fibres of polymer, produced by electrospinning. Nanotechnology 1996;7:216.

[30] Kaur T, Thirugnanam A. Tailoring in vitro biological and mechanical properties of polyvinyl alcohol reinforced with threshold carbon nanotube concentration for improved cellular response. RSC Advances 2016;6:39982-92.

[31] Matassi F, Nistri L, Paez DC, Innocenti M. New biomaterials for bone regeneration. Clinical cases in mineral and bone metabolism 2011;8:21-4.

[32] Liu X, Ma PX. Polymeric scaffolds for bone tissue engineering. 2004.

[33] Lee EJ, Huh BK, Kim SN, Lee JY, Park CG, Mikos AG, et al. Application of Materials as Medical Devices with Localized Drug Delivery Capabilities for Enhanced Wound Repair. Progress in Materials Science 2017.

[34] Gunatillake PA, Adhikari R. Biodegradable synthetic polymers for tissue engineering. Eur Cell Mater 2003;5:1-16.

[35] Paradossi G, Cavalieri F, Chiessi E, Spagnoli C, Cowman MK. Poly (vinyl alcohol) as versatile biomaterial for potential biomedical applications. Journal of Materials Science: Materials in Medicine 2003;14:687-91.

[36] Shuai C, Mao Z, Lu H, Nie Y, Hu H, Peng S. Fabrication of porous polyvinyl alcohol scaffold for bone tissue engineering via selective laser sintering. Biofabrication 2013;5:015014.

[37] Boland ED, Telemeco TA, Simpson DG, Wnek GE, Bowlin GL. Utilizing acid pretreatment and electrospinning to improve biocompatibility of poly (glycolic

acid) for tissue engineering. Journal of Biomedical Materials Research Part B: Applied Biomaterials 2004;71:144-52.

[38] Guo B, Ma PX. Synthetic biodegradable functional polymers for tissue engineering: a brief review. Science China Chemistry 2014;57:490-500.

[39] Park H, Park K, Shalaby WS. Biodegradable hydrogels for drug delivery: CRC Press; 2011.

[40] Cao H, Kuboyama N. A biodegradable porous composite scaffold of PGA/β-TCP for bone tissue engineering. Bone 2010;46:386-95.

[41] Tajbakhsh S, Hajiali F. A comprehensive study on the fabrication and properties of biocomposites of poly (lactic acid)/ceramics for bone tissue engineering. Materials Science and Engineering: C 2017;70:897-912.

[42] Zhou H, Touny AH, Bhaduri SB. Fabrication of novel PLA/CDHA bionanocomposite fibers for tissue engineering applications via electrospinning. Journal of Materials Science: Materials in Medicine 2011;22:1183-93.

[43] Zhang H, Chen Z. Fabrication and characterization of electrospun PLGA/MWNTs/hydroxyapatite biocomposite scaffolds for bone tissue engineering. Journal of Bioactive and Compatible Polymers 2010.

[44] Lin C, Wang Y, Lai Y, Yang W, Jiao F, Zhang H, et al. Incorporation of carboxylation multiwalled carbon nanotubes into biodegradable poly (lactic-co-glycolic acid) for bone tissue engineering. Colloids and Surfaces B: Biointerfaces 2011;83:367-75.

[45] Lee HJ, Yoon OJ, Kim DH, Jang YM, Kim HW, Lee WB, et al. Neurite outgrowth on nanocomposite scaffolds synthesized from PLGA and carboxylated carbon nanotubes. Advanced Engineering Materials 2009;11:B261-B6.

[46] Sheikh Z, Najeeb S, Khurshid Z, Verma V, Rashid H, Glogauer M. Biodegradable materials for bone repair and tissue engineering applications. Materials 2015;8:5744-94.

[47] Noshi T, Yoshikawa T, Ikeuchi M, Dohi Y, Ohgushi H, Horiuchi K, et al. Enhancement of the in vivo osteogenic potential of marrow/hydroxyapatite composites by bovine bone morphogenetic protein. Journal of biomedical materials research 2000;52:621-30.

[48] Hak DJ. The use of osteoconductive bone graft substitutes in orthopaedic trauma. Journal of the American Academy of Orthopaedic Surgeons 2007;15:525-36.

[49] Zhou H, Lee J. Nanoscale hydroxyapatite particles for bone tissue engineering. Acta biomaterialia 2011;7:2769-81.

[50] Samavedi S, Whittington AR, Goldstein AS. Calcium phosphate ceramics in bone tissue engineering: a review of properties and their influence on cell behavior. Acta Biomaterialia 2013;9:8037-45.

[51] Alvarez K, Nakajima H. Metallic scaffolds for bone regeneration. Materials 2009;2:790-832.

[52] Matassi F, Botti A, Sirleo L, Carulli C, Innocenti M. Porous metal for orthopedics implants. Clinical Cases in Mineral and Bone Metabolism 2013;10:111.

[53] Saris N-EL, Mervaala E, Karppanen H, Khawaja JA, Lewenstam A. Magnesium: an update on physiological, clinical and analytical aspects. Clinica chimica acta 2000;294:1-26.

[54] Cha C, Shin SR, Annabi N, Dokmeci MR, Khademhosseini A. Carbon-based nanomaterials: multifunctional materials for biomedical engineering. ACS nano 2013;7:2891-7.

[55] Usui Y, Aoki K, Narita N, Murakami N, Nakamura I, Nakamura K, et al. Carbon Nanotubes with High Bone-Tissue Compatibility and Bone-Formation Acceleration Effects. Small 2008;4:240-6.

[56] Ma P-C, Siddiqui NA, Marom G, Kim J-K. Dispersion and functionalization of carbon nanotubes for polymer-based nanocomposites: a review. Composites Part A: Applied Science and Manufacturing 2010;41:1345-67.

[57] Paiva M, Zhou B, Fernando K, Lin Y, Kennedy J, Sun Y-P. Mechanical and morphological characterization of polymer–carbon nanocomposites from functionalized carbon nanotubes. Carbon 2004;42:2849-54.

[58] Zhao B, Hu H, Mandal SK, Haddon RC. A bone mimic based on the self-assembly of hydroxyapatite on chemically functionalized single-walled carbon nanotubes. Chemistry of Materials 2005;17:3235-41.

[59] Kazi SN, Badarudin A, Zubir MNM, Ming HN, Misran M, Sadeghinezhad E, et al. Investigation on the use of graphene oxide as novel surfactant to stabilize weakly charged graphene nanoplatelets. Nanoscale Research Letters 2015;10:1-15.

[60] Mehrali M, Moghaddam E, Seyed Shirazi SF, Baradaran S, Mehrali M, Latibari ST, et al. Mechanical and <italic>In Vitro</italic> Biological Performance of Graphene

Nanoplatelets Reinforced Calcium Silicate Composite. PLoS ONE 2014;9:e106802.

[61] Thomas TD. The role of activated charcoal in plant tissue culture. Biotechnology advances 2008;26:618-31.

[62] COLEMAN WP. Surgical Management of Vitiligo by SOMESH GUPTA, MATS J. OLSSON, AMRINDER J. KANWAR, AND JEAN-PAUL ORTONNE, EDITORS. Dermatologic Surgery 2008;34:88-.

[63] Meyer U. The history of tissue engineering and regenerative medicine in perspective. Fundamentals of Tissue Engineering and Regenerative Medicine: Springer; 2009. p. 5-12.

[64] Fung Y. A proposal to the National science Foundation for An Engineering Research Centre at USCD. Center for the Engineering of Living Tissues UCSD 2001;865023:2001.

[65] Birla R. Introduction to tissue engineering: applications and challenges: John Wiley & Sons; 2014.

[66] Burke JF, Yannas IV, Quinby Jr WC, Bondoc CC, Jung WK. Successful use of a physiologically acceptable artificial skin in the treatment of extensive burn injury. Annals of surgery 1981;194:413.

[67] Peterson L, Vasiliadis HS, Brittberg M, Lindahl A. Autologous chondrocyte implantation a long-term follow-up. The American journal of sports medicine 2010;38:1117-24.

[68] Horch RE. New Developments and Trends in Tissue Engineering: An Update. Journal of Tissue Science & Engineering 2012;2012.

[69] Osteoporosis AP. Consensus statement of an expert group. Osteoporosis Society of India, New Delhi 2003.

[70] Johnell O, Kanis J. An estimate of the worldwide prevalence and disability associated with osteoporotic fractures. Osteoporosis international 2006;17:1726-33.

[71] Cooper C, Campion G, Melton Iii L. Hip fractures in the elderly: a world-wide projection. Osteoporosis international 1992;2:285-9.

[72] Lewandrowski K-U, Gresser JD, Wise DL, Trantolo DJ. Bioresorbable bone graft substitutes of different osteoconductivities: a histologic evaluation of

osteointegration of poly (propylene glycol-co-fumaric acid)-based cement implants in rats. Biomaterials 2000;21:757-64.

[73] Place ES, Evans ND, Stevens MM. Complexity in biomaterials for tissue engineering. Nature materials 2009;8:457-70.

[74] Brockbank KG. Tissue Engineering Constructs and Commercialization. Austin, Landes Bioscience 2000.

[75] Merritt K, Rodrigo JJ. Immune response to synthetic materials: sensitization of patients receiving orthopaedic implants. Clinical orthopaedics and related research 1996;326:71-9.

[76] Kong L, Gao Y, Cao W, Gong Y, Zhao N, Zhang X. Preparation and characterization of nano-hydroxyapatite/chitosan composite scaffolds. Journal of Biomedical Materials Research Part A 2005;75:275-82.

[77] Alsberg E, Anderson K, Albeiruti A, Franceschi R, Mooney D. Cell-interactive alginate hydrogels for bone tissue engineering. Journal of dental research 2001;80:2025-9.

[78] Xu XL, Lou J, Tang T, Ng KW, Zhang J, Yu C, et al. Evaluation of different scaffolds for BMP-2 genetic orthopedic tissue engineering. Journal of Biomedical Materials Research Part B: Applied Biomaterials 2005;75:289-303.

[79] Ferreira AM, Gentile P, Chiono V, Ciardelli G. Collagen for bone tissue regeneration. Acta biomaterialia 2012;8:3191-200.

[80] Brekke JH, Toth JM. Principles of tissue engineering applied to programmable osteogenesis. Journal of biomedical materials research 1998;43:380-98.

[81] Christel P, Chabot F, Leray J, Morin C, Vert M. Biodegradable composites for internal fixation. Biomaterials 1980;1:271-80.

[82] Linhart W, Peters F, Lehmann W, Schwarz K, Schilling AF, Amling M, et al. Biologically and chemically optimized composites of carbonated apatite and polyglycolide as bone substitution materials. Journal of biomedical materials research 2001;54:162-71.

[83] Xiong Z, Yan Y, Zhang R, Sun L. Fabrication of porous poly (L-lactic acid) scaffolds for bone tissue engineering via precise extrusion. Scripta Materialia 2001;45:773-9.

[84] Nejati E, Mirzadeh H, Zandi M. Synthesis and characterization of nano-hydroxyapatite rods/poly (l-lactide acid) composite scaffolds for bone tissue engineering. Composites Part A: Applied Science and Manufacturing 2008;39:1589-96.

[85] Sheikh FA, Ju HW, Moon BM, Lee OJ, Kim JH, Park HJ, et al. Hybrid scaffolds based on PLGA and silk for bone tissue engineering. Journal of tissue engineering and regenerative medicine 2015.

[86] Sabir MI, Xu X, Li L. A review on biodegradable polymeric materials for bone tissue engineering applications. Journal of Materials Science 2009;44:5713-24.

[87] Poursamar SA, Azami M, Mozafari M. Controllable synthesis and characterization of porous polyvinyl alcohol/hydroxyapatite nanocomposite scaffolds via an in situ colloidal technique. Colloids and Surfaces B: Biointerfaces 2011;84:310-6.

[88] Hofmann M, Mohammed A, Perrie Y, Gbureck U, Barralet J. High-strength resorbable brushite bone cement with controlled drug-releasing capabilities. Acta biomaterialia 2009;5:43-9.

[89] de Sousa Gomes P. Biological evaluation of biomaterials for bone tissue regeneration. 2011.

[90] van der Stok J, Koolen M, de Maat M, Yavari SA, Alblas J, Patka P, et al. Full regeneration of segmental bone defects using porous titanium implants loaded with BMP-2 containing fibrin gels. European cells & materials 2015;2015:141-54.

[91] Bender S, Chalivendra V, Rahbar N, El Wakil S. Mechanical characterization and modeling of graded porous stainless steel specimens for possible bone implant applications. International Journal of Engineering Science 2012;53:67-73.

[92] Staiger MP, Pietak AM, Huadmai J, Dias G. Magnesium and its alloys as orthopedic biomaterials: a review. Biomaterials 2006;27:1728-34.

[93] Zeng R, Dietzel W, Witte F, Hort N, Blawert C. Progress and challenge for magnesium alloys as biomaterials. Advanced Engineering Materials 2008;10:B3-B14.

[94] Chen EY, Wang YC, Mintz A, Richards A, Chen CS, Lu D, et al. Activated charcoal composite biomaterial promotes human embryonic stem cell differentiation toward neuronal lineage. Journal of Biomedical Materials Research Part A 2012;100:2006-17.

[95] Zhang L, Dou S, Li Y, Yuan Y, Ji Y, Wang Y, et al. Degradation and compatibility behaviors of poly (glycolic acid) grafted chitosan. Materials Science and Engineering: C 2013;33:2626-31.

[96] Wong WH, Mooney DJ. Synthesis and properties of biodegradable polymers used as synthetic matrices for tissue engineering. Synthetic biodegradable polymer scaffolds: Springer; 1997. p. 51-82.

[97] Zhao M-C, Liu M, Song G, Atrens A. Influence of the β-phase morphology on the corrosion of the Mg alloy AZ91. Corrosion Science 2008;50:1939-53.

[98] Lopes MS, Jardini A, Maciel Filho R. Poly (lactic acid) production for tissue engineering applications. Procedia Engineering 2012;42:1402-13.

[99] Mainil-Varlet P, Curtis R, Gogolewski S. Effect of in vivo and in vitro degradation on molecular and mechanical properties of various low-molecular-weight polylactides. Journal of Biomedical Materials Research Part A 1997;36:360-80.

[100] Kellomäki M, Niiranen H, Puumanen K, Ashammakhi N, Waris T, Törmälä P. Bioabsorbable scaffolds for guided bone regeneration and generation. Biomaterials 2000;21:2495-505.

[101] Santoro M, Shah SR, Walker JL, Mikos AG. Poly (lactic acid) nanofibrous scaffolds for tissue engineering. Advanced drug delivery reviews 2016;107:206-12.

[102] Lou T, Wang X, Song G, Gu Z, Yang Z. Fabrication of PLLA/β-TCP nanocomposite scaffolds with hierarchical porosity for bone tissue engineering. International journal of biological macromolecules 2014;69:464-70.

[103] Fang Z, Feng Q. Improved mechanical properties of hydroxyapatite whisker-reinforced poly (L-lactic acid) scaffold by surface modification of hydroxyapatite. Materials Science and Engineering: C 2014;35:190-4.

[104] Lasprilla AJ, Martinez GA, Lunelli BH, Jardini AL, Maciel Filho R. Poly-lactic acid synthesis for application in biomedical devices—A review. Biotechnology advances 2012;30:321-8.

[105] Fei Z, Hu Y, Wu D, Wu H, Lu R, Bai J, et al. Preparation and property of a novel bone graft composite consisting of rhBMP-2 loaded PLGA microspheres and calcium phosphate cement. Journal of Materials Science: Materials in Medicine 2008;19:1109-16.

[106] Murphy WL, Kohn DH, Mooney DJ. Growth of continuous bonelike mineral within porous poly (lactide-co-glycolide) scaffolds in vitro. Journal of biomedical materials research 2000;50:50-8.

[107] Gentile P, Chiono V, Carmagnola I, Hatton PV. An overview of poly (lactic-co-glycolic) acid (PLGA)-based biomaterials for bone tissue engineering. International journal of molecular sciences 2014;15:3640-59.

[108] Shi Y, Han H, Quan H, Zang Y, Wang N, Ren G, et al. Activated carbon fibers/poly (lactic-co-glycolic) acid composite scaffolds: Preparation and characterizations. Materials Science and Engineering: C 2014;43:102-8.

[109] Oh SH, Kang SG, Kim ES, Cho SH, Lee JH. Fabrication and characterization of hydrophilic poly (lactic-co-glycolic acid)/poly (vinyl alcohol) blend cell scaffolds by melt-molding particulate-leaching method. Biomaterials 2003;24:4011-21.

[110] Mooney D, Park S, Kaufmann P, Sano K, McNamara K, Vacanti J, et al. Biodegradable sponges for hepatocyte transplantation. Journal of biomedical materials research 1995;29:959-65.

[111] Stampella A, Papi A, Rizzitelli G, Costantini M, Colosi C, Barbetta A, et al. Synthesis and characterization of a novel poly (vinyl alcohol) 3D platform for the evaluation of hepatocytes' response to drug administration. Journal of Materials Chemistry B 2013;1:3083-98.

[112] Chua C, Leong K, Tan K, Wiria F, Cheah C. Development of tissue scaffolds using selective laser sintering of polyvinyl alcohol/hydroxyapatite biocomposite for craniofacial and joint defects. Journal of Materials Science: Materials in Medicine 2004;15:1113-21.

[113] Gao C, Gao Q, Li Y, Rahaman MN, Teramoto A, Abe K. Preparation and in vitro characterization of electrospun PVA scaffolds coated with bioactive glass for bone regeneration. Journal of Biomedical Materials Research Part A 2012;100:1324-34.

[114] Ma B, Lin L, Huang X, Hu Q, Fang M. Bone Tissue Engineering Using B-Tricalcium Phosphate Scaffolds Fabricated Via Selective Laser Sintering. Knowledge Enterprise: Intelligent Strategies in Product Design, Manufacturing, and Management 2006:710-6.

[115] Tarafder S, Balla VK, Davies NM, Bandyopadhyay A, Bose S. Microwave-sintered 3D printed tricalcium phosphate scaffolds for bone tissue engineering. Journal of tissue engineering and regenerative medicine 2013;7:631-41.

[116] Tarafder S, Davies NM, Bandyopadhyay A, Bose S. 3D printed tricalcium phosphate bone tissue engineering scaffolds: effect of SrO and MgO doping on in vivo osteogenesis in a rat distal femoral defect model. Biomaterials Science 2013;1:1250-9.

[117] Le Nihouannen D, Duval L, Lecomte A, Julien M, Guicheux J, Daculsi G, et al. Interactions of total bone marrow cells with increasing quantities of macroporous calcium phosphate ceramic granules. Journal of Materials Science: Materials in Medicine 2007;18:1983-90.

[118] Yang C, Wang Y, Chen X, Zhao N. Biomimetic fabrication of BCP/COL/HCA scaffolds for bone tissue engineering. Materials Letters 2005;59:3635-40.

[119] Leukers B, Gülkan H, Irsen SH, Milz S, Tille C, Schieker M, et al. Hydroxyapatite scaffolds for bone tissue engineering made by 3D printing. Journal of Materials Science: Materials in Medicine 2005;16:1121-4.

[120] Wang X, Li Y, Wei J, De Groot K. Development of biomimetic nano-hydroxyapatite/poly (hexamethylene adipamide) composites. Biomaterials 2002;23:4787-91.

[121] Sandeman SR, Jeffery H, Howell CA, Smith M, Mikhalovsky SV, Lloyd AW. The in vitro corneal biocompatibility of hydroxyapatite coated carbon mesh. Biomaterials 2009;30:3143-9.

[122] Domun N, Hadavinia H, Zhang T, Sainsbury T, Liaghat G, Vahid S. Improving the fracture toughness and the strength of epoxy using nanomaterials–a review of the current status. Nanoscale 2015;7:10294-329.

[123] Pan L, Pei X, He R, Wan Q, Wang J. Multiwall carbon nanotubes/polycaprolactone composites for bone tissue engineering application. Colloids and Surfaces B: Biointerfaces 2012;93:226-34.

[124] Lahiri D, Rouzaud F, Namin S, Keshri A, Valdes J, Kos L, et al. Carbon nanotube reinforced polylactide− caprolactone copolymer: mechanical strengthening and interaction with human osteoblasts in vitro. ACS applied materials & interfaces 2009;1:2470-6.

[125] Hu H, Ni Y, Mandal SK, Montana V, Zhao B, Haddon RC, et al. Polyethyleneimine functionalized single-walled carbon nanotubes as a substrate for neuronal growth. The Journal of Physical Chemistry B 2005;109:4285-9.

[126] Zhang D, Yi C, Zhang J, Chen Y, Yao X, Yang M. The effects of carbon nanotubes on the proliferation and differentiation of primary osteoblasts. Nanotechnology 2007;18:475102.

[127] Zancanela DC, de Faria AN, Simão AMS, Gonçalves RR, Ramos AP, Ciancaglini P. Multi and single walled carbon nanotubes: effects on cell responses and biomineralization of osteoblasts cultures. Journal of Materials Science: Materials in Medicine 2016;27:1-10.

[128] Zhu L, Chang DW, Dai L, Hong Y. DNA damage induced by multiwalled carbon nanotubes in mouse embryonic stem cells. Nano letters 2007;7:3592-7.

[129] Liu Z, Robinson JT, Sun X, Dai H. PEGylated nanographene oxide for delivery of water-insoluble cancer drugs. Journal of the American Chemical Society 2008;130:10876-7.

[130] Nayak TR, Andersen H, Makam VS, Khaw C, Bae S, Xu X, et al. Graphene for controlled and accelerated osteogenic differentiation of human mesenchymal stem cells. ACS nano 2011;5:4670-8.

[131] Kalbacova M, Broz A, Kong J, Kalbac M. Graphene substrates promote adherence of human osteoblasts and mesenchymal stromal cells. Carbon 2010;48:4323-9.

[132] Yoon OJ, Jung CY, Sohn IY, Kim HJ, Hong B, Jhon MS, et al. Nanocomposite nanofibers of poly (d, l-lactic-co-glycolic acid) and graphene oxide nanosheets. Composites Part A: Applied Science and Manufacturing 2011;42:1978-84.

[133] Ming HN. Fabrication and characterization of graphene hydrogel via hydrothermal approach as a scaffold for preliminary study of cell growth. International journal of nanomedicine 2011;6.

[134] Ku SH, Lee M, Park CB. Carbon-Based Nanomaterials for Tissue Engineering. Advanced healthcare materials 2013;2:244-60.

[135] Pinto AM, Moreira S, Gonçalves IC, Gama FM, Mendes AM, Magalhães FD. Biocompatibility of poly(lactic acid) with incorporated graphene-based materials. Colloids and Surfaces B: Biointerfaces 2013;104:229-38.

[136] Zhang L, Liu W, Yue C, Zhang T, Li P, Xing Z, et al. A tough graphene nanosheet/hydroxyapatite composite with improved in vitro biocompatibility. Carbon 2013;61:105-15.

[137] Guo X, Mei N. Assessment of the toxic potential of graphene family nanomaterials. Journal of Food and Drug Analysis 2014;22:105-15.

[138] Chang Y, Yang S-T, Liu J-H, Dong E, Wang Y, Cao A, et al. In vitro toxicity evaluation of graphene oxide on A549 cells. Toxicology letters 2011;200:201-10.

[139] Wang K, Ruan J, Song H, Zhang J, Wo Y, Guo S, et al. Biocompatibility of Graphene Oxide. Nanoscale Res Lett 2010;6:8.

[140] Zhang Y, Ali SF, Dervishi E, Xu Y, Li Z, Casciano D, et al. Cytotoxicity effects of graphene and single-wall carbon nanotubes in neural phaeochromocytoma-derived PC12 cells. Acs Nano 2010;4:3181-6.

[141] Liao K-H, Lin Y-S, Macosko CW, Haynes CL. Cytotoxicity of Graphene Oxide and Graphene in Human Erythrocytes and Skin Fibroblasts. ACS Applied Materials & Interfaces 2011;3:2607-15.

[142] Schinwald A, Murphy FA, Jones A, MacNee W, Donaldson K. Graphene-based nanoplatelets: a new risk to the respiratory system as a consequence of their unusual aerodynamic properties. ACS nano 2012;6:736-46.

[143] Kokubo T, Takadama H. How useful is SBF in predicting in vivo bone bioactivity? Biomaterials 2006;27:2907-15.

[144] Materials ACD-oC. Standard test method for tensile properties of polymer matrix composite materials: ASTM International; 2008.

[145] Parent P, Laffon C, Marhaba I, Ferry D, Regier T, Ortega I, et al. Nanoscale characterization of aircraft soot: A high-resolution transmission electron microscopy, Raman spectroscopy, X-ray photoelectron and near-edge X-ray absorption spectroscopy study. Carbon 2016;101:86-100.

[146] Annabi N. Porous Biomaterials. Integrated Biomaterials for Biomedical Technology: John Wiley & Sons, Inc.; 2012. p. 35-65.

[147] Lee SJ, Choi JS, Park KS, Khang G, Lee YM, Lee HB. Response of MG63 osteoblast-like cells onto polycarbonate membrane surfaces with different micropore sizes. Biomaterials 2004;25:4699-707.

[148] Loh QL, Choong C. Three-Dimensional Scaffolds for Tissue Engineering Applications: Role of Porosity and Pore Size. Tissue Engineering Part B, Reviews 2013;19:485-502.

[149] Noviana D, Paramitha D, Ulum MF, Hermawan H. The effect of hydrogen gas evolution of magnesium implant on the postimplantation mortality of rats. Journal of Orthopaedic Translation 2016;5:9-15.

[150] Aghion E, Levy G, Ovadia S. In vivo behavior of biodegradable Mg–Nd–Y–Zr–Ca alloy. Journal of Materials Science: Materials in Medicine 2012;23:805-12.

[151] Dahle AK, Lee YC, Nave MD, Schaffer PL, StJohn DH. Development of the as-cast microstructure in magnesium–aluminium alloys. Journal of light metals 2001;1:61-72.

[152] Rajavel K, Dinesh M, Saranya R, Kumar RR. Enhanced vacuum sensing performance of multiwalled carbon nanotubes: role of defects and carboxyl functionalization. RSC Advances 2015;5:20479-85.

[153] Zhu L, Ghosh T, Park C-Y, Meng Z-D, Oh W-C. Enhanced Sonocatalytic Degradation of Rhodamine B by Graphene-TiO2 Composites Synthesized by an Ultrasonic-Assisted Method. Chinese Journal of Catalysis 2012;33:1276-83.

[154] Witte F. Reprint of: The history of biodegradable magnesium implants: A review. Acta biomaterialia 2015;23:S28-S40.

[155] Mittal V, Nuzzo R, Kroto H. Polymer-graphene Nanocomposites: Royal Society of Chemistry; 2012.

[156] Atieh MA, Bakather OY, Al-Tawbini B, Bukhari AA, Abuilaiwi FA, Fettouhi MB. Effect of carboxylic functional group functionalized on carbon nanotubes surface on the removal of lead from water. Bioinorganic chemistry and applications 2011;2010.

[157] Lehman JH, Terrones M, Mansfield E, Hurst KE, Meunier V. Evaluating the characteristics of multiwall carbon nanotubes. Carbon 2011;49:2581-602.

[158] Zhang F, Weidmann A, Nebe JB, Burkel E. Osteoblast cell response to surface-modified carbon nanotubes. Materials Science and Engineering: C 2012;32:1057-61.

[159] Cuhadaroglu D, Uygun OA. Production and characterization of activated carbon from a bituminous coal by chemical activation. African journal of Biotechnology 2008;7.

[160] Mansur HS, Sadahira CM, Souza AN, Mansur AA. FTIR spectroscopy characterization of poly (vinyl alcohol) hydrogel with different hydrolysis degree and chemically crosslinked with glutaraldehyde. Materials Science and Engineering: C 2008;28:539-48.

[161] Yacob AR, Majid ZA, Dasril RSD, Inderan V. Comparison of various sources of high surface area carbon prepared by different types of activation. 2008.

[162] Gaharwar AK, Patel A, Dolatshahi-Pirouz A, Zhang H, Rangarajan K, Iviglia G, et al. Elastomeric nanocomposite scaffolds made from poly (glycerol sebacate) chemically crosslinked with carbon nanotubes. Biomaterials Science 2015.

[163] Shirazi Y, Tofighy MA, Mohammadi T. Synthesis and characterization of carbon nanotubes/poly vinyl alcohol nanocomposite membranes for dehydration of isopropanol. Journal of Membrane Science 2011;378:551-61.

[164] Hou L, Li Z, Pan Y, Du L, Li X, Zheng Y, et al. In vitro and in vivo studies on biodegradable magnesium alloy. Progress in Natural Science: Materials International 2014;24:466-71.

[165] Depan D, Misra RDK. The interplay between nanostructured carbon-grafted chitosan scaffolds and protein adsorption on the cellular response of osteoblasts: Structure–function property relationship. Acta Biomaterialia 2013;9:6084-94.

[166] Song J, Gao H, Zhu G, Cao X, Shi X, Wang Y. The preparation and characterization of polycaprolactone/graphene oxide biocomposite nanofiber scaffolds and their application for directing cell behaviors. Carbon 2015;95:1039-50.

[167] Yusong P, Dangsheng X, Xiaolin C. Mechanical properties of nanohydroxyapatite reinforced poly (vinyl alcohol) gel composites as biomaterial. Journal of materials science 2007;42:5129-34.

[168] Wang J, Wang X, Xu C, Zhang M, Shang X. Preparation of graphene/poly(vinyl alcohol) nanocomposites with enhanced mechanical properties and water resistance. Polymer International 2011;60:816-22.

[169] Duan S, Yang X, Mei F, Tang Y, Li X, Shi Y, et al. Enhanced osteogenic differentiation of mesenchymal stem cells on poly (l-lactide) nanofibrous scaffolds

containing carbon nanomaterials. Journal of Biomedical Materials Research Part A 2015;103:1424-35.

[170] Depan D, Misra R. The interplay between nanostructured carbon-grafted chitosan scaffolds and protein adsorption on the cellular response of osteoblasts: Structure–function property relationship. Acta biomaterialia 2013;9:6084-94.

[171] Keselowsky BG, Collard DM, García AJ. Surface chemistry modulates fibronectin conformation and directs integrin binding and specificity to control cell adhesion. Journal of Biomedical Materials Research Part A 2003;66:247-59.

[172] Aryaei A, Jayatissa AH, Jayasuriya AC. The effect of graphene substrate on osteoblast cell adhesion and proliferation. Journal of Biomedical Materials Research Part A 2014;102:3282-90.

[173] Lee SJ, San Choi J, Park KS, Khang G, Lee YM, Lee HB. Response of MG63 osteoblast-like cells onto polycarbonate membrane surfaces with different micropore sizes. Biomaterials 2004;25:4699-707.

[174] Yang C, Wang Y, Chen X. Mineralization regulation and biological influence of bioactive glass-collagen-phosphatidylserine composite scaffolds. Science China Life Sciences 2012;55:236-40.

[175] Watari F, Akasaka T, Li X, Uo M, Yokoyama A. Proliferation of osteoblast cells on nanotubes. Frontiers of Materials Science in China 2009;3:169-73.

[176] Chang H-I, Wang Y. Cell responses to surface and architecture of tissue engineering scaffolds: INTECH Open Access Publisher; 2011.

[177] Lee WC, Lim CHYX, Shi H, Tang LAL, Wang Y, Lim CT, et al. Origin of Enhanced Stem Cell Growth and Differentiation on Graphene and Graphene Oxide. ACS Nano 2011;5:7334-41.

[178] Yang Y, Shi S, Ding Q, Chen J, Peng J, Xu Y. Multiwalled carbon nanotube-modified poly (d, l-lactide-co-glycolide) scaffolds for dendritic cell load. Journal of Biomedical Materials Research Part A 2015;103:1045-52.

[179] Makar G, Kruger J. Corrosion of magnesium. International Materials Reviews 2013.

[180] Dong W, Hou L, Li T, Gong Z, Huang H, Wang G, et al. A Dual Role of Graphene Oxide Sheet Deposition on Titanate Nanowire Scaffolds for Osteo-implantation: Mechanical Hardener and Surface Activity Regulator. Scientific reports 2015;5.

[181] Kaur T, Thirugnanam A, Pramanik K. Effect of carboxylated graphene nanoplatelets on mechanical and in-vitro biological properties of polyvinyl alcohol nanocomposite scaffolds for bone tissue engineering. Materials Today Communications 2017.

[182] Holmes B, Fang X, Zarate A, Keidar M, Zhang LG. Enhanced human bone marrow mesenchymal stem cell chondrogenic differentiation in electrospun constructs with carbon nanomaterials. Carbon 2016;97:1-13.

[183] Ahmad I, Yazdani B, Zhu Y. Recent advances on carbon nanotubes and graphene reinforced ceramics nanocomposites. Nanomaterials 2015;5:90-114.

Dissemination

Journal Articles (Published)

1. Tejinder Kaur, A. Thirugnanam and Krishna Pramanik, "Tailoring the in vitro characteristics of poly(vinyl alcohol)-nanohydroxyapatite composite scaffolds for bone tissue engineering", Journal of Polymer Engineering, 2016, 36:771-784.
2. Tejinder Kaur, A. Thirugnanam, "Tailoring in-vitro biological and mechanical properties of polyvinyl alcohol reinforced with threshold carbon nanotube concentration for improved cellular response", RSC Advances, 2016, 6:39982-39992.
3. Tejinder Kaur, A. Thirugnanam, "Effect of porous activated charcoal reinforcement on mechanical and in-vitro biological properties of polyvinyl alcohol composite scaffolds", Journal of Materials Sciences and Technology, 2016, http://dx.doi.org/doi: 10.1016/j.jmst.2016.06.020.
4. Tejinder Kaur, Senthilguru Kulanthaivel, Thirugnanam Arunachalam, Indranil Banerjee and Krishna Pramanik, "Biological and mechanical evaluation of poly(lactic-co-glycolic acid) based composites reinforced with one, two and three dimensional carbon biomaterials for bone tissue regeneration", Biomedical Materials, 2017, 12:025012.
5. Tejinder Kaur, A. Thirugnanam and Krishna Pramanik, "Effect of carboxylated graphene nanoplatelets on mechanical and in-vitro biological properties of polyvinyl alcohol nanocomposite scaffolds for bone tissue engineering", Materials Today Communication, 2017, 12:34-42.

Conferences

1. Tejinder Kaur, A. Thirugnanam, "Carbon Nanomaterials Reinforced Poly(lactic-co-glycolic acid) Composites for Bone Tissue Engineering", 10th World Biomaterials Congress (WBC), 2016, Montreal, Canada.
2. Tejinder Kaur, A. Thirugnanam, "Tailoring in-vitro biological and mechanical properties of polyvinyl alcohol-activated charcoal composite scaffolds for bone tissue engineering" International Conference on Materials for the Millennium (MATCON), 2016, Kochi, India.
3. Tejinder Kaur, A. Thirugnanam and K. Pramanik, "Polyvinyl alcohol/nano-hydroxyapatite biocomposite scaffolds for bone tissue engineering", IInd International Conference on Medical Materials, Devices and Regenerative Medicine, 2014, Kathmandu, Nepal.
4. Tejinder Kaur, A. Thirugnanam and K. Pramanik, "Preparation and Characterization of PVA/nHA Scaffold for Tissue Engineering", 2nd International Conference on Tissue Engineering & Regenerative Medicine (ICTERM), 2013, India.

Vitae

TEJINDER KAUR

+91-9078822642, k.tejinder12@gmail.com
Biomechanics and Biotransport Lab
Dept. of Biotechnology and Medical Engineering
National Institute of Technology Rourkela, Odisha-769008, India

EDUCATION

Doctor of Philosophy in **2017**
Biotechnology and Medical Engineering
National Institute of Technology Rourkela, Odisha, India (NITR)
Dissertation: "Development of Carbon Reinforced Polymer-Ceramic Composites for Bone Tissue Engineering"
Advisor: Professor A. Thirugnanam

Master of Technology-Bachelor of Technology (integrated)
in Biotechnology **2011**
Lovely Professional University, Punjab, India

RESEARCH EXPERIENCE

Graduate Research Assistant **2012 - Present**
Department of Biotechnology and Medical Engineering, NITR

- Comparative study of carboxymethyl tamarind seed powder coated chitosan/montmorillonite/ hydroxyapatite composite macro sphere scaffolds.
- Shape memory behavior of polyethylene glycol in polymethyl methacrylate polymer network for biomedical application.
- Poly(vinyl alcohol)- bentonite nanocomposite hydrogels with marigold extract for wound healing applications.
- Biofunctionalization of titanium implants with biocomposite coatings via silanization.
- Corrosion resistant coatings on magnesium alloy (AE42) for cardiovascular stent application.
- Microwave assisted synthesis of porous chitosan-modified montmorillonite-hydroxyapatite composite scaffolds.
- Collaborate and coordinate with faculty and fellow graduate students across the departments.

Masters Research Experience **2011**
Department of Biotechnology, Lovely Professional University
- Quality analysis of curd with reference to microorganism and production of Bacteriocin.

TEACHING AND MENTORING EXPERIENCE

Teaching Assistant, Computational Biomechanics Laboratory **2013**
National Institute of Technology Rourkela
- Static and dynamic structural analysis, heat transfer and fluid dynamics using ANSYS 13.0.
- Human GAIT analysis using multiaxial force plate.

Teaching Assistant, Bioprocess Instrumentation Laboratory **2013**
National Institute of Technology Rourkela
- Applications and operations of various analytical instruments.

Teaching Assistant, Biomechanics and Advanced Biomechanics **2013-2015**
National Institute of Technology Rourkela
- Prepared practice tutorials focusing on application of biomechanics for 15-20 sophomores and 10 graduate students

Teaching Assistant, Computer Aided Tissue Engineering Laboratory **2014**
National Institute of Technology Rourkela
- Computer aided modelling and designing of various tissue substitutes

Graduate Mentor, Biomechanics and Biotransport Lab **2013-present**
National Institute of Technology Rourkela
- Mentored 5 undergraduates and 4 graduate students.
- Guided the students in preparation and presentation of research findings.

Graduate Mentor, Summer Internship Program
Biomechanics and Biotransport Lab **2014, 2015**
National Institute of Technology Rourkela
- Mentored 4 undergraduates in polymer composite for wound healing.

PUBLICATIONS

JOURNAL ARTICLES

- **Tejinder Kaur**, A. Thirugnanam and Krishna Pramanik. (2017). "Effect of carboxylated graphene nanoplatelets on mechanical and in-vitro biological properties of polyvinyl alcohol nanocomposite scaffolds for bone tissue engineering", Materials Today Communication, 12:34-42.

- Veena Vyas, **Tejinder Kaur** and A. Thirugnanam. (2016). "Chitosan composite three dimensional macrospheric scaffolds for bone tissue engineering", International Journal of Biological Macromolecules, https://doi.org/10.1016/j.ijbiomac.2017.04.055.
- **Tejinder Kaur**, Senthilguru Kulanthaivel, Thirugnanam Arunachalam, Indranil Banerjee and Krishna Pramanik. (2017). "Biological and mechanical evaluation of poly(lactic-co-glycolic acid) based composites reinforced with one, two and three dimensional carbon biomaterials for bone tissue regeneration", Biomedical Materials, 12:025012.
- Veena Vyas, **Tejinder Kaur**, Sumanta Kar and A. Thirugnanam. (2017). "Biofunctionalization of commercially pure titanium with chitosan/hydroxyapatite biocomposite via silanization: evaluation of biological performances", Journal of Adhesion Science and Technology, doi: 10.1080/01694243.2016.1278070.
- **Tejinder Kaur**, A. Thirugnanam and Krishna Pramanik. (2016). "Tailoring the in vitro characteristics of poly(vinyl alcohol)-nanohydroxyapatite composite scaffolds for bone tissue engineering", Journal of Polymer Engineering, 36:771-784.
- **Tejinder Kaur**, A. Thirugnanam. (2016). "Tailoring in-vitro biological and mechanical properties of polyvinyl alcohol reinforced with threshold carbon nanotube concentration for improved cellular response", RSC Advances, 6:39982-39992.
- **Tejinder Kaur**, A. Thirugnanam. (2016). "Effect of porous activated charcoal reinforcement on mechanical and in-vitro biological properties of polyvinyl alcohol composite scaffolds", Journal of Materials Sciences and Technology, doi: 10.1016/j.jmst.2016.06.020.
- Sumanta Kar, **Tejinder Kaur** and A. Thirugnanam, "Microwave-assisted synthesis of porous chitosan-modified montmorillonite-hydroxyapatite composite scaffolds", International Journal of Biological Macromolecules, 2016, 82; 628-636.
- Omkar Majumder, Anil Kumar Singh Bankoti, **Tejinder Kaur**, A. Thirugnanam and Ashok Kumar Mondal, "The influence of silane and silane-PMMA coatings on the in vitro biodegradation behavior of AE42 magnesium alloy for cardiovascular stent applications", RSC Advances, 2016, 6:107344-107354.

CONFERENCE PRESENTATIONS

- **Tejinder Kaur**, A. Thirugnanam. (2016) "Carbon Nanomaterials Reinforced Poly(lactic-co-glycolic acid) composites for bone tissue engineering", 10th World Biomaterials Congress (WBC), Montreal, Canada.
- **Tejinder Kaur**, A. Thirugnanam. (2016) "Tailoring in-vitro biological and mechanical properties of polyvinyl alcohol-activated charcoal composite scaffolds for bone tissue engineering" International Conference on Materials for the Millennium (MATCON), Kochi, India.
- **Tejinder Kaur**, , Kiran Y Vajanthari and A. Thirugnanam, "Development of PVA bentonite hydrogel composites for wound dressing", 2nd International Conference on Frontiers in Biological Sciences, 2015, Rourkela, India.

- Artatrana Tandi, **Tejinder Kaur**, Rethina Ebinesan, A. Thirugnanam and Ashok Mondal. (2015). "Drug loaded polyvinyl alcohol-cellulose composite hydrogels for wound dressings", 8th International Conference on Materials for Advanced Technologies (ICMAT), Singapore.
- **Tejinder Kaur**, A. Thirugnanam and K. Pramanik. (2014). "Polyvinyl alcohol/nano-hydroxyapatite biocomposite scaffolds for bone tissue engineering", IInd International Conference on Medical Materials, Devices and Regenerative Medicine, Kathmandu, Nepal.
- **Tejinder Kaur,** A. Thirugnanam and K. Pramanik. (2013). "Preparation and characterization of PVA/nHA scaffold for tissue engineering", 2nd International Conference on Tissue Engineering & Regenerative Medicine (ICTERM), Rourkela, India.

AWARDS AND FELLOWSHIPS

Travel award from Centre for International Cooperation in Science (CICS), India

- For attending the World Biomaterials Congress (WBC), Canada **2016**

Graduate Aptitude Test in Engineering (GATE) Fellowship **2012-2017**
from Ministry of Human Resource Development (MHRD), Government of India

TRAININGS

EMSI Symposium – Punjab University, Punjab, India **2012**

- Recent updates on mutation and cancer research

Verka Milk Plant, Punjab, India **2008**

- Production and quality analysis of various milk products

Lovely Professional University, Punjab, India **2007**

- Basics of Bioinformatics

SKILLS

- Materials processing and characterization techniques
- Tissue culture techniques
- Cell biology techniques
- Molecular biology techniques

REFERENCES

- **Dr. A. Thirugnanam, Ph.D.**
  Assistant Professor
  Department of Biotechnology and Medical Engineering,
  National Institute of Technology Rourkela,
  Odisha-769008, India.
  Email: thirugnanam.a@nitrkl.ac.in

- **Dr. Ashok Kumar Mondal, Ph.D.**
  Assistant Professor
  Department of Metallurgical and Materials Engineering
  National Institute of Technology Rourkela
  Odisha-769008, India.
  Email: mondala@nitrkl.ac.in; Phone- +91-661-2462571

- **Dr. Krishna Pramanik, Ph.D.**
  Professor
  Department of Biotechnology and Medical Engineering
  National Institute of Technology Rourkela
  Odisha-769008, India.
  Email: kpr@nitrkl.ac.in; Phone- +91-661-2462283

- **Dr. P. Balasubramanian, Ph.D.**
  Assistant Professor
  Department of Biotechnology and Medical Engineering
  National Institute of Technology Rourkela
  Odisha-769008, India.
  Email: biobala@nitrkl.ac.in; Phone- +91-661-2462297

Index

absorbance, 41, 42
activated carbon, 15, 31
agglomeration, 36
allografts, 2
ALP activity, 43, 83, 113
Apatite, 66, 101
ATR-FTIR, 54, 92
autografts, 2

bioactivity, 40, 66, 101
biocompatibility, 5
biodegradability, 6
biphasic calcium phosphate, 12
bone, 1
bone modeling, 1
bone tissue engineering, 3, 18
Bouin's fluid, 44
Bradford assay, 41
Bradford reagent, 41
Brownian motion, 46

calcein-AM, 44
carbon, 14
carbon nanotubes, 14, 28
carbonaceous, 28
calibration curve, 43
cell viability, 42, 76, 108
ceramics, 12, 27
chitosan, 22
collagen, 22, 44
composites, 26
confocal microscope, 43
contact angle, 40, 58, 94

degradation, 40, 62, 98
destaining, 43

electrospinning, 8

functionalized, 36
freeze drying, 8

gas foaming, 7
goat blood, 41
graphene nanoplatelets, 15, 30
graphene oxide, 30

hemocompatibility, 41, 99
hemolysis, 41, 64, 99
Hoechst dye, 43
hyaluronic acid, 22
hydroxyapatite, 12

inert, 32
interconnected, 5

magnesium, 14
mesenchymal stem cells, 4
metal, 13
mineralization, 43, 85

osteoblasts, 4

particulate leaching, 7
phase separation, 7
physicochemical characterization, 39
polycaprolactone, 5
poly(glycolic acid), 5, 25
poly(lactic acid), 5, 25
poly(lactic-co-glycolic acid, 10, 26
polymers, 9
poly(vinyl alcohol), 9, 26
porosity, 5
protein adsorption, 41, 70, 103

reinforcement, 14

scaffold, 5
scanning electron microscope, 39
solvent casting, 7
stainless steel, 24
swelling, 40, 59, 96

tensile properties, 42, 106
tissue engineering, 17
titanium, 13
tri-calcium phosphate, 27
TRITC-phalloidin, 43
transmission electron microscope, 39

X-ray diffraction, 39, 91